

# Evaluation of floor accelerations and spectra in linear and nonlinear regular RC frame buildings

by

Rahaf SHEIKH ALARD

THESIS PRESENTED TO ÉCOLE DE TECHNOLOGIE SUPÉRIEURE  
IN PARTIAL FULFILLMENT FOR A MASTER'S DEGREE  
WITH THESIS IN CONSTRUCTION ENGINEERING  
M.A.Sc.

MONTREAL, JULY 15, 2020

ÉCOLE DE TECHNOLOGIE SUPÉRIEURE  
UNIVERSITÉ DU QUÉBEC



Rahaf Sheikh Alard, 2020



This [Creative Commons](https://creativecommons.org/licenses/by-nc-nd/4.0/) license allows readers to download this work and share it with others as long as the author is credited. The content of this work can't be modified in any way or used commercially.

**BOARD OF EXAMINERS THESIS M.Sc.A.**  
**THIS THESIS HAS BEEN EVALUATED**  
**BY THE FOLLOWING BOARD OF EXAMINERS**

Mrs. Rola Assi, Thesis Supervisor  
Department of Construction Engineering, École de Technologie Supérieure

Mr. Alan Carter, President of the jury  
Department of Construction Engineering, École de Technologie Supérieure

Mr. Lotfi Guizani, Member of the jury  
Department of Construction Engineering, École de Technologie Supérieure

**THIS THESIS WAS PRESENTED AND DEFENDED**  
**IN THE PRESENCE OF A BOARD OF EXAMINERS AND PUBLIC**  
**JUNE 04, 2020**  
**AT ÉCOLE DE TECHNOLOGIE SUPÉRIEURE**



## **ACKNOWLEDGMENT**

I would like to thank my Master's supervisor, Ms. Rola Assi, for her efforts in this project, availability, and financial support through the NSERC Discovery Grant. .

I wish to express my sincere thanks to École de technologie supérieure (ÉTS) for providing me with all the necessary facilities. I am grateful to the library team of ÉTS for their commitment to service and dedication to the job. I am also thankful to the team of ÉTS student services and ÉTS Student Association for their support and organizing friendly and helpful activities.

I take this opportunity to thank my family for almost four decades of love, support, and encouragement. And to my lover Mohamed, whose love, wisdom, and generosity have enriched my life.

I also express my gratitude to my friends and all who, directly or indirectly, have lent their hand for helping in this journey.



# **Évaluation des accélérations et des spectres de plancher dans les bâtiments réguliers à ossature en béton armé dans le domaine linéaire et non linéaire**

Rahaf SHEIKH ALARD

## **RÉSUMÉ**

Ce projet vise à étudier l'effet de la ductilité des bâtiments sur les demandes en termes d'accélérations des composants non structuraux (CNS). Il vise également à évaluer les méthodes simplifiées disponibles dans la littérature ainsi que l'équation proposée dans la récente norme NIST.GCR.18.917.43 pour calculer les demandes d'accélération des CNS dans les bâtiments inélastiques. À cette fin, un bâtiment typique de 6 étages est conçu selon l'édition 2015 du Code national du bâtiment du Canada (CNB) pour quatre cas : 1) cadre modérément ductile à Montréal, 2) cadre conventionnel à Montréal, 3) cadre ductile à Vancouver, et 4) cadre conventionnel à Vancouver. Montréal et Vancouver ont été choisies pour représenter la sismicité de l'est et de l'ouest du Canada, respectivement. Les structures susmentionnées ont été soumises à douze et dix-sept enregistrements artificiels avec une probabilité de 2 et 10% sur 50 ans à Montréal et Vancouver, respectivement. La sélection et l'étalonnage des enregistrements sont compatibles avec les spectres d'aléa uniforme spécifiés dans l'édition 2015 du CNB. Les demandes d'accélération sismique des CNS exprimés en termes de l'amplification en fonction de la hauteur ( $A_x$ ), du facteur d'amplification de réponse ( $A_r$ ) et de spectres de réponse du plancher (FRS) sont générées en effectuant une analyse dynamique linéaire et non linéaire, et en appliquant la méthode simplifiée de Kothari et al. (2017), à l'aide du logiciel SAP2000®. Le profil PFA/PGA obtenu et  $A_r$  sont comparés à ceux proposés dans le CNB 2015 et le rapport NIST.GCR.18.917.43. Les résultats ont montré que la ductilité du cadre tend à réduire les demandes d'accélération des CNS et que cet avantage est moindre dans les cadres de construction conventionnelle par rapport aux cadres ductiles et modérément ductiles. Les demandes d'accélération sismique des CNS à Vancouver sont plus élevées qu'à Montréal pour tous les cas étudiés. Les FRS générés par la méthode simplifiée sont en bon accord en termes de forme avec ceux obtenus par l'analyse dynamique non linéaire, mais sous-estiment les ordonnées des FRS. Enfin, la demande PFA/PGA suggérée par le CNB 2015 est conservatrice pour les bâtiments inélastiques alors que la valeur de  $A_r$  est sous-estimée. Les demandes suggérées par NIST.GCR.18.917.43 correspondent mieux aux demandes requises que le NBC 2015.

**Mots-clés:** Spectres de réponse du plancher, composants non structuraux, composants opérationnels et fonctionnels, analyse non-linéaire, ductilité, béton armé et cadres résistants aux moments.





# **Evaluation of floor accelerations and spectra in linear and nonlinear Regular RC Frame Buildings**

Rahaf SHEIKH ALARD

## **ABSTRACT**

This project aims to investigate the influence of building ductility on nonstructural components (NSCs) acceleration demands. It targets also to evaluate simplified methods available in the literature as well as the equation proposed in the recent report NIST.GCR.18.917.43 to compute the NSCs acceleration demands in inelastic buildings. For this purpose, a typical 6-story frame building is designed according to 2015 edition of National Building Code of Canada (NBC) for four cases: 1) moderately ductile frame in Montreal, 2) conventional frame in Montreal, 3) ductile frame in Vancouver, and 4) conventional frame in Vancouver. Montreal and Vancouver were chosen to represent the seismicity in east and west of Canada, respectively. The aforementioned structures were subjected to twelve and seventeen artificial records with 2 and 10% per 50 year probability in Montreal and Vancouver, respectively. The selected and scaled records are compatible with the Uniform Hazard Spectra specified in the 2015 edition of the NBC. The seismic acceleration demands of NSCs in terms of height factor ( $A_x$ ), component amplification factor ( $A_r$ ), and floor response spectra (FRS) are generated by performing linear and nonlinear dynamic analysis, and applying the simplified method of Kothari et al. (2017), using SAP2000<sup>®</sup> software. The obtained factors  $A_x$  and  $A_r$  are compared to the ones proposed by NBC 2015 and the report NIST.GCR.18.917.43. The results showed that the frame ductility tends to reduce the NSCs acceleration demands and this benefit is less in the conventional construction frames as compared to the ductile and moderately ductile frames. Also, it was found that the seismic acceleration demands of NSCs are higher in Vancouver than in Montreal. The FRS generated by the simplified method are in a good agreement in terms of the shape with the ones obtained from the nonlinear dynamic analysis, but underestimate the ordinates of the FRS. Finally, the PFA/PGA demand suggested by the NBC 2015 is conservative for the inelastic building while the value of  $A_r$  is underestimated. The demands suggested by NIST.GCR.18.917.43 fit the required demands better than NBC 2015.

**Keywords:** Floor response spectra, nonstructural components, operational and functional components, nonlinear analysis, ductility, reinforced concrete, and moment-resisting frames.



## TABLE OF CONTENTS

	Page
INTRODUCTION .....	1
CHAPITRE 1 LITERATURE REVIEW .....	7
1.1 Introduction.....	7
1.2 The importance of NSCs seismic design .....	9
1.3 Approaches to estimate the seismic demands of NSCs .....	11
1.3.1 Code provisions for horizontal seismic force demands on NSCs .....	12
1.3.2 Floor acceleration demands according to NIST.GCR.18.917.43 .....	17
1.3.3 Floor Response Spectra approach .....	19
1.4 Proposed methods to determine seismic demands on NSCs mounted to inelastic buildings.....	22
1.4.1 PFAs distribution along the relative height.....	22
1.4.2 Peak component acceleration (PCA).....	23
1.5 Summary .....	31
CHAPITRE 2 SEISMIC DESIGN OF REINFORCED CONCRETE MOMENT RESISTING FRAMES .....	33
2.1 Introduction.....	33
2.2 Description of building .....	34
2.3 Load combinations.....	34
2.4 Seismic design considerations .....	36
2.5 Modal Analysis .....	36
2.6 Determination of seismic design forces.....	38
2.6.1 Gravity loads .....	38
2.6.2 Seismic base shear forces .....	40
2.7 Static Analyses.....	43
2.8 Seismic design .....	44
2.8.1 Design of the ductile frame .....	44
2.8.2 Design of the moderately ductile frame .....	46
2.8.3 Design conventional construction frames .....	47
2.9 Drift ratio .....	50
2.10 Summary .....	51
CHAPITRE 3 SELECTION AND SCALING OF GROUND MOTION RECORDS .....	53
3.1 Introduction.....	53
3.2 Selection and scaling of ground motion records.....	53
3.2.1 Moderately ductile frame in Montreal.....	55
3.2.2 Conventional construction frame in Montreal.....	58
3.2.3 Ductile frame in Vancouver .....	61
3.2.4 Conventional construction frame in Vancouver.....	65
3.3 Summary .....	69

CHAPITRE 4	LINEAR AND NONLINEAR ANALYSIS OF THE CASE STUDY BUILDINGS .....	70
4.1	Linear Dynamic Analysis .....	70
4.2	Nonlinear Dynamic Analysis.....	71
4.3	Simplified method of Kothari et al. (2017).....	77
4.3.1	Ductile frame in Vancouver .....	77
4.3.2	Conventional construction frame in Vancouver.....	84
4.3.3	Moderately ductile frame in Montreal.....	89
4.3.4	Conventional construction frame in Montreal.....	93
4.4	Summary .....	97
CHAPITRE 5	RESULTS .....	98
5.1	Evaluation the effect of ductility.....	98
5.1.1	Height factor $A_x$ .....	98
5.1.2	Floor response spectra (FRS) .....	100
5.1.3	Component amplification factor, $A_r$ .....	105
5.2	Effect of building location .....	108
5.3	Evaluation the simplified method of Kothari et al. (2017) .....	110
5.3.1	Height factor $A_x$ .....	110
5.3.2	Floor response spectra (FRS) .....	112
5.4	Evaluation of NIST GCR 18-917-43 (2018) .....	114
5.4.1	Height factor $A_x$ .....	114
5.4.2	Component amplification factor $A_r$ .....	116
5.5	Evaluation of the product ( $A_x.A_r$ ).....	118
5.6	Summary .....	121
CONCLUSIONS	.....	123
RECOMMENDATIONS	.....	127
APPENDIX I	SELECTION AND SCALING OF GROUND MOTIONS .....	128
APPENDIX II	SECTION ANALYSIS OF PHB1 SECTION BY RESPONSE 2000.....	132
APPENDIX III	PLASTIC HINGES PROPERTIES AND ACCEPTTANCE CRITERIA .....	134
APPENDIX IV	FRS, $R_{cb}$ , and $A_r$ IN FLOORS 1, 3, 4, and 5 .....	145
LIST OF BIBLIOGRAPHICAL REFERENCES	.....	150

## LIST OF TABLES

	Page
Table 1.1	Codes formulas of horizontal seismic design forces on NSCs .....13
Table 1.2	Design ground accelerations and amplification factors in the codes formulas .....13
Table 1.3	PCA/PFA and component ductility values .....19
Table 1.4	Suggested frequencies in (Hz) for generating FRS.....20
Table 1.5	Values of parameter $\alpha$ .....22
Table 1.6	Values of parameter $\beta$ .....23
Table 1.7	Values of $m_l$ , $m_r$ , and $A_{rmax}$ .....26
Table 1.8	Values of $a$ , $b$ and $A_r$ for different ranges of structural periods .....27
Table 2.1	The values of gravity loads used in the design .....34
Table 2.2	Load combinations considered for seismic design of building as per NBC .....34
Table 2.3	Types of flexural resistance and their relationship as per CSA A23.3 .....36
Table 2.4	Modal periods, NBC 2015 limit, and the considered period in the seismic design .....37
Table 2.5	Force modification factors in concrete structures as per NBC 2015 .....41
Table 2.6	Factors $M_v$ for moment resisting frames as per NBC 2015.....42
Table 2.7	Base shear force calculations for case of studied buildings.....42
Table 2.8	Lateral loads for each floor level for buildings in Vancouver .....43
Table 2.9	Lateral loads for each floor level for buildings in Montreal.....43
Table 2.10	Shear resistance of frame joints at different levels of ductility as per CSA A23.3 .....45

Table 3.1	Modal periods and ranges for ground motion scaling for the studied buildings.....	55
Table 3.2	Scaling factors of selected records of moderately ductile frame in Montreal.....	56
Table 3.3	Scaling factors of selected records of moderately ductile frame in Montreal.....	56
Table 3.4	Scaling factors of selected records of conventional frame in Montreal.....	59
Table 3.5	Scaling factors of selected records of conventional frame in Montreal.....	59
Table 3.6	Scaling factors of selected records of ductile frame in Vancouver .....	62
Table 3.7	Scaling factors of selected records of ductile frame in Vancouver .....	62
Table 3.8	Scaling factors of selected records of conventional frame in Vancouver..	66
Table 3.9	Scaling factors of selected records of conventional frame in Vancouver..	66
Table 4.1	Obtained parameters from idealized relationship .....	79
Table 4.2	Equivalent stiffness and stiffness reduction factors at IO and LS performance levels for the 2D ductile frame in Vancouver.....	79
Table 4.3	Ground motion records and scaling factors (SF) at IO and LS performance levels used in the 1 <sup>st</sup> iteration for the ductile frame in Vancouver .....	81
Table 4.4	Mean values of maximum roof displacement, maximum base shear, and SRF at IO and LS performance level of the ductile frame in Vancouver .....	82
Table 4.5	Iterations results at IO and LS performance levels for the ductile frame in Vancouver .....	83
Table 4.6	Obtained parameters from idealized relationship .....	85
Table 4.7	Equivalent stiffness and stiffness reduction factors at IO and LS performance levels for the 2D conventional construction frame in Vancouver .....	85
Table 4.8	Used ground motion at IO and LS performance levels in the 1 <sup>st</sup> iteration for the conventional construction frame in Vancouver .....	86

Table 4.9	Mean value of maximum roof displacement, maximum base shear, and SRF at IO and LS performance levels of the conventional construction frame in Vancouver.....	87
Table 4.10	Equivalents stiffness and damping iterations results at IO and LS performance levels for conventional construction frame in Vancouver ....	88
Table 4.11	Obtained parameters from idealized relationship .....	90
Table 4.12	Equivalent stiffness and stiffness reduction factors at IO and LS performance levels for the 2D moderately ductile frame in Montreal.....	90
Table 4.13	Used ground motion at IO and LS performance levels in the 1 <sup>st</sup> iteration for the moderately ductile frame in Montreal.....	91
Table 4.14	Mean value of maximum roof displacement, maximum base shear, and SRF at IO and LS performance levels of the moderately ductile frame in Montreal .....	91
Table 4.15	Equivalents stiffness and damping iterations results at IO and LS performance levels for moderately ductile frame in Montreal .....	92
Table 4.16	Obtained parameters from idealized relationship .....	94
Table 4.17	Equivalent stiffness and stiffness reduction factors at IO and LS performance levels for the 2D conventional frame in Montreal.....	94
Table 4.18	Used ground motion at IO and LS performance levels in the 1 <sup>st</sup> iteration for the conventional frame in Montreal.....	95
Table 4.19	Mean value of maximum roof displacement, maximum base shear, and SRF at IO and LS performance levels of the conventional frame in Montreal.....	95
Table 4.20	Equivalents stiffness and damping iterations results at IO and LS performance levels for conventional frame in Montreal.....	96





## LIST OF FIGURES

		Page
Figure 1.1	Structural and nonstructural components of a typical building .....	8
Figure 1.2	Relative investments in typical buildings .....	9
Figure 1.3	Failure of suspended lighting fixtures in an office building in 2001 Nisqually earthquake ( $M_w=6.8$ ) .....	10
Figure 1.4	Severe damage to the masonry cladding of the former Montreal East City Hall during the 1988 Saguenay earthquake ( $M_w=5.9$ ) .....	10
Figure 1.5	Nonstructural damage in 2011 Christchurch earthquake ( $M_w= 6.2$ ) .....	11
Figure 1.6	The distribution of PGA amplification along the relative height according to the NBC 2015, ASCE 7-16 and Eurocode 8 .....	15
Figure 1.7	The component amplification factor $A_r$ according to the current codes ....	16
Figure 1.8	Time history and direct spectra to spectra methods to generate FRS .....	21
Figure 1.9	$R_{acc}$ values at roof level for various component damping ratios at the 1 <sup>st</sup> period.....	24
Figure 1.10	$R_{acc}$ values at roof level for various component damping ratios at the 2 <sup>nd</sup> period.....	24
Figure 1.11	Flowchart for the simplified method.....	29
Figure 2.1	Plan view of RC moment resisting frame building model.....	35
Figure 2.2	Elevation view of the RC moment resisting frame building model.....	35
Figure 2.3	Three dimensional model of a case study building created by SAP2000® .....	37
Figure 2.4	Assigning the floor seismic mass as a weight in the floor diaphragm of the SAP2000® model .....	38
Figure 2.5	Unfactored gravity loads considered to design a typical interior ductile frame in Vancouver and moderately ductile frame in Montreal. Values include only the self-weight of beams (Unit is kN).....	39

Figure 2.6	Unfactored gravity loads considered in design of typical interior conventional constructed frame in Vancouver and Montreal. Values include only the self-weight of beams (Unit is kN).....	39
Figure 2.7	UHS with a probabilities of exceedance 2% per 50 years (a) Vancouver, and (b) Montreal .....	41
Figure 2.8	Arrangement of longitudinal reinforcement in beams in ductile frames ...	45
Figure 2.9	Arrangement of longitudinal reinforcement in beams in moderately ductile frames.....	46
Figure 2.10	Dimensions of beams and columns for buildings in Vancouver .....	47
Figure 2.11	Dimensions of beams and columns for buildings in Montreal .....	48
Figure 2.12	Reinforcing details of the ductile frame members in Vancouver .....	48
Figure 2.13	Reinforcing details of the conventionally constructed frames in Vancouver .....	49
Figure 2.14	Reinforcing details of the moderately ductile frame members in Montreal .....	49
Figure 2.15	Reinforcing details of the conventionally constructed frames in Montreal .....	50
Figure 2.16	Inter-storey drift ratio for frame models in (a) Vancouver; (b) Montreal..	50
Figure 3.1	Target spectrum with probabilities of exceedance of 2% and 10% per 50 years (a) Montreal, and (b) Vancouver .....	54
Figure 3.2	Acceleration spectra of the selected and scaled input ground motion for the moderately ductile frame in Montreal using the target spectrum at a probability of exceedance 2% per 50 years in (a) $T_{R1}$ , and (b) $T_{R2}$ .....	57
Figure 3.3	(a) Mean acceleration spectra for scenarios 1 and 2 compared with the target spectrum (b) Difference between the mean acceleration spectra of the scaled records and the target spectrum at a probability of exceedance 2% per 50 years within $T_{R1}$ and $T_{R2}$ .....	57
Figure 3.4	Acceleration spectra of the selected and scaled input ground motion for the moderately ductile frame in Montreal using the target spectrum at a probability of exceedance 10% per 50 years in (a) $T_{R1}$ , and (b) $T_{R2}$ ...	58

Figure 3.5	(a) Mean acceleration spectra for scenarios 1 and 2 compared with the target spectrum (b) Difference between the mean acceleration spectra of the scaled records and the target spectrum at a probability of exceedance 10% per 50 years within $T_{R1}$ and $T_{R2}$ .....58
Figure 3.6	Acceleration spectra of the selected and scaled input ground motion for the conventional construction frame in Montreal using the target spectrum at a probability of exceedance 10% per 50 years in (a) $T_{R1}$ , and (b) $T_{R2}$ .....60
Figure 3.7	(a) Mean acceleration spectra for scenario 1 and 2 compared with the target spectrum (b) Difference between the mean acceleration spectra of the scaled records and the target spectrum at a probability of exceedance 2% per 50 years within $T_{R1}$ and $T_{R2}$ .....60
Figure 3.8	Acceleration spectra of the selected and scaled input ground motion for the conventional frame in Montreal using the target spectrum at a probability of exceedance 10% per 50 years in (a) $T_{R1}$ , and (b) $T_{R2}$ .....61
Figure 3.9	(a) Mean acceleration spectra for scenarios 1 and 2 compared with the target spectrum (b) Difference between the mean acceleration spectra of the scaled records and the target spectrum at a probability of exceedance 10% per 50 years within $T_{R1}$ and $T_{R2}$ .....61
Figure 3.10	Acceleration spectra of the selected and scaled input ground motion for the ductile frame in Vancouver using the target spectrum at a probability of exceedance 2% per 50 years in (a) $T_{R1}$ , (b) $T_{R2}$ , and (c) $T_{R3}$ .....63
Figure 3.11	(a) Mean acceleration spectra for scenario 1, 2 and 3 compared with the target spectrum (b) Difference between the mean acceleration spectra of the scaled records and the target spectrum at a probability of exceedance 2% per 50 years within $T_{R1}$ , $T_{R2}$ , and $T_{R3}$ .....64
Figure 3.12	Acceleration spectra of the selected and scaled input ground motion for the ductile frame in Vancouver using the target spectrum at a probability of exceedance 10% per 50 years in (a) $T_{R1}$ , (b) $T_{R2}$ , and (c) $T_{R3}$ .....64
Figure 3.13	(a) Mean acceleration spectra for scenario 1, 2 and 3 compared with the target spectrum (b) Difference between the mean acceleration spectra of the scaled records and the target spectrum at a probability of exceedance 10% per 50 years within $T_{R1}$ , $T_{R2}$ , and $T_{R3}$ .....65
Figure 3.14	Acceleration spectra of the selected and scaled input ground motion for the conventional construction frame in Vancouver using the target

	spectrum at a probability of exceedance 2% per 50 years in (a) $T_{R1}$ , (b) $T_{R2}$ , and (c) $T_{R3}$ .....67
Figure 3.15	(a) Mean acceleration spectra for scenario 1, 2 and 3 compared with the target spectrum (b) Difference between the mean acceleration spectra of the scaled records and the target spectrum at a probability of exceedance 2% per 50 years within $T_{R1}$ $T_{R2}$ , and $T_{R3}$ .....67
Figure 3.16	Acceleration spectra of the selected and scaled input ground motion for the conventional frame in Vancouver using the target spectrum at a probability of exceedance 10% per 50 years in (a) $T_{R1}$ , (b) $T_{R2}$ , and (c) $T_{R3}$ .....68
Figure 3.17	(a) Mean acceleration spectra for scenario 1, 2 and 3 compared with the target spectrum (b) Difference between the mean acceleration spectra of the scaled records and the target spectrum at a probability of exceedance 10% per 50 years within $T_{R1}$ , $T_{R2}$ , and $T_{R3}$ .....68
Figure 4.1	Floors seismic weight applied to floor nodes in a typical model.....71
Figure 4.2	Typical frame model with assigned plastic hinges .....72
Figure 4.3	Definition of plastic hinge properties of a symmetric section in SAP2000 .....73
Figure 4.4	Definition of plastic hinge of a non-symmetric section in SAP 2000 .....74
Figure 4.5	Generalized Force–Deformation Relation for Concrete Elements or Components .....74
Figure 4.6	Isotropic hysteresis model.....75
Figure 4.7	Hinges formation at the end of pushover analysis of ductile frame in Vancouver .....78
Figure 4.8	Obtained pushover capacity curve of ductile frame in Vancouver.....78
Figure 4.9	The roof displacement and base shear time histories obtained from the linear dynamic analysis of 2D ductile frame in Vancouver subjected to W6C1_02 record, considering $SRF_{IO}=0.324$ , $\zeta_{eqIO} = 22.01\%$ .....80
Figure 4.10	Hinges formation at the end of pushover analysis of conventional frame in Vancouver.....84

Figure 4.11	Computed pushover capacity curve of conventional frame in Vancouver .....	85
Figure 4.12	Hinges formation at the end of pushover analysis of moderately ductile frame in Montreal .....	89
Figure 4.13	Computed pushover capacity curve of moderately ductile frame in Montreal.....	90
Figure 4.14	Hinges formation at the end of pushover analysis of conventional frame in Montreal .....	93
Figure 4.15	Computed pushover capacity curve of conventional frame in Montreal...	94
Figure 5.1	Computed mean $A_x$ factor along the height of the studied buildings compared to NBC 2015 provision: (a) elastic analyses (b) inelastic analyses using ground motion with 10% per 50 years probability of exceedance, and (c) inelastic analyses using ground motion with 2% per 50 years probability of exceedance.....	99
Figure 5.2	Effect of building ductility on the roof level mean FRS with component damping ratio 5% .....	100
Figure 5.3	Effect of building ductility on the 2 <sup>nd</sup> floor mean FRS with component damping ratio 5% .....	101
Figure 5.4	Effect of building ductility on the amplitudes of mean FRS in the 2 <sup>nd</sup> and 6 <sup>th</sup> floor for component damping ratio 5% and ground motion with 2% per 50 years probability of exceedance .....	102
Figure 5.5	Effect of ground motion level on $R_{cb}$ factor in the 6 <sup>th</sup> floor of the studied frames using component damping ratio 5% .....	103
Figure 5.6	Effect of ground motion level on $R_{cb}$ factor in the 2 <sup>nd</sup> floor of the studied frames using component damping ratio 5% .....	104
Figure 5.7	Effect of building ductility on the shape of mean FRS in the 2 <sup>nd</sup> and 6 <sup>th</sup> floors for component damping ratio 5% .....	105
Figure 5.8	Effect of building ductility on $A_r$ in the 6 <sup>th</sup> floor for component damping ratio 5%.....	106
Figure 5.9	Effect of building ductility on $A_r$ in the 2 <sup>nd</sup> floor for component damping ratio 5%.....	107

Figure 5.10	Computed mean $A_r$ factor along the height of the studied buildings compared to NBC 2015 provision: (a) elastic analyses (b) inelastic analyses using ground motion with 10% per 50 years probability of exceedance, and (c) inelastic analyses using ground motion with 2% per 50 years probability of exceedance.....	108
Figure 5.11	Mean inelastic FRS at each floor for ductile and conventional studied buildings in Vancouver .....	109
Figure 5.12	Mean inelastic FRS at each floor for moderately ductile and conventional studied buildings in Montreal.....	109
Figure 5.13	Mean PFA/PGA ratio along the height of the case of study buildings obtained from the Kothari's simplified method at IO and LS performance levels and the nonlinear dynamic analysis: (a) ductile frame in Vancouver, (b) conventional frame in Vancouver, (c) moderately ductile frame in Montreal, and (d) conventional frame in Montreal .....	111
Figure 5.14	Computed mean FRS in the 6 <sup>th</sup> floor obtained from the simplified method and from nonlinear dynamic analysis .....	113
Figure 5.15	Mean FRS in the 2 <sup>nd</sup> floor obtained from the simplified method in the studied frames compared to those obtained from nonlinear dynamic analysis.....	114
Figure 5.16	Comparison of computed mean elastic and inelastic $A_x$ profiles with the NIST.GCR.18-917-43 (2018) provisions.....	115
Figure 5.17	Comparison of computed $A_r$ values in the 6 <sup>th</sup> floor compared to the value proposed in NIST.GCR.18-917-43 (2018).....	117
Figure 5.18	Comparison of computed $A_r$ values in the 2 <sup>nd</sup> floor compared to the value proposed in NIST.GCR.18-917-43 (2018).....	118
Figure 5.19	Comparison of computed mean ( $A_x.A_r$ ) in the 6 <sup>th</sup> level of the studied buildings compared to NBC 2015 and NIST.GCR.18-917-43 (2018) provisions.....	119
Figure 5.20	Comparison of computed max $A_x.A_r$ factor of the studied buildings along the building height to NBC 2015 and NIST.GCR.18-917-43 (2018) provisions .....	120

## **LIST OF ABBREVIATIONS**

ASCE	American Society of Civil Engineers
CC	Conventional construction
CSA	Canadian Standards Association
D	Ductile
EC8	Eurocode 8
E-W	East – West direction
FEMA	Federal Emergency Management Agency
FRS	Floor response spectrum
GRS	Ground response spectrum
IO	Immediate Occupancy performance level
LDP	Linear dynamic procedure
LS	Life safety performance level
MD	Moderately ductile
MDOF	Multi degree of freedom
NBC	National building code of Canada
NDP	Nonlinear dynamic procedure
NEHRP	National Earthquake Hazards Reduction Program
N-S	North – South direction
NSCs	Nonstructural components
NSP	Nonlinear static procedure
OFCs	Operational and functional components
PCA	Peak component acceleration
PFA	Peak floor acceleration
PGA	Peak ground acceleration
RC	Reinforced concrete
SDOF	Single degree of freedom





## LIST OF SYMBOLS

### Greek alphabet

$\alpha$	Post-yield slope of idealized bilinear relationship as per FEMA 356
$\gamma_a$	Component importance factor as per EC 8
$\delta_{avg}$	Average of displacements at the extreme points of the diaphragm at level x
$\delta_{max}$	Maximum displacement at any point of the diaphragm at level x
$\Delta_{LS}$	Displacement at life safety performance level
$\Delta_y$	Yield displacement
$\zeta_0$	Structural damping
$\zeta_{eq}$	Equivalent damping
$\zeta_{hys}$	Hysteretic damping
$\lambda$	Factor to account for low-density concrete
$\phi_c$	Resistance factor for concrete
$\phi_y$	Yield rotation
$\omega_i$	Angular frequency at mode i

### Lowercase Latin alphabet

$a$	Parameter used to measure deformation capacity in component load–deformation curve given by ASCE 41-17
$a_0$	Mass proportional coefficient
$a_1$	Stiffness proportional coefficient
$a_i$	The maximum acceleration at level i obtained from the modal analysis
$a_g$	Design ground acceleration on type A ground as per Eurocode 8
$a_p$	The dynamic amplification factor as per ASCE 7-16
$b$	Parameter used to measure deformation capacity in component load–deformation curve given by ASCE 41-17

$c$	Parameter used to measure residual strength in component load–deformation curve given by ASCE 41-17
$f'_c$	Concrete compressive strength at 28 days
$f_y$	Yield strength of longitudinal reinforcing steel bars
$f_{yt}$	Yield strength of transverse reinforcing steel bars
$h_n$	The total height of the supporting structure
$h_x$	The height of NSC in the building starting from the ground level as per NBC 2015
$k_e$	Initial effective slope of idealized bilinear relationship as per FEMA 356
$k_{eq}$	Equivalent stiffness of a structure
$k_i$	Initial stiffness of a structure before cracking
$q_a$	Component response modification factor
$z$	The height of NSC in the building starting from the ground level as per ASCE 7-16

### Uppercase Latin alphabet

$A_j$	Minimum cross-sectional area within a joint in a plane parallel to the axis of the reinforcement generating the shear in the joint
$A_r$	The dynamic amplification factor as per NBC 2015
$A_x$	Height factor in NBC and accidental torsion amplification factor in ASCE 7-16
$C_p$	The component factor
$D$	Dead load
$E$	Earthquake load
$E_c$	Young modulus of concrete
$E_s$	Young modulus of steel
$F_a$	The acceleration-based site coefficient
$F_p$	Component seismic design force applied horizontally at the center of gravity of the component
$F_t$	Concentrated force applied at the top of the building
$F_x$	Portion of design base shear that is located at level x

$h_i$	The height above the base to level $i$
$h_x$	The height above the base to level $x$
$I_E$	The importance factor of the building as per NBC 2015
$I_p$	Component importance factor as per ASCE 7-16
$L$	Live Load
$M$	Moment magnitude of an earthquake event
$M_n$	Nominal flexural resistance
$M_p$	Probable flexural resistance
$M_r$	Factored flexural resistance
$M_v$	Factor accounts for higher mode effect on the base shear force
$M_y$	Yield moment
$R$	Fault distance
$R_{cb}$	The ratio of elastic FRS to the inelastic FRS
$R_d$	Ductility-related force modification factor
$R_o$	Overstrength-related force modification factor
$R_p$	Component response modification factor
$S$	Snow load
$S_a(0.2)$	The spectral acceleration value for a period of 0.2 s
$S(T)$	The spectral acceleration value for a period of $T$
$S_{DS}$	Design spectral acceleration at short period
$S_p$	Horizontal force factor
$S_T(T)$	Spectral acceleration of target spectrum
$T_a$	Building period defined by code expression (Equation 1-10)
$T_p$	Nonstructural component period
$T_{1Bldg}$	The fundamental period of the building
$T_{iBldg}$	The building period of mode $i$
$T_{max}$	The upper limit of period range $T_R$
$T_{min}$	The lower limit of period range $T_R$
$T_R$	Period range of interest for selection and scaling ground motion

$T_{90\%}$	The period of the highest vibration mode required to cumulate a minimum participating mass of 90% of the structure mass
$V$	Design base shear
$V_{\max}$	Upper limit of design base shear
$V_{\min}$	Lower limit of design base shear
$V_y$	Base shear force at yielding point
$W$	Seismic weight of building
$W_i$	Portion of $W$ that is located at level $i$
$W_p$	Nonstructural component weight
$W_x$	Portion of $W$ that is located at level $x$

## INTRODUCTION

### Background and problem definition

Several regions in Canada are seismically active. The most active region is western Canada such as the coastal area of British Columbia including Victoria and Vancouver, and to a lesser extent, the eastern Canada such as the region from the St. Lawrence River Valley to the Ottawa Valley including Quebec City, Montreal and Ottawa.

The largest earthquake in eastern North America in the last 50 years struck Quebec on November 25, 1988 with a moment magnitude of 5.9. This earthquake, referred to as the Saguenay earthquake, did point out the tremendous impact of the failure of the NSCs of buildings and economic losses upon life safety. In this event, a great majority of the injuries, property damage and economic loss was caused by the failure of NSCs in buildings while very little structural damage was observed (Foo & Cheung, 2004).

In 1995, National Building Code of Canada (NBC) expressed the force modification factor,  $R$  in the minimum lateral seismic force at the base of the structure to design and detail the building components for different levels of ductility. This factor reflected the capability of a structure to dissipate energy through inelastic behaviour. The values of  $R$  ranged from 1.0 for very brittle systems to 4.0 for the most ductile systems. Each value of  $R$  factor must be used only in conjunction with the corresponding design and detailing requirements of a structural system, and design level of ground motion. In the 2005 to 2015 editions of the NBC, two force modification factors,  $R_d$  and  $R_o$  are proposed in the base shear equation for seismic design (Mitchell et al., 2003), where  $R_d$  is the ductility-related factor and  $R_o$  is the overstrength-related factor. Consequently, the reinforced concrete moment-resisting frame buildings can be designed according to NBC 2015 as ductile (D), moderately ductile (MD) or conventional construction (CC).

On the other hand, the proposed equation in all editions of NBC to determine the seismic design forces on NSCs considers their supporting structure as elastic and ignores the impact of force modification factors of the building. Thus, evaluating the NSCs acceleration demands in terms

of height factor ( $A_x$ ) and the component amplification factor ( $A_r$ ) in inelastic buildings is a very essential research need.

Recent studies have shown that the building ductility affects the NSC response expressed in terms of the height factor,  $A_x$ , and the shape and peak values of floor response spectra (FRS) (Chaudhuri & Villaverde, 2008; Medina et al., 2006; Miranda & Taghavi, 2009; Oropeza et al., 2010; Petrone et al., 2015; Shooshtari, Saatcioglu, Naumoski, & Foo, 2010; Sullivan, Calvi, & Nascimbene, 2013; Surana et al., 2016, 2017; Vukobratović & Fajfar, 2017; Wieser et al., 2011). In fact, if an earthquake event induces inelastic response in the supporting structure, the component response reduces. Several methods were proposed to consider the benefit of building nonlinearity in reducing NSC demands in terms of  $A_x$  and FRS (Fathali & Lizundia, 2011; Medina et al., 2006; Petrone et al., 2015; Shooshtari et al., 2010; Surana et al., 2016; Wieser et al., 2013). These methods proposed the distribution of  $A_x$  factor along the building height as a function of the relative height, the ground motion intensity, and the period of the supporting structure. As for FRS, proposed methods were in general amplification functions to generate the FRS from the ground response spectrum (GRS) or the uniform hazard spectra (UHS). However, these methods either consider the shaking intensity of the study location as a surrogate of building ductility; thus ignoring the corresponding building design and detailing requirements for each ductility level or are limited to one level of building ductility. On the other hand, simplified methods were recently suggested to carry out nonlinear static analysis (pushover) together with linear time history analysis to generate inelastic FRS (Jha et al., 2017; Kothari et al., 2017). The method proposed by Kothari et al (2017) was derived for a conventional RC frame with three stories, and was not evaluated for other levels of ductility nor different number of stories. In addition to the aforementioned methods, a new equation was proposed in the document NIST GCR 18-917-43 (2018) to determine the seismic design forces for NSCs attached to inelastic buildings. This equation considers that the building ductility only affects the  $A_x$  factor.

The current study aims to investigate the influence of different levels of building ductility on seismic demands expressed in terms of  $A_x$ ,  $A_r$ , and FRS of light acceleration-sensitive NSCs. For this purpose, a 6-story regular reinforced concrete frame office building assumed to be

located in Montreal and Vancouver was used in this project. The building was designed according to requirements stated by CSA A23.3 (2014a)44 as ductile and conventional construction in Vancouver, moderately ductile and conventional construction in Montreal. Ground motion records with probability of exceedance of 2 and 10% per 50 years were selected and scaled to be compatible with the uniform hazard spectra (UHS) of Montreal and Vancouver. Linear and nonlinear dynamic analyses were performed to compute the elastic and inelastic NSCs seismic demands in the four mentioned case studies using SAP2000® software (CSI, 2019). In addition, this project is interested in evaluating the most recent simplified method available in the literature (Kothari et al., 2017) as well as the new equation proposed in NIST GCR 18-917-43 (2018) to evaluate the aforementioned seismic demands of NSCs.

## Objectives

The main objective of this study is to evaluate the seismic demands of acceleration sensitive NSCs attached to regular reinforced concrete moment resisting frames buildings that can develop inelastic deformations when subjected to strong and moderate ground motions in Canada.

The specific objectives of this project are as follows:

- 1) Evaluate the influence of building ductility and severity of ground motion on the NSCs acceleration demands in terms of  $A_x$ ,  $A_r$  and FRS.
- 2) Investigate the influence of building location (east and west of Canada) on the seismic acceleration demands of NSCs.
- 3) Evaluate the following approaches to compute the NSCs acceleration demands (PFA, the PCA and FRS) in inelastic buildings:
  - The simplified method of Kothari et al. (2017),
  - The simplified equation of NBC (2015)
  - The simplified equation of the document NIST GCR 18-917-43 (2018).

## Methodology

The methodology used to achieve the general and the specific objectives includes the following steps:

- 1) Perform a literature review on the seismic response of NSC with a focus on the different methods proposed to consider the influence of building ductility on the acceleration seismic demands of light NSCs.
- 2) Select the 6-story case study RC frame building and carry out the seismic design process. Excel sheets have been created in order to design it according to the standard CSA A23.3-14 (2014a). Four cases studies were considered as follows:
  - Ductile and conventional construction in Vancouver,
  - Moderately ductile and conventional construction in Montreal.
- 3) Create 2-D linear and nonlinear models for the aforementioned cases studies using SAP2000® software. Properties of concentrated plastic hinges were calculated according to ASCE 41-17 (2017).
- 4) Select and scale the input ground motions with probability of exceedance 2 and 10% per 50 years. Excel sheets were created to select and scale ground motions as per to method A proposed in NBC 2015 – Appendix J. The considered ground motions are extracted from the synthetic time histories database provided by Atkinson (2009) for the east and west of Canada.
- 5) Perform linear and nonlinear dynamic analysis procedures to the aforementioned studied cases in order to determine acceleration demands on NSCs attached to them.
- 6) Apply the steps of the simplified method in Kothari et al. (2017) to the aforementioned case study buildings.
- 7) Discuss the results of the aforementioned analyses and compare them to those stated by NBC 2015 and NIST GCR 18-917-43 in order to achieve the current project objectives.



### **Limit of study**

This study is limited to the following points:

- 1) The structural system consists of regular symmetric reinforced concrete moment-resisting frames. Irregular structural systems and building with shear walls are beyond the scope of this study.
- 2) The height of the selected building is limited to 6 stories.
- 3) The case study buildings were considered as two-dimensional frames subjected to uni-directional seismic excitation.
- 4) Only site class C (based on NBC 2015) was considered. Other soil types are not included.
- 5) Only lightweight acceleration-sensitive NSCs were considered in this study, and the dynamic interaction with the building was neglected.
- 6) NSCs considered in this study are linear elastic, and NSCs ductility was not taken into account.

### **Thesis organization**

The thesis consists of five chapters in addition to this introduction and the conclusions. The first chapter overviews the approaches of determining the seismic acceleration demands on acceleration sensitive NSCs. In addition, the first chapter critically reviews the proposed methods in previous studies to consider the building ductility in determining the NSCs seismic acceleration demands. The second chapter describes the selected building (geometry, loads, and material properties), and the seismic design process of four case study buildings. The selection and scaling of the input ground motions are given in the third chapter. In chapter four, the linear and nonlinear analyses of case study buildings are presented. The fifth chapter presents the analyses, and discusses the obtained results in each part of the study. Finally, conclusions from the current work and recommendations for future work are presented.



## **CHAPITRE 1**

### **LITERATURE REVIEW**

This chapter gives a brief information about NSCs classification and their seismic performance in recent earthquakes followed by an overview of the code approaches for determining the seismic demands on NSCs. This chapter presents also a detailed literature review about the influence of building ductility on NSCs seismic response as well as the proposed methods in the previous studies to include the effect of building ductility in the NSCs seismic demands computation.

#### **1.1 Introduction**

A building is composed of various components that can be divided into two groups, structural components and nonstructural components (NSCs). The structural components (or primary system) of a building are designed to resist and transfer vertical and horizontal loads such as gravity, earthquake, wind loads. These components include columns, beams, braces, slabs, load-bearing walls and foundations. NSCs are elements within or attached to buildings to provide them with essential services and functions and do not contribute to the building's resistance such as suspended ceiling, heating and ventilation systems and building contents as shown in Figure 1.1. The NSCs can be also named operational and functional components (OFCs) according to CSA S832 (CSA, 2014b), or secondary systems (FEMA 74, 2005).

NSCs can be divided into three categories of sub-components based on their function (CSA, 2014b) as follows:

- 1) Architectural that are either external such as cladding, glazing, roofing, balconies, etc. or internal such as partitions, ceilings, atriums, etc.
- 2) Building services that include mechanical, plumbing, electrical and telecommunications.
- 3) Building contents that are either common such as movable partitions, office equipment, storage lockers, etc. or specialized such as antiques, works of art, hazardous materials, medical supplies, etc.

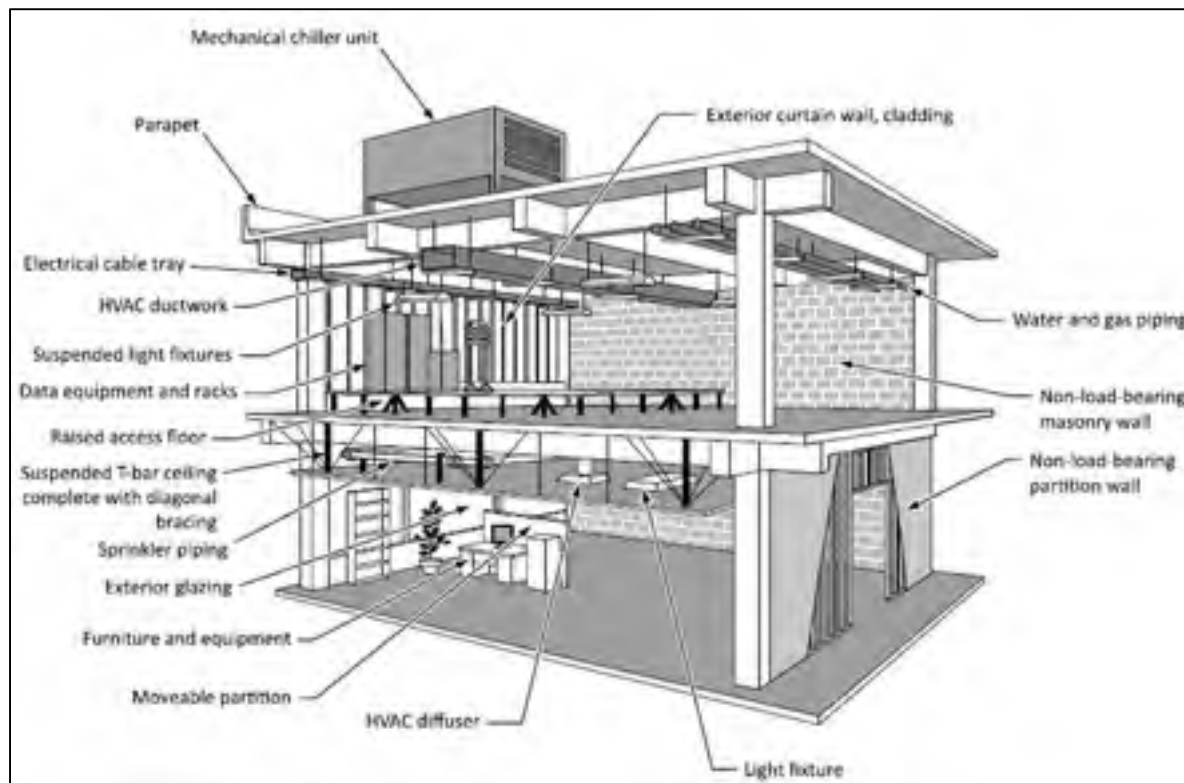


Figure 1.1 Structural and nonstructural components of a typical building  
Taken from CSA S832 (CSA, 2014b)

In addition, NSCs can be classified according to the main reason causing their seismic damage as follows (FEMA74, 2005):

- 1) Acceleration-sensitive components: the main cause of seismic damage in this category (such as parapets and suspended ceilings) is the building seismic inertial forces.
- 2) Displacement-sensitive components: the main cause of seismic damage in this category (such as windows and elevator cabins) is the building displacement or inter-story drift.
- 3) Both acceleration- and displacement-sensitive components: the seismic damage in this category (such as fire sprinklers and heavy infill walls) is due to the inertia forces and building displacement.

NSCs can also be classified based on their fundamental period ( $T_p$ ) into rigid and flexible. According to NEHRP (2009), rigid components are short period elements ( $T_p \leq 0.06 \text{ s}$ ) while flexible components are longer period elements ( $T_p > 0.06 \text{ s}$ ).

Finally, NSCs can be categorized into light and heavy based on the ratio of their weight to that of the supporting structure. According to CSA S832 (2014b), NSCs are considered light when their weight doesn't exceed 20% of the total weight of the floor on which they are located or 10% of the total weight of the supporting structure.

## 1.2 The importance of NSCs seismic design

Proper seismic design of NSCs is important for several reasons. First, the failure of NSCs can cause injuries or deaths. For instance, the failure of cladding panels in precast buildings was the main cause of fatalities in the 2012 Emilia earthquake in north Italy (Magliulo et al., 2014). Second, the cost of NSCs represents the largest portion of construction cost in facilities such as hospitals, offices and hotels as shown in Figure 1.2 (Miranda & Taghavi, 2009).

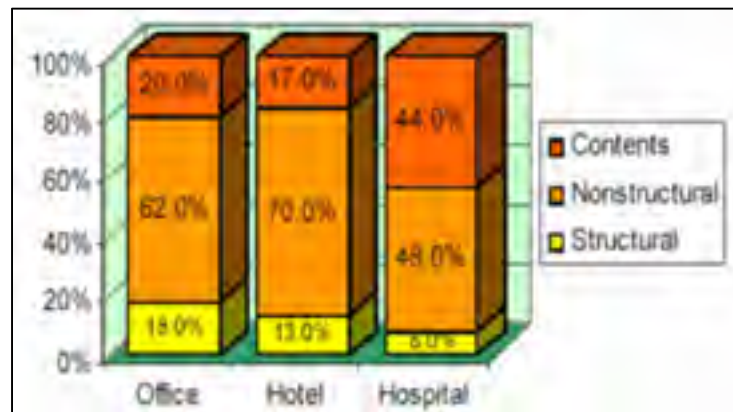


Figure 1.2 Relative investments in typical buildings  
Taken from Miranda and Taghavi (2009)

The economic costs resulting from damage to NSCs include not only the physical repair work, but also downtime cost when the damage affects the building occupancy. For example, the damage of NSCs in Santiago airport during 2010 Maule, Chile Earthquake ( $M_w$  8.8) led airline

companies to suffer US\$10 million loss as a result of business interruption (Filiatrault & Sullivan, 2014). Finally, NSCs are very sensitive to ground motion shaking so low or moderate earthquakes, which cause very little structural damage, can lead to severe economic losses due to NSCs damage or failure. For example, the 1988 Saguenay earthquake ( $M_w$  5.9) that struck Quebec, Canada caused very little structural damage while a great majority of the properties damage and economic loss was caused by the failure of NSCs in buildings (Foo & Cheung, 2004; Mitchell et al., 1990). Examples of NSC damage in different earthquakes are illustrated in Figures 1.3 to 1.5.



Figure 1.3 Failure of suspended lighting fixtures in an office building in 2001 Nisqually earthquake ( $M_w=6.8$ )  
Taken from Filiatrault et al. (2001)



Figure 1.4 Severe damage to the masonry cladding of the former Montreal East City Hall during the 1988 Saguenay earthquake ( $M_w=5.9$ )  
Taken from Mitchell et al. (1990)



Figure 1.5 Nonstructural damage in 2011 Christchurch earthquake ( $M_w=6.2$ )  
Taken from Baird and Yeow (2016)

### 1.3 Approaches to estimate the seismic demands of NSCs

The seismic force demands of NSCs can be determined by four approaches summarized as follows:

- 1) Simplified formulas suggested by current code provisions such as NBC (2015), CSA S832 (2014b), ASCE 7-16 (2016), ASCE 41-17 (2017), Eurocode 8 (2004), and NIST GCR 18-917-43 (2018). These simplified formulas are based on equivalent static methods that are usually applied in the current design practice for ordinary and industrial structures and serve as convenient means when no or just little information about the NSCs and the supporting structure are available at the design phase.
- 2) Simplified formulas enhanced by refined determination of peak floor accelerations (PFA) by means of modal superposition methods available in ASCE 7-16 (2016) and ASCE 41-17 (2017), and require knowing the building dynamic properties.
- 3) Decoupled time history analyses also known as floor response spectrum method. They are usually used when dealing with critical facilities such as nuclear power plants (ASCE 4-98, 2000; CSA N289.3-10, 2010). In these methods, only the supporting structure is modelled, so they are recommended for light components where the dynamic interaction between supporting structure and NSCs is neglected.

- 4) Coupled time history analyses where the supporting structure and NSCs are modelled as an integral part. Although this approach gives accurate responses of NSCs, it is not widely used because it involves several difficulties such as large differences between supporting structure characteristics (mass and stiffness) and that of NSCs, and large number of degrees-of-freedom in a combined system (Chen & Soong, 1988).

### 1.3.1 Code provisions for horizontal seismic force demands on NSCs

In Canada, the seismic design of NSCs in new buildings is addressed in the CSA-S832 standard (2014b) and NBC (2015). The previous versions of NBC also contained some provisions regarding the seismic design of NSCs in terms of the seismic force and inter-story drift demand requirements (Assi & McClure, 2015). In the United States, the seismic design of NSCs is addressed in the National Earthquake Hazard Reduction Program (NEHRP) documents, ASCE 7-16 (2016) and ASCE 41-17 (2017). In Europe, it is addressed in the Eurocode 8 (EN 1998-1, 2004).

Table 1.1 presents the proposed equations in NBC 2015, ASCE 7-16, and Eurocode 8 to determine the horizontal seismic design force acting on the mass center of a NSC. These are inertia forces equal to the product of NSC weight,  $W_p$  and the peak component acceleration, PCA. According to these formulations, the product of design ground acceleration and the height factor,  $A_x$  (see Table 1.2) gives the peak floor acceleration (PFA) where the NSC is attached. Then the PFA is scaled by two factors to determine the PCA: the component dynamic amplification factor,  $A_r$  and the component response modification factor,  $R_p$  (see Table 1.2). The factor  $A_r$  is explained in details in section 1.3.1.2, while the component response modification factor represents the energy absorption capacity of the element and its attachment. The term  $F_a$  is the acceleration-based site coefficient while  $S_a(0.2)$  is the spectral acceleration value for a period of 0.2 s. The terms  $S_{DS}$  and  $a_g$  are the design ground acceleration in ASCE and Eurocode 8, respectively.

The term  $I_E$  is the importance factor of the building and the term  $C_p$  is the seismic coefficient for components of mechanical and electrical equipment. The terms  $I_p$  and  $\gamma_a$  are the component importance factor in ASCE and Eurocode 8, respectively.



Table 1.1 Codes formulas of horizontal seismic design forces on NSCs

Code	Seismic horizontal design force	
NBC 2015	$0.3F_a S_a (0.2) I_E (C_p A_r / R_p) (1 + 2h_x / h_n) W_p$	(1.1)
ASCE 7-16	$0.4S_{DS} (a_p I_p / R_p) (1 + 2h_x / h_n) W_p$	(1.2)
Eurocode 8	$a_g S [3(1 + z / h_n) / (1 + (1 - T_p / T)^2) - 0.5] (\gamma_a / q_a) W_p$	(1.3)

Table 1.2 Design ground accelerations and amplification factors in the codes formulas

Code	Design ground acceleration	Height factor	Component dynamic amplification factor	NSC response factor	Importance factor
NBC	$0.3F_a S_a (0.2)$	$(1 + 2h_x / h_n)$	$A_r$	$R_p$	$I_E$
ASCE	$0.4S_{DS}$	$(1 + 2h_x / h_n)$	$a_p$	$R_p$	$I_p$
EC 8	$a_g S$	$[1.5(1 + h_x / h_n) - 0.5]$	$\frac{[3(1 + h_x / h_n) - 0.5]}{[1.5(1 + h_x / h_n) - 0.5]}$	$q_a$	$\gamma_a$

Equations 1.1 to 1.3 are mainly empirical and do not rely on analytical analysis or experimental works (Bachman et al., 1994; Filiatrault & Sullivan, 2014).

In case more information about the supporting structure is available in terms of modal periods and shapes, ASCE 7-16 and NEHRP (2009) permit to use Equation 1.4 to determine the seismic force demand on NSCs at any level based on the dynamic properties of the structure as follow:

$$F_p = \left( \frac{a_i a_p W_p}{R_p / I_p} \right) A_x \quad (1.4)$$

Where  $a_i$  is the acceleration at level i obtained from the modal analysis procedure explained in ASCE 7-16 and  $A_x$  is the torsional amplification factor used to amplify the accidental torsional moment at each level and is given by Equation 1.5 as follow:

$$1.0 \leq A_x = \left( \frac{\delta_{\max}}{1.2\delta_{\text{avg}}} \right)^2 \leq 3.0 \quad (1.5)$$

Where  $\delta_{\max}$  and  $\delta_{\text{avg}}$  are the maximum and average displacements at level  $x$ , respectively. This method gives more realistic results than the simplified codes formulas because  $a_i$  is determined by using modal analysis method. More details about using the refined approach to determine the amplification of PFA along the height are available in Pinkawa et al. (2014) and Wieser et al. (2011).

Common limitations were pointed out concerning the code approaches for horizontal seismic demands on NSCs and criticized in several studies as follows:

### 1.3.1.1 Height factor, $A_x$

The factor  $A_x$  represents the amplification of PGA along the building height, it is equal to the ratio (PFA/PGA). This distribution is linear and ranges from 1.0 at ground level to 3.0 at the roof level as per NBC and ASCE, while it ranges from 1.0 at ground level to 2.5 at the roof level as per EC8 as shown in Figure 1.6.

The linear increase of  $A_x$  factor (Figure 1.6) is a function of the relative height  $h_x/h_n$ , where  $h_x$  is the height of the NSC relative to the ground level, and  $h_n$  is the total height of the supporting structure. However, it is shown in Miranda and Taghavi (2009) that a longer fundamental period of elastic building resulted in a lower ratio of PFA/PGA for shear wall buildings, moment-resisting frame buildings, and buildings with lateral system stiffness somewhere in between. In Fathali and Lizundia (2011), it was shown that the distribution of  $A_x$  factor is affected by the level of seismicity along with fundamental period of the supporting structure and relative height. It has been concluded in that study that the profile of  $A_x$  proposed in ASCE 7-16 is a good fit just for short-period buildings (fundamental period less than 0.5 s) in low-seismicity areas ( $\text{PGA} < 0.067 \text{ g}$ ), but conservative for the other ranges of periods. It was also

observed that the PFAs are relatively constant over most of the building height in the long-period buildings (fundamental period larger than 1.5 s).

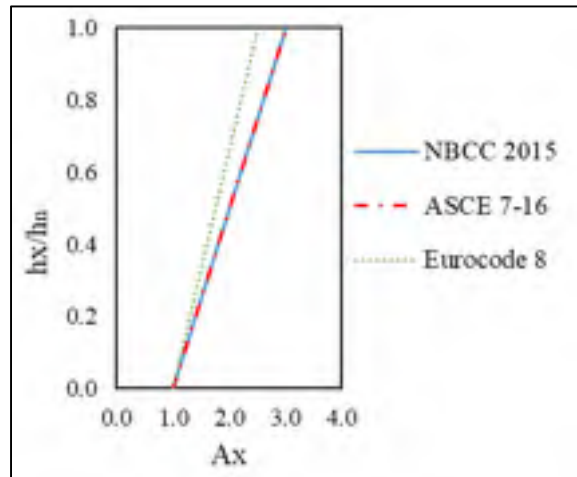


Figure 1.6 The distribution of PGA amplification along the relative height according to the NBC 2015, ASCE 7-16 and Eurocode 8

In addition to the effect of building fundamental period on  $A_x$  factor, a sudden increase in the PFA in the top stories was reported in recent studies (Petrone et al., 2015; Rodriguez, Restrepo, & Carr, 2002; Taghavi & Miranda, 2005) due to the large contribution of the higher modes to the PFAs. This phenomenon called whiplash happens in the most top floors of mid and high-rise buildings.

Beside the aforementioned parameters, building ductility has also an effect on the  $A_x$  factor along the building height. Typically, the ratio PFA/PGA tends to be lower when the building is inelastic. This is due to the fact that the yielding in the structure leads to elongation of the building period during the response (Surana et al., 2016; Wieser et al., 2013; Wieser et al., 2011). According to Petrone et al. (2015) whose studies are oriented to the Eurocode 8. A linear trend that varies from 1.0 at the base to 3.0 at the top is on the safe side for the linear response of RC frames supporting structures, while this range is conservative based on the nonlinear analysis results and a linear trend that goes from 1.0 at the base to 2.0 at the top would better fit the outcomes of the nonlinear analyses.

### 1.3.1.2 Dynamic amplification factor, $A_r$

The Codes approaches consider the dynamic interaction between the NSC and the building by means of a component amplification factor,  $A_r$ , which is defined as the floor response spectrum normalized by the PFA of the elastic frame (Medina et al., 2006).

The factor  $A_r$  is given in different codes and standards (ASCE 7-16, 2016; NBC, 2015) as a tabulated value. A value of 1.0 is given for a rigid NSC while a value of 2.5 is given for a flexible NSC. This is because the flexible NSC vibrates independently around its point of attachment to the building leading to dynamic amplification of acceleration at the attachment point. The values of  $A_r$  are assumed constant for all the building floors. Unlike ASCE 7-16 (2016) and NBC (2015), NEHRP (2009) and EC8 (2004) give the  $A_r$  factor as a function of the ratio of NSCs periods to fundamental period of building ( $T_p/T_{1Bldg}$ ) as shown in Figure 1.7.

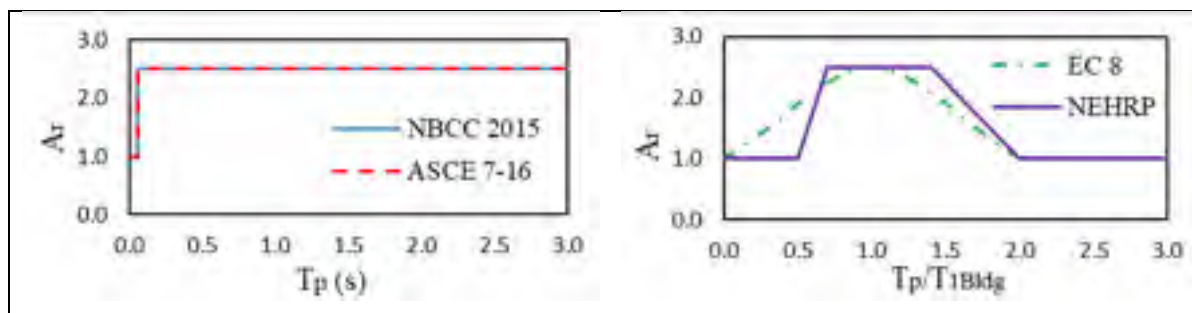


Figure 1.7 The component amplification factor  $A_r$  according to the current codes

Several studies showed that the aforementioned codes recommendations underestimate the  $A_r$  factors. In Medina et al. (2006), it was observed that the maximum value 2.5 of  $A_r$  underestimates the component amplification in elastic buildings, where the value of  $A_r$  reaches a value up to 5.5 at the roof of a low-rise elastic building (3 stories) and reduces to 2.5 at the roof of a mid-rise elastic building (9 stories). As for the case of inelastic response of supporting structures, the  $A_r$  value of 2.5 is on the safe side if the damping ratio of NSCs exceeds 5%. Otherwise, it should be increased based on the selected damping ratio.

In Fathali and Lizundia (2011), it was shown based on recorded floor accelerations in 169 buildings in Los Angeles that the value of  $A_r$  exceeds the code value of 2.5 and reaches a maximum value of 3.3 for a range of  $T_p$  between 0.1 s and 0.75 s. On the other hand, the code value outside this range of periods is conservative. These results are in a good agreement with those found by Wieser et al. (2013) in a study on steel resisting moment frames, which showed that the peak value of  $A_r$  that corresponds to the first mode is reduced as the level of yielding in the structure increases while no remarkable reduction was observed at the second modal period. In Petrone et al. (2015) study on RC moment resisting frames, the value of  $A_r$  given in the codes was also criticized, and a linear distribution for  $A_r$  along the height was proposed to range from 3.0 at ground level to 5.2 at roof in elastic supporting structures and from 2.6 to 4.8 in inelastic buildings. Recently, NIST GCR 18-917-43 (2018) gives the value of  $A_r$  based on the relative height and ductility of the component. For example, for an elastic component,  $A_r$  equals 2.5 at the ground floor and 4.0 in the roof and elevated floors (see section 1.3.2).

### 1.3.2 Floor acceleration demands according to NIST.GCR.18.917.43

The proposed NSCs design equation by NIST GCR 18-917-43 (2018) is given in Equation 1.6:

$$\frac{F_p}{W_p} = PGA \left[ \frac{\frac{PFA}{PGA}}{R_{\mu Bldg}} \right] \times \left[ \frac{\frac{PCA}{PFA}}{R_{pcomp}} \right] \times I_p \quad (1.6)$$

Where:

- $F_p$  Horizontal design force for NSCs
- $W_p$  Component operating weight
- PGA Peak ground acceleration and considered equal to  $0.4S_a(0.2)$ , where  $S_a(0.2)$  is the spectral acceleration at structure period of 0.2 s.
- PFA/PGA Peak ground acceleration to peak floor acceleration ratio given by the following equation:

$$\left[ \frac{PFA}{PGA} \right] = 1 + \alpha_1 \left[ \frac{z}{h} \right] + \alpha_2 \left[ \frac{z}{h} \right]^{10} \quad (1.7)$$

Where:

$$\alpha_1 = (1 / T_{aBldg}) \leq 2.5 \quad (1.8)$$

$$\alpha_2 = [1 - (0.4 / T_{aBldg})^2] > 0 \quad (1.9)$$

$$T_{aBldg} = C_t h^x \quad (1.10)$$

where  $C_t$  and  $x$  are defined by standards according to the lateral force resisting system of the building

$R_{\mu Bldg} = (R_d)^{1/2}$  where  $R_{\mu Bldg}$  is a reduction factor to account for building global ductility calculated based on the value of  $R_d$  (see Table 2.5).

**PCA/PFA** Factor to account for component amplification, inherent component damping, and component ductility. Values of PCA/PFA shown in Table 1.3 are based on the location of NSCs and the component ductility assuming the inherent component damping is 5%.

$R_{pcomp}$  Inherent component reserve strength margin factor that accounts for its ductility.

$I_p$  Component importance Factor

We can note that PFA/PGA is affected by the building parameters such as the lateral force resisting system (LFRS), modal periods, ductility, and vertical location of the component term. While PCA/PFA is affected by the component period, its ductility, and its damping, so the PFA/PGA and PCA/PFA terms are separated for simplicity.

Equation 1.6 is a refinement of Equation 1.2, whereas the building period, relative height, type of lateral force resisting system, and building ductility are taken into account to compute (PFA/PGA). As for (PCA/PFA) value in Equation 1.6, it becomes a function to the component ductility and height instead of component period in Equation 1.2.

Table 1.3 PCA/PFA and component ductility values  
Taken from NIST GCR 18-917-43 (2018)

Location of Component	Possibility of Being in Resonance with Building	Component Ductility		(PCA) (PFA) <sup>(2)</sup>
		Category <sup>(1)</sup>	Assumed Ductility	
Ground	None Likely	Elastic	$\mu_{comp}=1$	2.0
		Low	$\mu_{comp}=1.25$	2.0
		Moderate	$\mu_{comp}=1.5$	1.8
		High	$\mu_{comp}=2$	1.4
Roof or Elevated Floor	Less Likely	Any	—	1.0
		Elastic	$\mu_{comp}=1$	4.0
	None Likely	Low	$\mu_{comp}=1.25$	2.0
		Moderate	$\mu_{comp}=1.5$	2.2
		High	$\mu_{comp}=2$	1.4
	Less Likely	Any	—	1.0

<sup>(1)</sup> Categories will be assigned to components similar to ASCE/SEI 7-16 Table 13.5-1. Categories need to be determined.

<sup>(2)</sup> Inherent component damping of 5% is assumed as a default.

### 1.3.3 Floor Response Spectra approach

Floor Response Spectra (FRS) is a decoupled analysis method called also systems-in-cascade method (Villaverde, 1996). This method is used for light weight NSCs, so the dynamic analysis is performed for the supporting structure without considering the effect of the NSCs. FRS represents the peak acceleration response of a nonstructural component and is typically used to estimate the acceleration demands on flexible NSCs while PFA is used to estimate the acceleration demands on rigid NSCs (Flores et al., 2015).

This method is simple in concept, somewhat rational and far from the numerical complexity in the coupled analyses. However, it doesn't account for multiple points of NSCs attachments, and requires lengthy numerical integrations when using time history analysis. More details about the advantages and limitations of this method are available in Villaverde (1997) and Chen and Soong (1988).

The procedure of floor response spectra is described in a number of official documents related to the seismic analysis of nuclear structures such as the CSA N289.3-10 (2010) and ASCE 4-98 (2000). ASCE 4-98 states the nonlinear time history and direct spectra-to-spectra as methods to generate floor response spectra, and gives recommendation about frequency interval, treatment of uncertainties and damping ratio. For example, ASCE 4-98 recommends a frequency increment to compute FRS at each frequency range listed in Table 1.4 to produce an accurate FRS including the significant peaks that are expected at the natural frequencies of the supporting structure. It also recommends to consider the uncertainties in the supporting structure frequencies by broadening the peaks of FRS by a minimum of  $\pm 15\%$ . Explanation about nonlinear time history method and direct spectra to spectra method is given in the following sections.

Table 1.4 Suggested frequencies in (Hz) for generating FRS  
Taken from ASCE 4-98 (2000)

Frequency range	0.5-3.0	3.0-3.6	3.6-5.0	5.0-8.0	8.0-15	15-18	18-22	22-34
Increment	0.10	0.15	0.20	0.25	0.50	1.0	2.0	3.0

### 1.3.3.1 Time history method

In this method, the supporting structure is subjected to a set of recorded or synthetic time histories compatible with a given seismic design spectrum. Then, the floor acceleration at the locations of the NSCs attachments can be obtained and utilized as the input to a single degree-of-freedom oscillator to generate a floor response spectrum (FRS), which is a plot of the maximum responses of the oscillator versus the frequency of the oscillator (Villaverde, 1997). To obtain a reliable FRS, a large number of sets of earthquake time histories may be required (Villaverde, 1997).



### 1.3.3.2 Direct spectra to spectra method

To avoid the complexity of the aforementioned time history method, several methods were proposed to generate FRS directly from a specified ground response spectrum, or design spectrum. These methods use as input a specified ground response spectrum and the dynamic properties of the structure (modal frequencies, damping ratios, mode shapes and modal participation factors). Figure 1.8 illustrates the procedure of both time history and direct spectra to spectra methods.

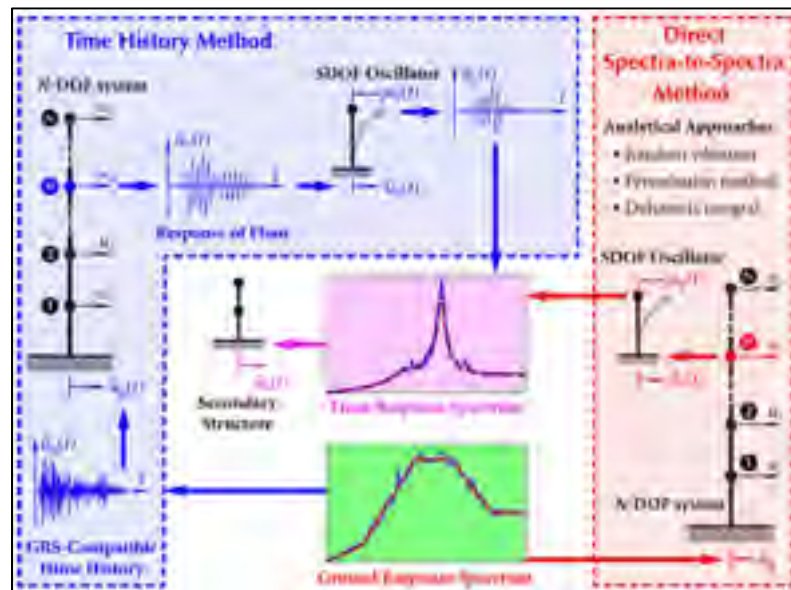


Figure 1.8 Time history and direct spectra to spectra methods to generate FRS  
Taken from Jiang (2016)

There are different direct approaches to generate the floor response spectra from the design response spectra such as random vibration (Der Kiureghian, 1980), perturbation method (Singh & Suarez, 1986) and Duhamel integral (ASCE 4-98, 2000). Recently, new and simplified methods were proposed (Surana et al., 2016; Vukobratović & Fajfar, 2017) to generate elastic and inelastic floor response spectrum directly from the ground response spectra. In Surana et al. (2016), amplification functions have been proposed to amplify the ground response spectrum in case of elastic and inelastic supporting structure depending on incremental

dynamic analysis performed on 3D RC frame buildings. Whereas, a new method that takes into account the dynamic properties of the structure is proposed in Vukobratović and Fajfar (2017) and can be used for both elastic and inelastic multi-degree-of-freedom structures, based on the response spectrum concept. However, the results for inelastic supporting systems was considered approximate and not accurate enough when compared with results obtained by nonlinear response history analysis.

#### 1.4 Proposed methods to determine seismic demands on NSCs mounted to inelastic buildings

In the following sections, a critical review of the most recent proposed methods to include the effect of building ductility on the seismic acceleration demands of NSCs in terms of PFA/PGA distribution along the relative height and PCA.

##### 1.4.1 PFAs distribution along the relative height

Fathali and Lizundia (2011) proposed Equation 1.11 to determine PFA/PGA ratio based on recorded data from instrumented buildings. In Equation 1.11, PFA/PGA ratio is a function to the relative height,  $\alpha$  and  $\beta$  parameters which are determined based on the  $PGA$  and the building fundamental period,  $T_{Bldg1}$ , as shown in Tables 1.5 and 1.6.

$$PFA / PGA = 1 + \alpha(z / h)^\beta \quad (1.11)$$

Table 1.5 Values of parameter  $\alpha$   
Taken from Fathali and Lizundia (2011)

	$0.4S_{DS}$ $=PGA < 0.067g$	$0.067 \leq 0.4S_{DS} = PGA < 0.2g$	$0.4S_{DS}$ $=PGA \geq 0.2g$
$T_{Bldg1} < 0.5s$	1.26	1.04	0.99
$0.5s < T_{Bldg1} < 1.5s$	1.52	1.02	0.65
$T_{Bldg1} > 1.5s$	0.90	0.72	0.00

Table 1.6 Values of parameter  $\beta$   
Taken from Fathali and Lizundia (2011)

	$0.4S_{DS}$ $=PGA < 0.067g$	$0.067 \leq 0.4S_{DS} = PGA < 0.2g$	$0.4S_{DS}$ $=PGA \geq 0.2g$
$T_{Bldg1} < 0.5s$	1.09	1.29	0.89
$0.5s < T_{Bldg1} < 1.5s$	1.57	1.63	1.55
$T_{Bldg1} > 1.5s$	1.69	3.00	1.00

Petrone et al. (2015) performed nonlinear analysis for ductile RC moment resisting frame buildings at five different heights (1, 2, 3, 5 and 10 stories). Based on the PFA/PGA profiles obtained from the nonlinear analysis, a linear range of PFA/PGA distribution along the height from 1.0 at ground to 2.0 at roof level is proposed.

## 1.4.2 Peak component acceleration (PCA)

### 1.4.2.1 Proposed methods based on amplification functions

In the following a summary of studies which proposed functions and equations to include the effect of building ductility in the seismic acceleration demands of NSCs in terms of FRS and/or  $A_r$ .

Medina et al. (2006) performed linear and nonlinear dynamic analysis on four special moment resisting steel frames (3, 6, 9 and 18 stories). The values of  $A_r$  factor in the elastic and inelastic steel frames were determined. The ratios of elastic to the inelastic  $A_r$  factors were computed and defined as a modification factor  $R_{acc}$ . The study recommended  $R_{acc} = 1.0$  for the bottom half of the frame; while it provided charts to determine the value of  $R_{acc}$  at the roof level corresponding to the first and second building period as shown in Figures 1.9 and 1.10, respectively. We can note that the reduction in the component acceleration at the first mode is larger than that at the second one. In addition, the reduction in the component acceleration at the first mode is weakly dependant on the building height in opposite to reduction at the second mode, which tends to increase with  $T_{1Bldg}$ . The proposed functions in this study take into

account the location of the component in the building, the damping ratio of the component, the modal periods, and base shear strength of the frame structure,  $RI$ . However, the study is limited to the special moment resisting steel frames.

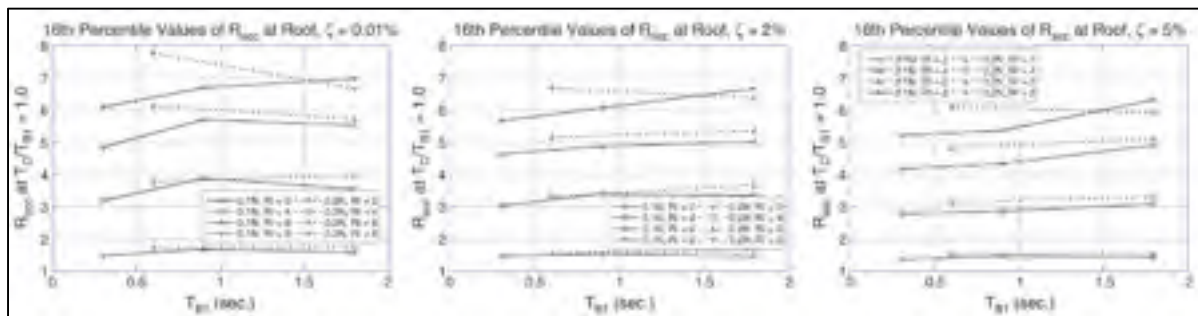


Figure 1.9  $R_{acc}$  values at roof level for various component damping ratios at the 1<sup>st</sup> period  
Taken from Medina et al. (2006)

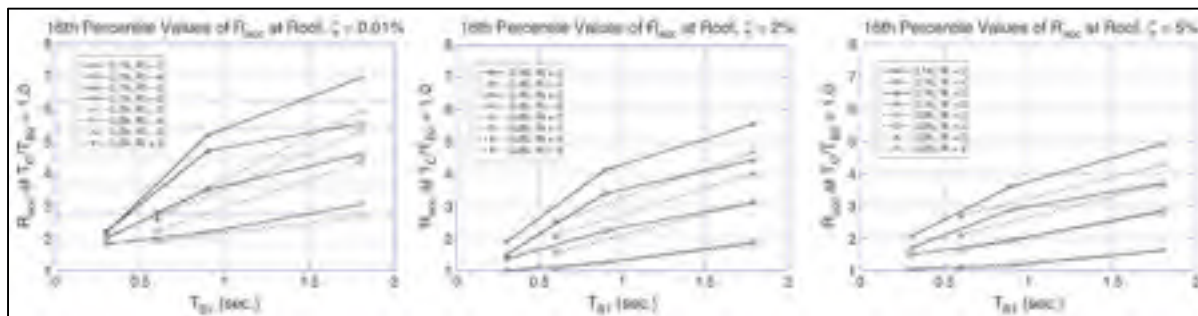


Figure 1.10  $R_{acc}$  values at roof level for various component damping ratios at the 2<sup>nd</sup> period  
Taken from Medina et al. (2006)

Shooshtari et al. (2010) performed nonlinear dynamic analysis on twelve RC buildings consisting of 5, 10, and 15 storey heights. Both moment resisting frame and shear walls structural systems were considered as lateral force resisting systems. Consequently, three moment resisting frame buildings and three shear wall buildings (5, 10, and 15 stories) were considered in Vancouver and Ottawa, separately. The buildings in Vancouver were designed to be ductile while they were designed to be moderately ductile in Ottawa. The mean FRS were generated at the roof level for the buildings and consequently the Equation 1.12 was proposed to generate the roof design spectrum for NSCs mounted on RC buildings in Canada. The

proposed equation was derived based on the nonlinear response of the supporting structure and considers the effect of the fundamental period of the supporting structure, structure location, and the lateral force resisting system type. However, this method is limited to the ductile buildings in western Canada and moderately ductile buildings in eastern Canada.

$$FRS(T) = (5.0 - 0.5T_{aBldg1})S(T_{aBldg1}) \leq BS(0.2) \text{ for } T_s \prec T \leq 2.0s \quad (1.12)$$

Where  $S(T_{aBldg1})$  is the UHS value specified by NBC at  $T_{aBldg1}$ .  $B$  is a coefficient to consider the type of the lateral force resisting systems. The value of the lower limit of period,  $T_s$  is determined based on the building location (Vancouver or Ottawa).

Wieser et al. (2011) performed incremental dynamic analysis on four special moment steel frame buildings (3, 9, 20 stories office building, and 3 stories hospital building). Based on the results of the incremental dynamic analysis, this study proposed amplification functions to compute the ratio (FRS/GRS) as shown in Equation 1.13, where GRS is the ground response spectra. This method is limited to the special moment resisting steel frames.

Fathali and Lizundia (2011) proposed functions shown in Equation 1.14 to determine the component amplification factor ( $A_r$ ) based on a recorded data in instrumented buildings. Where  $m_1$ ,  $m_r$ , and  $A_{rmax}$  are coefficients defined based on  $T_{Bldg1}$  and given in Table 1.7.

$$FRS / GRS = \begin{cases} 1 + \frac{2.5 - T_{Bldg1}}{T_{Bldg1}} \frac{h_x}{h_n} & \text{for } T_p / T_{Bldg1} = 0 \\ 2.0 & \text{if } T_{1Bldg} \prec 1.3s \text{ for } 0.2 \leq T_p / T_{Bldg1} \leq 0.5 \\ 3.0 & \text{if } T_{1Bldg} \succ 1.3s \text{ for } 0.2 \leq T_p / T_{Bldg1} \leq 0.5 \\ 1 + 6.5 \frac{h_x}{h_n} & \text{for } 0.9 \leq T_p / T_{Bldg1} \leq 1.1 \\ 2.5 \sqrt{\frac{h_x}{h_n}} & \text{for } T_p / T_{Bldg1} \succ 2.0 \end{cases} \quad (1.13)$$

$$A_r = \begin{cases} 1.0 & \text{for } T_p = 0 \\ A_{r \max} & \text{for } m_1 T_{Bldg1} \prec T_p \prec m_r \cdot T_{Bldg1} \\ A_{r \max} \frac{m_r \cdot T_{Bldg1}}{T_p} & \text{for } T_p \succ m_r \cdot T_{Bldg1} \end{cases} \quad (1.14)$$

Table 1.7 Values of  $m_1$ ,  $m_r$ , and  $A_{r \max}$   
Taken from Fathali and Lizundia (2011)

	$m_1$	$m_r$	$A_{r \max}$
$T_{Bldg1} < 0.5 \text{ s}$	0.9	1.2	2.5
$0.5 \text{ s} < T_{Bldg1} < 1.5 \text{ s}$	0.3	0.8	2.1
$T_{Bldg1} > 1.5 \text{ s}$	0.1	0.3	2.1

Petrone et al. (2015) performed linear and nonlinear analysis for five ductile RC moment resisting frame buildings (1, 2, 3, 5 and 10 stories). This study proposed a simplified method to generate FRS shown in Equation 1.15. The proposed FRS in this method consists of three branches. The 1<sup>st</sup> and 3<sup>rd</sup> branch depends on Equation 1.3 with a slight modification while the 2<sup>nd</sup> branch is flat in order to consider the peaks of FRS at  $T_{Bldgi}$ . The modifications consist of: 1) propose new parameters  $a$  and  $b$  determined from Table 1.8 to ensure a good matching between the proposed floor spectra and the one obtained from analysis, and 2) the value of  $A_r$  factor is determined from Table 1.8 based on the  $T_{Bldg1}$ .

Since this method proposed based on matching the FRS data obtained from the nonlinear dynamic analysis, the method is limited to the ductile RC frames and ignores the other levels of ductility.

$$FRS(T_p) = \begin{cases} \alpha.S.g.(1 + h_x / h_n) \cdot \left[ \frac{A_r}{1 + (A_r - 1)((1 - T_p)/(a.T_{Bldg1}))^2} \right] \geq \alpha.S.g \text{ for } T_p < a.T_{Bldg1} \\ \alpha.S.g.(1 + h_x / h_n) \cdot A_r & \text{for } a.T_{Bldg1} < T_p < b.T_{Bldg1} \\ \alpha.S.g.(1 + h_x / h_n) \cdot \left[ \frac{A_r}{1 + (A_r - 1)((1 - T_p)/(b.T_{Bldg1}))^2} \right] \geq \alpha.S.g \text{ for } T_p > b.T_{Bldg1} \end{cases} \quad (1.15)$$

Table 1.8 Values of a, b and  $A_r$  for different ranges of structural periods  
Taken from Petrone et al. (2015)

	<b>a</b>	<b>b</b>	<b><math>A_r</math></b>
<b><math>T_{Bldg1} &lt; 0.5 \text{ s}</math></b>	0.8	1.4	5.0
<b><math>0.5 \text{ s} &lt; T_{Bldg1} &lt; 1.0 \text{ s}</math></b>	0.3	1.2	4.0
<b><math>T_{Bldg1} &gt; 1.0 \text{ s}</math></b>	0.3	1.0	2.5

Surana et al. (2016) performed incremental dynamic analysis on RC special moment resisting frame building at four different heights (2, 4, 8, and 12 stories). Based on the results obtained from the nonlinear analysis, the amplification functions  $A(T_p)$  to generate the floor spectrum at any level by amplifying the ground response spectrum (GRS) were proposed as presented in Equation 1.16. The proposed amplification functions consider the relative height, building period and inelasticity. However, the different levels of building ductility were carried out by applying the input ground motion at different intensities on the same RC moment resisting frame design.

$$A(T_p) = \begin{cases} \frac{C_1}{1 + \left( \frac{T_{Bldg2}}{T_{Bldg1}} - \frac{T_p}{T_{Bldg1}} \right)^2} - C_2 & \text{for } 0.0 < T_p / T_{Bldg1} < 0.5 \\ \frac{C_3}{1 + \left( 1 - \frac{T_p}{T_{Bldg1}} \right)^2} - C_4 & \text{for } 0.5 < T_p / T_{Bldg1} < T_L \\ 1 + 2 \frac{h_x}{h_n} & \text{for } T_p / T_{Bldg1} > T_L \end{cases} \quad (1.16)$$

Where  $C_1$ ,  $C_2$ ,  $C_3$ , and  $C_4$  are constants that can be obtained using the known values of the amplification function  $A(T_p)$  at specific values of period,  $T_p$  (i.e. at  $T_p = 0$ ,  $T_{Bldg2}$ ,  $0.5T_{Bldg1}$ , and  $T_{Bldg1}$ ).

#### 1.4.2.2 Proposed simplified methods based on pushover analysis

Floor response spectra that consider a structure nonlinearity may be developed using nonlinear time history analysis of the structure. However, nonlinear analysis is deemed complicated, time-consuming and along with lack of clear guidance. In order to avoid conducting nonlinear dynamic analysis, Jha et al. (2017) and later Kothari et al. (2017) proposed simplified methods to generate FRS using pushover analysis. The simplified method of Kothari et al. (2017) is a point of interest in this project since it is the most recent. Therefore, a detailed explanation of this method is shown in Figure 1.11 and presented as follow.

The simplified method of Kothari et al. (2017) is an experimental method derived for a 3 stories conventional RC frame building. Linear time history of an equivalent linear structural model was carried out to obtain the floor time histories which are then converted to FRS. The equivalent linear model accounts for the stiffness degradation and equivalent damping that result from the nonlinear behavior of the structure at a predefined performance level.

The equivalent stiffness at a performance level determined from the idealized relationship as per FEMA 356 (2000) at the value of the roof displacement at the desired performance level. The idealized relationship is bilinear, with initial effective slope  $k_e$  and post-yield slope  $\alpha$ . Line segments of this relationship is located using an iterative graphical procedure that approximately balances the area above and below the pushover curve. According to FEMA 356 (2000),  $k_e$  is taken as the secant stiffness calculated at a base shear force equal to 60% of the effective yield strength of the structure. The roof displacement at a desired performance level is computed based on the allowable drift value at each performance level provided in. When the global stiffness reduction of the structure is defined, it is distributed to column



elements with ratios depending on the hinge formation status in each column given by the pushover analysis at a predefined performance level.

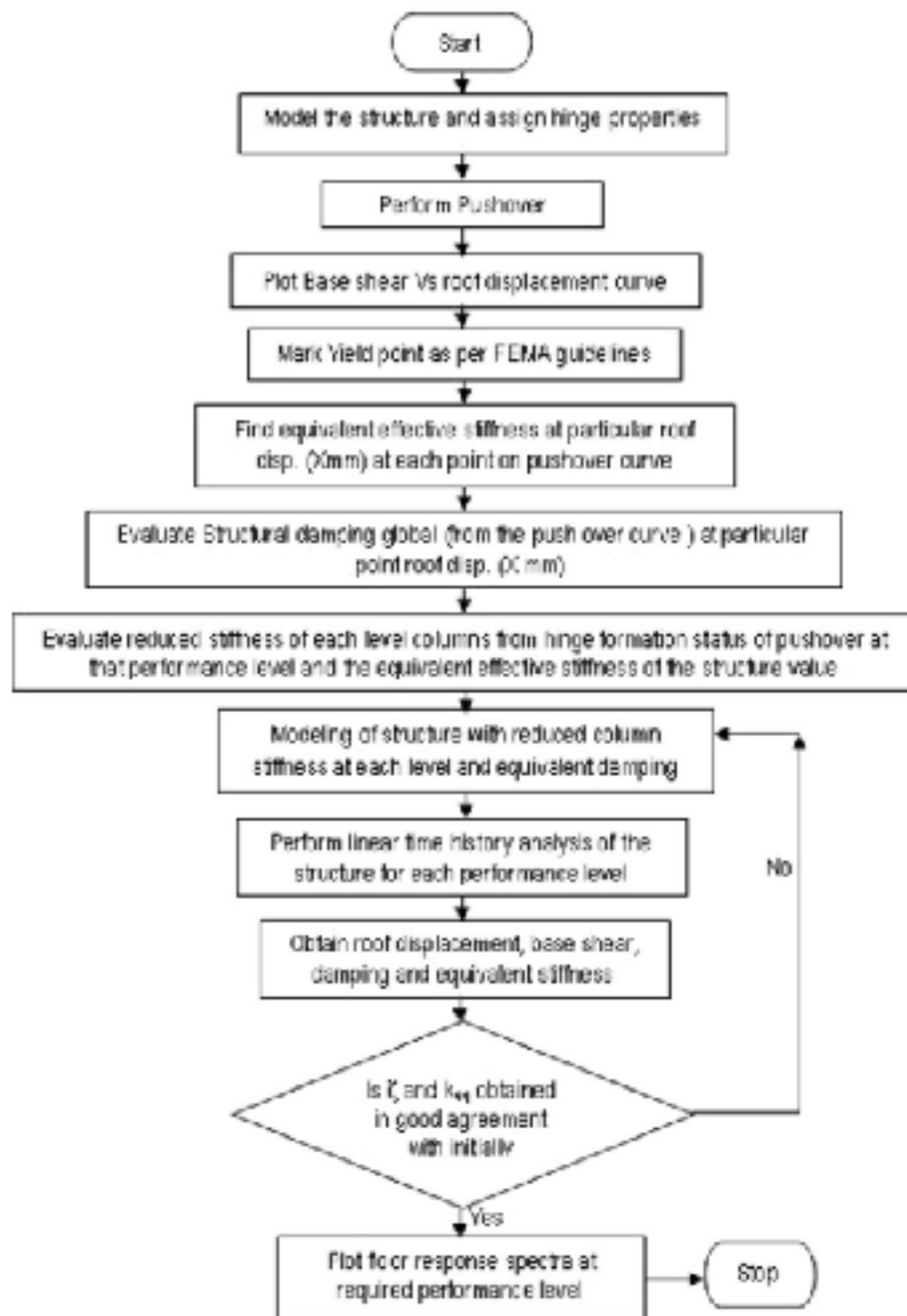


Figure 1.11 Flowchart for the simplified method  
Taken from Kothari et al. (2017)

The equivalent damping  $\zeta_{eq}$  considered in the equivalent linear model is divided into two parts as given in Equation 1.11.

$$\zeta_{eq} = \zeta_0 + \zeta_{hys} \quad (1.17)$$

Where  $\zeta_0$  is the structural damping, usually considered equal to 5% in concrete structures, and  $\zeta_{hys}$  is the hysteretic damping that represents the energy dissipation due to nonlinear hysteretic behavior of the structure.  $\zeta_{hys}$  was evaluated using Sucuoğlu and Erberik (2004) model, which accounts for stiffness and strength degrading and given by Equation 1.18 as follows:

$$\zeta_{hys} = \frac{1}{4\pi} [3.0(\mu - 1) / \mu] \quad (1.18)$$

Where  $\mu$ , is the displacement ductility obtained from the pushover curve by dividing the displacement at a pre-selected performance level  $\Delta_{PerformanceLevel}$ , by the yield displacement  $\Delta_y$ . This study showed also that the equivalent damping calculated by Equation 1.18 is in close agreement with that given by Priestley (2003) and presented in Equation 1.19 as follows:

$$\zeta_{hys} = \frac{120}{\pi} (1 - 1/\sqrt{\mu}) \quad (1.19)$$

After defining the equivalent stiffness and damping, linear time history analysis is performed for the equivalent linear model. The initial values of equivalent stiffness and damping are determined from the pushover curve. The maximum roof displacement and the base shear obtained from linear time history analysis is used to evaluate the equivalent stiffness and damping in the first iteration. If the evaluated equivalent stiffness is equal to previously considered stiffness from pushover analysis, then used equivalent stiffness and damping values are considered as final. If not, then the equivalent stiffness and damping values resulting from

time history analysis are considered as new values and the iterations are repeated till reaching convergence.

## 1.5 Summary

This chapter provided a brief summary about NSCs classification and their seismic performance in past seismic events, followed by an overview of the codes equations for determining the seismic demands on NSCs. These equations assume that the supporting structure is elastic and ignore its ductility. In general, codes overestimate the values of  $A_x$  factor and underestimate the values of  $A_r$  factor, which explains why NIST GCR 18-917-43 and several other studies proposed lower values to  $A_x$  factor and higher values to  $A_r$  factor.

In addition to the codes approaches, this chapter presented the proposed methods in previous studies to include the effect of building ductility in computing the NSCs seismic demands. In general, the proposed solutions to consider the supporting structure nonlinearity can be divided into two groups: the first group of studies considered different values of  $R_d$  (Surana et al., 2016; Wieser et al., 2013) regardless of the reinforcement detailing corresponding to each value of  $R_d$  although this factor  $R_d$  reflects the capability of a structure to dissipate energy through inelastic behavior (Mitchell et al., 2003). The factor  $R_d$  includes several parameters such as structure ductility, energy absorption, the ability to sustain load and stiffness under reversed cyclic loading. Therefore, this factor must be used only in conjunction with specific reinforcement detailing and the corresponding ground motion design level (Mitchell et al., 2003).

On the other hand, the second group of studies (Petrone et al., 2015; Shooshtari et al., 2010) considered the reinforcement detailing and the failure modes corresponding to  $R_d$  value. However, they included just one level of ductility in their studies. Therefore, the current study will follow this group of studies, but with extension to different ductility levels stated by NBC 2015.

Therefore, the next chapter presents the design of a selected frame building at four levels of ductility taking into account the reinforcement detailing that corresponds to each level of ductility in accordance with CSA A23.3 (2014a).



## **CHAPITRE 2**

### **SEISMIC DESIGN OF REINFORCED CONCRETE MOMENT RESISTING FRAMES**

#### **2.1 Introduction**

The detailed design of studied reinforced concrete moment resisting frames buildings are presented in this chapter. The considered 6-story building model used in this project has a common regular building configuration (Cement Association of Canada, 2006). In this study, this building model is designed in accordance with NBC (2015) and CSA A23.3 (2014a) for four case studies: Ductile and conventional construction moment resisting frame buildings assumed to be located in Vancouver, and moderately ductile and conventional construction moment resisting frame buildings assumed to be located in Montreal.

The seismic design process of frames includes performing modal analysis by SAP 2000® (CSI, 2019) to determine the fundamental period of each frame model. The frames are considered bare without any participation from nonstructural components (masonry enclosures or partition walls).

Three dimensional structural models were created by SAP 2000® in order to consider the effect of accidental torsion in the determination of the frames internal forces. Also, the exterior and interior frame sections were kept similar for the sake of simplicity and the analyses were conducted in the short direction of plan. Then, the seismic loads were calculated by using the Equivalent Static Force Procedure (ESFP) on the basis of the seismic design provisions of NBC 2015. All buildings were assumed to be located on firm soil (Class “C” in NBC 2015) with a normal importance category.

## 2.2 Description of building

Figures 2.1 and 2.2 show the plan and elevation views of the considered building model. The building has seven 6.0 m bays in the N-S direction and three bays in E-W direction, two 9.0 m office bays and a central 6.0 m corridor bay. The story height is 3.65 m. The preliminary dimensions of interior columns are all 500 x 500 mm while the exterior columns are 450 x 450 mm. The beams of both the N-S and E-W frames are 400 mm wide x 600 mm deep for the first three stories and 400 x 550 mm for the top three storeys. The yield stress for longitudinal and transverse reinforcing steel,  $f_y$  and  $f_{yt}$ , is equal to 400 MPa. The compressive strength of concrete at 28 day,  $f_c'$  is equal to 30 MPa. The gravity loads used in the design are presented in Table 2.1.

Table 2.1 The values of gravity loads used in the design

Dead Load (kN/m <sup>2</sup> )		Live Load (kN/m <sup>2</sup> )		Roof Load (kN/m <sup>2</sup> )	
Type	Value	Type	Value	Type	Value
Self weight (kN/m <sup>3</sup> )	24.0	Office floor	2.4	Snow	2.2
Partition	1.0	Corridor bay	4.8	Mechanical service	1.6
Mechanical service	0.5				
Roofing	0.5				

## 2.3 Load combinations

The load combinations stated by NBC 2015 and used in this project to design the frame buildings are illustrated in Table 2.2. Where D, L, S and E are the actions resulting from dead, live, snow and earthquake with accidental torsion loads, respectively. Other combinations are stated by NBC 2015, but not considered in this project.

Table 2.2 Load combinations considered for seismic design of building as per NBC

$1.25 D + 1.5 L + 1.0 S$	(2.1)
$1.0 D + 1.0 E$	(2.2)
$1.0 D - 1.0 E$	(2.3)
$1.0 D + 0.5 L + 1.0 E + 0.25 S$	(2.4)
$1.0 D + 0.5 L - 1.0 E + 0.25 S$	(2.5)

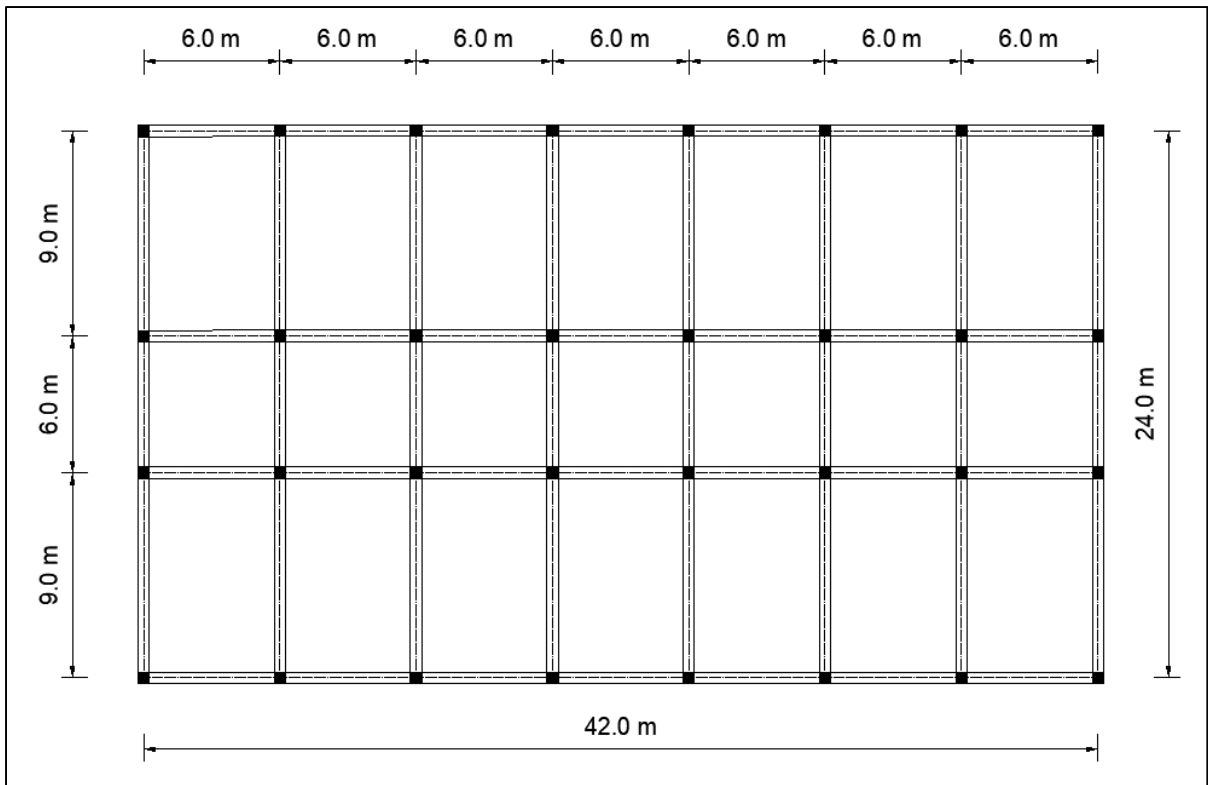


Figure 2.1 Plan view of RC moment resisting frame building model

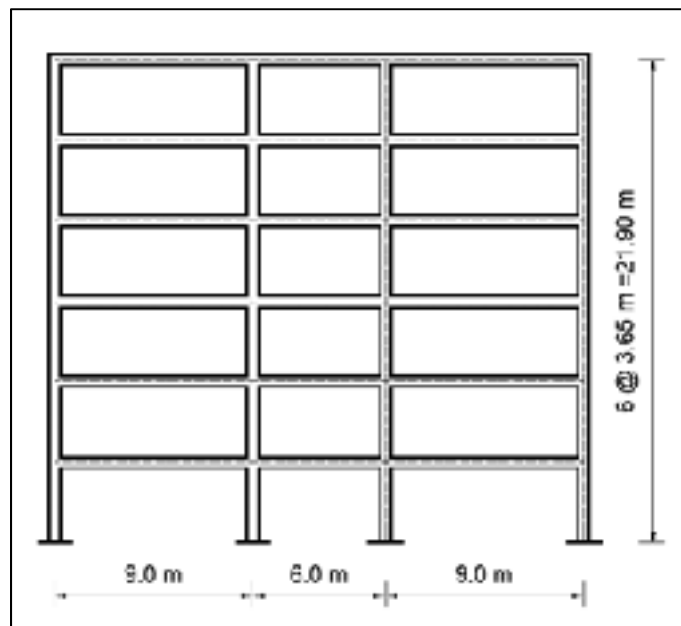


Figure 2.2 Elevation view of the RC moment resisting frame building model

## 2.4 Seismic design considerations

The standard CSA A23.3-14 (2014a) defines three types of flexural resistance: probable, nominal, and factored in order to ensure the hierarchy of strength of different members in the seismic design process of ductile and moderately ductile structures. Table 2.3 shows the types of flexural resistance and the relationship between them as suggested by CSA A23.3-14 (2014a) and used in designing the buildings.

Table 2.3 Types of flexural resistance and their relationship as per CSA A23.3

Type of flexural resistance	Approximate relationships
Factored resistance, $M_r$	-
Nominal resistance, $M_n$	$M_n = 1.2 M_r$
Probable resistance, $M_p$	$M_p = 1.47 M_r$

## 2.5 Modal Analysis

Modal analysis has been performed for a three dimensional model of each case study using the software SAP2000® (CSI, 2019).

Figure 2.3 shows a typical three dimensional model of the selected building in this project. Two materials were defined. The first material is concrete. The weight per unit volume was considered zero in order to avoid considering the self-weight two times. The modulus of elasticity of concrete  $E_c$ , is calculated as  $4500\sqrt{f'_c}$  as per CSA A23.3 (2014a), which equals 24648 MPa. The second defined material is the reinforcing steel. The modulus of elasticity of steel  $E_s$ , is considered equal to 200.0 GPa.

The columns of the buildings are all fixed at the bottom. In each floor, a diaphragm constrain was defined. The seismic mass of each floor (see Tables 2.8 and 2.9) was assigned to the floor diaphragm as shown in Figure 2.4. In order to consider the cracking, sections moment inertia were assumed to be 0.4, 0.6, and 0.7 of the gross moment inertia for all beams, columns in the top three storeys, and columns in the bottom three storeys, respectively as required by CSA



A23.3-14 (2014a). End length offset were considered with a rigid zone factor 0.5 which is the recommended value for RC frames (CSI, 2011). Table 2.4 presents the first three modal periods of all case study buildings. The fundamental period used in seismic design does not exceed 1.5 times the empirical period for RC frame buildings proposed in NBC 2015 (see Equation 1.10) that is equal to:  $1.5 (0.075h_n^{0.75}) = 1.14$  s as shown in Table 2.4.

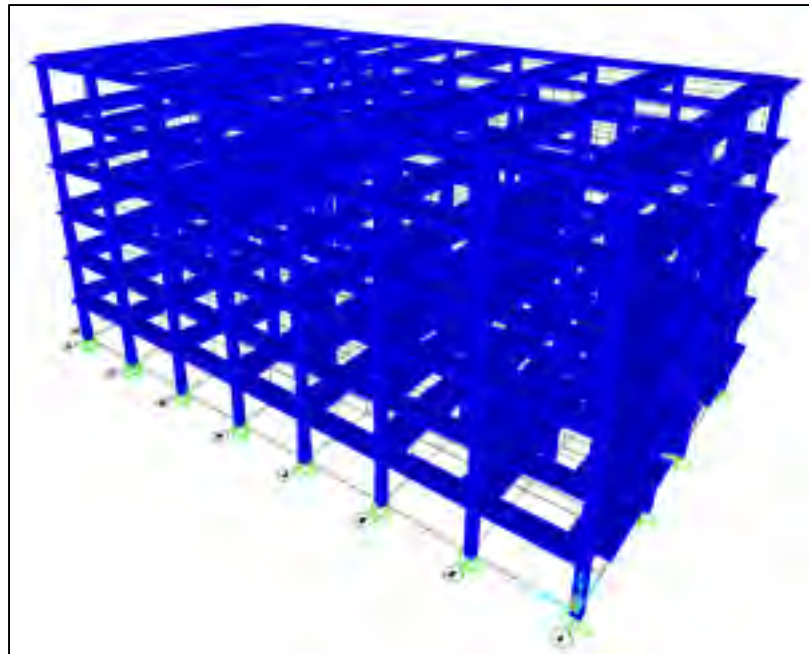


Figure 2.3 Three dimensional model of a case study building created by SAP2000®

Table 2.4 Modal periods, NBC 2015 limit, and the considered period in the seismic design

Case of study building	$T_{Bldg1}$	$T_{Bldg2}$	$T_{Bldg3}$	$1.5T_a$	$T_{considered}$
Ductile in Vancouver (D)	1.656	0.550	0.295	1.14	1.14
Conventional in Vancouver (CC)	1.010	0.315	0.160	1.14	1.01
Moderately ductile in Montreal (MD)	1.507	0.481	0.242	1.14	1.14
Conventional in Montreal (CC)	1.142	0.381	0.209	1.14	1.14

Unit is in second

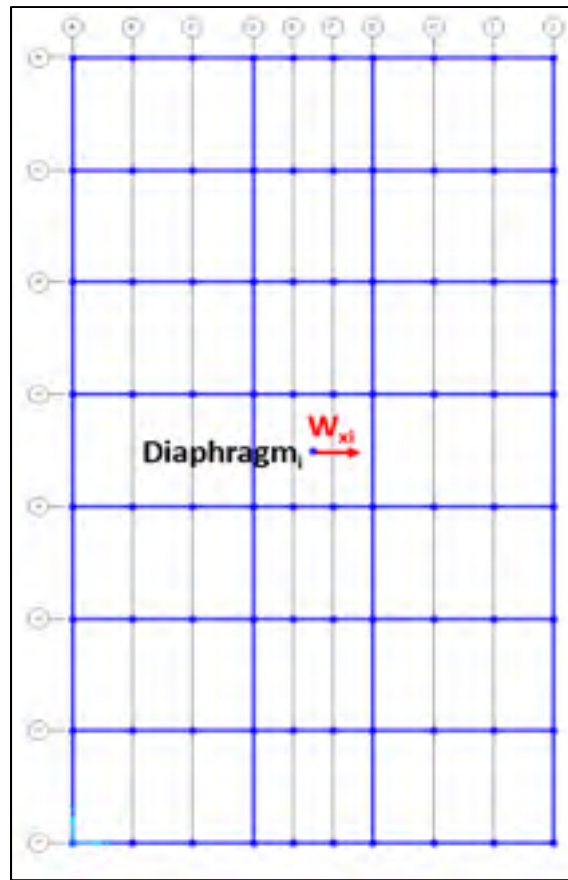


Figure 2.4 Assigning the floor seismic mass as a weight in the floor diaphragm of the SAP2000® model

## 2.6 Determination of seismic design forces

### 2.6.1 Gravity loads

In order to determine the internal forces (axial loads, shear loads, and bending moments) in the members, the studied buildings were analysed using SAP2000®. The loads applied to the ductile frame model in Vancouver and the moderately ductile frame model in Montreal are illustrated in Figure 2.5, where the loads applied to the conventional construction frame models in Vancouver and Montreal are presented in Figure 2.6.

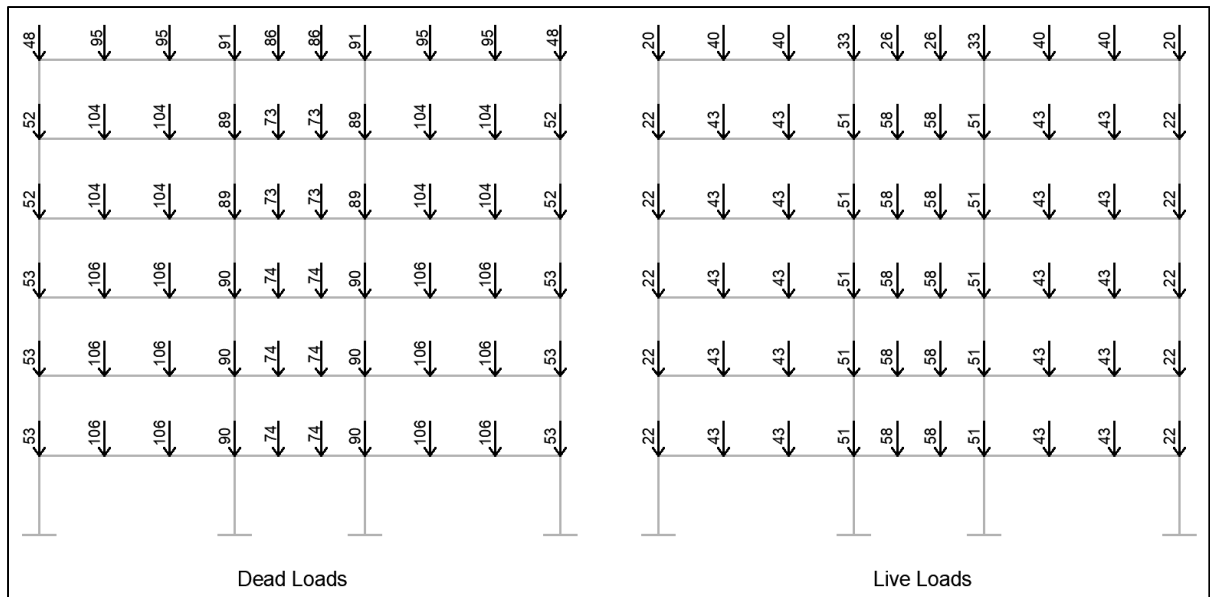


Figure 2.5 Unfactored gravity loads considered to design a typical interior ductile frame in Vancouver and moderately ductile frame in Montreal. Values include only the self-weight of beams (Unit is kN)

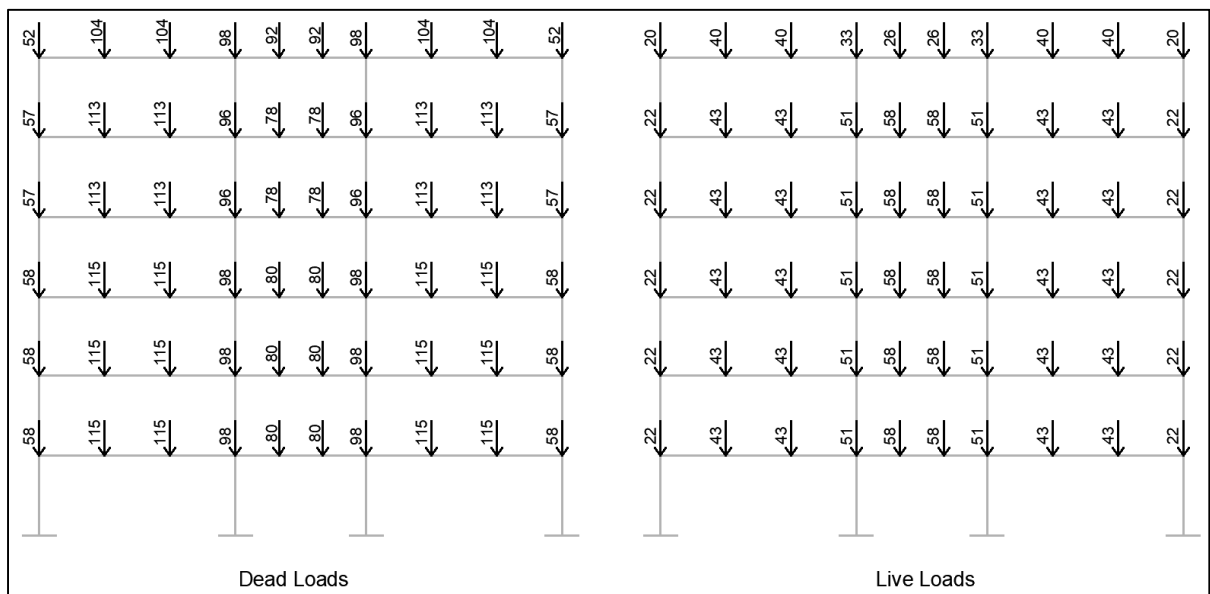


Figure 2.6 Unfactored gravity loads considered in design of typical interior conventional constructed frame in Vancouver and Montreal. Values include only the self-weight of beams (Unit is kN)

### 2.6.2 Seismic base shear forces

The design base shear force is obtained by Equation 2.6 as given in NBC 2015. The design base shear force should not exceed the limit given by Equation 2.7, or considered less than the limit given by Equation 2.8.

$$V = \frac{S(T)M_v I_E W}{R_d R_o} \quad (2.6)$$

$$V_{\max} = \frac{2}{3} \frac{S(0.2) I_E W}{R_d R_o} \quad (2.7)$$

$$V_{\min} = \frac{S(2.0)M_v I_E W}{R_d R_o} \quad (2.8)$$

Where  $R_d$  is the ductility related force modification factor, and  $R_o$  is the overstrength related force modification factor (see Table 2.5).  $I_E$  is the building importance factor, and it is considered 1.0 for normal importance category.  $W$  is the seismic weight of building that equals the dead load plus 25% of the snow load.  $M_v$  is a factor that accounts for higher modes effect on the base shear force (see Table 2.4).

Figure 2.7 presents the UHS given by NBC 2015 in Vancouver and Montreal with probability of exceedance 2% per 50 years. The spectral acceleration at periods 0.05, 0.1, 0.2, 0.3, 0.5, 1.0, 2.0, 5.0, and 10.0 s are obtained from the website of Natural Resource of Canada (Natural Resources Canada, 2018) by providing the latitude and longitude of Vancouver and Montreal.

The base shear force was distributed along the buildings height using Equation 2.9, where  $F_t$  is a concentrated force applied at the top of the building and given by Equation 2.10,  $W_x$  is the seismic weight of floor  $x$ , and  $h_x$  is the height of level  $x$  relative to the ground level. Table 2.7 presents the calculations of base shear force for all case of study buildings and the values of factors used in these calculations.

The accidental torsion is calculated by applying the lateral forces  $F_x$  (see Equation 2.9) at an accidental eccentricity of  $\pm 0.1D_{nx}$ , where  $D_{nx}$  is the plan dimension of the building perpendicular to the direction of seismic loading. In this project,  $D_{nx}$  equals 42.0 m, which gives accidental eccentricity 4.2 m from the center of mass. The calculations of the seismic lateral forces  $F_x$  and torques  $T_x$  at each floor level are presented in Tables 2.8 and 2.9 for studied buildings in Vancouver and Montreal, respectively.

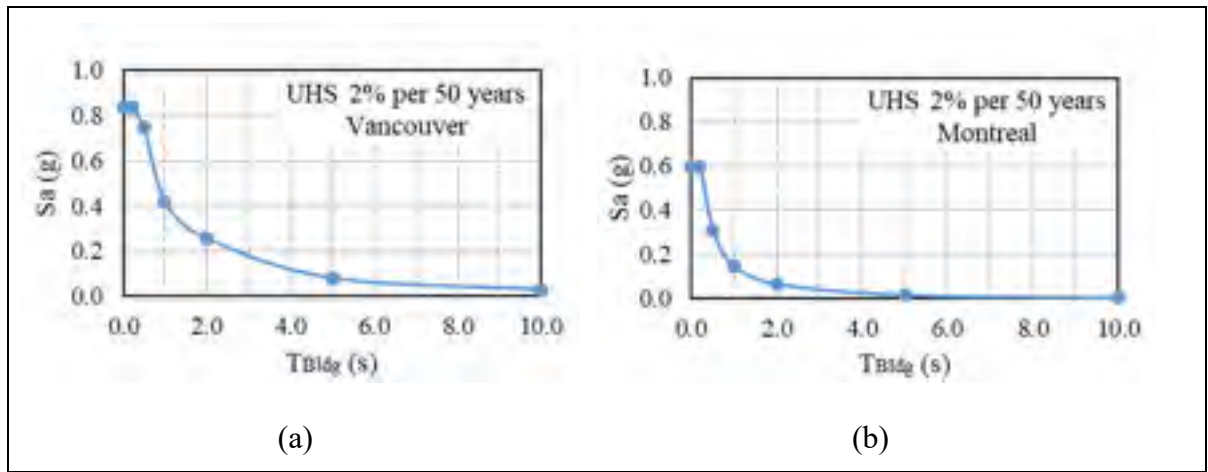


Figure 2.7 UHS with a probabilities of exceedance 2% per 50 years  
(a) Vancouver, and (b) Montreal

Table 2.5 Force modification factors in concrete structures as per NBC 2015

LFRS is RC Moment-resisting frames	$R_d$	$R_o$	Restrictions on Structure Height				
			$I_E F_a S_a(0.2)$				$I_E F_a S_a(1.0)$
			< 0.2	$\geq 0.2$ to < 0.35	$\geq 0.35$ to $\leq 0.75$	> 0.75	> 0.3
Ductile	4.0	1.7	NL	NL	NL	NL	NL
Moderately ductile	2.5	1.4	NL	NL	60	40	40
Conventional construction	1.5	1.3	NL	NL	20	15	10

$$F_x = (V - F_t) \frac{W_x h_x}{\sum_{i=1}^n W_i h_i} \quad (2.9)$$

$$F_t = \begin{cases} 0.07TV \leq 0.25V & \text{for } T > 0.7s \\ 0 & \text{for } T \leq 0.7s \end{cases} \quad (2.10)$$

Table 2.6 Factors  $M_v$  for moment resisting frames as per NBC 2015

<b>S(0.2)/S(5.0)</b>	<b>T ≤ 0.5</b>	<b>T = 1.0</b>	<b>T = 2.0</b>	<b>T ≥ 5.0</b>
5	1.00	1.00	1.00	1.00
20	1.00	1.00	1.00	1.00
40	1.00	1.00	1.00	1.00
65	1.00	1.00	1.00	1.03

Table 2.7 Base shear force calculations for case of studied buildings

<b>Model</b>	<b>S(T)</b>	<b>R<sub>d</sub></b>	<b>R<sub>o</sub></b>	<b>W<sub>total</sub></b>	<b>V</b>	<b>V<sub>min</sub></b>	<b>V<sub>max</sub></b>	<b>F<sub>t</sub></b>	<b>F<sub>t max</sub></b>
D Vancouver	0.397	4.0	1.7	44021.6	2570.6	1650.8	3616.7	204.9	642.6
CC Vancouver	0.532	1.5	1.3	52015.0	14192.4	6802.0	14902.1	822.2	3548.
MD Montreal	0.137	2.4	1.4	45235.8	1769.2	878.9	5126.7	141.0	442.3
CC Montreal	0.156	1.5	1.3	47448.0	3784.4	1654.6	9651.7	258.7	946.1

Forces unit is kN, and accelerations unit is (g)

Table 2.8 Lateral loads for each floor level for buildings in Vancouver

Floor	$h_x$	Ductile Building				Conventional Building			
		$W_x$	$F_x$	$V_x$	$T_x$	$W_x$	$F_x$	$V_x$	$T_x$
6	21.90	7488.6	689.0	0.0	2894.0	8383.0	3717.0	0.0	15612.0
5	18.25	7251.3	556.0	689.0	2335.0	8671.0	3204.0	3717.0	13457.0
4	14.60	7251.3	445.0	1245.0	1868.0	8671.0	2563.0	6921.0	10766.0
3	10.95	7343.5	338.0	1690.0	1419.0	8763.0	1943.0	9484.0	8160.0
2	7.30	7343.5	225.0	2028.0	946.0	8763.0	1295.0	11427.0	5440.0
1	3.65	7343.5	113.0	2253.0	473.0	8763.0	648.0	12723.0	2720.0
0	0.00	-	-	2366.0	-	-	-	13370.0	-

Units are in kN, m

Table 2.9 Lateral loads for each floor level for buildings in Montreal

Floor	$h_x$	Moderately Ductile Building				Conventional Building			
		$W_x$	$F_x$	$V_x$	$T_x$	$W_x$	$F_x$	$V_x$	$T_x$
6	21.90	7599.0	469.0	0.0	1970.0	7968.0	1016.0	0	4265.0
5	18.25	7472.1	384.0	469.0	1615.0	7841.0	833.0	1016.0	3498.0
4	14.60	7472.1	308.0	854.0	1292.0	7841.0	666.0	1848.0	2798.0
3	10.95	7564.2	234.0	1161.0	981.0	7933.0	506.0	2515.0	2123.0
2	7.30	7564.2	156.0	1395.0	654.0	7933.0	337.0	3020.0	1416.0
1	3.65	7564.2	78.0	1550.0	327.0	7933.0	169.0	3357.0	708.0
0	0.00	-	-	1628.0	-	-	-	3526.0	-

Units are in kN, m

## 2.7 Static Analyses

In order to determine the internal forces required for the seismic design of buildings, static analysis have been done to each case study building under dead loads, live loads, seismic loads, and torques moments. The typical model shown in Figure 2.3 has been used. The dead and live loads have been applied to the frames as shown in Figures 2.5 and 2.6. In addition, the self-weights of the columns were added as distributed forces along the columns. The forces  $F_{xi}$  and torques  $T_{xi}$  were applied to the floor diaphragms. The analyses cases are defined according to Table 2.2 and the internal forces and moments obtained from the analysis are considered in the design.

## 2.8 Seismic design

Four Excel sheets have been created to design the studied frames as per the requirements of CSA A23.3-14. The Excel sheets include the seismic design details of the ductile, moderately ductile, two conventional construction frames in Vancouver, and in Montreal, respectively. The main points considered in designing the ductile, moderately ductile, and conventional construction frames are presented in the following sections along with the final dimensions and reinforcing details of frames members.

### 2.8.1 Design of the ductile frame

The ductile frame in Vancouver is designed according to the items in section 21.3.1 of CSA A23.3 (2014a). The capacity design philosophy was considered in the design, so that the flexural resistance of the columns and the beams shall satisfy Equation 2.11 as follows:

$$\sum M_{nc} \geq \sum M_{pb} \quad (2.11)$$

Where  $\sum M_{nc}$  is the sum of moments corresponding to the nominal resistance (see section 2.4) of the columns framing into the joint.  $\sum M_{pb}$  is the sum of moments corresponding to the probable resistance (see section 2.4) of the beams framing into that joint.

The longitudinal reinforcement in the bottom of beam sections were arranged in the ductile frame so that the positive moment resistance at the face of a joint is not less than one-half of the negative moment resistance provided at that face of the joint as shown in Figure 2.8. In addition, the negative and the positive moment resistance at any section along the member length is not less than one-quarter of the maximum moment resistance provided at the face of end joints (see Figure 2.8).



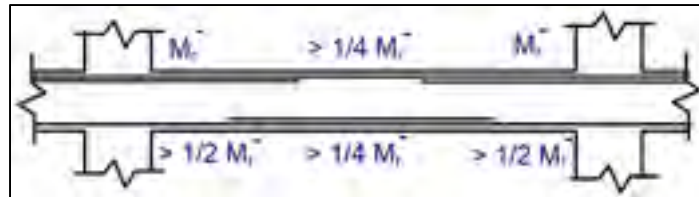

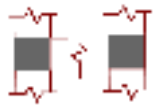



Figure 2.8 Arrangement of longitudinal reinforcement in beams in ductile frames  
Taken from M. Saatcioglu (2004)

The factored shear resistance of the joints in the ductile frame were designed to not exceed the limits shown in Table 2.10 for three types of joints. Where the factor  $\lambda$  that accounts for low-density concrete, is considered equal to 1.0.  $\phi_c$ , a resistance factor for concrete, was considered equal to 0.65 according to CSA A.23.3 (2014a).  $A_j$  is the minimum cross-sectional area within a joint in a plane parallel to the axis of the reinforcement generating the shear in the joint.

The final members' dimensions of ductile frame in Vancouver and the reinforcing details of members sections are illustrated in Figures 2.10 and 2.12, respectively.

Table 2.10 Shear resistance of frame joints at different levels of ductility as per CSA A23.3

<b>Confined joints</b>		Ductile	$V_j = 2.2\lambda\phi_c\sqrt{f'_c}A_j$	(2.12)
		Moderately ductile Conventional construction	$V_j = 1.7\lambda\phi_c\sqrt{f'_c}A_j$	(2.13)
<b>Joints confined on three faces or on two opposite faces</b>		Ductile	$V_j = 1.6\lambda\phi_c\sqrt{f'_c}A_j$	(2.14)
		Moderately ductile Conventional construction	$V_j = 1.2\lambda\phi_c\sqrt{f'_c}A_j$	(2.15)
<b>Other joints</b>		Ductile	$V_j = 1.3\lambda\phi_c\sqrt{f'_c}A_j$	(2.16)
		Moderately ductile Conventional construction	$V_j = 1.0\lambda\phi_c\sqrt{f'_c}A_j$	(2.17)

### 2.8.2 Design of the moderately ductile frame

The moderately ductile frame in Montreal is designed according to the items in section 21.4 in CSA A23.3-14 (2014a). The capacity design philosophy was considered in the design, so that the flexural resistance of the columns and the beams shall satisfy Equation 2.18 as follows:

$$\sum M_{rc} \geq \sum M_{nb} \quad (2.18)$$

Where  $\sum M_{rc}$  is the sum of moments corresponding to the factored resistance (see Section 2.4) of the columns framing into the joint.  $\sum M_{nb}$  is the sum of moments corresponding to the nominal resistance (see Section 2.4) of the beams framing into that joint.

The longitudinal reinforcement in the bottom of beam sections were arranged in the ductile frame so that the positive moment resistance at the face of a joint is not less than one-third of the negative moment resistance provided at that face of the joint as shown in Figure 2.9. In addition, the negative and the positive moment resistance at any section along the member length is not less than one-fifth of the maximum moment resistance provided at the face of end joints (see Figure 2.9).

The factored shear resistance of the joint in the moderately ductile frame were designed not exceed the limits shown in Table 2.10 for the three types of joints. The Final members' dimensions of moderately ductile frame in Montreal and the reinforcing details of members sections are illustrated in Figures 2.11 and 2.14, respectively.

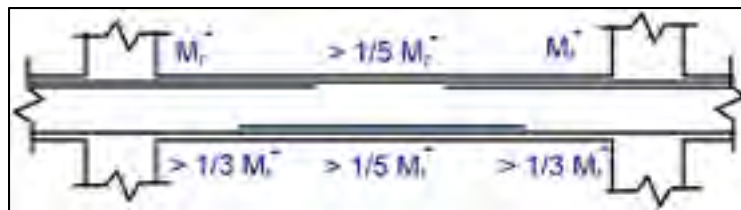


Figure 2.9 Arrangement of longitudinal reinforcement in beams in moderately ductile frames  
Taken from M. Saatcioglu (2004)

### 2.8.3 Design conventional construction frames

The conventional construction frames in Vancouver and Montreal are designed according to the items in section 21.6.2 in CSA A23.3-14 (2014a). The capacity design philosophy was not applied in the design of conventional construction frames, and no restrictions regarding the arrangement of longitudinal reinforcement in beams should be applied. The factored shear resistance of the joints in the conventional construction frames were designed not to exceed the same limits for the joints of the moderately ductile frame as shown in Table 2.10. The final members' dimensions of conventional construction frames in Vancouver and Montreal are illustrated in Figures 2.10 and 2.11, respectively.

400x550				400x550				400x550			
450x450	400x550	500x500	400x550	450x450	400x550	500x500	400x550	450x450	400x550	500x500	400x550
450x450	400x550	500x500	400x550	450x450	400x550	500x500	400x550	450x450	400x550	500x500	400x550
450x450	400x550	500x500	400x550	450x450	400x550	500x500	400x550	450x450	400x550	500x500	400x550
450x450	400x600	500x500	400x600	450x450	400x600	500x500	400x600	450x450	400x600	500x500	400x600
450x450	400x600	500x500	400x600	450x450	400x600	500x500	400x600	450x450	400x600	500x500	400x600
450x450	400x600	500x500	400x600	450x450	400x600	500x500	400x600	450x450	400x600	500x500	400x600
450x450	500x500	500x500	500x500	450x450	500x500	500x500	500x500	450x450	500x500	500x500	500x500
(a)				(b)							
400x750				400x750				400x750			
650x650	400x750	700x700	400x750	650x650	400x750	700x700	400x750	650x650	400x750	700x700	400x750
650x650	400x750	700x700	400x750	650x650	400x750	700x700	400x750	650x650	400x750	700x700	400x750
650x650	400x750	700x700	400x750	650x650	400x750	700x700	400x750	650x650	400x750	700x700	400x750
650x650	400x800	700x700	400x800	650x650	400x800	700x700	400x800	650x650	400x800	700x700	400x800
750x750	400x800	800x800	400x800	750x750	400x800	800x800	400x800	750x750	400x800	800x800	400x800
750x750	400x800	800x800	400x800	750x750	400x800	800x800	400x800	750x750	400x800	800x800	400x800
750x750	800x800	800x800	800x800	750x750	800x800	800x800	800x800	750x750	800x800	800x800	800x800
(a)				(b)							

Figure 2.10 Dimensions of beams and columns for buildings in Vancouver  
(a) Ductile, and (b) conventional constructed

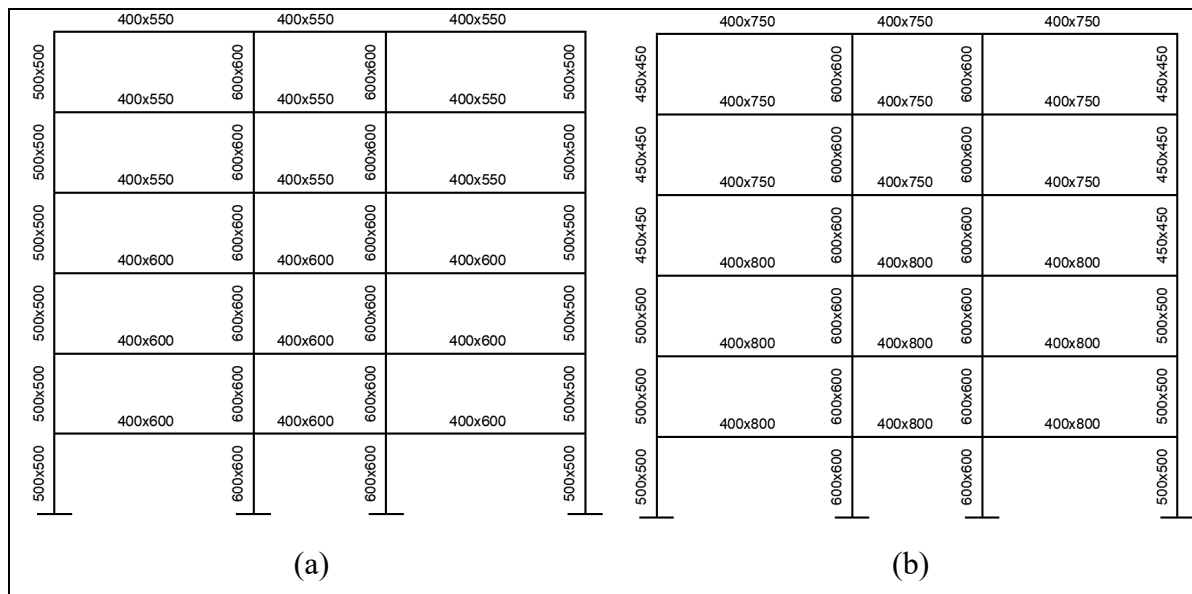


Figure 2.11 Dimensions of beams and columns for buildings in Montreal  
(a) Moderately ductile, and (b) conventional constructed

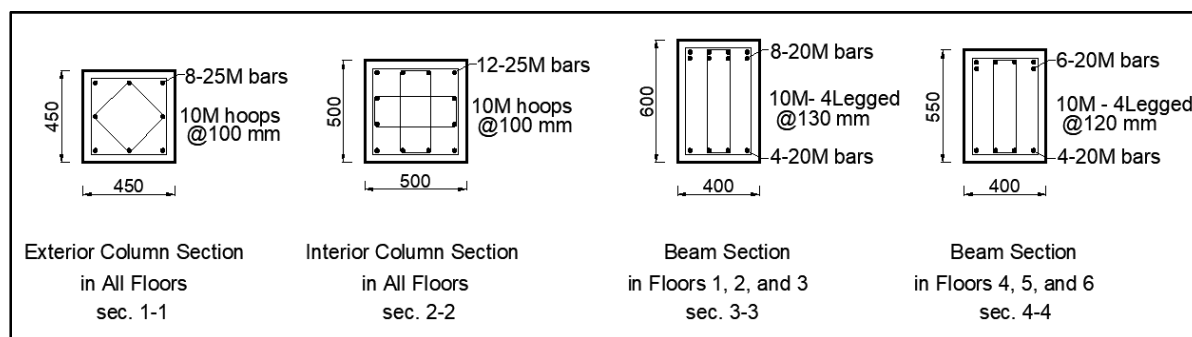


Figure 2.12 Reinforcing details of the ductile frame members in Vancouver

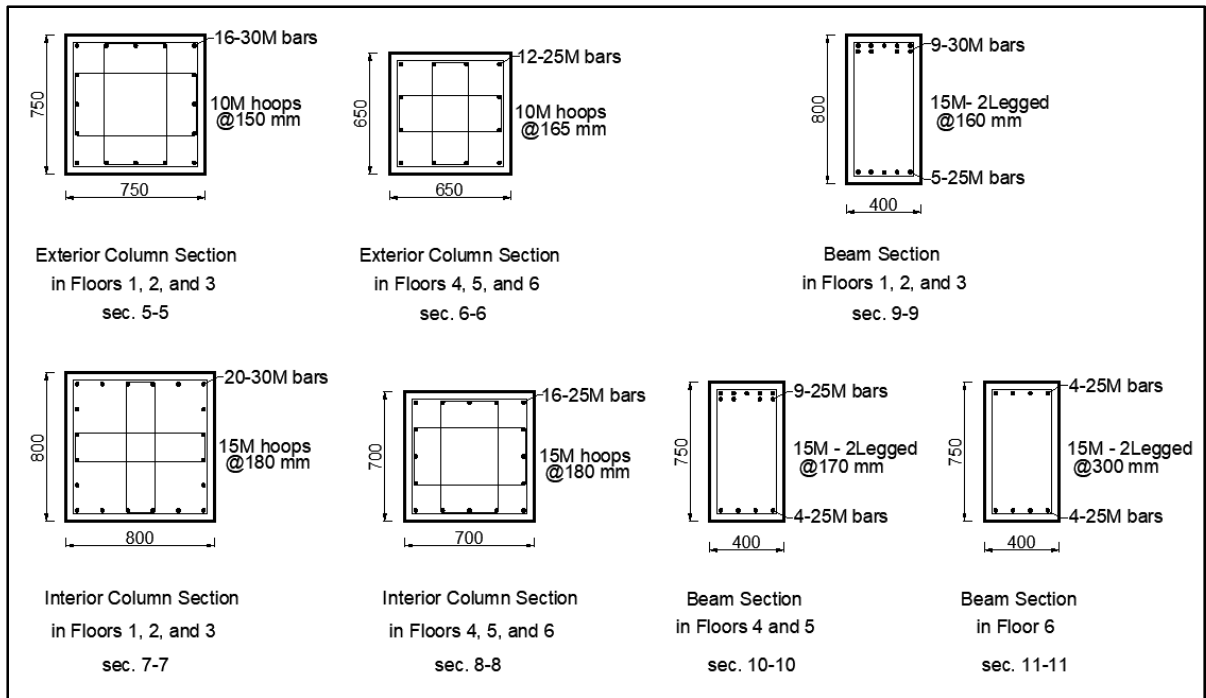


Figure 2.13 Reinforcing details of the conventionally constructed frames in Vancouver

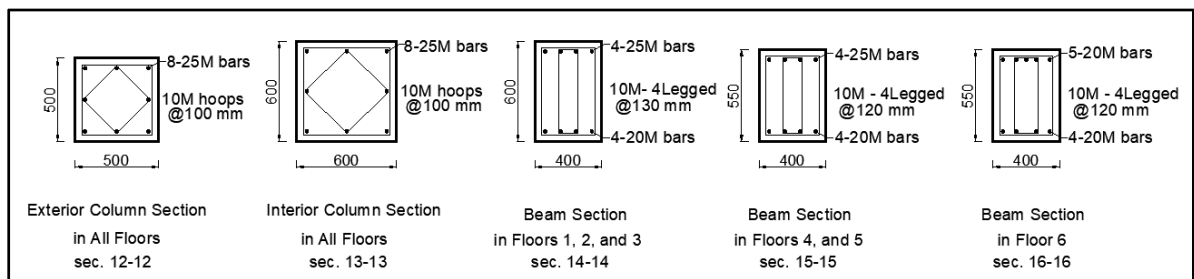


Figure 2.14 Reinforcing details of the moderately ductile frame members in Montreal

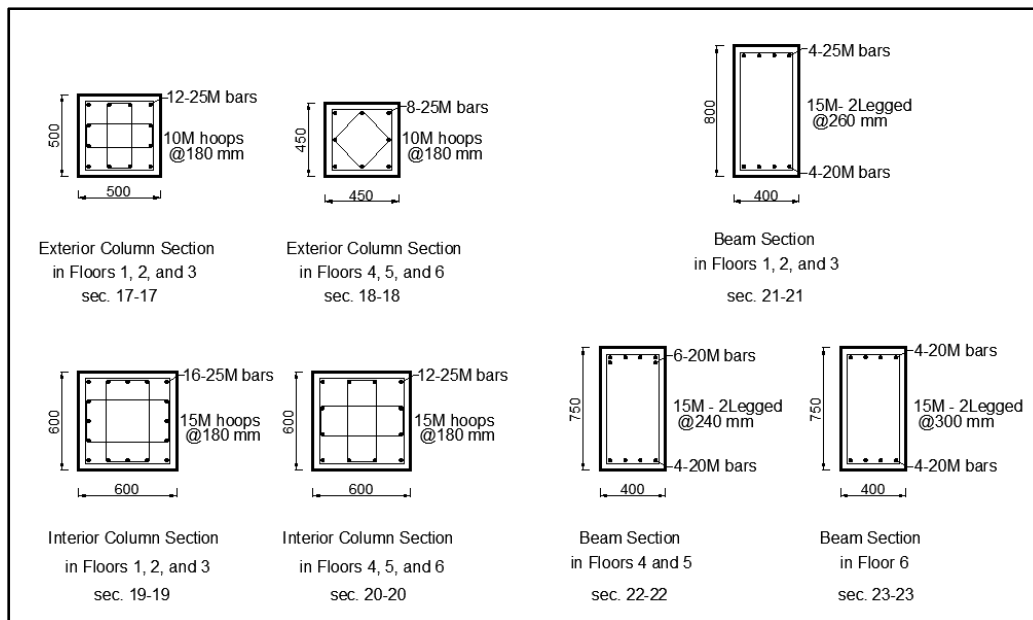


Figure 2.15 Reinforcing details of the conventionally constructed frames in Montreal

## 2.9 Drift ratio

The maximum inter-storey drift ratio occurs in frames 1 and 8. Figure 2.16 presents the inter-storey drift ratio in frame 1 for all of studied buildings under the lateral loads and accidental torsion. It can be noted that the drift ratios of models are less than the NBC 2015 limit of 2.5%.

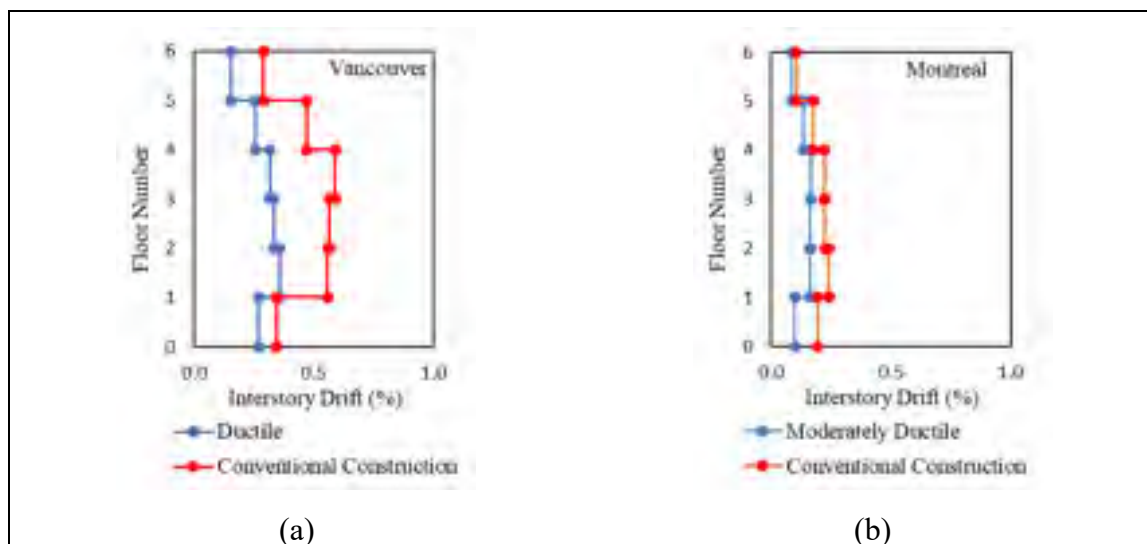


Figure 2.16 Inter-storey drift ratio for frame models in (a) Vancouver; (b) Montreal

## **2.10 Summary**

This chapter presented in detail the seismic design steps of the four studied frames and how the design requirements and reinforcement detailing differ when the ductility level changes. The next chapter presents the selection and scaling of ground motions required for performing the dynamic analyses for all studied frames.





## CHAPITRE 3

### SELECTION AND SCALING OF GROUND MOTION RECORDS

#### 3.1 Introduction

The details of selection and scaling of input ground motion records are presented in this chapter. Method-A proposed in the structural commentaries of the NBC 2015 was followed. The considered ground motion are chosen from the synthetic time histories database provided by Atkinson (2009) in east and west of Canada, and available from [www.seismotoolbox.ca](http://www.seismotoolbox.ca), along with their response spectra.

Four Excel sheets have been created in this project to select and scale the aforementioned ground motion in eastern and western Canada to match the target spectra with 2 and 10% probability of exceedance in Montreal and Vancouver, respectively. The Excel sheets are presented in Appendix I.

#### 3.2 Selection and scaling of ground motion records

Synthetic ground motion records for dynamic analysis are selected and scaled to match the target spectrum  $S_T(T)$  given in NBC 2015. Two methods, A and B, are proposed in NBC *commentary – Part J (2017)* to select and scale ground motions. According to Method A, the spectral accelerations corresponding to periods shorter than 0.5 s are obtained by linear interpolation between PGA,  $S_a(0.05)$ ,  $S_a(0.1)$ ,  $S_a(0.2)$ ,  $S_a(0.3)$ , and  $S_a(0.5)$  instead of defining a plateau at short periods. Figure 3.1 shows the target spectra in Montreal and Vancouver with a probability of exceedance 2% and 10% per 50 years as per NBC 2015.

The input ground motion records are selected and scaled to match the target spectrum in a period range  $T_R$  specified in NBC 2015. The lower and upper limits of this period range,  $T_{min}$  and  $T_{max}$ , are determined using Equations 3.1 and 3.2, respectively. Where  $T_{90\%}$  is the period of the highest vibration mode required to cumulate a minimum participating mass of 90% of the structure mass. The values of  $T_{Bldg1}$  and  $T_{90\%}$  used for the selection and scaling ground motion are shown in Table 3.1.

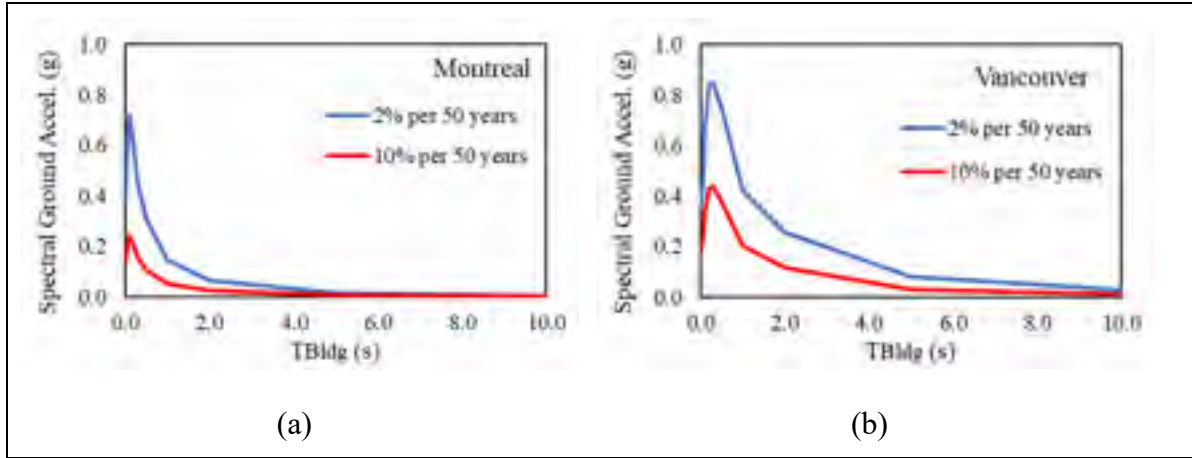


Figure 3.1 Target spectrum with probabilities of exceedance of 2% and 10% per 50 years  
(a) Montreal, and (b) Vancouver

$$T_{\min} = \min[0.2T_{Bldg1}, T_{90\%}] \quad (3.1)$$

$$T_{\max} = \max[2.0T_{Bldg1}, 1.5 \text{ s}] \quad (3.2)$$

The synthetic ground motions database in Atkinson (2009) was generated for two scenarios in Montreal assumed to be the source of hazard in eastern Canada. The first scenario includes the events with moment magnitude  $M = 6.0$  at a fault distance  $R$ , ranging between 10 and 30 km. These events contribute to the hazard at period range  $T_{R1}$ , which varies from  $T_{\min}$  to 1.0 s. The second scenario includes events with  $M = 7.0$  at larger distances between 20 and 70 km. These events contribute to the hazard at period range  $T_{R2}$ , which varies from 0.5 s to  $T_{\max}$ .

In Vancouver, the synthetic ground motions have been generated for three scenarios assumed to be the source of hazard in western Canada. The first scenario includes the events with a moment magnitude  $M = 6.5$  at a fault distance  $R$ , ranging between 12 and 30 km. These events contribute to the hazard at period range  $T_{R1}$ , varies from  $T_{\min}$  to 0.8 s portion. The second scenario includes events with  $M = 7.5$  at larger distances between 25 and 100 km. These events contribute to the hazard at period range  $T_{R2}$ , varies from 0.3 s to 1.5 s. The third scenario includes events with  $M = 9.0$  at large distance reaches 360 km. These events contribute to the hazard at period range  $T_{R3}$ , varies from 1.0 s to  $T_{\max}$ .

Table 3.1 Modal periods and ranges for ground motion scaling for the studied buildings

Case of study building	$T_{Bldg1}$	$T_{90\%}$	$T_{R1}$	$T_{R2}$	$T_{R3}$
Ductile in Vancouver (D)	1.167	0.390	0.23-0.8	0.3-1.5	1.0-2.33
Conventional in Vancouver (CC)	0.703	0.223	0.14-0.8	0.3-1.5	1.0-1.5
Moderately ductile in Montreal (MD)	1.033	0.339	0.21-1.0	0.5-2.1	-
Conventional in Montreal (CC)	0.818	0.275	0.16-1.0	0.5-1.6	-

Units are seconds. The values of modal periods are defined without considering the cracks effect

The minimum number of ground motion time histories required for dynamic analysis is eleven as per NBC 2015 provided that a minimum of five ground motions must be selected for each hazard scenario. Therefore, twelve and seventeen synthetic ground motions were selected and scaled for each studied frames in Montreal and Vancouver, respectively as follows.

### 3.2.1 Moderately ductile frame in Montreal

Tables 3.2 and 3.3 illustrate the selected ground motions for the moderately ductile frame in Montreal in each (M-R) scenario, the time step of the ground motion records, and the scaling factor required for matching with the target spectrum at a probability of exceedance 2% and 10% per 50 years as per NBC 2015, respectively.

Figures 3.2 and 3.4 present the scaled acceleration spectra of the selected ground motion in  $T_{R1}$  and  $T_{R2}$  for the moderately ductile frame using the target spectrum at a probability of exceedance 2% and 10% per 50 years, respectively. Figures 3.3 and 3.5 present the difference between the mean acceleration spectra of the scaled ground motion and the target spectrum at a probability of exceedance 2% and 10% per 50 years, respectively. It is noted that when the mean spectra of the scaled ground motion for both scenarios in Figures 3.3 and 3.5 are lesser than the target spectrum, the reduction does not exceed 10% which satisfies NBC 2015 limit.

Table 3.2 Scaling factors of selected records of moderately ductile frame in Montreal using the target spectrum at a probability of exceedance 2% per 50 years

Scenario	M	R	Record	Duration	Time step	Scaling factor	PGA
1	6.0	15.0	E6C1_07	43.598	0.002	0.563	0.295
			E6C1_32			0.968	0.415
			E6C1_31			0.785	0.312
		30.0	E6C2_08	47.530		0.943	0.297
			E6C2_26			1.701	0.398
			E6C2_31			1.504	0.278
2	7.0	25.0	E7C1_11	51.126		0.534	0.518
			E7C1_25			0.564	0.311
			E7C1_28			0.702	0.403
		100.0	E7C2_01	57.352		1.439	1.046
			E7C2_11			1.991	1.933
			E7C2_02			1.570	0.939

Units are in km, seconds, and g

Table 3.3 Scaling factors of selected records of moderately ductile frame in Montreal using the target spectrum at a probability of exceedance 10% per 50 years

Scenario	M	R	Record	Duration	Time step	Scaling factor	PGA
1	6.0	15.0	E6C1_31	43.598	0.002	0.258	0.103
			E6C1_01			0.174	0.132
			E6C1_07			0.201	0.105
		30.0	E6C2_26	47.530		0.536	0.125
			E6C2_31			0.524	0.097
			E6C2_12			0.652	0.142
2	7.0	25.0	E7C1_07	51.126		0.102	0.094
			E7C1_43			0.075	0.091
			E7C1_24			0.084	0.089
		100.0	E7C2_11	57.352		0.635	0.616
			E7C2_44			0.698	0.661
			E7C2_27			0.869	0.405

Units are in km, seconds, and g

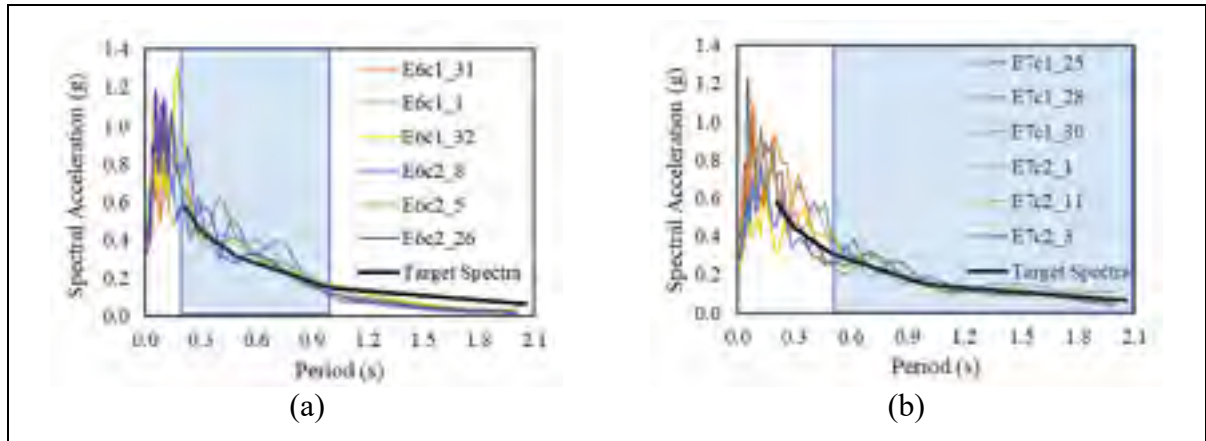


Figure 3.2 Acceleration spectra of the selected and scaled input ground motion for the moderately ductile frame in Montreal using the target spectrum at a probability of exceedance 2% per 50 years in (a)  $T_{R1}$ , and (b)  $T_{R2}$

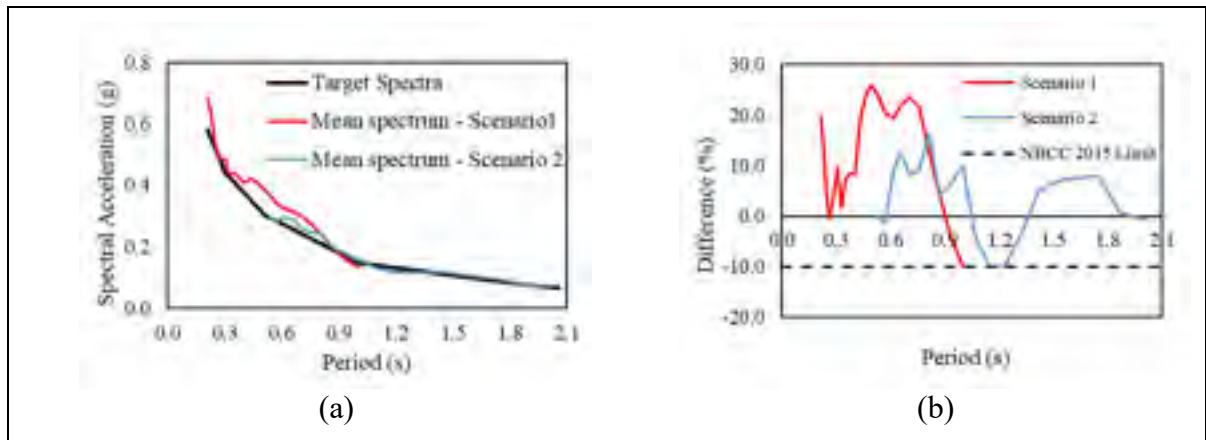


Figure 3.3 (a) Mean acceleration spectra for scenarios 1 and 2 compared with the target spectrum (b) Difference between the mean acceleration spectra of the scaled records and the target spectrum at a probability of exceedance 2% per 50 years within  $T_{R1}$  and  $T_{R2}$

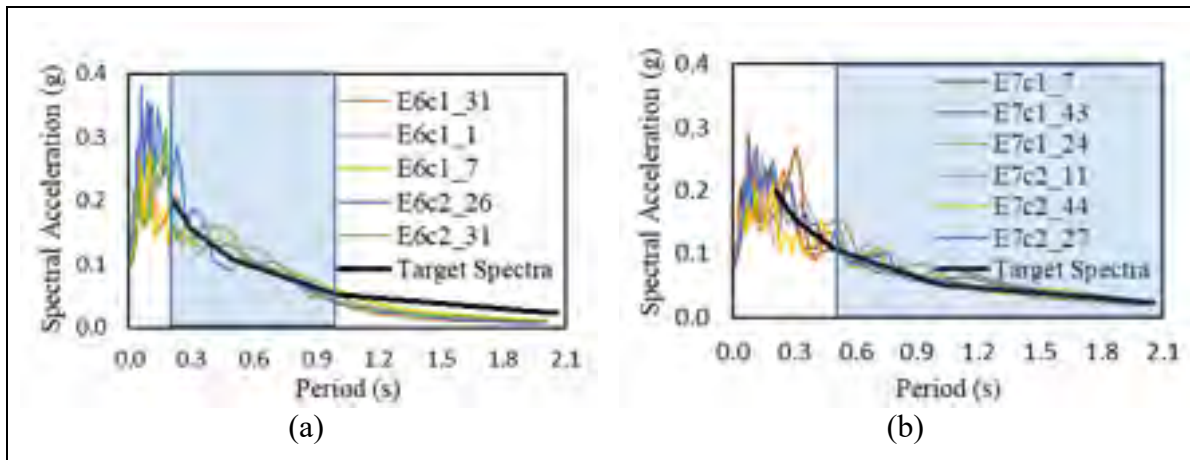


Figure 3.4 Acceleration spectra of the selected and scaled input ground motion for the moderately ductile frame in Montreal using the target spectrum at a probability of exceedance 10% per 50 years in (a)  $T_{R1}$ , and (b)  $T_{R2}$

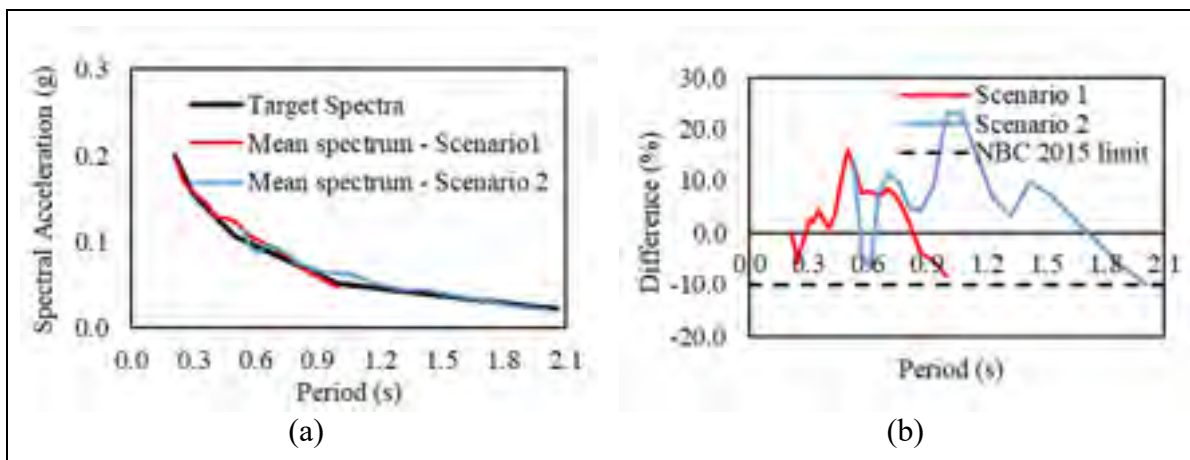


Figure 3.5 (a) Mean acceleration spectra for scenarios 1 and 2 compared with the target spectrum (b) Difference between the mean acceleration spectra of the scaled records and the target spectrum at a probability of exceedance 10% per 50 years within  $T_{R1}$  and  $T_{R2}$

### 3.2.2 Conventional construction frame in Montreal

Tables 3.4 and 3.5 illustrate the selected ground motions for the conventional construction frame in Montreal in each (M-R) scenario, the time step of the ground motion records, and the scaling factor required for matching with the target spectrum at probability of exceedance 2% and 10% per 50 years as per NBC 2015, respectively.

Table 3.4 Scaling factors of selected records of conventional frame in Montreal using the target spectrum at a probability of exceedance 2% per 50 years

Scenario	M	R	Record	Duration	Time step	Scaling factor	PGA
1	6.0	15.0	E6C1_07	43.598	0.002	0.523	0.351
			E6C1_16			0.643	0.428
			E6C1_31			0.397	0.331
		30.0	E6C2_05	47.530		0.279	0.429
			E6C2_08			0.315	0.333
			E6C2_26			0.234	0.390
2	7.0	25.0	E7C1_25	51.126		0.551	0.286
			E7C1_28			0.574	0.385
			E7C1_30			0.689	0.366
		100.0	E7C2_03	57.352		0.770	0.908
			E7C2_07			0.922	0.932
			E7C2_11			0.971	1.627

Units are in km and seconds

Table 3.5 Scaling factors of selected records of conventional frame in Montreal using the target spectrum at a probability of exceedance 10% per 50 years

Scenario	M	R	Record	Duration	Time step	Scaling factor	PGA
1	6.0	15.0	E6C1_01	43.598	0.002	0.194	0.147
			E6C1_31			0.295	0.117
			E6C1_15			0.191	0.176
		30.0	E6C2_26	47.530		0.589	0.138
			E6C2_31			0.583	0.108
			E6C2_38			0.661	0.123
2	7.0	25.0	E7C1_43	51.126		0.070	0.086
			E7C1_07			0.100	0.092
			E7C1_24			0.079	0.083
		100.0	E7C2_11	57.352		0.594	0.577
			E7C2_45			0.959	1.034
			E7C2_44			0.684	0.648

Units are in km, seconds, and g

Figures 3.6 and 3.8 present the scaled acceleration spectra of the selected ground motion in  $T_{R1}$  and  $T_{R2}$  for the conventional construction frame in Montreal at probability of exceedance 2% and 10% per 50 years, respectively. Figures 3.6 and 3.8 present the difference between the

mean acceleration spectra of the scaled ground motion and the target spectrum at probability of exceedance 2% and 10% per 50 years, respectively.

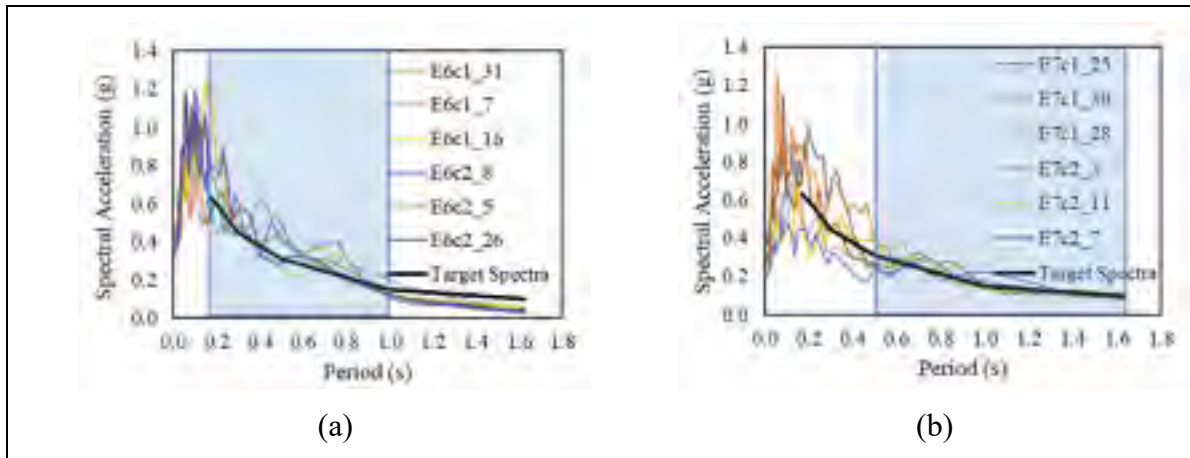


Figure 3.6 Acceleration spectra of the selected and scaled input ground motion for the conventional construction frame in Montreal using the target spectrum at a probability of exceedance 10% per 50 years in (a)  $T_{R1}$ , and (b)  $T_{R2}$

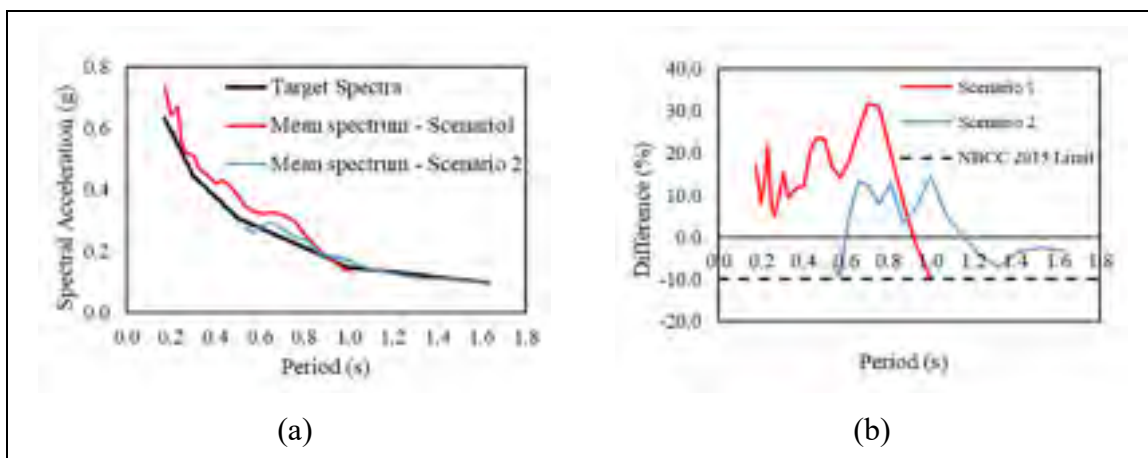


Figure 3.7 (a) Mean acceleration spectra for scenario 1 and 2 compared with the target spectrum (b) Difference between the mean acceleration spectra of the scaled records and the target spectrum at a probability of exceedance 2% per 50 years within  $T_{R1}$  and  $T_{R2}$



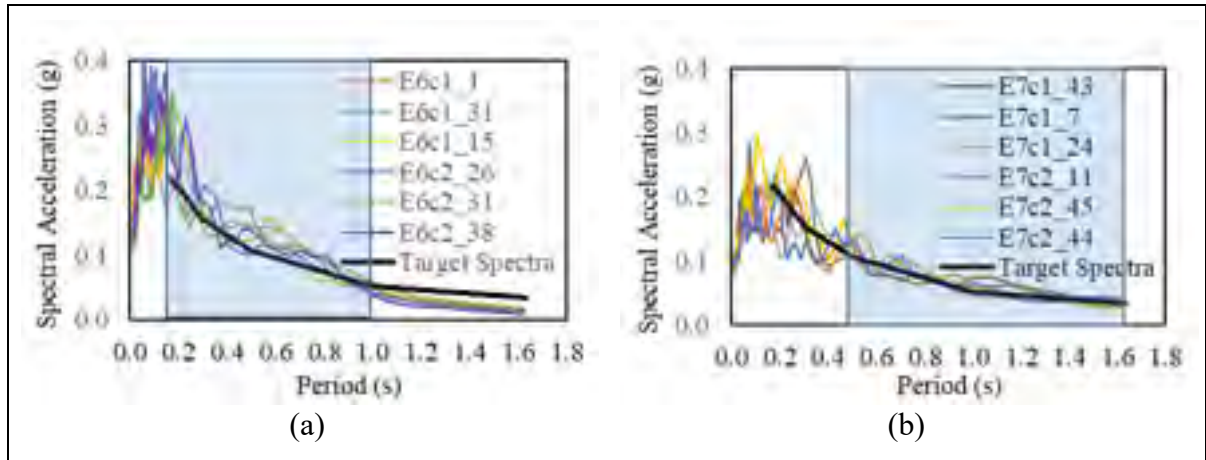


Figure 3.8 Acceleration spectra of the selected and scaled input ground motion for the conventional frame in Montreal using the target spectrum at a probability of exceedance 10% per 50 years in (a)  $T_{R1}$ , and (b)  $T_{R2}$

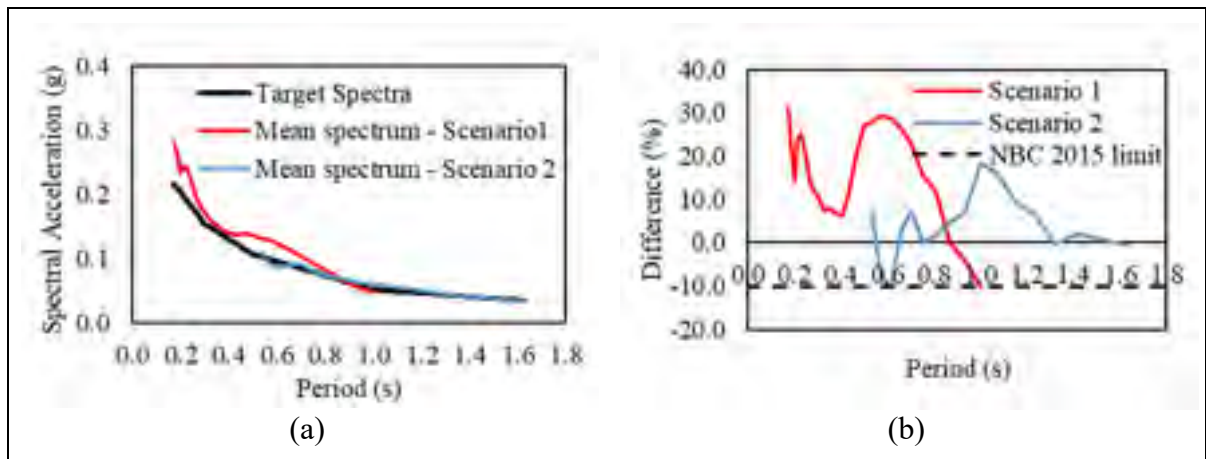


Figure 3.9 (a) Mean acceleration spectra for scenarios 1 and 2 compared with the target spectrum (b) Difference between the mean acceleration spectra of the scaled records and the target spectrum at a probability of exceedance 10% per 50 years within  $T_{R1}$  and  $T_{R2}$

### 3.2.3 Ductile frame in Vancouver

Tables 3.6 and 3.7 illustrate the selected ground motions for the ductile frame in Vancouver in each (M-R) scenario, the time step of the ground motion records, and the scaling factor required for matching with the target spectrum at probability of exceedance 2% and 10% per 50 years, respectively as per NBC 2015.

Table 3.6 Scaling factors of selected records of ductile frame in Vancouver using the target spectrum at a probability of exceedance 2% per 50 years

Scenario	M	R	Record	Duration	Time step	Scaling factor	PGA
1	6.5	12.0	W6C1 02	49.305	0.005	0.766	0.374
			W6C1 27			1.101	0.398
			W6C1 31			0.862	0.422
		30.0	W6C2 10	53.630		1.172	0.203
			W6C2 20			1.492	0.344
			W6C2 44			1.500	0.376
2	7.5	25.0	W7C1 09	102.025		0.666	0.399
			W7C1 28			0.925	0.490
			W7C1 31			0.775	0.256
		100.0	W7C2 16	93.390		1.711	0.303
			W7C2 15			1.731	0.421
			W7C2 06			1.913	0.376
3	9.0	360.8	W9C 05	309.42	0.010	1.599	0.220
			W9C 09			1.553	0.199
			W9C 07			1.693	0.211
			W9C 15			1.734	0.295
			W9C 08			1.755	0.203

Units are in km and seconds

Table 3.7 Scaling factors of selected records of ductile frame in Vancouver using the target spectrum at a probability of exceedance 10% per 50 years

Scenario	M	R	Record	Duration	Time step	Scaling factor	PGA
1	6.5	12.0	W6C1 27	49.305	0.005	0.559	0.202
			W6C1 17			0.623	0.188
			W6C1 25			0.716	0.216
		30.0	W6C2 10	53.630		0.595	0.103
			W6C2 44			0.761	0.191
			W6C2 20			0.758	0.175
2	7.5	25.0	W7C1 22	102.025		0.582	0.198
			W7C1 26			0.512	0.264
			W7C1 18			0.654	0.250
		100.0	W7C2 16	93.390		0.794	0.141
			W7C2 15			0.803	0.195
			W7C2 06			0.887	0.174
3	9.0	360.8	W9C 15	309.42	0.010	0.806	0.137
			W9C 09			0.722	0.093
			W9C 05			0.744	0.102
			W9C 08			0.815	0.094
			W9C 07			0.788	0.098

Units are in km, seconds, and g

Figures 3.10 and 3.13 present the scaled acceleration spectra of the selected ground motion in  $T_{R1}$ ,  $T_{R2}$ , and  $T_{R3}$  for the ductile frame in Vancouver at probability of exceedance 2% and 10% per 50 years, respectively. Figures 3.11 and 3.14 present the difference between the mean acceleration spectra of the scaled ground motion and the target spectra at probability of exceedance 2% and 10% per 50 years.

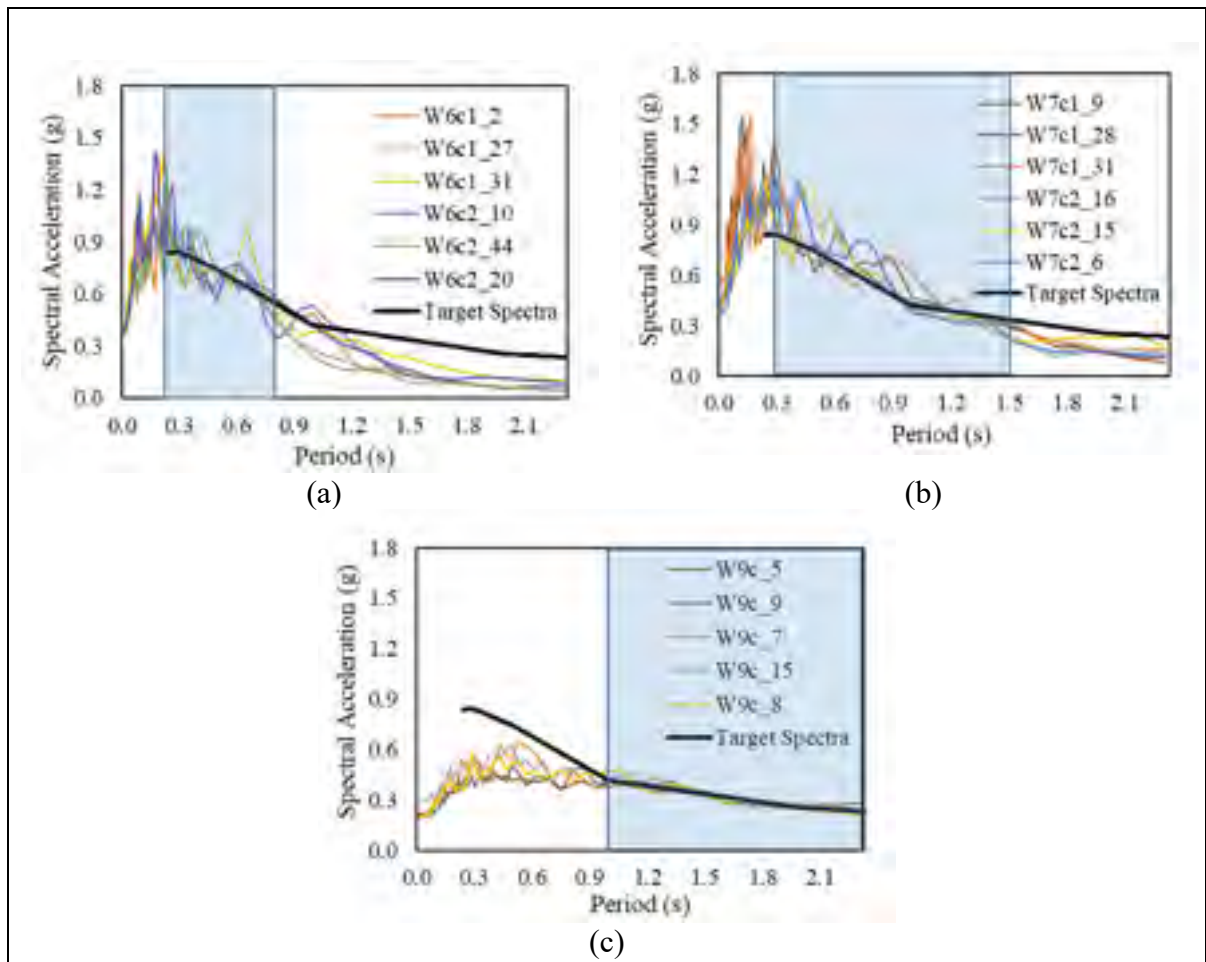


Figure 3.10 Acceleration spectra of the selected and scaled input ground motion for the ductile frame in Vancouver using the target spectrum at a probability of exceedance 2% per 50 years in (a)  $T_{R1}$ , (b)  $T_{R2}$ , and (c)  $T_{R3}$

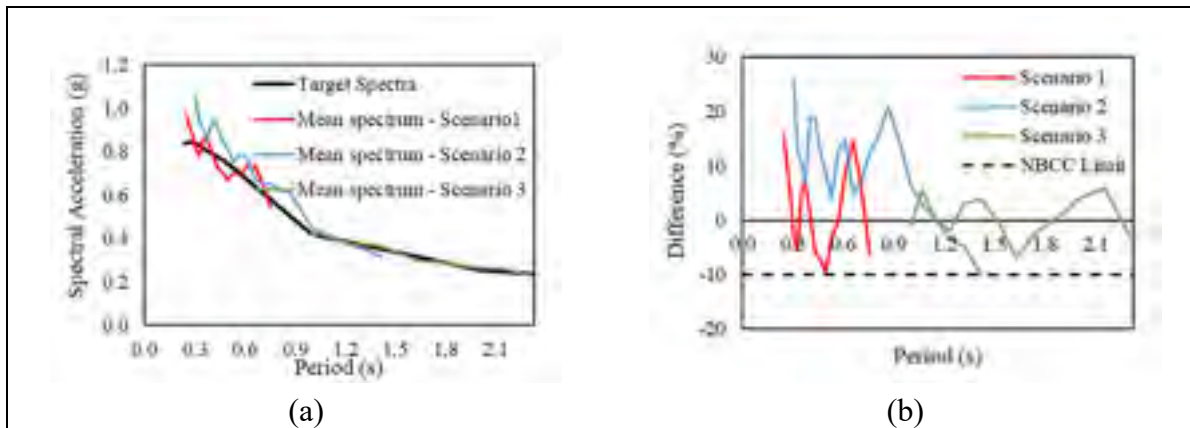


Figure 3.11 (a) Mean acceleration spectra for scenario 1, 2 and 3 compared with the target spectrum (b) Difference between the mean acceleration spectra of the scaled records and the target spectrum at a probability of exceedance 2% per 50 years within  $T_{R1}$ ,  $T_{R2}$ , and  $T_{R3}$

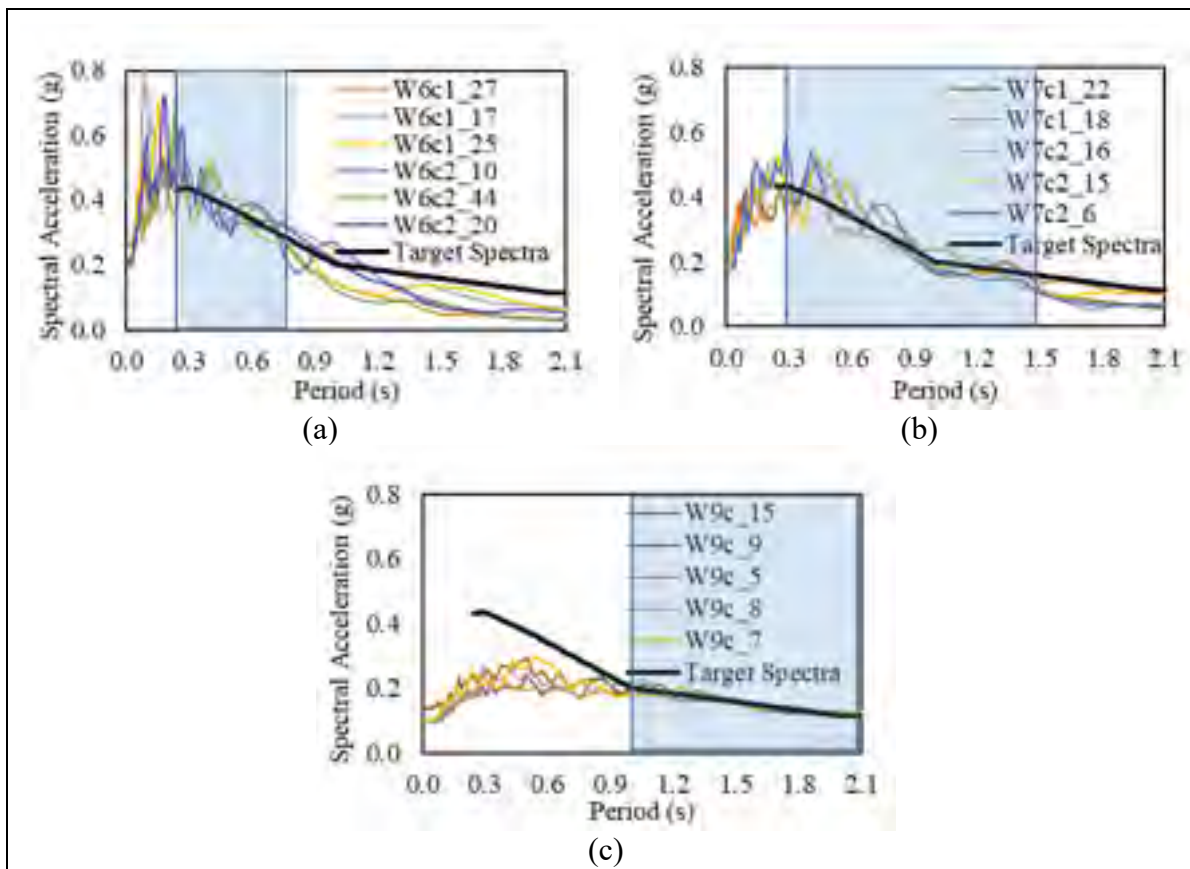


Figure 3.12 Acceleration spectra of the selected and scaled input ground motion for the ductile frame in Vancouver using the target spectrum at a probability of exceedance 10% per 50 years in (a)  $T_{R1}$ , (b)  $T_{R2}$ , and (c)  $T_{R3}$

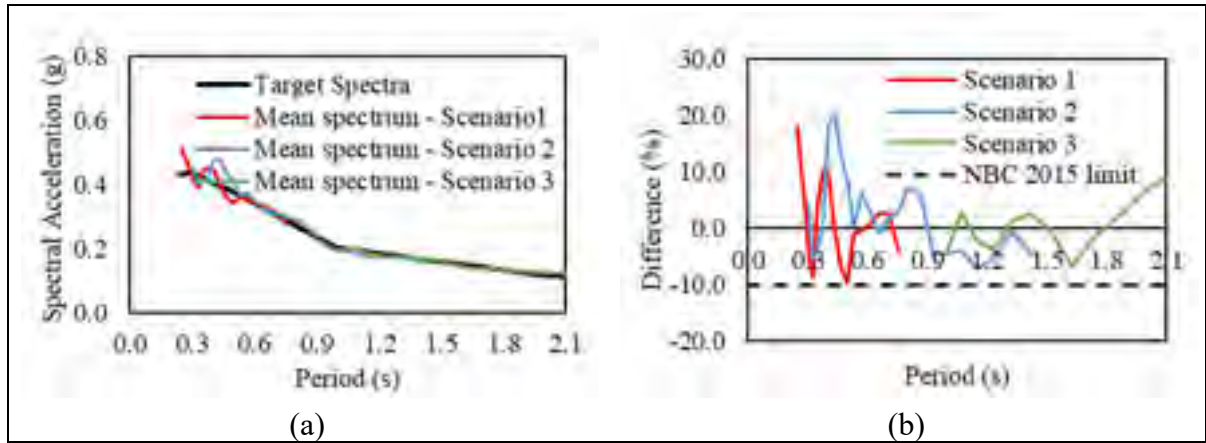


Figure 3.13 (a) Mean acceleration spectra for scenario 1, 2 and 3 compared with the target spectrum (b) Difference between the mean acceleration spectra of the scaled records and the target spectrum at a probability of exceedance 10% per 50 years within  $T_{R1}$ ,  $T_{R2}$ , and  $T_{R3}$

### 3.2.4 Conventional construction frame in Vancouver

Tables 3.8 and 3.9 illustrate the selected ground motions for the conventional construction frame in Vancouver in each (M-R) scenario, the time step of the ground motion records, and the scaling factor required for matching with the target spectrum at probabilities of exceedance 2% and 10% per 50 years, respectively as per NBC 2015.

Figure 3.14 presents the scaled acceleration spectra of the selected ground motion in  $T_{R1}$ ,  $T_{R2}$ , and  $T_{R3}$  for the conventional construction frame in Vancouver. Figure 3.15 presents the difference between the mean acceleration spectra of the scaled ground motion and the target spectrum, which satisfies NBC 2015 limit.

Table 3.8 Scaling factors of selected records of conventional frame in Vancouver using the target spectrum at a probability of exceedance 2% per 50 years

Scenario	M	R	Record	Duration	Time step	Scaling factor	PGA
1	6.5	12.0	W6C1 02	49.305	0.005	0.771	0.378
			W6C1 27			1.123	0.397
			W6C1 21			0.933	0.520
		30.0	W6C2 10	53.630		1.157	0.195
			W6C2 20			1.482	0.322
			W6C2 44			1.455	0.358
2	7.5	25.0	W7C1 09	102.025		0.666	0.399
			W7C1 28			0.926	0.490
			W7C1 31			0.775	0.256
		100.0	W7C2 16	93.390		1.711	0.303
			W7C2 15			1.731	0.421
			W7C2 06			1.913	0.376
3	9.0	360.8	W9C 05	309.42	0.010	1.638	0.228
			W9C 09			1.553	0.196
			W9C 02			1.705	0.283
			W9C 11			1.716	0.234
			W9C 17			1.726	0.170

Units are in km and seconds

Table 3.9 Scaling factors of selected records of conventional frame in Vancouver using the target spectrum at a probability of exceedance 10% per 50 years

Scenario	M	R	Record	Duration	Time step	Scaling factor	PGA
1	6.5	12.0	W6C1 27	49.305	0.005	0.558	0.202
			W6C1 17			0.621	0.188
			W6C1 09			0.558	0.197
		30.0	W6C2 10	53.630		0.570	0.099
			W6C2 44			0.725	0.182
			W6C2 20			0.709	0.164
2	7.5	25.0	W7C1 22	102.025		0.582	0.198
			W7C1 26			0.512	0.264
			W7C1 18			0.654	0.250
		100.0	W7C2 16	93.390		0.794	0.141
			W7C2 15			0.803	0.195
			W7C2 06			0.887	0.174
3	9.0	360.8	W9C 05	309.42	0.010	0.787	0.108
			W9C 32			1.279	0.094
			W9C 02			0.939	0.135
			W9C 11			0.792	0.111
			W9C 29			1.103	0.092

Units are in km, seconds, and g



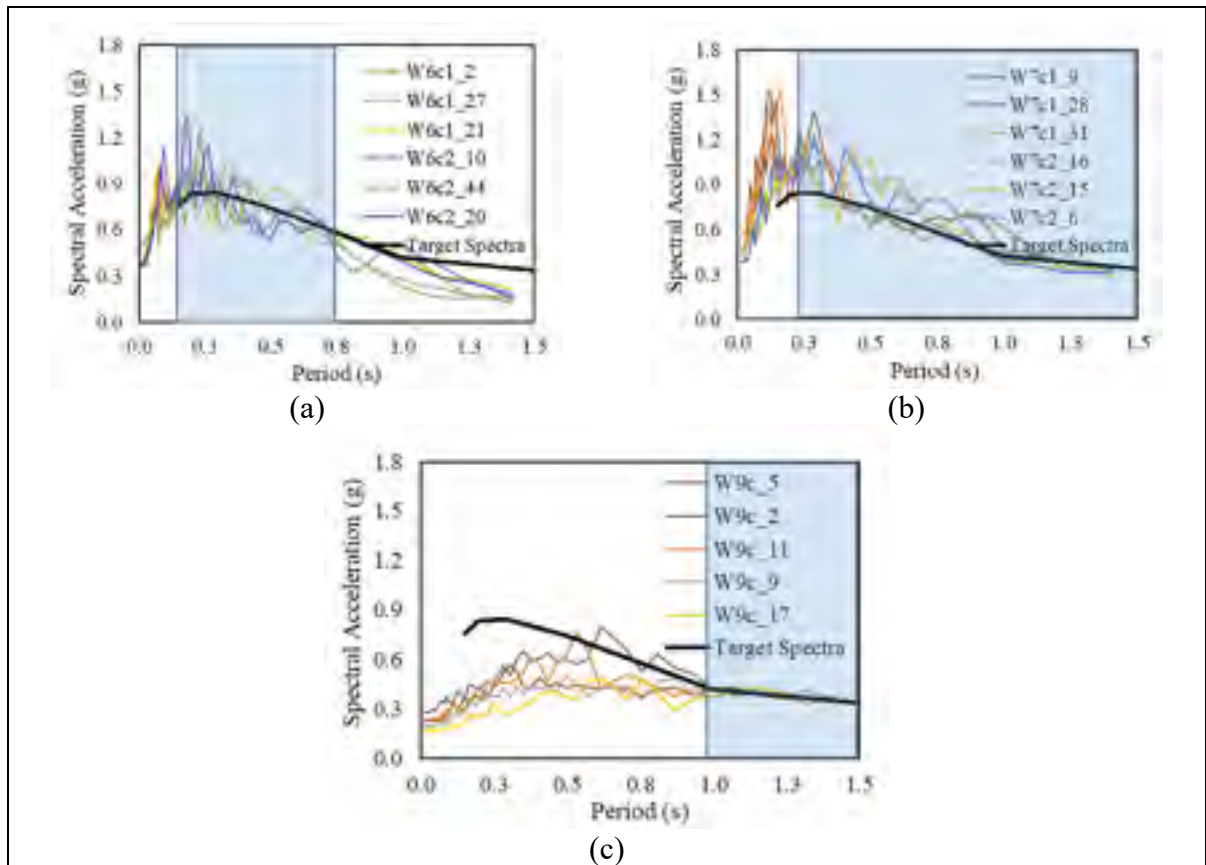


Figure 3.14 Acceleration spectra of the selected and scaled input ground motion for the conventional construction frame in Vancouver using the target spectrum at a probability of exceedance 2% per 50 years in (a)  $T_{R1}$ , (b)  $T_{R2}$ , and (c)  $T_{R3}$

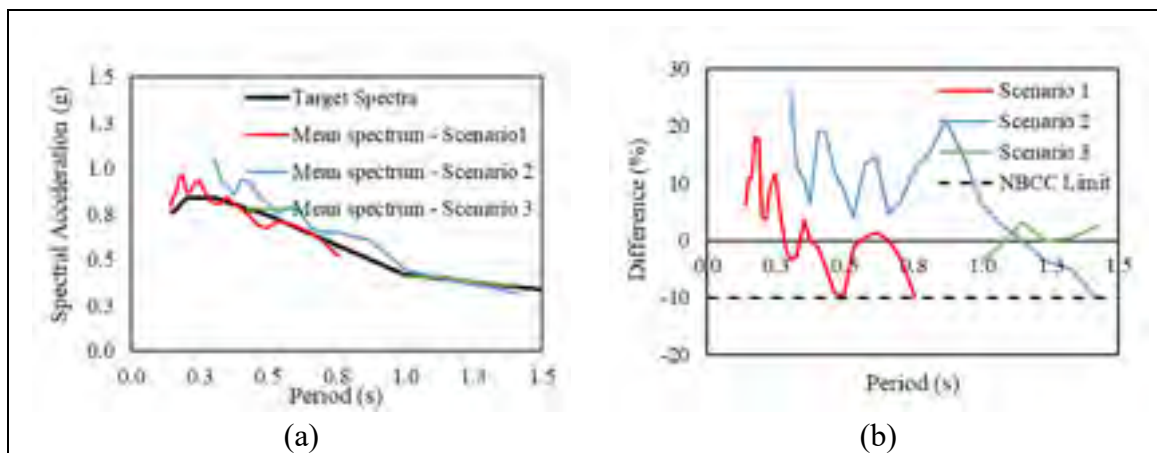


Figure 3.15 (a) Mean acceleration spectra for scenario 1, 2 and 3 compared with the target spectrum (b) Difference between the mean acceleration spectra of the scaled records and the target spectrum at a probability of exceedance 2% per 50 years within  $T_{R1}$   $T_{R2}$ , and  $T_{R3}$

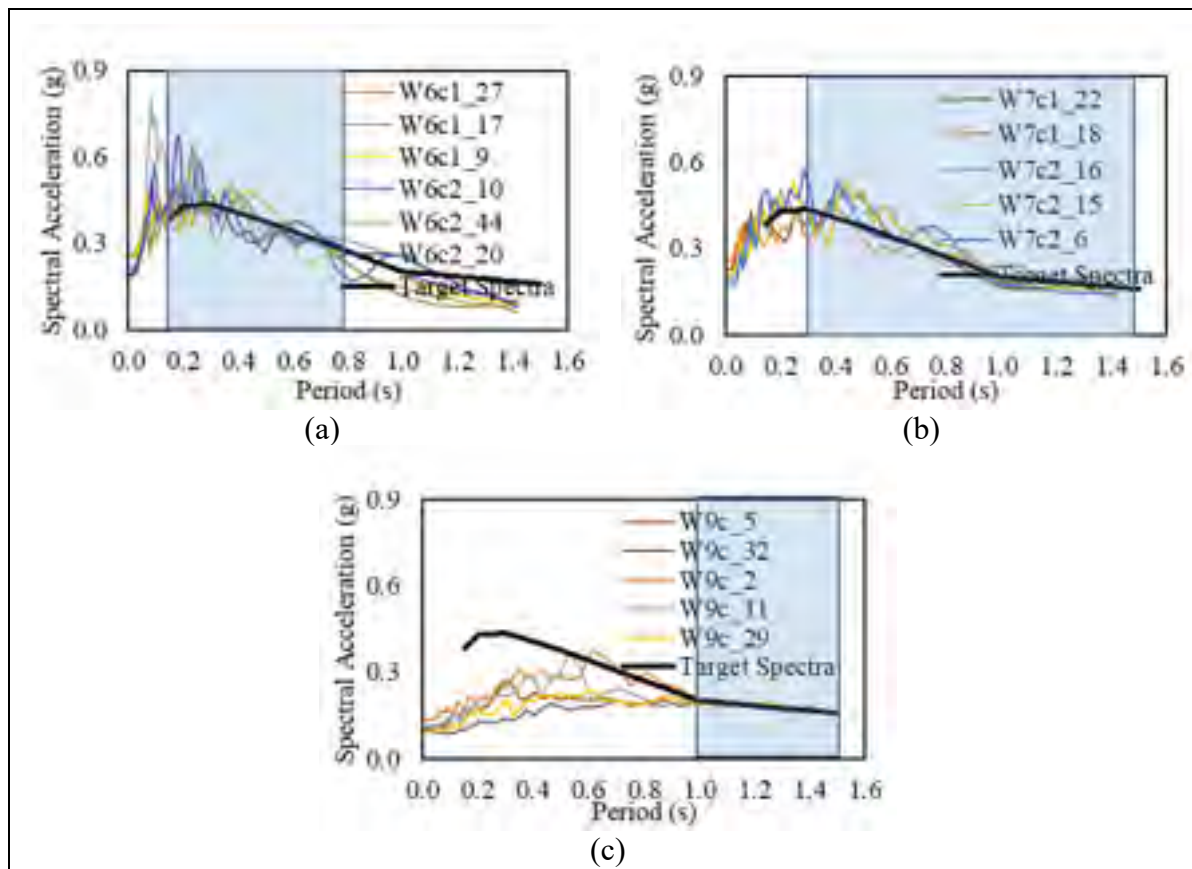


Figure 3.16 Acceleration spectra of the selected and scaled input ground motion for the conventional frame in Vancouver using the target spectrum at a probability of exceedance 10% per 50 years in (a)  $T_{R1}$ , (b)  $T_{R2}$ , and (c)  $T_{R3}$

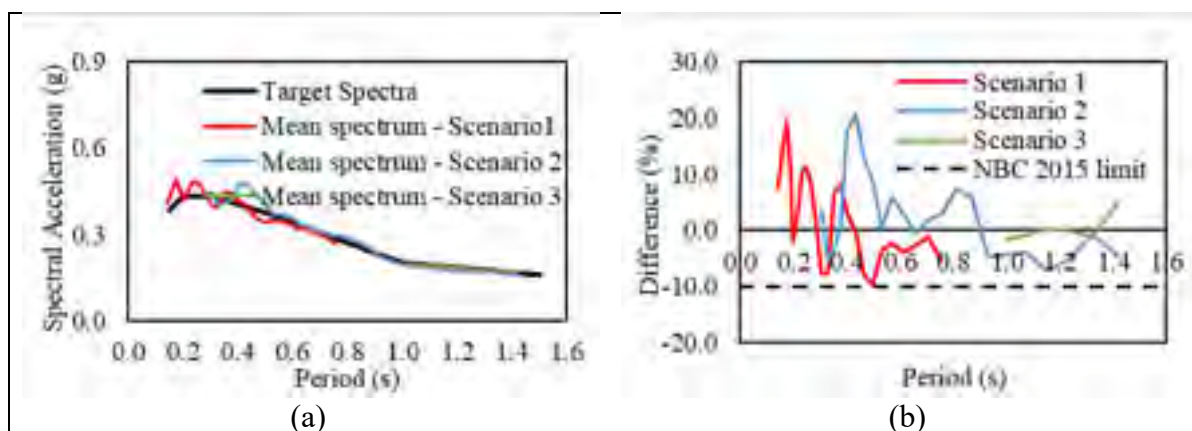


Figure 3.17 (a) Mean acceleration spectra for scenario 1, 2 and 3 compared with the target spectrum (b) Difference between the mean acceleration spectra of the scaled records and the target spectrum at a probability of exceedance 10% per 50 years within  $T_{R1}$ ,  $T_{R2}$ , and  $T_{R3}$



### **3.3        Summary**

This chapter presented in detail the steps of selecting and scaling the synthetic ground motions at 2% and 10% probability of exceedance per 50 years for the four studied frames. These ground motions will be applied to the studied frames to perform the dynamic analyses as will be illustrated in the next chapter.

## CHAPITRE 4

### LINEAR AND NONLINEAR ANALYSIS OF THE CASE STUDY BUILDINGS

This chapter presents the modeling details and calculations required for the linear and nonlinear time history analyses of all frame models.

#### 4.1 Linear Dynamic Analysis

Two-dimensional linear models have been created for the studied frames using SAP2000® (CSI, 2019). Members' geometry, materials, end length offset, and boundary conditions are defined as explained in Section 2.5. Floors seismic weight  $W_x$  calculated in Chapter two for each frame model were applied as per Tables 2.8 and 2.9 to floor nodes as illustrated in Figure 4.1. Three types of analysis cases were defined as follows:

- **Modal:** the load case type is modal, and type of modes was Eigen vectors.
- **Gravity:** the load case type is static, and the type of analysis is linear. The initial conditions were considered zero. The loads applied in this analysis case is (D + 0.25 L + S). D, L, and S loads are shown in Figures 2.5 and 2.6.
- **Linear dynamic analysis:** the load case type is time history, type of analysis is linear, solution type is direct integration, and history type is transient. Proportional damping was selected. The mass and stiffness proportional coefficients,  $a_0$  and  $a_1$ , are determined from Equations 4.1 and 4.2, respectively as per Chopra (2012). Where  $\zeta$  is considered equal to 5% and the angular frequencies  $\omega_1$  and  $\omega_2$  at the first and second modes of a building are determined based on the modal periods (see Table 2.4) as per Equation 4.3.

$$a_0 = \zeta \frac{2\omega_1\omega_2}{\omega_1 + \omega_2} \quad (4.1)$$

$$a_1 = \zeta \frac{2}{\omega_1 + \omega_2} \quad (4.2)$$

$$\omega_i = \frac{2\pi}{T_{Bldgi}} \quad (4.3)$$

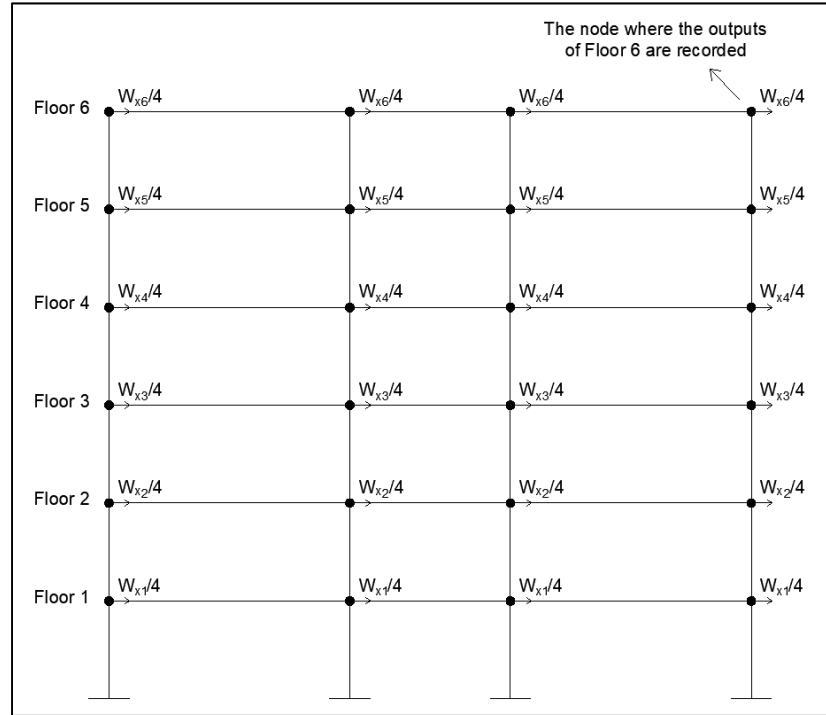


Figure 4.1 Floors seismic weight applied to floor nodes in a typical model

Results in terms of floor accelerations and floor response spectra are obtained directly from SAP2000® in all floors, and presented in the next chapter.

## 4.2 Nonlinear Dynamic Analysis

Two-dimensional nonlinear models have been created for the studied frames using SAP2000®. Similar to the linear models, materials, members' geometry, end length offset, and floors seismic weight are defined. Deformation controlled plastic hinges (ductile) were assigned at the end of the rigid zones of beams and columns so that the plastic hinges form at the face of joints. Figure 4.2 shows a typical frame with the assigned plastic hinges.

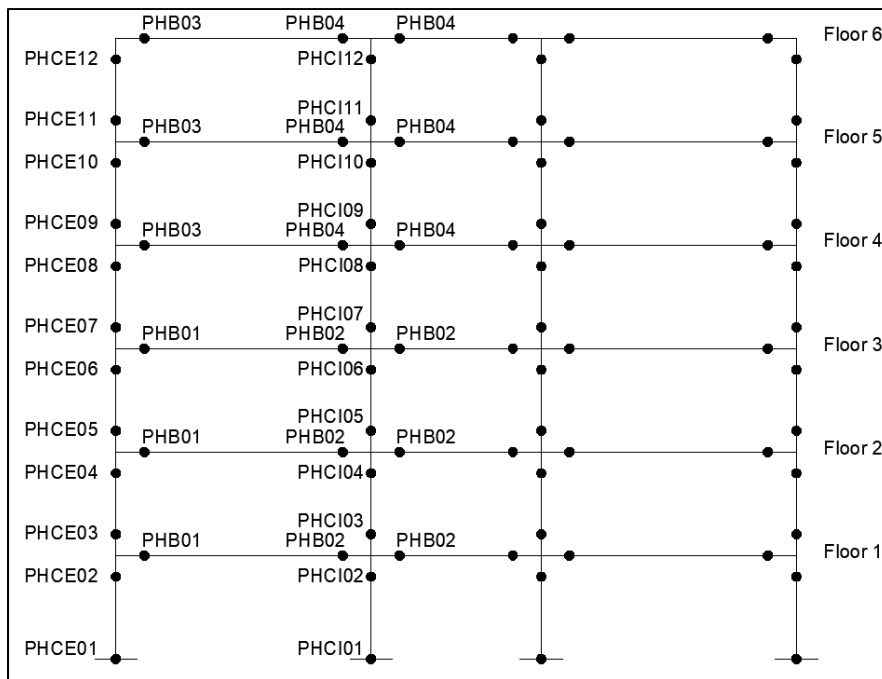


Figure 4.2 Typical frame model with assigned plastic hinges

Nonlinear flexural characteristics of the individual frame members were defined by moment-rotation relationships of plastic hinges assigned at the member ends. Flexural moment capacities were based on the section and material properties of members. In order to define plastic hinges by SAP2000, the backbone and acceptance criteria were determined according to the backbone given by ASCE 41-17 as shown in Figures 4.3 to 4.5.

The isotropic hysteresis type was selected (Figure 4.6). In this model, the strength increases in both directions simultaneously. As for the stiffness, the unloading and reverse loading occur along a path parallel to the elastic line. More details about the isotropic hysteresis model is available in CSI (2017).

The yield moment of a section,  $M_y$  is used as a moment scale factor (Moment SF), and the yield rotation,  $\theta_y$  is used as a rotation scale factor (Rotation SF). Consequently, the moment and hinge rotation at the four points (B, C, D and E) are assigned as a ratio to the yield moment and rotation (Figure 4.3). Similarly, the acceptance criteria hinge rotation at different performance levels are assigned as a ratio to the yield rotation. The point B in Figure 4.3 to Figure 4.5 represents the section yield. The moment  $M_y$  of a section is determined by software

Response2000<sup>®</sup> (Bentz, 1999). Examples to determine  $M_y$  of sections using Response2000<sup>®</sup> is available in Appendix II. The rotation  $\theta_y$  is equal to  $0.5\varepsilon_y L_b / h_b$  for columns and  $0.283\varepsilon_y L_b / h_b$  for beams as per (Calvi et al., 2008). Where  $\varepsilon_y$  is the yield strain considered 0.002,  $h_b$  is the beam section depth, and  $L_b$  is the beam span.

**Frame Hinge Property Data for PHCE6 - Moment M3**

Edit

Displacement Control Parameters

Point	Moment/SF	Rotation/SF
E	-0.2	-8.4
D-	-0.2	-5.6
C-	-1.1	-5.6
B-	-1	0
A	0	0
B	1	0
C	1.1	5.6
D	0.2	5.6
E	0.2	8.4

Load Carrying Capacity Beyond Point E

☒ Drops To Zero

☐ Is Extrapolated

Scaling for Moment and Rotation

☐ Use Yield Moment: Moment SF: 309.5

☐ Use Yield Rotation: Rotation SF: 7.500E-03 (Steel Objects Only)

Acceptance Criteria (Plastic Rotation/SF)

☒ Immediate Occupancy: 0.667

☐ Life Safety: 2.667

☐ Collapse Prevention: 3.762

☒ Show Acceptance Criteria on Plot

Type

☒ Moment - Rotation

☐ Moment - Curvature

Hysteresis Type And Parameters

Hysteresis Type: isotropic

No Parameters Are Required For This Hysteresis Type

OK Cancel

Figure 4.3 Definition of plastic hinge properties of a symmetric section in SAP2000

Frame Hinge Property Data for PHB3 - Moment M3

Edit

Displacement Control Parameters

Point	Moment/SF	Rotation/SF
B	-0.2	-11.4
D	-0.2	-6.2
C	-1.1	-6.2
E	-1	-1
A	0	0
F	1	1
G	1.1	5.3
H	0.2	5.3
I	0.3	2.6

☐ Symmetric

Type

☒ Moment - Rotation

☐ Moment - Curvature

Hysteresis Type And Parameters

Hysteresis Type:

No Parameters Are Required For This Hysteresis Type

Load Carrying Capacity Beyond Point E

☒ Drops To Zero

☐ Is Extrapolated

Scaling for Moment and Rotation

☐ Use Yield Moment

☐ Use Yield Rotation (Steel Objects Only)

	Positive	Negative
Moment SF	175.6	259.4
Rotation SF	4.600E-03	4.600E-03

Acceptance Criteria (Plastic Rotation/SF)

☒ Immediate Occupancy

☐ Life Safety

☐ Collapse Prevention

☒ Show Acceptance Criteria on Plot

OK Cancel

Figure 4.4 Definition of plastic hinge of a non-symmetric section in SAP 2000

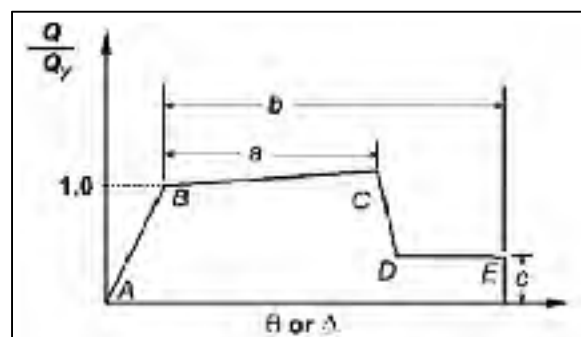


Figure 4.5 Generalized Force–Deformation Relation for Concrete Elements or Components  
Taken from ASCE 41-17

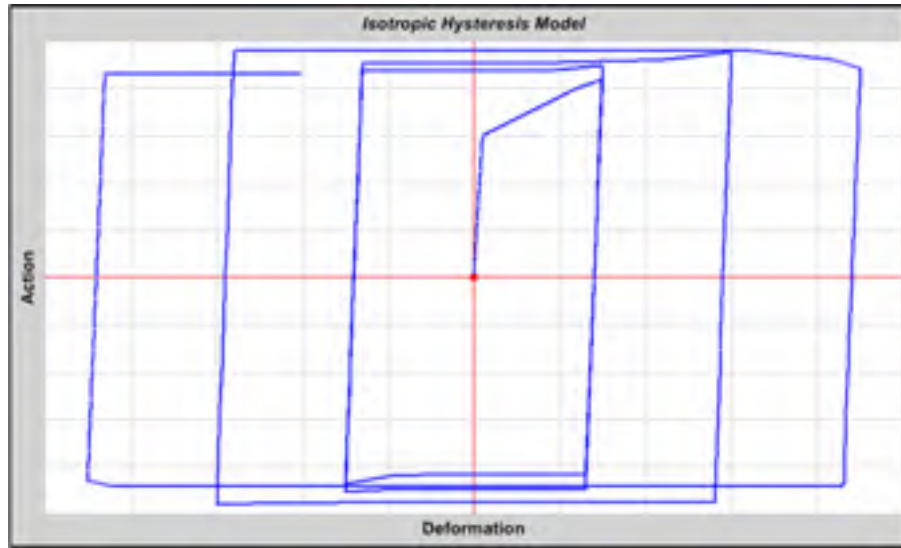


Figure 4.6 Isotropic hysteresis model  
Taken from CSI (2017)

The point C represents the section when it reaches the post-capping. The Moment  $M_C$  is assumed to be equal to  $1.1M_y$  as per NIST GCR 17-917-46v3 (2017). The rotation  $\theta_C$  is determined from Equation 4.4. The point D represents the section when it reaches the residual strength. The Moment  $M_D$  is determined from Equation 4.5. The rotation  $\theta_D$  is assumed to be equal to  $\theta_C$ . The point E represents the section it reaches to the ultimate capacity. The Moment  $M_E$  is equal to  $M_D$ , and the rotation  $\theta_E$  is determined from Equation 4.6.

$$\theta_C = \theta_y + a \quad (4.4)$$

$$M_D = M_E = c \quad (4.5)$$

$$\theta_E = \theta_y + b \quad (4.6)$$

Where:

- a, b    Parameters used to measure deformation capacity in component load–deformation curves based on section properties given by Table 10.7 for beams and Table 10.8 for columns in ASCE 41-17.

- c Parameter used to measure residual strength given by Table 10.7 for beams and Table 10.8 for columns in ASCE 41-17 based on section properties.

The acceptance criteria of the hinge rotations are determined from Table 10.7 for beams and Table 10.8 for columns in ASCE 41-17 based on the section properties.

In Table 10.7, the modelling parameters of conforming transverse reinforcement beams controlled by flexure are used for calculating the plastic hinges properties and acceptance criteria in ductile and moderately ductile frames. On the other hand, the modelling parameters of non-conforming transverse reinforcement beams are used for the conventional construction frames.

In Table 10.8, the equations of columns not controlled by inadequate development or splicing along the clear height are used for calculating the plastic hinges properties and acceptance criteria in ductile and moderately ductile frames. On the other hand, the equations of columns controlled by inadequate development or splicing along the clear height are used for the conventional construction frames.

The plastic hinge properties are calculated and presented for all frame models in the Appendix III. Three types of analysis cases were defined: modal, gravity, and nonlinear dynamic analysis. The loads applied in the gravity analysis case consist of  $D + 0.25 L + S$ .

Direct integration nonlinear time history analysis was performed using the ground motion with 2% and 10% probabilities of exceedance described in chapter 3. The performance level of the studied frames were assessed at 2% and 10% probabilities of exceedance according to FEMA 356 (2000) and following the procedure in Hakim et al. (2014). The assessment showed that all the studied frames reach to the IO performance level under the ground motions with 10% probability of exceedance while they reach LS performance level under the ground motions with 2% probability of exceedance.

Results of the nonlinear time history analyses in terms of floor accelerations and floor response spectra are obtained directly from SAP2000<sup>®</sup>, and presented in the next chapter.



### 4.3 Simplified method of Kothari et al. (2017)

The simplified method explained in section 1.4.2.2 was applied to frame models in Vancouver and Montreal as follows:

#### 4.3.1 Ductile frame in Vancouver

##### 4.3.1.1 Pushover analysis

The nonlinear model explained in section 4.2 was used for performing pushover analysis to the ductile frame in Vancouver. Three analysis cases were defined: modal, gravity, and pushover. The loads applied in the gravity analysis case are (D+0.25L+S). The pushover analysis case is a static load case type with nonlinear analysis type. The type of applied loads was considered the first mode. Displacement control with an applied displacement 2.19 m (10% of frame height) at the frame roof was selected.

The formation of hinges of structure and acceptance criteria are shown in Figure 4.7. Pushover analysis stopped when the rotations of all the plastic hinges in the ground floor columns near the base of structure reach their ultimate values. This happened after plastic hinges developed in most of beams and their rotations ranged between yielding to ultimate, which means columns of the frame are stronger than beams.

Pushover capacity curve and the idealized bilinear force-displacement relationship as per Federal Emergency Management Agency (FEMA) (2000) are obtained by SAP2000 as shown in Figure 4.8. Table 4.1 presents the yield strength of frame  $V_y$ , the yield displacement  $\Delta_y$ , the initial stiffness before concrete cracking  $k_i$ , and initial effective slope  $k_e$  obtained from above procedure. The points IO and LS are chosen on the obtained pushover curve (Figure 4.8) such that the performance level of point IO will correspond to immediate occupancy and that of LS will correspond to life safety as per FEMA-356 (2000) guidelines. Table C1-3 in FEMA-356 (2000) guidelines provides global drifts,  $\theta$  of a structure at different performance levels. For concrete frames, the drifts corresponding to IO and LS performance levels are 1% and 2%,

respectively. The global displacement,  $\Delta$  of a structure at a performance level is obtained from multiplying  $\theta$  at the same performance level by the total height of a structure. Therefore, the displacement of point IO,  $\Delta_{IO}$  is equal to 219 mm and that of point LS,  $\Delta_{LS}$  is equal to 438 mm.

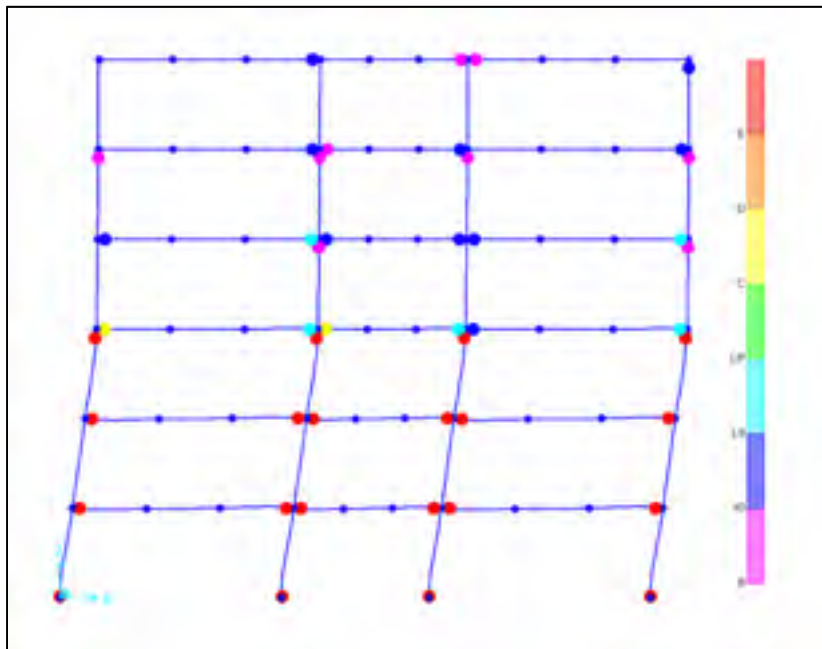


Figure 4.7 Hinges formation at the end of pushover analysis of ductile frame in Vancouver

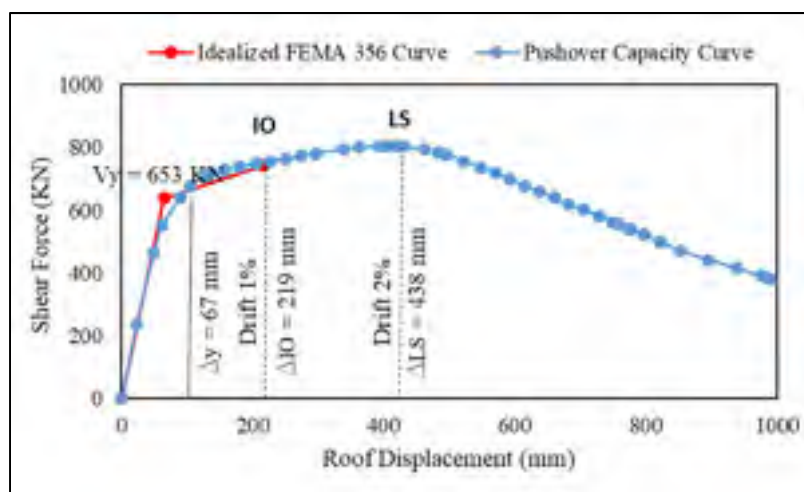


Figure 4.8 Obtained pushover capacity curve of ductile frame in Vancouver

Table 4.1 Obtained parameters from idealized relationship of ductile frame in Vancouver

$V_y$ (KN)	$\Delta_y$ (mm)	$k_i$ (KN/m)	$k_e$ (KN/m)
653.0	67.0	10548.82	9696.12

After obtaining the displacements at the aforementioned performance levels, getting the equivalent stiffness at that performance levels becomes possible using Equation 4.4 as follows:

$$k_{eqIO} = \frac{V_{IO}}{\Delta_{IO}} \quad \text{and} \quad k_{eqLS} = \frac{V_{LS}}{\Delta_{LS}} \quad (4.4)$$

Where  $V_{IO}$  and  $V_{LS}$  are the structure strength at IO and LS performance levels, respectively. Table 4.2 presents the structure strength, global displacement, equivalent stiffness, stiffness reduction factor, SRF ( $k_{eq}/k_i$ ), and equivalent damping calculated using Equations 1.17 and 1.19 at IO and LS performance levels for the 2D ductile frame in Vancouver.

Table 4.2 Equivalent stiffness and stiffness reduction factors at IO and LS performance levels for the 2D ductile frame in Vancouver

Immediate Occupancy (IO)						Life Safety (LS)					
$V_{IO}$	$\Delta_{IO}$	$k_{eqIO}$	SRF <sub>IO</sub>	$\mu_{IO}$	$\zeta_{eqIO}$	$V_{LS}$	$\Delta_{LS}$	$k_{eqLS}$	SRF <sub>LS</sub>	$\mu_{LS}$	$\zeta_{eqLS}$
748.3	0.219	3416.7	0.324	3.25	22.01	801.6	0.438	1830.2	0.173	6.5	28.22

Unites are in kN, m

#### 4.3.1.2 Linear dynamic analysis

Two-dimensional equivalent linear model was created at IO performance level for the ductile frame in Vancouver. This model is similar to the linear model described in section 4.1 for the ductile frame in Vancouver, but its stiffness was reduced by applying  $SRF_{IOi}$  (see Table 4.2) to the moment inertia of all elements. Therefore, modal analysis was performed to define the new

modal periods (see 1<sup>st</sup> iteration in Table 4.5 for IO) because of stiffness reduction. The new values of modal periods were used to select and scale the synthetic ground motion of western Canada as given in Table 4.3. The value of viscous damping  $\zeta_{eqIOi}$  (see Table 4.2) is constant for all modes. The resulting roof displacement and base shear time histories were recorded as shown in Figure 4.9 when subjected to W6C1\_02.

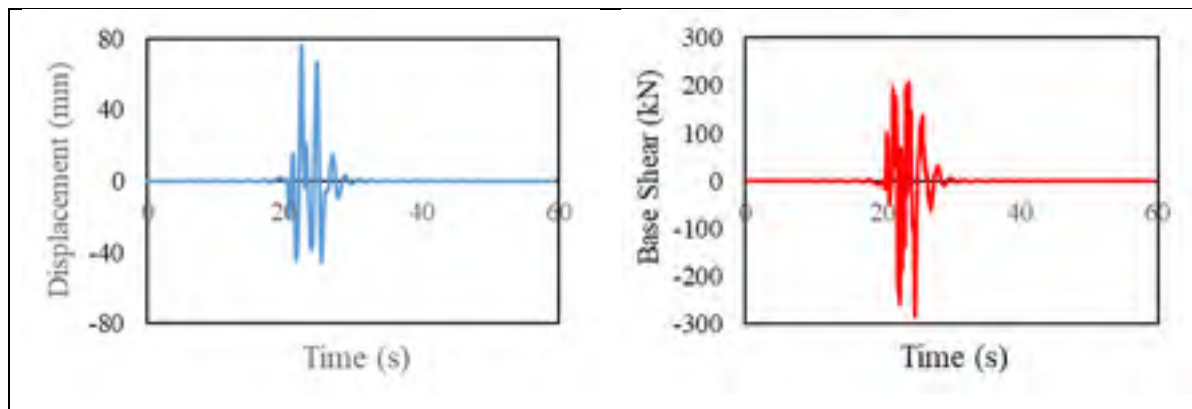


Figure 4.9 The roof displacement and base shear time histories obtained from the linear dynamic analysis of 2D ductile frame in Vancouver subjected to W6C1\_02 record, considering  $SRF_{IO}=0.324$ ,  $\zeta_{eqIO} = 22.01\%$

The maximum values of roof displacement and base shear obtained from each record are presented in Table 4.4 where the new values of  $k_{eqIO}$  are calculated using Equations 4.4 for each record of ground motion. The mean value of  $k_{eqIO}$  is divided by  $k_i$  (see Table 4.1) to determine the new value of  $SRF_{IO(i+1)}$  as shown in Table 4.5. The mean value of the maximum roof displacement is divided by  $\Delta_y$  (see Table 4.1) to calculate  $\mu$  and consequently compute  $\zeta_{eqIO(i+1)}$  using Equations 1.11 and 1.13. The difference between the new and initial values of stiffness reduction,  $(\Delta SRF / SRF_i)$  and equivalent damping  $(\Delta \zeta_{eq} / \zeta_{eqi})$  were calculated as shown in Table 4.5. The iteration procedure presented in this section was applied until the obtained  $\Delta SRF / SRF_i$  and  $\Delta \zeta_{eq} / \zeta_{eqi}$  reach around 10% as shown in Table 4.5.

Similar to the procedure followed for IO performance level, two-dimensional equivalent linear model was created at LS performance level for the ductile frame in Vancouver using SRFLS

and  $\zeta_{eqLS}$  (see Table 4.2). The used ground motion in the 1<sup>st</sup> iteration, mean values of  $k_{eqLS}$ , and results of iterations for the ductile frame in Vancouver at LS performance level are illustrated in Tables 4.3, 4.4 and 4.5, respectively.

Table 4.3 Ground motion records and scaling factors (SF) at IO and LS performance levels used in the 1<sup>st</sup> iteration for the ductile frame in Vancouver

	M	R (km)	duration (s)	Time step	IO		LS	
					record	SF	record	SF
1	6.5	12.0	49.305	0.005	W6C1_02	0.7922	W6C1_25	1.6057
		30.0	53.630		W6C1_17	1.2683	W6C1_24	1.1103
					W6C2_44	1.4742	W6C2_09	1.5454
					W6C2_20	1.5856	W6C2_44	1.5628
					W6C2_10	1.2354	W6C2_20	1.4524
2	7.5	25.0	102.025	0.005	W7C1_09	0.6663	W7C1_09	0.6663
		100.0	93.390		W7C1_31	0.7753	W7C1_31	0.7753
					W7C2_16	1.7112	W7C2_16	1.7112
					W7C2_15	1.7305	W7C2_15	1.7305
					W7C2_06	1.9126	W7C2_06	1.9126
3	9.0	360.8	309.42	0.010	W9C_15	1.6804	W9C_05	1.4049
					W9C_09	1.5514	W9C_09	1.6371
					W9C_03	1.2958	W9C_06	1.4654
					W9C_04	1.2906	W9C_04	1.3487
					W9C_22	1.7917	W9C_03	1.4777

Table 4.4 Mean values of maximum roof displacement, maximum base shear, and SRF at IO and LS performance level of the ductile frame in Vancouver

IO					LS				
Record	$\Delta_{IO}$	$V_{IOmax}$	$k_{eqIO}$	$SRF_{IO}$	Record	$\Delta_{LS}$	$V_{LSmax}$	$k_{eqLS}$	$SRF_{LS}$
W6c1_02	0.076	285.50	3740.78	0.355	W6c1_25	0.119	317.60	2664.61	0.253
W6c1_17	0.163	595.40	3647.10	0.346	W6c1_24	0.065	195.50	3014.79	0.286
W6c2_44	0.100	531.70	5308.14	0.503	W6c2_09	0.130	366.80	2829.00	0.268
W6c2_20	0.069	261.90	3795.21	0.360	W6c2_44	0.110	302.80	2745.51	0.260
W6c2_10	0.054	199.00	3693.94	0.350	W6c2_20	0.051	217.80	4287.74	0.406
W7c1_09	0.134	526.70	3923.66	0.372	W7c1_09	0.126	326.10	2587.87	0.245
W7c1_31	0.092	374.70	4085.93	0.387	W7c1_31	0.113	259.40	2286.59	0.217
W7c2_16	0.108	422.90	3914.94	0.371	W7c2_16	0.157	304.10	1932.06	0.183
W7c2_15	0.109	466.10	4291.15	0.407	W7c2_15	0.144	328.70	2280.11	0.216
W7c2_06	0.188	729.50	3880.20	0.368	W7c2_06	0.237	525.20	2220.20	0.210
W9c_15	0.180	790.80	4389.82	0.416	W9c_05	0.351	816.30	2325.08	0.220
W9c_09	0.184	705.00	3825.12	0.363	W9c_09	0.257	563.70	2190.42	0.208
W9c_03	0.221	904.80	4091.01	0.388	W9c_06	0.336	700.90	2083.04	0.197
W9c_40	0.139	626.80	4496.16	0.426	W9c_04	0.274	649.20	2372.54	0.225
W9c_22	0.183	717.60	3931.77	0.373	W9c_03	0.304	649.60	2134.54	0.202
<b>Mean</b>	<b>0.133</b>	<b>542.56</b>	<b>4067.66</b>	<b>0.386</b>	<b>Mean</b>	<b>0.185</b>	<b>434.91</b>	<b>2530.27</b>	<b>0.240</b>

Table 4.5 Iterations results at IO and LS performance levels for the ductile frame in Vancouver

PL	Iteration	SRF <sub>i</sub>	$\zeta_{eqi}\%$	T <sub>Bldg1</sub>	T <sub>Bldg2</sub>	$\Delta_{max}$	V <sub>max</sub>	$\mu$	k <sub>eq</sub>	SRF <sub>(i+1)</sub>	$\zeta_{eq(i+1)}\%$	$\Delta SRF/SRF_i$	$\Delta\zeta_{eq}/\zeta_{eqi}$
-	-	1.000	5.00	1.167	0.390	0.142	1469.34	-	10378.86	0.984	-	0.02	-
IO	1	0.324	22.01	2.018	0.676	0.133	542.56	1.98	4182.85	0.386	16.05	0.19	0.37
	2	0.386	16.05	1.852	0.620	0.143	659.53	2.12	4632.15	0.439	16.94	0.14	0.05
	3	0.439	16.94	1.739	0.582	0.131	680.28	1.94	5170.23	0.490	15.79	0.12	0.07
	4	0.490	15.79	1.648	0.552	0.127	736.60	1.89	5757.85	0.546	15.43	0.11	0.02
	5	0.546	15.43	1.563	0.523	0.122	787.63	1.81	6444.72	0.611	14.83	0.12	0.04
LS	1	0.173	28.22	2.752	0.922	0.185	434.91	2.75	2530.27	0.240	20.15	0.38	0.40
	2	0.240	20.15	2.336	0.783	0.167	529.01	2.49	3161.49	0.300	18.97	0.25	0.06
	3	0.300	18.97	2.096	0.702	0.149	578.12	2.22	3942.55	0.374	17.54	0.25	0.08
	4	0.374	17.54	1.881	0.63	0.139	628.11	2.06	4523.82	0.429	16.61	0.15	0.06
	5	0.429	16.61	1.758	0.589	0.134	679.41	1.98	5062.45	0.480	16.07	0.12	0.03
	6	0.480	16.07	1.664	0.557	0.128	701.31	1.90	5498.26	0.521	15.47	0.09	0.04
	7	0.521	15.47	1.599	0.535	0.125	772.34	1.85	6171.88	0.585	15.14	0.12	0.02

Units are kN, m, and second

### 4.3.2 Conventional construction frame in Vancouver

#### 4.3.2.1 Pushover analysis

The development of plastic hinges and acceptance criteria are shown in Figure 4.10. The rotational capacity of plastic hinges in the ground floor columns near the base of structure was reached before that of plastic hinges in most of beams, which means columns of frame are not stronger than beams at all joints.

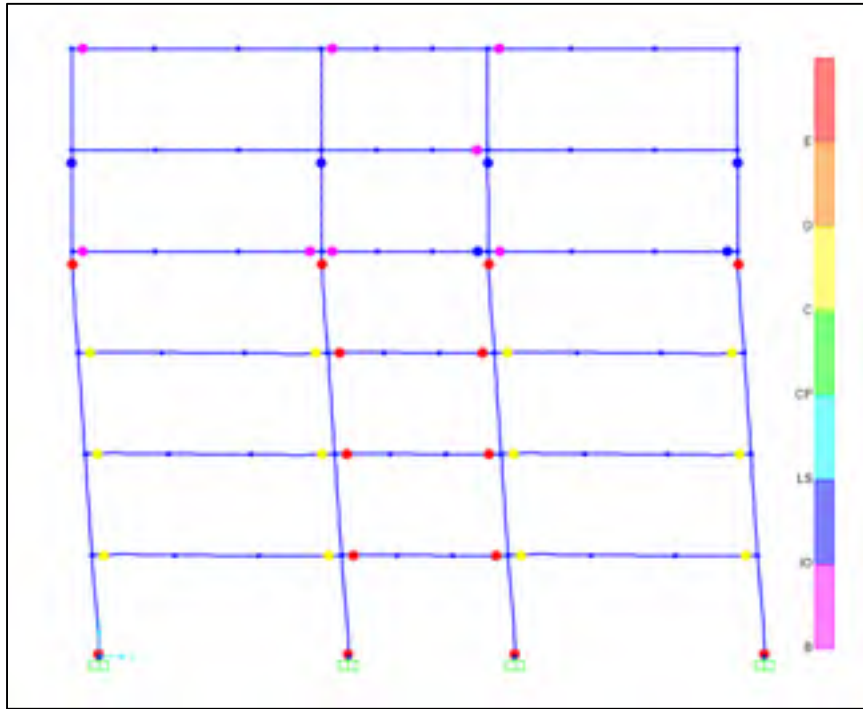


Figure 4.10 Hinges formation at the end of pushover analysis of conventional frame in Vancouver

Figure 4.11 presents the obtained pushover capacity curve and Table 4.6 presents  $V_y, \Delta_y, k_i$ , and  $k_e$  obtained from above procedure. Table 4.7 presents  $V, \Delta, k_{eq}$ , SRF, and  $\zeta_{eq}$  at IO and LS performance levels using the same procedure explained in section 4.3.1.1.



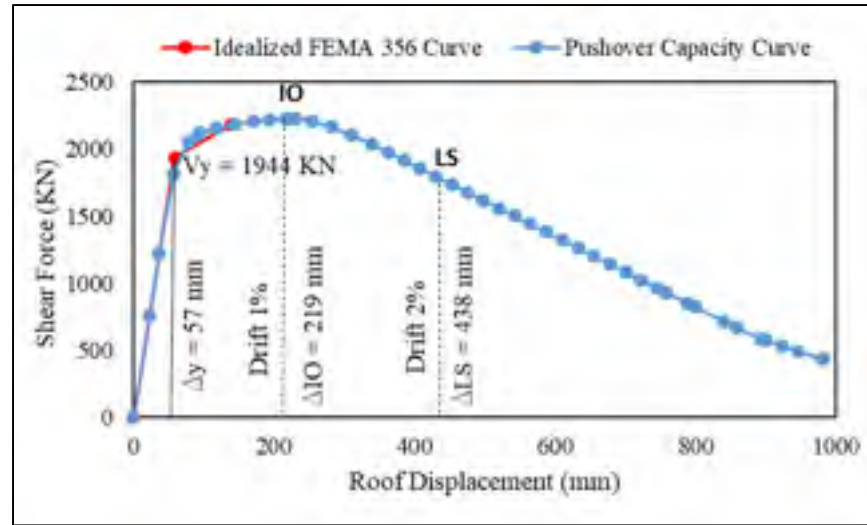


Figure 4.11 Computed pushover capacity curve of conventional frame in Vancouver

Table 4.6 Obtained parameters from idealized relationship of conventional construction frame in Vancouver

$V_y$ (kN)	$\Delta_y$ (mm)	$k_i$ (kN/m)	$k_e$ (kN/m)
1944.0	57.0	33840.75	33840.75

Table 4.7 Equivalent stiffness and stiffness reduction factors at IO and LS performance levels for the 2D conventional construction frame in Vancouver

Immediate Occupancy (IO)						Life Safety (LS)					
$V_{IO}$	$\Delta_{IO}$	$k_{eqIO}$	$SRF_{IO}$	$\mu_{IO}$	$\zeta_{eqIO}$	$V_{LS}$	$\Delta_{LS}$	$k_{eqLS}$	$SRF_{LS}$	$\mu_{LS}$	$\zeta_{eqLS}$
2230.7	0.219	10186	0.301	3.81	23.6	1778.1	0.438	4059.5	0.120	7.62	29.4

Units are in kN, m

#### 4.3.2.2 Linear dynamic analysis

The used ground motion in the 1<sup>st</sup> iteration, mean values of  $k_{eq}$  and SRF, and results of iterations for the conventional frame in Vancouver at IO and LS performance level are illustrated in Tables 4.8, 4.9, and 4.10, respectively.

Table 4.8 Used ground motion at IO and LS performance levels in the 1<sup>st</sup> iteration for the conventional construction frame in Vancouver

	M	R (km)	duration (s)	Time step	IO		LS	
					record	SF	record	SF
1	6.5	12.0	49.305	0.005	W6C1_02	0.7843	W6C1_02	0.7922
					W6C1_17	1.2690	W6C1_17	1.2683
					W6C1_27	1.1126	W6C1_06	1.4141
		30.0	53.630		W6C2_10	1.1884	W6C2_44	1.4742
					W6C2_44	1.5397	W6C2_20	1.5856
					W6C2_20	1.5415	W6C2_10	1.2354
2	7.5	25.0	102.025	0.005	W7C1_28	0.9255	W7C1_09	0.6663
					W7C1_31	0.7753	W7C1_28	0.9255
					W7C1_09	0.6663	W7C1_31	0.7753
		100.0	93.390		W7C2_16	1.7112	W7C2_16	1.7112
					W7C2_15	1.7305	W7C2_15	1.7305
					W7C2_06	1.9126	W7C2_06	1.9126
3	9.0	360.8	309.42	0.010	W9C_05	1.5883	W9C_09	1.6221
					W9C_07	1.6904	W9C_15	1.7478
					W9C_15	1.7452	W9C_03	1.3580
					W9C_08	1.7545	W9C_13	1.5530
					W9C_09	1.5781	W9C_04	1.3488

Table 4.9 Mean value of maximum roof displacement, maximum base shear, and SRF at IO and LS performance levels of the conventional construction frame in Vancouver

IO					LS				
Record	$\Delta_{IO}$	$V_{IOmax}$	$k_{eqIO}$	$SRF_{IO}$	Record	$\Delta_{LS}$	$V_{LSmax}$	$k_{eqLS}$	$SRF_{LS}$
W6c1_02	0.047	217.90	4610.66	0.136	W6c1_02	0.058	732.30	12578.15	0.372
W6c1_17	0.096	453.80	4732.01	0.140	W6c1_17	0.072	670.50	9333.24	0.276
W6c1_27	0.0638	397.00	6222.57	0.184	W6c1_06	0.1027	1164.00	11333.98	0.335
W6c2_10	0.031	144.60	4652.51	0.137	W6c2_44	0.038	382.90	10055.15	0.297
W6c2_44	0.062	402.10	6445.98	0.190	W6c2_20	0.055	765.80	14020.51	0.414
W6c2_20	0.040	208.50	5229.50	0.155	W6c2_10	0.069	709.80	10266.13	0.303
W7c1_28	0.078	544.10	6991.78	0.207	W7c1_09	0.062	747.60	12083.40	0.357
W7c1_31	0.049	255.00	5216.86	0.154	W7c1_28	0.062	638.40	10230.77	0.302
W7c1_09	0.119	495.90	4167.23	0.123	W7c1_31	0.087	958.90	11074.03	0.327
W7c2_16	0.062	318.60	5117.25	0.151	W7c2_16	0.090	886.20	9879.60	0.292
W7c2_15	0.066	315.00	4793.06	0.142	W7c2_15	0.092	1034.00	11192.90	0.331
W7c2_06	0.112	487.50	4341.05	0.128	W7c2_06	0.131	1297.00	9893.21	0.292
W9c_05	0.109	530.70	4873.28	0.144	W9c_09	0.099	1193.00	12076.12	0.357
W9c_07	0.116	609.40	5235.40	0.155	W9c_15	0.084	898.00	10629.73	0.314
W9c_15	0.137	693.50	5073.15	0.150	W9c_03	0.112	1187.00	10645.74	0.315
W9c_08	0.844	424.00	502.49	0.015	W9c_13	0.102	1135.00	11182.27	0.330
W9c_09	0.095	485.40	5108.40	0.151	W9c_04	0.098	1147.00	11690.96	0.345
<b>Mean</b>	<b>0.125</b>	<b>410.76</b>	<b>4900.77</b>	<b>0.145</b>	<b>Mean</b>	<b>0.083</b>	<b>914.55</b>	<b>11068.58</b>	<b>0.327</b>

Units are in kN, m

Table 4.10 Equivalents stiffness and damping iterations results at IO and LS performance levels for conventional construction frame in Vancouver

PL	Iteration	SRF <sub>i</sub>	$\zeta_{eqi}\%$	T <sub>Bldg1</sub>	T <sub>Bldg2</sub>	$\Delta_{max}$	V <sub>max</sub>	$\mu$	keq	SRF <sub>(i+1)</sub>	$\zeta_{eq(i+1)}\%$	$\Delta SRF/SRF_i$	$\Delta \zeta_{eq} / \zeta_{eqi}$
-	-	1.00	5.00	0.7025	0.223	0.054	1869.41	-	34420.57	1.017	-	0.02	-
IO	1	0.301	23.63	1.2476	0.397	0.083	914.55	1.45	11068.58	0.327	11.44	0.09	1.07
	2	0.327	11.44	1.198	0.381	0.098	1197.80	1.71	17145.39	0.507	14.02	0.55	0.18
	3	0.507	14.02	0.9690	0.308	0.079	1484.60	1.37	19035.10	0.562	10.57	0.11	0.33
	4	0.562	10.57	0.9223	0.2931	0.085	1706.47	1.47	19897.56	0.588	11.72	0.05	0.10
LS	1	0.120	29.36	1.962	0.624	0.125	410.76	2.18	4900.77	0.145	17.31	0.21	0.70
	2	0.145	17.31	1.818	0.578	0.093	532.70	1.63	5815.22	0.172	13.23	0.19	0.31
	3	0.172	13.23	1.642	0.522	0.095	645.34	1.66	6790.94	0.201	13.57	0.17	0.02
	4	0.201	13.57	1.521	0.484	0.086	670.25	1.49	7889.49	0.233	11.90	0.16	0.14
	5	0.233	11.90	1.414	0.450	0.084	730.92	1.47	8718.34	0.258	11.68	0.11	0.02

Units are kN, m, and second

### 4.3.3 Moderately ductile frame in Montreal

#### 4.3.3.1 Pushover analysis

The development of plastic hinges and acceptance criteria are shown in Figure 4.12. The rotational capacity of plastic hinges in the ground floor columns near the base of structure was reached after the plastic hinges in most of beams reach their rotational capacity, which means columns of frame are stronger than beams at most of joints.

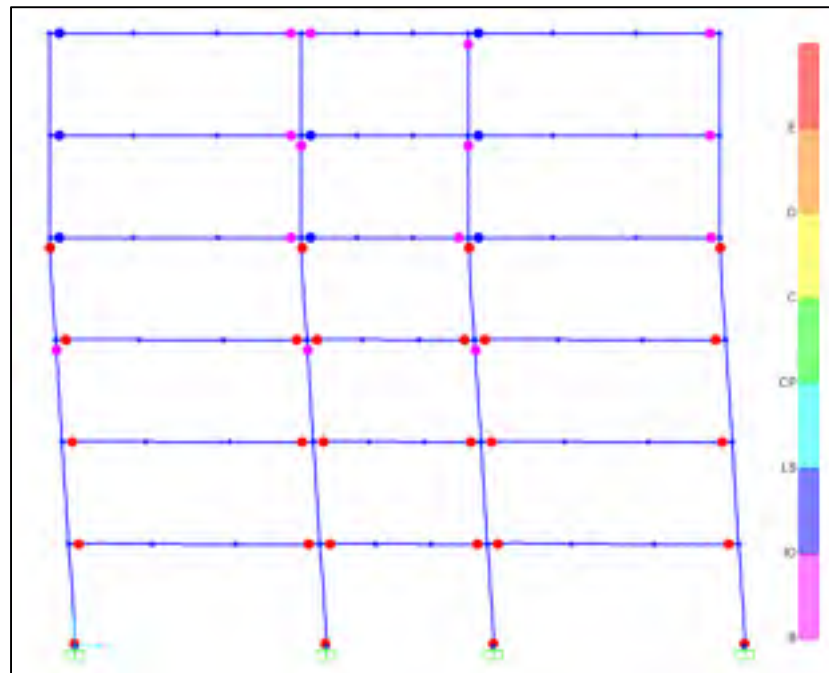


Figure 4.12 Hinges formation at the end of pushover analysis of moderately ductile frame in Montreal

Figure 4.13 presents the obtained pushover capacity curve and Table 4.6 presents  $V_y, \Delta_y, k_i$ , and  $k_e$  obtained from above procedure. Table 4.7 presents  $V, \Delta, k_{eq}$ , SRF, and  $\zeta_{eq}$  at IO and LS performance levels using the same procedure explained in section 4.3.1.1.

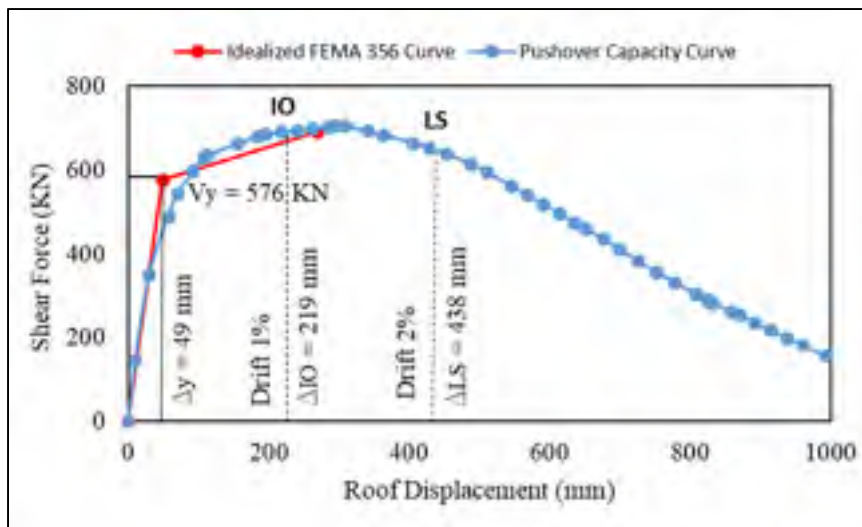


Figure 4.13 Computed pushover capacity curve of moderately ductile frame in Montreal

Table 4.11 Obtained parameters from idealized relationship of moderately ductile frame in Montreal

$V_y$ (kN)	$\Delta_y$ (mm)	$k_i$ (kN/m)	$k_e$ (kN/m)
576.3	48.8	17890.43	11799.87

Table 4.12 Equivalent stiffness and stiffness reduction factors at IO and LS performance levels for the 2D moderately ductile frame in Montreal

Immediate Occupancy (IO)						Life Safety (LS)					
$V_{IO}$	$\Delta_{IO}$	$k_{eqIO}$	$SRF_{IO}$	$\mu_{IO}$	$\zeta_{eqIO}$	$V_{LS}$	$\Delta_{LS}$	$k_{eqLS}$	$SRF_{LS}$	$\mu_{LS}$	$\zeta_{eqLS}$
690.1	0.219	3151	0.176	4.48	25.2	646.9	0.438	1477.0	0.083	8.97	30.4

Units are in kN, m

#### 4.3.3.2 Linear dynamic analysis

The used ground motion in the 1<sup>st</sup> iteration, mean values of  $k_{eq}$  and SRF, and results of iterations for the moderately ductile frame in Montreal at IO and LS performance level are illustrated in Tables 4.13 to 4.15.

Table 4.13 Used ground motion at IO and LS performance levels in the 1<sup>st</sup> iteration for the moderately ductile frame in Montreal

	M	R (km)	duration (s)	Time step	IO		LS	
					record	SF	record	SF
1	6.0	15.0	43.598	0.002	E6C1_07	0.5227	W6C1_07	0.5007
					E6C1_32	0.9115	W6C1_24	0.8645
					E6C1_42	1.0563	W6C1_32	0.8996
		30.0	47.530		E6C2_26	1.7345	W6C2_10	1.2445
					E6C2_33	1.7286	W6C2_15	1.1060
					E6C2_08	0.8809	W6C2_37	1.4107
2	7.0	25.0	51.126		E7C1_11	0.5612	W7C1_19	0.6057
					E7C1_19	0.5571	W7C1_25	0.6574
					E7C1_36	0.9363	W7C1_11	0.6396
		100.0	57.352		E7C2_01	1.4391	W7C2_44	2.154
					E7C2_02	1.6009	W7C2_01	1.4661
					E7C2_09	1.4704	W7C2_09	1.5884

Table 4.14 Mean value of maximum roof displacement, maximum base shear, and SRF at IO and LS performance levels of the moderately ductile frame in Montreal

<b>IO</b>					<b>LS</b>				
Record	$\Delta_{IO}$	$V_{IOmax}$	$k_{eqIO}$	$SRF_{IO}$	Record	$\Delta_{LS}$	$V_{LSmax}$	$k_{eqLS}$	$SRF_{LS}$
E6c1_07	0.030	166.20	5601.99	0.313	E6c1_07	0.020	104.60	5109.17	0.286
E6c1_42	0.042	202.20	4764.94	0.266	E6c1_24	0.026	180.50	6987.19	0.391
E6c1_32	0.027	198.90	7411.41	0.414	E6c1_32	0.024	135.50	5637.14	0.315
E6c2_33	0.030	172.20	5824.26	0.326	E6c2_10	0.017	82.11	4862.61	0.272
E6c2_10	0.023	145.00	6192.08	0.346	E6c2_15	0.031	103.00	3329.99	0.186
E6c2_26	0.025	132.50	5399.13	0.302	E6c2_37	0.024	82.19	3358.67	0.188
E7c1_06	0.089	340.60	3842.47	0.215	E7c1_19	0.113	184.30	1635.40	0.091
E7c1_11	0.066	252.00	3841.58	0.215	E7c1_25	0.090	181.10	2023.26	0.113
E7c1_19	0.111	291.90	2639.57	0.148	E7c1_11	0.088	168.60	1905.11	0.106
E7c2_09	0.277	884.10	3189.08	0.178	E7c2_44	0.510	1027.0	2012.19	0.112
E7c2_44	0.469	1393.0	2969.43	0.166	E7c2_01	0.237	475.60	2008.84	0.112
E7c2_01	0.163	581.70	3568.56	0.199	E7c2_09	0.461	824.60	1789.93	0.100
<b>Mean</b>	<b>0.113</b>	<b>396.69</b>	<b>4603.71</b>	<b>0.257</b>	<b>Mean</b>	<b>0.137</b>	<b>295.76</b>	<b>3388.29</b>	<b>0.189</b>

Units are in kN, m

Table 4.15 Equivalents stiffness and damping iterations results at IO and LS performance levels for moderately ductile frame in Montreal

PL	Iteration	SRF <sub>i</sub>	$\zeta_{eqi}\%$	T <sub>Bldg1</sub>	T <sub>Bldg2</sub>	$\Delta_{max}$	V <sub>max</sub>	$\mu$	keq	SRF <sub>(i+1)</sub>	$\zeta_{eq(i+1)}\%$	$\Delta SRF/SRF_i$	$\Delta \zeta_{eq} / \zeta_{eqi}$
-	-	1.00	5.00	1.034	0.339	0.083	1422.69	-	17528.12	0.980	-	0.02	-
IO	1	0.176	25.16	2.417	0.794	0.113	396.69	2.30	4603.71	0.257	18.04	0.46	0.39
	2	0.257	18.04	2.000	0.658	0.089	475.41	1.83	6092.74	0.341	14.93	0.32	0.21
	3	0.341	14.93	1.743	0.572	0.102	627.71	2.09	7115.67	0.398	16.77	0.17	0.11
	4	0.398	16.77	1.616	0.530	0.083	603.55	1.70	8106.83	0.453	13.91	0.14	0.21
	5	0.453	13.91	1.516	0.498	0.080	650.39	1.63	8601.33	0.481	13.29	0.06	0.05
LS	1	0.083	30.44	3.512	1.154	0.137	295.76	2.80	3388.29	0.189	20.37	1.29	0.49
	2	0.189	20.37	2.333	0.766	0.120	315.63	2.45	4464.30	0.250	18.82	0.32	0.08
	3	0.250	18.82	2.031	0.667	0.091	468.64	1.87	5894.01	0.329	15.26	0.32	0.23
	4	0.329	15.26	1.774	0.583	0.092	588.85	1.89	6954.34	0.389	15.42	0.18	0.01
	5	0.389	15.42	1.634	0.536	0.085	605.12	1.74	7970.84	0.446	14.24	0.15	0.08
	6	0.446	14.24	1.528	0.502	0.080	645.63	1.64	8492.62	0.475	13.40	0.07	0.06

Units are kN, m, and second



#### 4.3.4 Conventional construction frame in Montreal

##### 4.3.4.1 Pushover analysis

The development of plastic hinges and acceptance criteria are shown in Figure 4.14. The rotational capacity of plastic hinges in the ground floor columns near the base of structure was reached after the plastic hinges in beams did in the first three floors, which means columns of frame are not stronger than beams at all of joints.

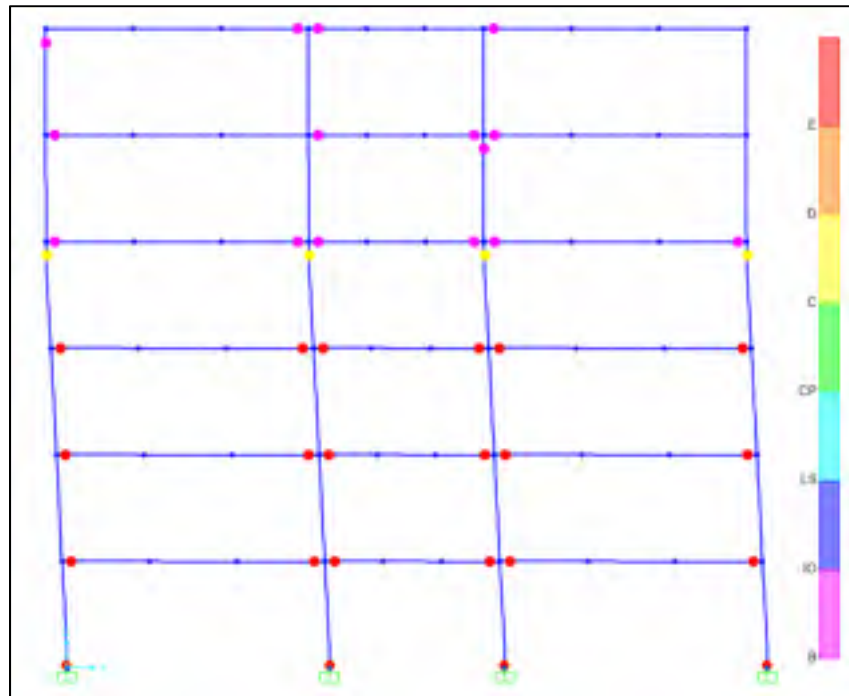


Figure 4.14 Hinges formation at the end of pushover analysis of conventional frame in Montreal

Figure 4.15 presents the obtained pushover capacity curve and Table 4.16 presents  $V_y, \Delta_y, k_i$ , and  $k_e$  obtained from above procedure. Table 4.17 presents  $V, \Delta, k_{eq}$ , SRF, and  $\zeta_{eq}$  at IO and LS performance levels using the same procedure explained in section 4.3.1.1.

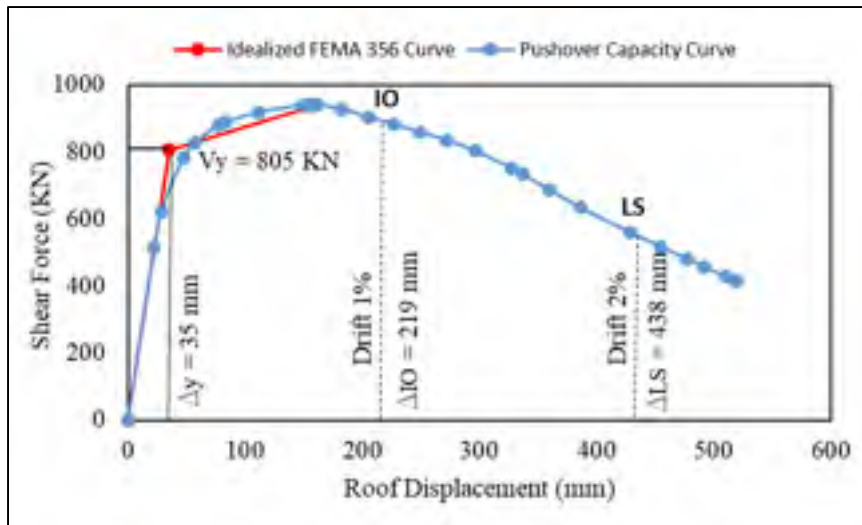


Figure 4.15 Computed pushover capacity curve of conventional frame in Montreal

Table 4.16 Obtained parameters from idealized relationship of conventional frame in Montreal

$V_y$ (kN)	$\Delta_y$ (mm)	$k_i$ (kN/m)	$k_e$ (kN/m)
805.34	35.1	22927.7	22927.7

Table 4.17 Equivalent stiffness and stiffness reduction factors at IO and LS performance levels for the 2D conventional frame in Montreal

Immediate Occupancy (IO)						Life Safety (LS)					
$V_{IO}$	$\Delta_{IO}$	$k_{eqIO}$	$SRF_{IO}$	$\mu_{IO}$	$\zeta_{eqIO}$	$V_{LS}$	$\Delta_{LS}$	$k_{eqLS}$	$SRF_{LS}$	$\mu_{LS}$	$\zeta_{eqLS}$
889.2	0.219	4060	0.177	6.23	27.9	544.45	0.438	1243.1	0.054	12.5	32.4

Units are in kN, m

#### 4.3.4.2 Linear dynamic analysis

The used ground motion in the 1<sup>st</sup> iteration, mean values of  $k_{eq}$  and SRF, and results of iterations for the moderately ductile frame in Montreal at IO and LS performance level are illustrated in Tables 4.18 to 4.20.

Table 4.18 Used ground motion at IO and LS performance levels in the 1<sup>st</sup> iteration for the conventional frame in Montreal

	M	R (km)	duration (s)	Time step	IO		LS	
					record	SF	record	SF
1	6.0	15.0	43.598	0.002	E6C1_07	0.5190	W6C1_07	0.5007
					E6C1_32	0.9063	W6C1_24	0.8645
					E6C1_42	1.0292	W6C1_32	0.8996
		30.0	47.530		E6C2_26	1.6903	W6C2_10	1.2445
					E6C2_08	0.8859	W6C2_15	1.1060
					E6C2_10	1.1956	W6C2_37	1.4107
2	7.0	25.0	51.126		E7C1_11	0.5612	W7C1_19	0.6057
					E7C1_19	0.5571	W7C1_25	0.6574
					E7C1_36	0.9363	W7C1_11	0.6396
		100.0	57.352		E7C2_01	1.4391	W7C2_44	2.1540
					E7C2_02	1.6009	W7C2_1	1.4661
					E7C2_09	1.4704	W7C2_9	1.5884

Table 4.19 Mean value of maximum roof displacement, maximum base shear, and SRF at IO and LS performance levels of the conventional frame in Montreal

<b>IO</b>					<b>LS</b>				
<b>Record</b>	$\Delta_{IO}$	$V_{IOmax}$	$k_{eqIO}$	$SRF_{IO}$	<b>Record</b>	$\Delta_{LS}$	$V_{LSmax}$	$k_{eqLS}$	$SRF_{LS}$
E6c1_07	0.031	177.00	5774.88	0.252	E6c1_07	0.021	81.77	3867.66	0.169
E6c1_32	0.026	212.90	8049.76	0.351	E6c1_24	0.026	115.90	4489.29	0.196
E6c1_42	0.042	222.20	5341.73	0.233	E6c1_32	0.024	100.50	4234.97	0.185
E6c2_26	0.023	134.30	5933.81	0.259	E6c2_10	0.017	64.27	3824.23	0.167
E6c2_08	0.014	128.80	9033.53	0.394	E6c2_15	0.031	87.79	2828.10	0.123
E6c2_10	0.024	143.00	5870.04	0.256	E6c2_37	0.024	64.30	2670.82	0.116
E7c1_11	0.052	274.80	5277.61	0.230	E7c1_19	0.105	161.10	1536.32	0.067
E7c1_19	0.082	379.70	4637.27	0.202	E7c1_25	0.080	154.60	1926.31	0.084
E7c1_36	0.059	389.10	6594.80	0.288	E7c1_11	0.082	136.30	1652.20	0.072
E7c2_01	0.124	601.20	4863.64	0.212	E7c2_44	0.461	854.50	1854.95	0.081
E7c2_02	0.178	1023.00	5731.16	0.250	E7c2_01	0.209	428.80	2050.66	0.089
E7c2_09	0.160	856.10	5347.18	0.233	E7c2_09	0.420	732.20	1744.91	0.076
<b>Mean</b>	<b>0.068</b>	<b>378.51</b>	<b>6037.95</b>	<b>0.263</b>	<b>Mean</b>	<b>0.125</b>	<b>248.50</b>	<b>2723.37</b>	<b>0.119</b>

Units are in kN, m

Table 4.20 Equivalent stiffness and damping iterations results at IO and LS performance levels for conventional frame in Montreal

PL	Iteration	SRF <sub>i</sub>	$\zeta_{eqi}\%$	T <sub>Bldg1</sub>	T <sub>Bldg2</sub>	$\Delta_{max}$	V <sub>max</sub>	$\mu$	keq	SRF <sub>(i+1)</sub>	$\zeta_{eq(i+1)}\%$	$\Delta SRF/SRF_i$	$\Delta \zeta_{eq} / \zeta_{eqi}$
-	-	1.00	5.00	0.818	0.275	0.079	1943.61	-	24009.45	1.05	-	0.05	-
IO	1	0.177	27.90	1.882	0.634	0.068	378.51	1.93	6037.95	0.263	15.73	0.49	0.77
	2	0.263	15.73	1.549	0.522	0.079	591.87	2.26	7714.92	0.336	17.78	0.28	0.12
	3	0.336	17.78	1.375	0.463	0.067	651.88	1.91	9241.74	0.407	15.57	0.21	0.14
	4	0.407	15.57	1.253	0.422	0.064	757.01	1.82	10961.11	0.478	14.87	0.17	0.05
	5	0.478	14.87	1.160	0.390	0.081	943.71	2.30	11974.52	0.522	17.99	0.09	0.17
	6	0.522	17.99	1.109	0.373	0.072	938.22	2.05	13640.15	0.595	16.51	0.14	0.09
	7	0.595	16.51	1.044	0.351	0.054	853.18	1.53	15933.05	0.695	12.32	0.17	0.34
LS	1	0.054	32.38	3.389	1.142	0.125	248.50	3.56	2723.37	0.119	22.95	1.19	0.41
	2	0.119	22.95	2.289	0.771	0.093	338.25	2.64	4201.33	0.183	19.67	0.54	0.17
	3	0.183	19.67	1.851	0.624	0.083	453.33	2.37	5872.60	0.256	18.40	0.40	0.07
	4	0.256	18.4	1.570	0.529	0.075	546.54	2.12	7625.18	0.333	16.98	0.30	0.08
	5	0.333	16.98	1.381	0.465	0.069	655.97	1.95	9222.69	0.402	15.85	0.21	0.07
	6	0.402	15.85	1.261	0.424	0.064	747.85	1.82	10845.47	0.460	14.87	0.14	0.07
	7	0.460	14.87	1.165	0.392	0.081	977.93	2.32	12198.98	0.532	18.10	0.16	0.18

Units are kN, m, and second

#### **4.4 Summary**

This chapter presented the modeling details of the performed linear and nonlinear dynamic analyses for the studied frames. In addition, the simplified method of Kothari et al. (2017) was applied to the studied frames which requires performing pushover analysis to all models. The output of the mentioned analyses will be presented and discussed in the next chapter.

## CHAPITRE 5

### RESULTS

This chapter presents the results of the linear and nonlinear dynamic analyses in order to fulfill the first and second objectives of this study, which are evaluating the effect of frame ductility and location on horizontal floor acceleration demands for NSCs. In addition, the results of applying the simplified method of Kothari et al. (2017) explained in section 4.3, and the equation proposed by NIST GCR 18-917-43 (2018) to determine the NSCs acceleration demands are evaluated and discussed. The factor  $A_r$  and FRS were plotted using component damping ratio equal to 5% which is the value stated by NBC (2015). The results obtained at the 2<sup>nd</sup> and 6<sup>th</sup> floor of frames are presented in this chapter while the results at the other floors are shown in Appendix IV.

#### 5.1 Evaluation the effect of ductility

##### 5.1.1 Height factor $A_x$

The mean values of the height factor were computed from both linear and nonlinear dynamic analyses as shown in Figure 5.1. We can note that the  $A_x$  factor has a linear trend with values ranging from 1.0 at the ground level to 2.0 and 2.5 at the roof level in the ductile and conventional construction frames in Vancouver, and 1.1 and 1.35 at the roof level in the moderately ductile and conventional construction frames in Montreal (Figure 5.1a). A reduction in the  $A_x$  factor is noted in the inelastic models (Figures 5.1b and 5.1c) in comparison with the elastic ones. The reduction in the  $A_x$  factor is larger when the ground motion with 2% per 50 years probability of exceedance is used as compared to the reduction when the ground motion with 10% per 50 years probability of exceedance is used. The whiplash phenomenon explained in section 1.3.1.1 was observed in the upper floors of all models. The results are in

a good agreement with the results of Petrone et al. (2015) in terms of value, form and whiplash phenomenon.

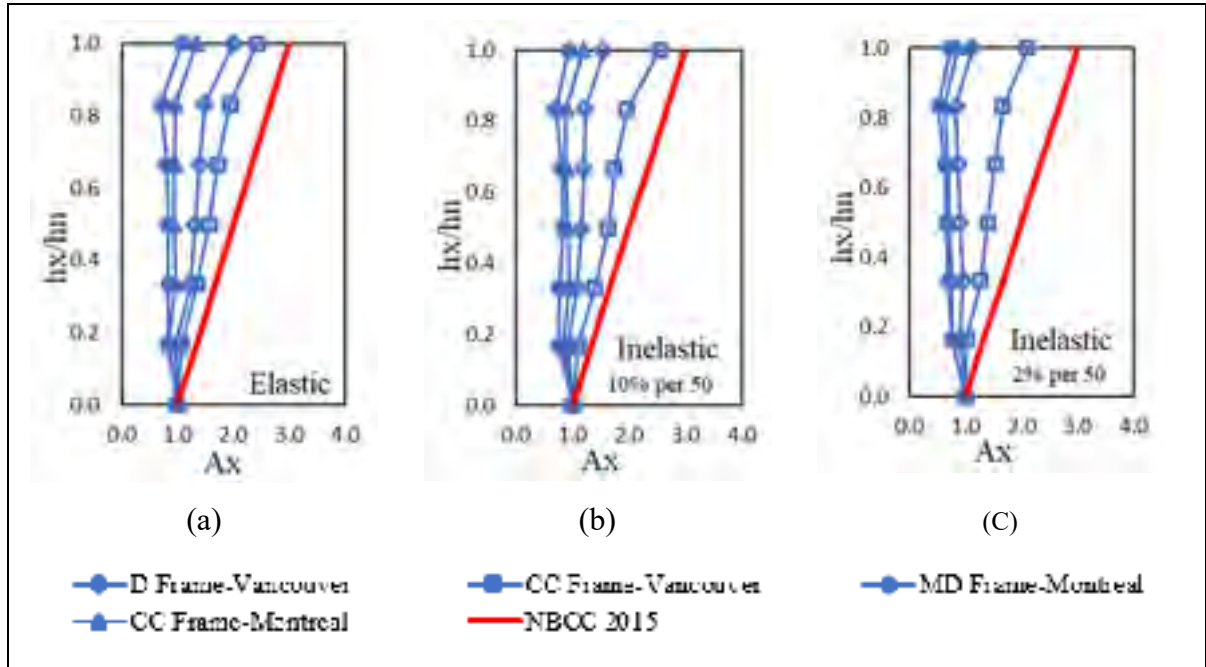


Figure 5.1 Computed mean  $A_x$  factor along the height of the studied buildings compared to NBC 2015 provision: (a) elastic analyses (b) inelastic analyses using ground motion with 10% per 50 years probability of exceedance, and (c) inelastic analyses using ground motion with 2% per 50 years probability of exceedance

In Figure 5.1, it is observed that both elastic and inelastic PFA/PGA ratios of conventional construction models in Montreal and Vancouver are larger than ratios of the ductile and moderately ductile models in Vancouver and Montreal. This is because the conventional construction models are more rigid than that the ductile or moderately ductile models, which leads to higher acceleration demands, which conforms with results found by Miranda and Taghavi (2009) and Shooshtari et al. (2010).

The continuous red line in Figure 5.1 represents distribution of  $A_x$  along  $h_x/h_n$  according to NBC 2015. In the elastic range, this distribution is in a good agreement with results obtained for frames in Vancouver while it is conservative in Montreal. On the other hand, the NBC distribution is conservative for all models when the frame models are inelastic. A linear

distribution that ranges from 1.0 at the base of the structure to 2.5 and 2.0 at the top would better fit the results when the frame models are inelastic using ground motion with 10% and 2% probability of exceedance per 50 years, respectively.

### 5.1.2 Floor response spectra (FRS)

Figures 5.2 and 5.3 presents the mean elastic and inelastic FRS generated for the studied models at the 2<sup>nd</sup> and 6<sup>th</sup> floor levels, respectively. Results for other intermediate floors are presented in Appendix IV.

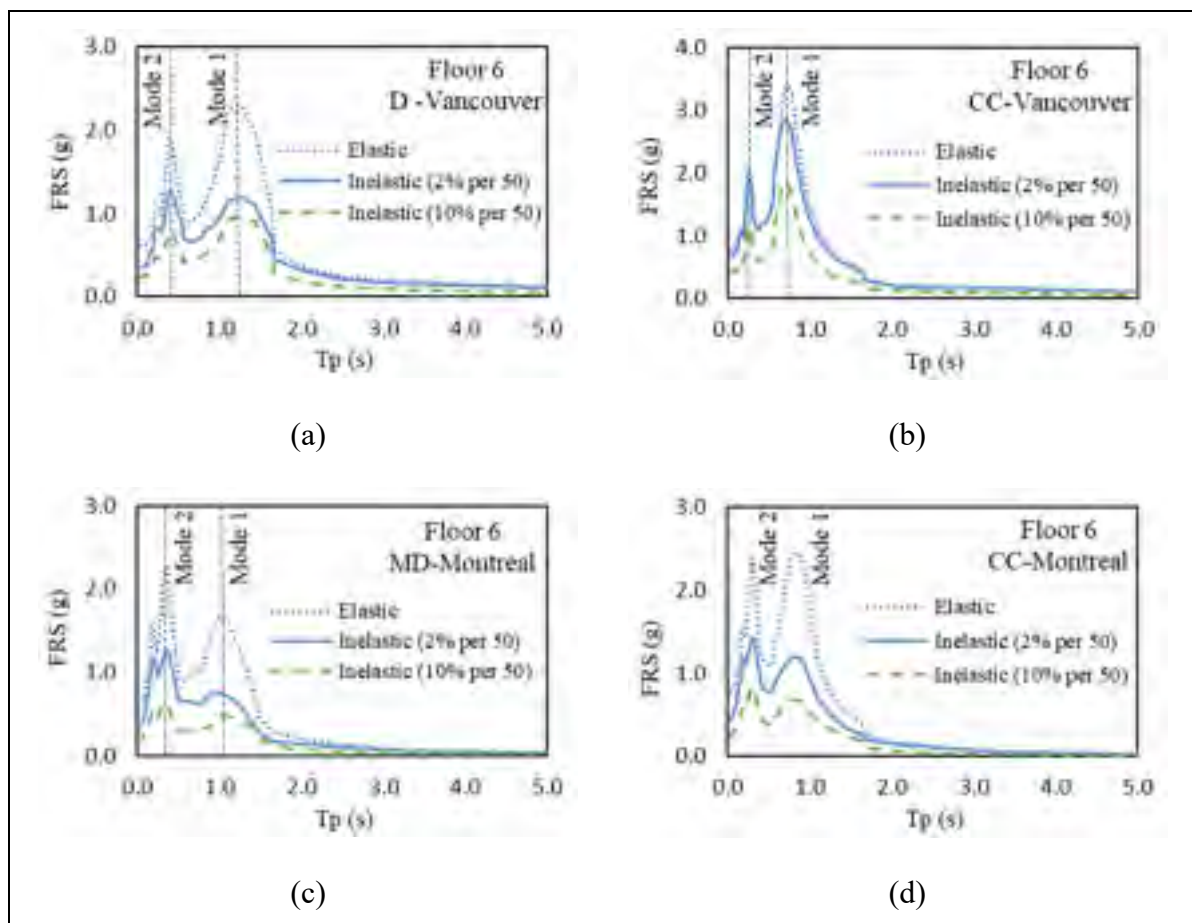


Figure 5.2 Effect of building ductility on the roof level mean FRS with component damping ratio 5%



It is observed that the mean elastic and inelastic FRS of each frame model have the same shape, but with a reduction in the FRS ordinates of the inelastic models with respect to the elastic ones, which complies with the results of Petrone et al. (2015) and Surana et al. (2016). The ordinates values of the mean FRS of the ductile frame in Vancouver and moderately ductile frame in Montreal are in a good agreements in terms of value and form with the ones presented by Shooshtari et al. (2010) for -5 floor RC ductile frame in Vancouver and -5 floor RC moderately ductile frame in Ottawa. It is noted that the effect of frame ductility is more significant around the frame modal periods  $T_{Bldg1}$  and  $T_{Bldg2}$  (Figures 5.2 and 5.3). At the roof level of all frame models, the reduction in the component acceleration is more pronounced around  $T_{Bldg1}$  than  $T_{Bldg2}$ , and vice versa in the 2<sup>nd</sup> floor. Similar observation were reported by Medina et al. (2006).

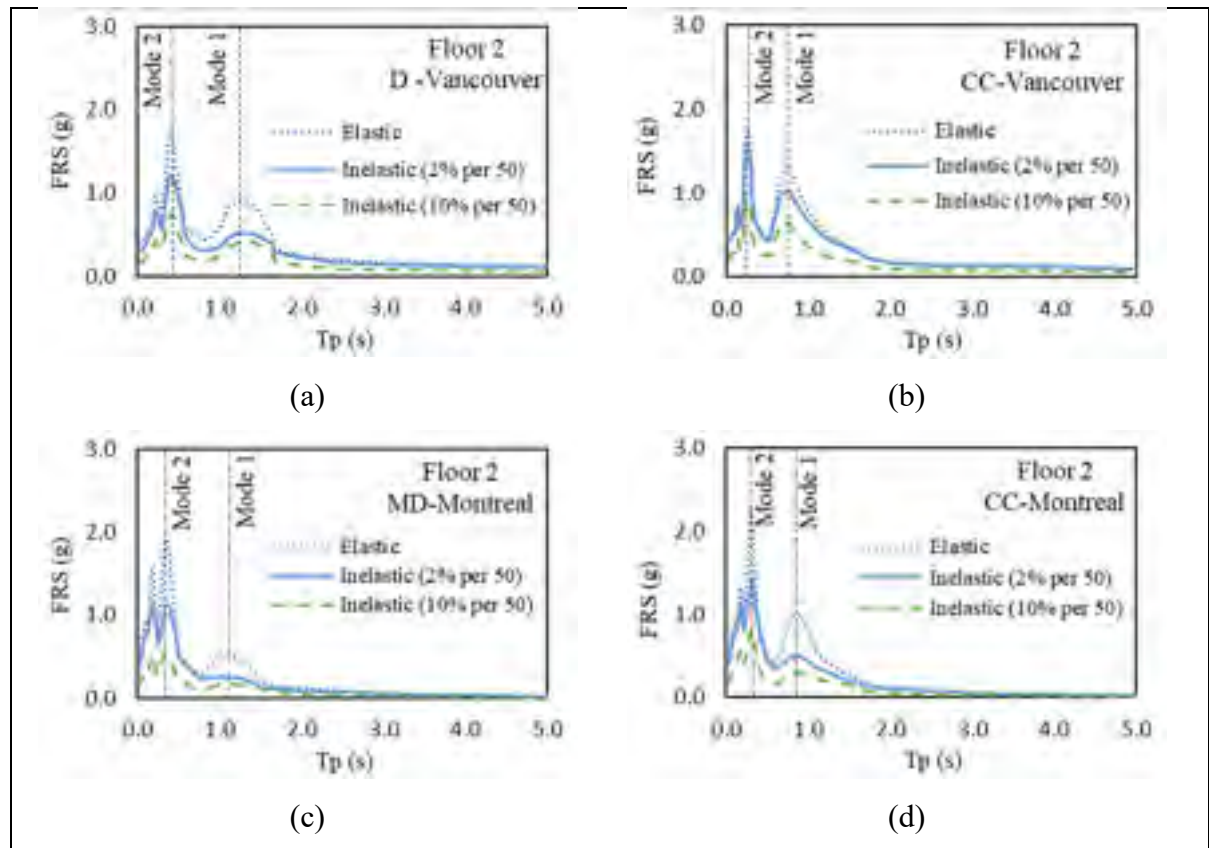


Figure 5.3 Effect of building ductility on the 2<sup>nd</sup> floor mean FRS with component damping ratio 5%

In order to evaluate the effect of frame ductility in reducing the FRS, the parameter  $R_{cb}$  that represents the ratios of mean FRS of the elastic to the one of inelastic frame models were computed in the roof and second floors and plotted in Figure 5.4. This means that a value of  $R_{cb} > 1.0$  implies that frame ductility reduces PCA response.

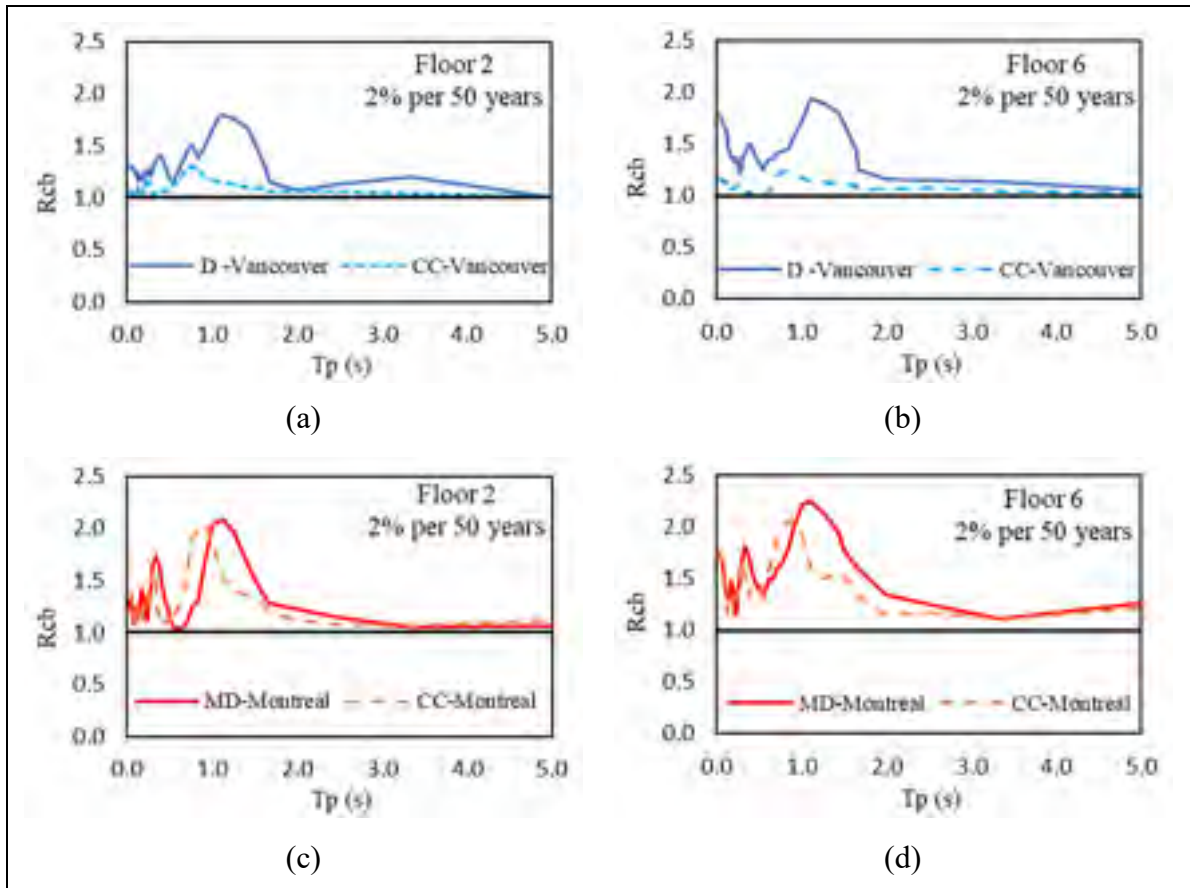


Figure 5.4 Effect of building ductility on the amplitudes of mean FRS in the 2nd and 6th floor for component damping ratio 5% and ground motion with 2% per 50 years probability of exceedance

It is observed in this figure that  $R_{cb}$  is above 1.0 for both floor levels in all the frame models. In the roof level (Figure 5.4b), the frame ductility reduces PCA in the ductile frame in Vancouver by a factor of 2.0 and 1.4 compared to an elastic version of the same frame model at  $T_{Bldg1}$  and  $T_{Bldg2}$ , respectively. However, in the conventional construction frame model in

Vancouver, the benefit of frame ductility in reducing NSCs demands is less, where PCA is reduced by a factor 1.25 and 1.15 compared to an elastic frame model at  $T_{Bldg1}$  and  $T_{Bldg2}$ , respectively. Similarly in Figure 5.4d, PCA was reduced by a factor 2.25 and 1.8 in the moderately ductile frame in Montreal, and a factor 2.0 and 1.5 in the conventional construction frame in Montreal compared to an elastic frame model at  $T_{Bldg1}$  and  $T_{Bldg2}$ , respectively.

Figures 5.5 and 5.6 compare  $R_{cb}$  using ground motion with 2% per 50 years probability of exceedance with the one using ground motion with 10% per 50 years probability of exceedance for all the studied frames at the 2<sup>nd</sup> and 6<sup>th</sup> floor level, respectively.

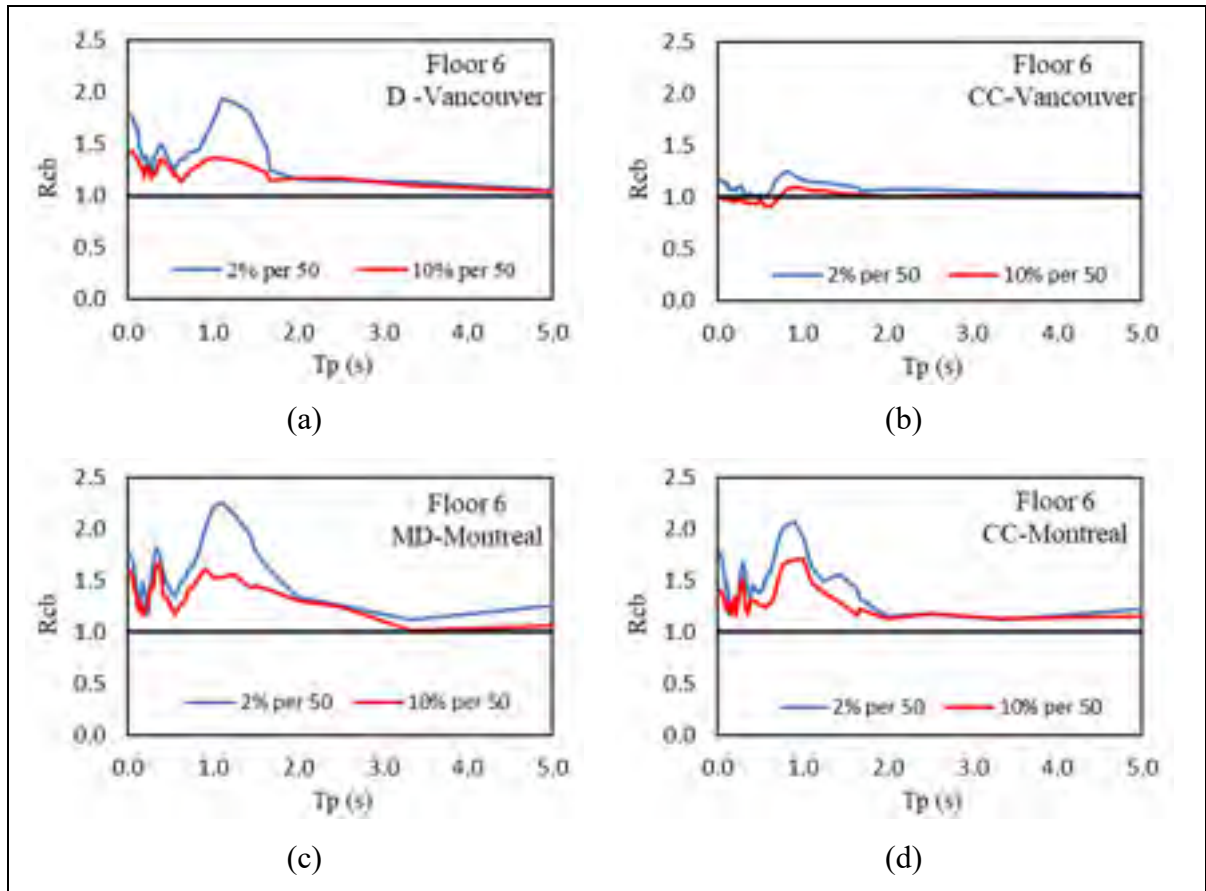


Figure 5.5 Effect of ground motion level on  $R_{cb}$  factor in the 6<sup>th</sup> floor of the studied frames using component damping ratio 5%

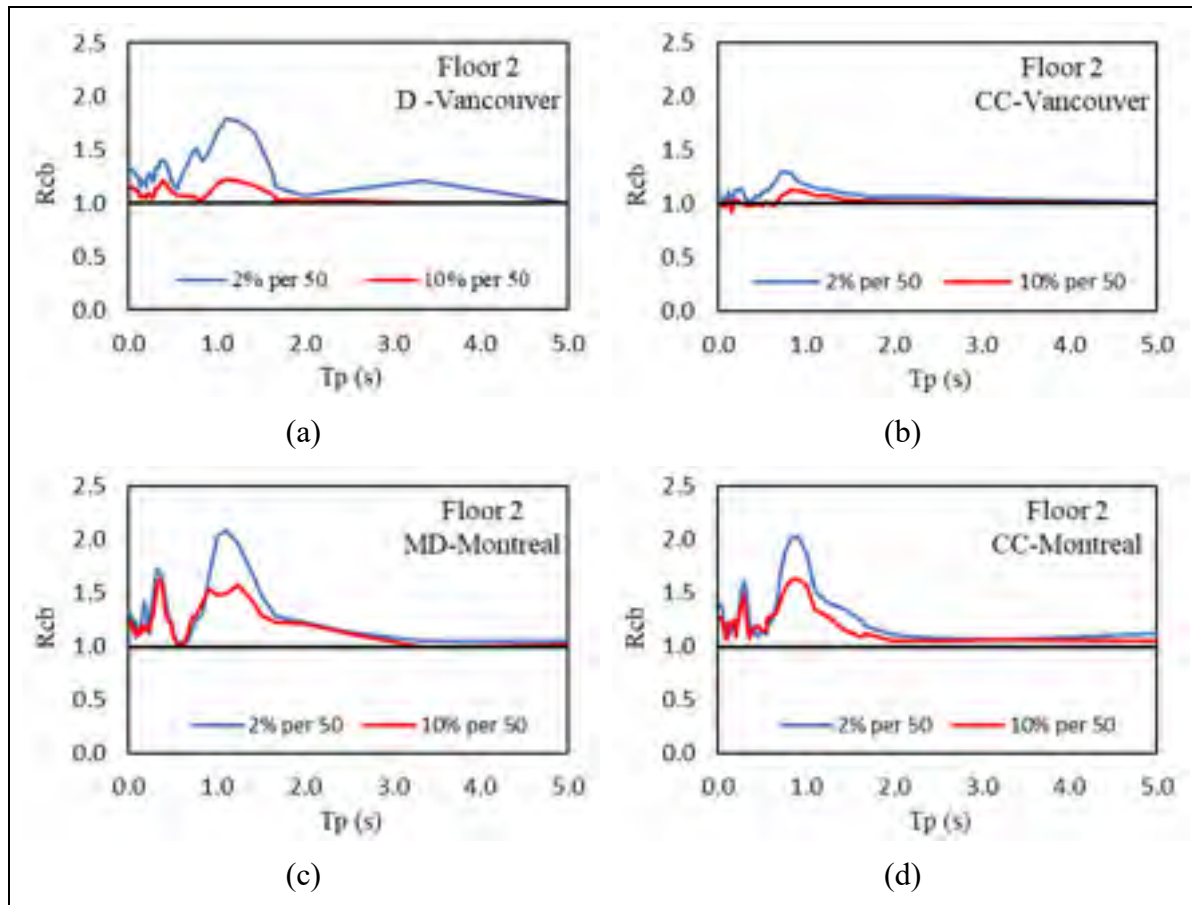


Figure 5.6 Effect of ground motion level on  $R_{cb}$  factor in the 2<sup>nd</sup> floor of the studied frames using component damping ratio 5%

It is noted that  $R_{cb}$  values obtained using ground motion with 10% per 50 years probability of exceedance is less than those obtained using ground motion with 2% per 50 years probability of exceedance is used. This means the reduction in the component accelerations mounted on inelastic structures depends on the level of yielding that the building experiences.

The computed mean inelastic FRS of the ductile and conventional construction frames in Vancouver were compared in Figures 5.7a and 5.7b.

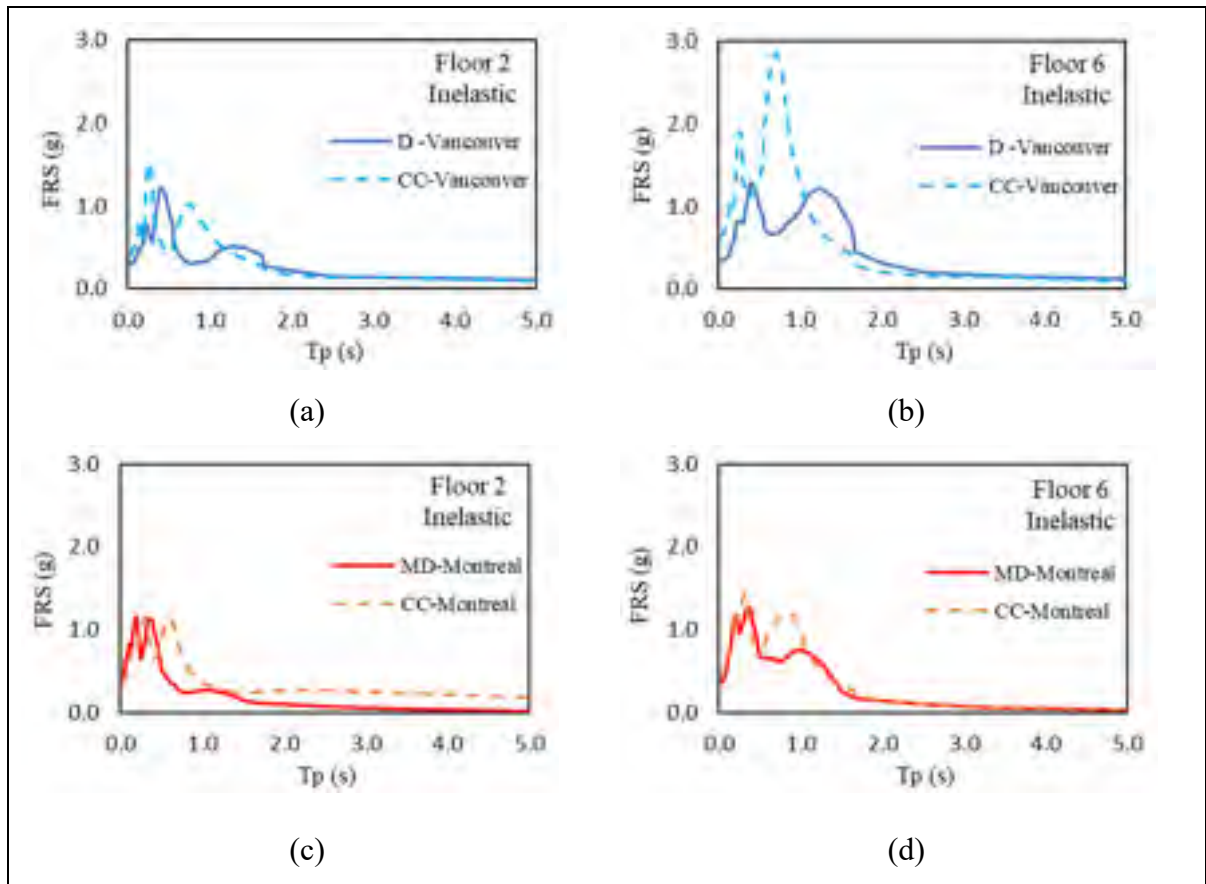


Figure 5.7 Effect of building ductility on the shape of mean FRS in the 2<sup>nd</sup> and 6<sup>th</sup> floors for component damping ratio 5%

It can be noted that the peaks of the FRS of the conventional construction frame are larger and happen earlier than those of the ductile frame in Vancouver (Figures 5.7 a and 5.7b). Similar observations were made for the moderately ductile and conventional construction frame in Montreal (Figure 5.7c and 5.7d). This is due to the fact that the conventional construction frames are more rigid than the ductile and moderately ductile frames.

### 5.1.3 Component amplification factor, $A_r$

The mean values of  $A_r$  factor versus  $T_p$  normalized to  $T_{Bldg1}$  for the elastic and inelastic case of study models in Montreal and Vancouver are presented in Figures 5.8 and 5.9 for the 2<sup>nd</sup> and

the roof ( $6t^h$ ) levels, respectively. A significant amplification in  $A_r$  value is observed when  $T_p$  matches one of the building periods.

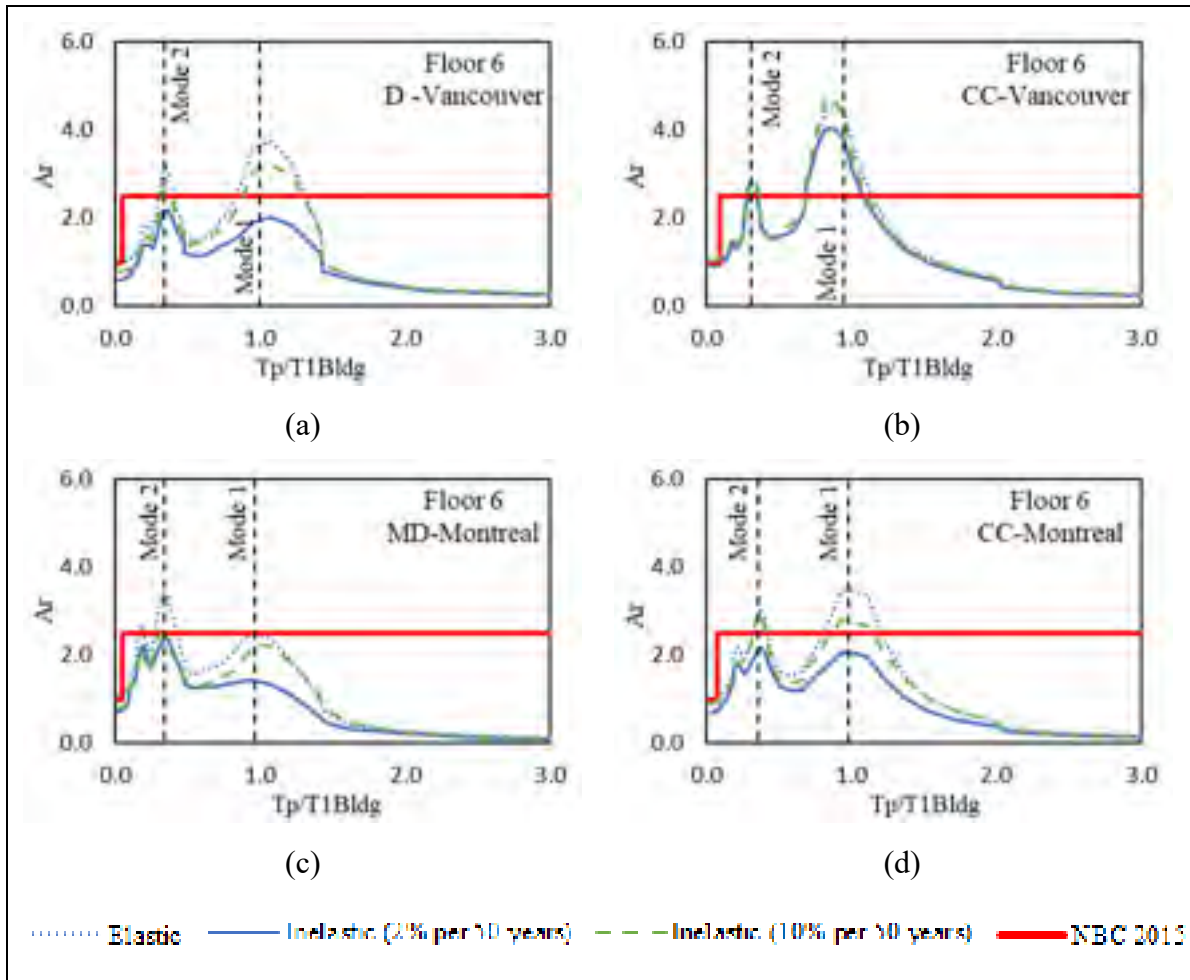


Figure 5.8 Effect of building ductility on  $A_r$  in the 6<sup>th</sup> floor for component damping ratio 5%



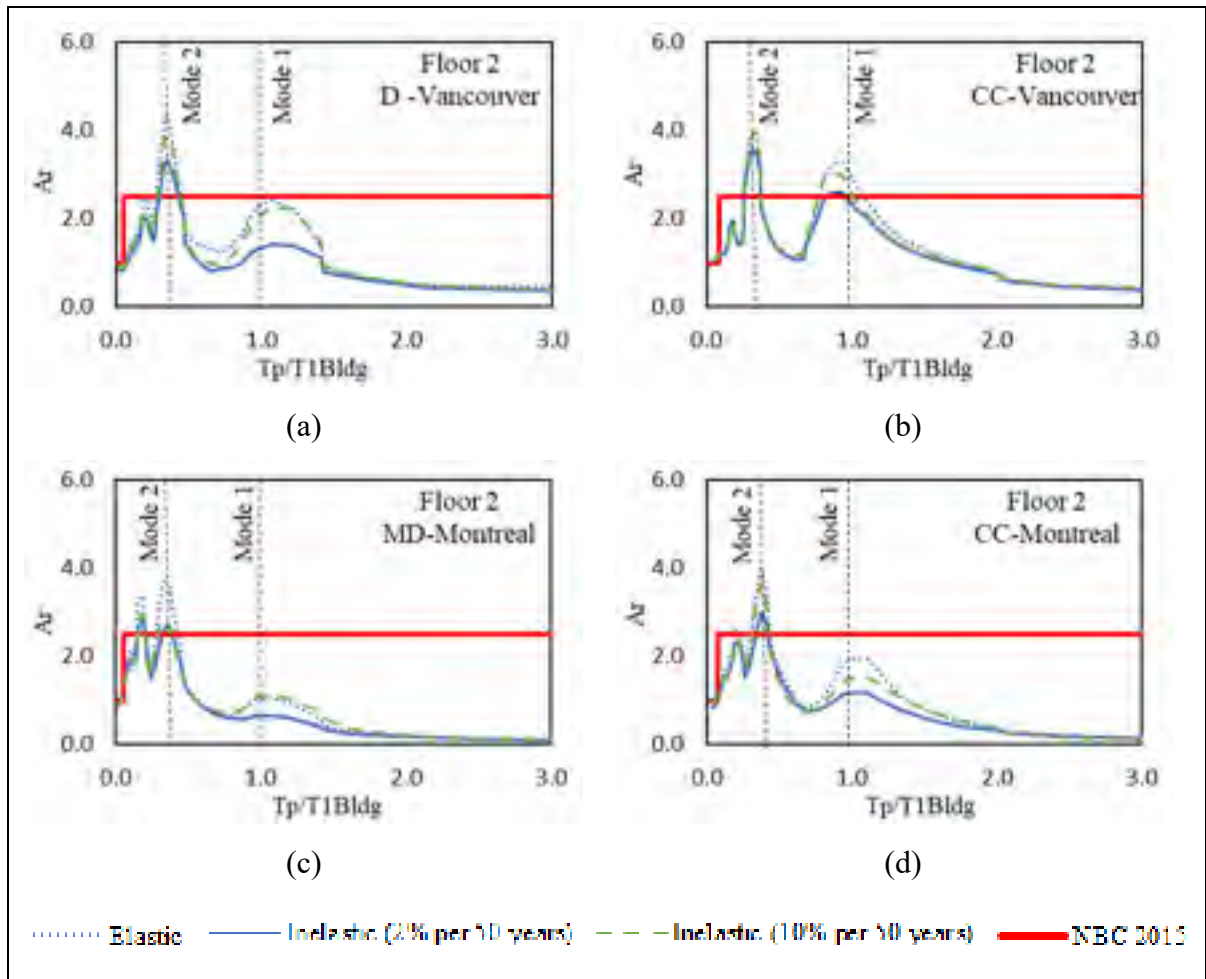


Figure 5.9 Effect of building ductility on  $A_r$  in the 2<sup>nd</sup> floor for component damping ratio 5%

It is noted that the recommended values of  $A_r$  by NBC 2015 (represented by red lines) are underestimated when the studied buildings are elastic. When the studied buildings are inelastic, the values of  $A_r$  proposed by NBC 2015 are also underestimated, but to a lesser extent, except the roof level of the moderately ductile buildings in Montreal.

The mean values of  $A_r$  factor versus the building height are plotted in Figure 5.10. It is observed in this figure that the  $A_r$  factors are almost constant in the lower part of the building, and there is an increase in values in the upper floors, especially for CC frame in Vancouver. According to Figure 5.10, it is recommended to use an  $A_r$  factor equal to 4.0 for all floor levels in the elastic RC moment resisting frames in Montreal and 5.0 in Vancouver. Same values are

suggested for the inelastic models when the ground motions at 10% per 50 years probability of exceedance are used. On the other hand, an  $A_r$  factor equals to 3.0 is recommended for frames in Montreal and 4.0 for those in Vancouver when the ground motion when subjected to ground motion with 2% per 50 years probability of exceedance. These values are in a good agreement with the suggested values in Fathali and Lizundia (2011) and Petrone et al. (2015) mentioned in section 1.4.2, and NIST GCR 18-917-43 (2018) mentioned in section 1.3.2.

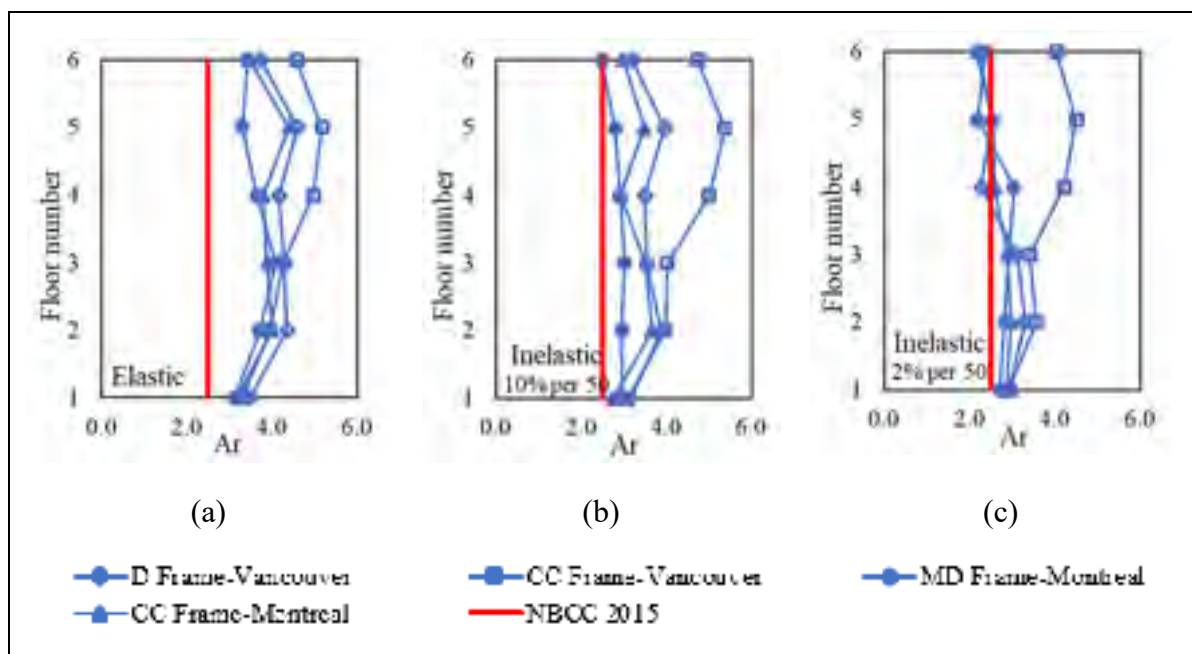


Figure 5.10 Computed mean  $A_r$  factor along the height of the studied buildings compared to NBC 2015 provision: (a) elastic analyses (b) inelastic analyses using ground motion with 10% per 50 years probability of exceedance, and (c) inelastic analyses using ground motion with 2% per 50 years probability of exceedance

## 5.2 Effect of building location

The mean inelastic FRS at each floor for the -6 floors frame models in Vancouver and Montreal are presented in Figures 5.11 and 5.12, respectively. It is observed that a progressive increase in response going from the first floor to upper floors. Higher amplifications are noted for frame models in Vancouver, which were subjected to stronger ground motions relative to those in



Montreal. An amplification of approximately a factor of 4.0 and 5.0 for the roof response relative to that of the first-storey for the ductile and conventional construction frames, respectively is observed in Vancouver. However this amplification factor was approximately 3.0 and 3.5 for the moderately ductile and conventional construction frames in Montreal. The UHS for Vancouver and Montreal cities are included also in Figures 5.11 and 5.12, respectively to depict the amount of amplification resulted at each floor relative to ground. It is observed that UHS in Vancouver can be used as representative of FRS in the first floor for design while the UHS in Montreal is less than the FRS in the first floor.

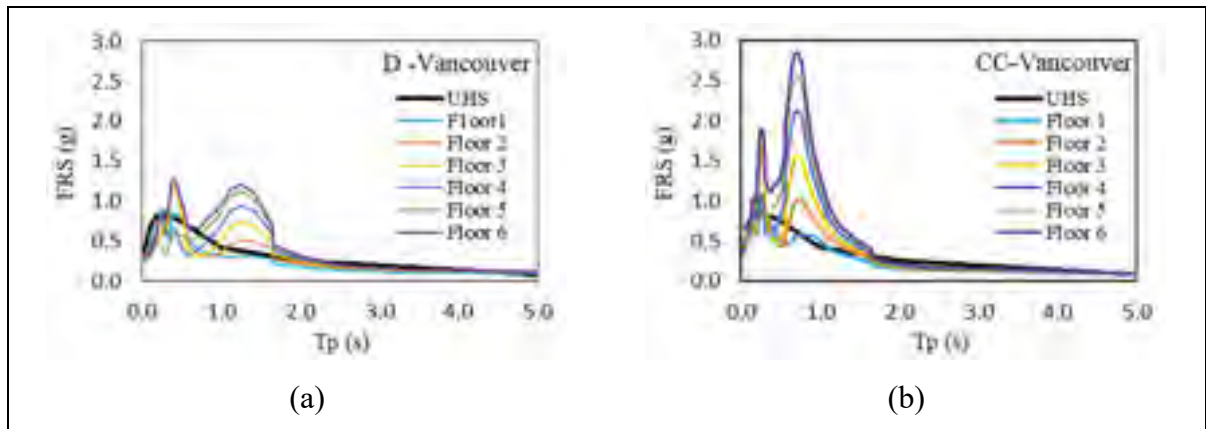


Figure 5.11 Mean inelastic FRS at each floor for ductile and conventional studied buildings in Vancouver

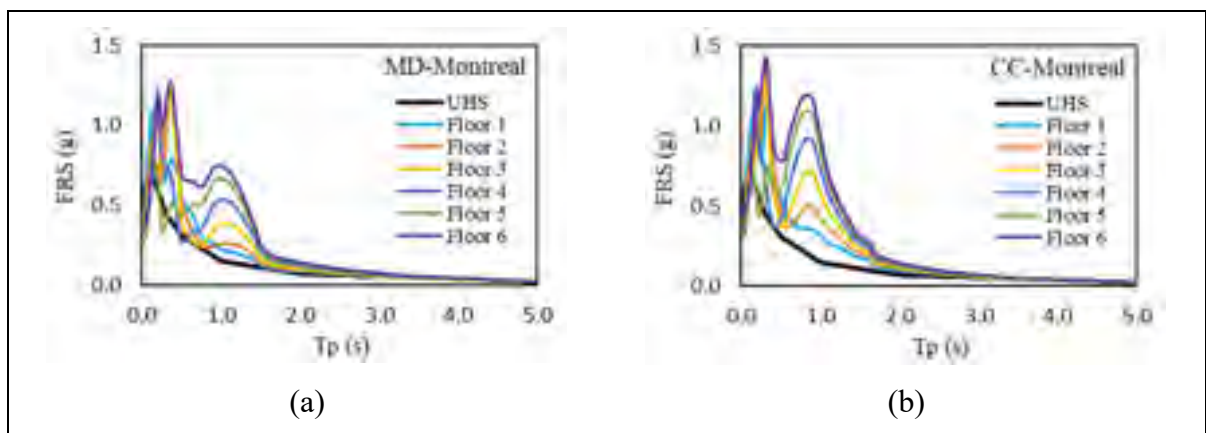


Figure 5.12 Mean inelastic FRS at each floor for moderately ductile and conventional studied buildings in Montreal

### 5.3 Evaluation the simplified method of Kothari et al. (2017)

In this section, results of simplified method of Kothari et al. (2017) in terms of height factor  $A_x$  and FRS are plotted at IO and LS performance levels. The results at IO performance level are compared with those of nonlinear dynamic analysis using ground motions at 10% per 50 years probability of exceedance while the results at LS performance level are compared with those of nonlinear dynamic analysis using ground motions at 2% per 50 years probability of exceedance.

#### 5.3.1 Height factor $A_x$

Figure 5.13 presents the mean  $A_x$  factor along the relative height of the studied buildings obtained from the simplified method at performance levels IO and LS compared to the one obtained from the nonlinear dynamic analysis.

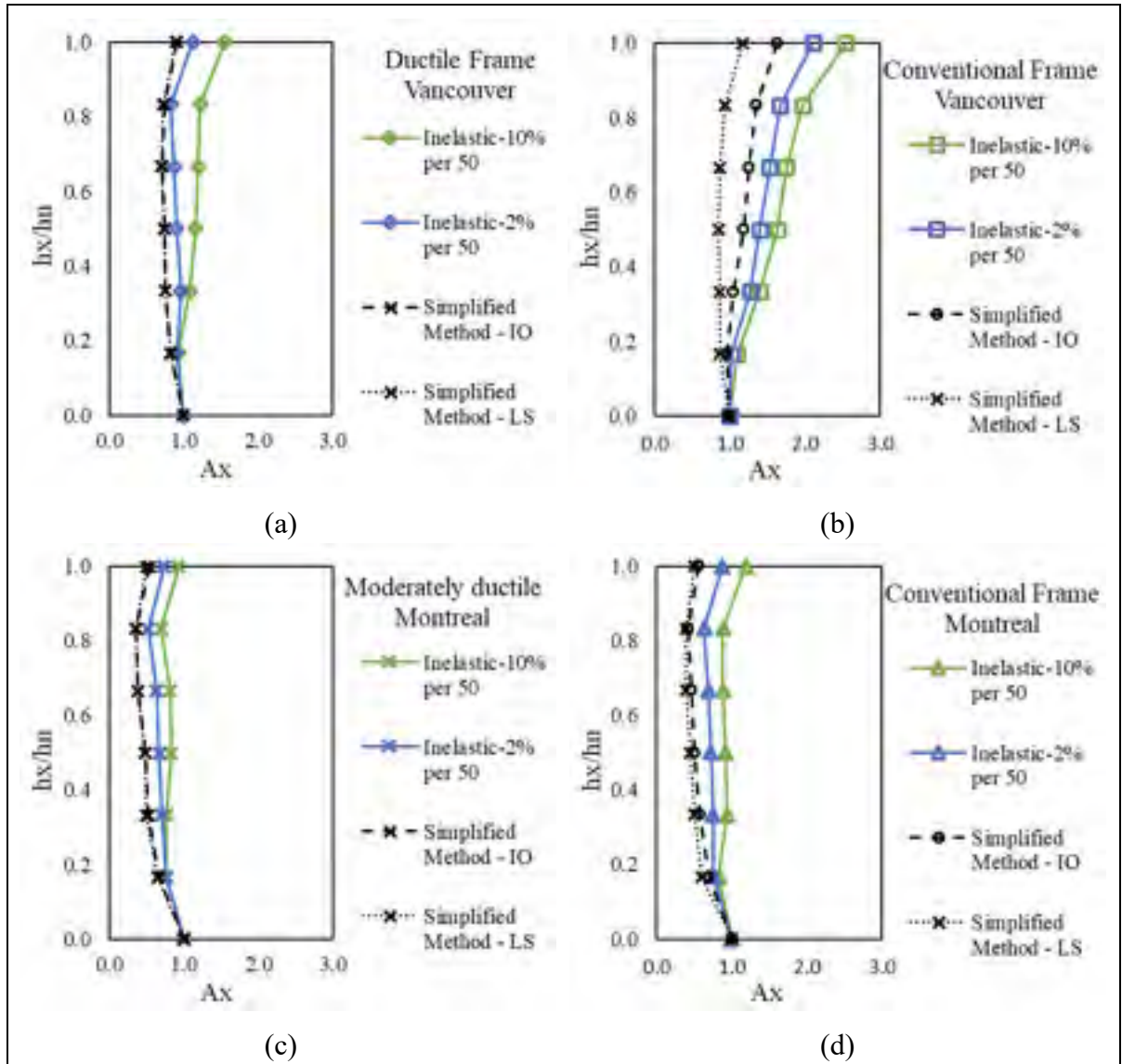


Figure 5.13 Mean PFA/PGA ratio along the height of the case of study buildings obtained from the Kothari's simplified method at IO and LS performance levels and the nonlinear dynamic analysis: (a) ductile frame in Vancouver, (b) conventional frame in Vancouver, (c) moderately ductile frame in Montreal, and (d) conventional frame in Montreal

It is observed that the mean  $A_x$  factor along the relative height  $h_x/h_n$  obtained from the simplified method at IO and LS has a constant trend except for the conventional frame in Vancouver where  $A_x$  factor has a linear trend. Additionally, the whiplash phenomenon at the roof level is observed for all the studied buildings.

In the ductile and moderately ductile frames, no difference was observed between the  $A_x$  profile at IO and at LS (Figure 5.13a and 5.13c). In the conventional construction frames, the profile  $A_x$  ranges from 1.0 at the ground level to 1.63 and 1.18 at IO and LS, respectively in Vancouver. While it ranges from 1.0 to 0.5 and 0.6 at IO and LS, respectively in Montreal (Figure 5.13b and 5.13d). In general, the simplified method succeeded in predicting the shape of the  $A_x$  profile along the relative height. However, the results obtained from the simplified method underestimates the values of  $A_x$  profile as compared to those obtained from the nonlinear dynamic analyses.

### 5.3.2 Floor response spectra (FRS)

Figures 5.14 and 5.15 present the mean FRS obtained from the simplified method of Kothari et al. (2017) for the studied frame models compared to those obtained from the nonlinear dynamic analysis at the 6<sup>th</sup> and 2<sup>nd</sup> floor levels.

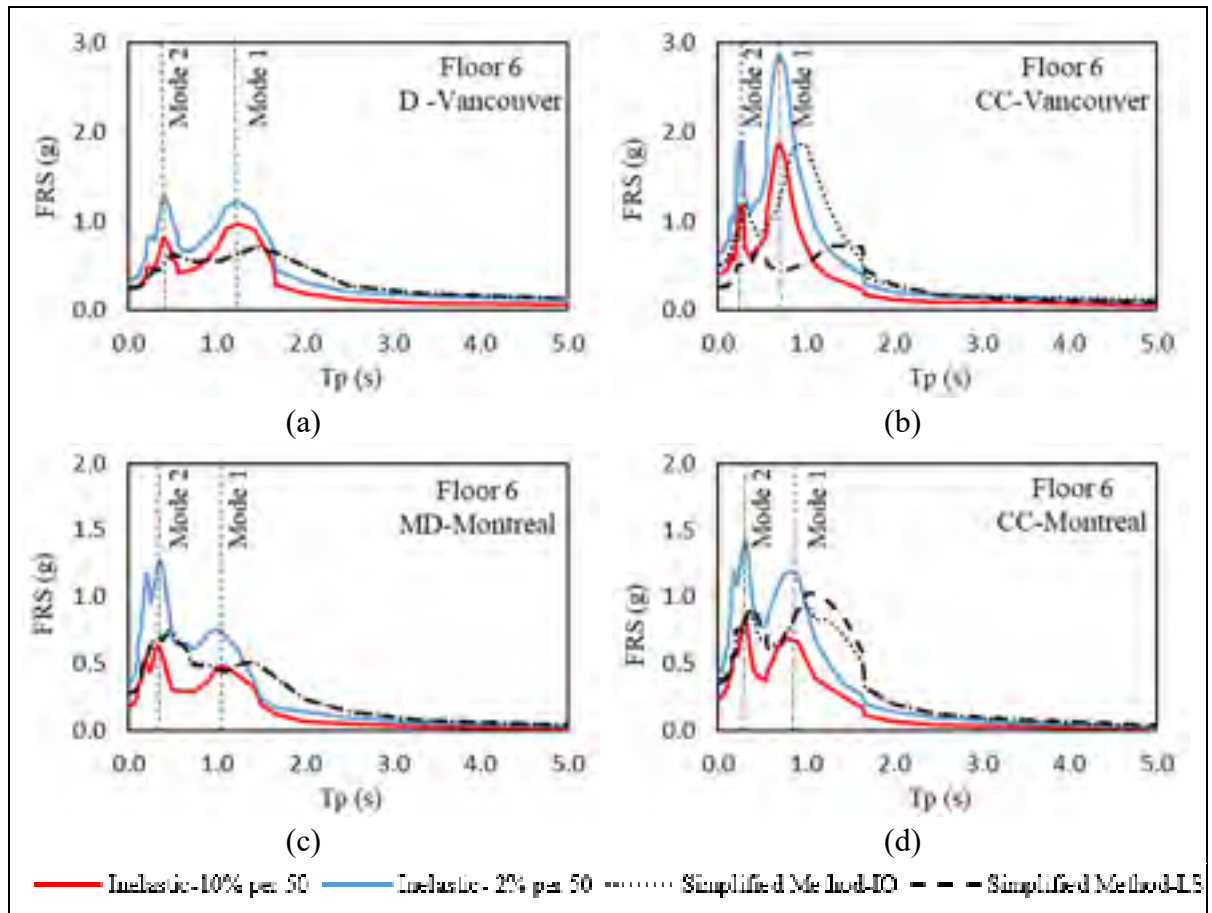


Figure 5.14 Computed mean FRS in the 6<sup>th</sup> floor obtained from the simplified method and from nonlinear dynamic analysis

Similarity in the results is observed at the IO and LS performance levels in the ductile and moderately ductile frames (Figures 5.14a and 5.14c) unlike the conventional frames at the different performance levels (Figures 5.14b and 5.14d). In the conventional frames, the mean FRS obtained from the simplified method at the IO performance level are in a good agreement in terms of shape and value with those obtained from the nonlinear dynamic analysis at IO performance level. However, the mean FRS obtained from the simplified method at the LS performance level underestimates the FRS ordinates comparing to what obtained from the nonlinear dynamic analysis at LS performance level.

In general, it can be concluded that applying the simplified method on ductile or moderately ductile buildings do not lead to accurate results since the simplified method was derived based on a conventional frame building.

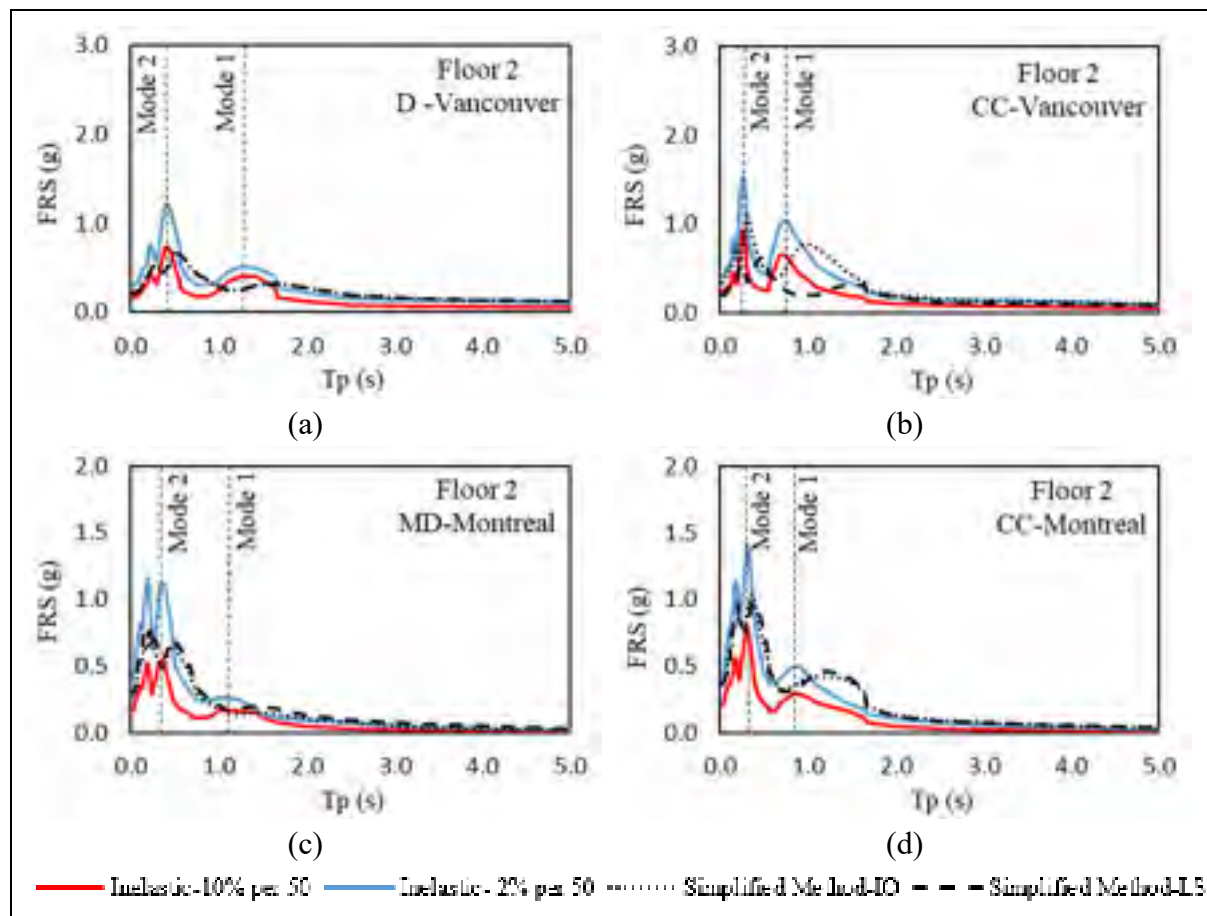


Figure 5.15 Mean FRS in the 2<sup>nd</sup> floor obtained from the simplified method in the studied frames compared to those obtained from nonlinear dynamic analysis

## 5.4 Evaluation of NIST GCR 18-917-43 (2018)

### 5.4.1 Height factor $A_x$

The elastic and inelastic mean value of  $A_x$  profiles along the relative height  $h_x/h_n$  for the studied building models are compared to the one proposed by NIST GCR 18-917-43 (2018) (given by

Equation 1.6) as shown in Figure 5.16. The  $A_x$  profiles recommended by NIST GCR 18-917-43 (2018) were determined for four cases: 1)  $R_d = 1.0$  for elastic frames, 2)  $R_d = 4.0$  for inelastic ductile frame, 3)  $R_d = 2.5$  for moderately ductile frame, and 4)  $R_d = 1.5$  for conventional construction frames.

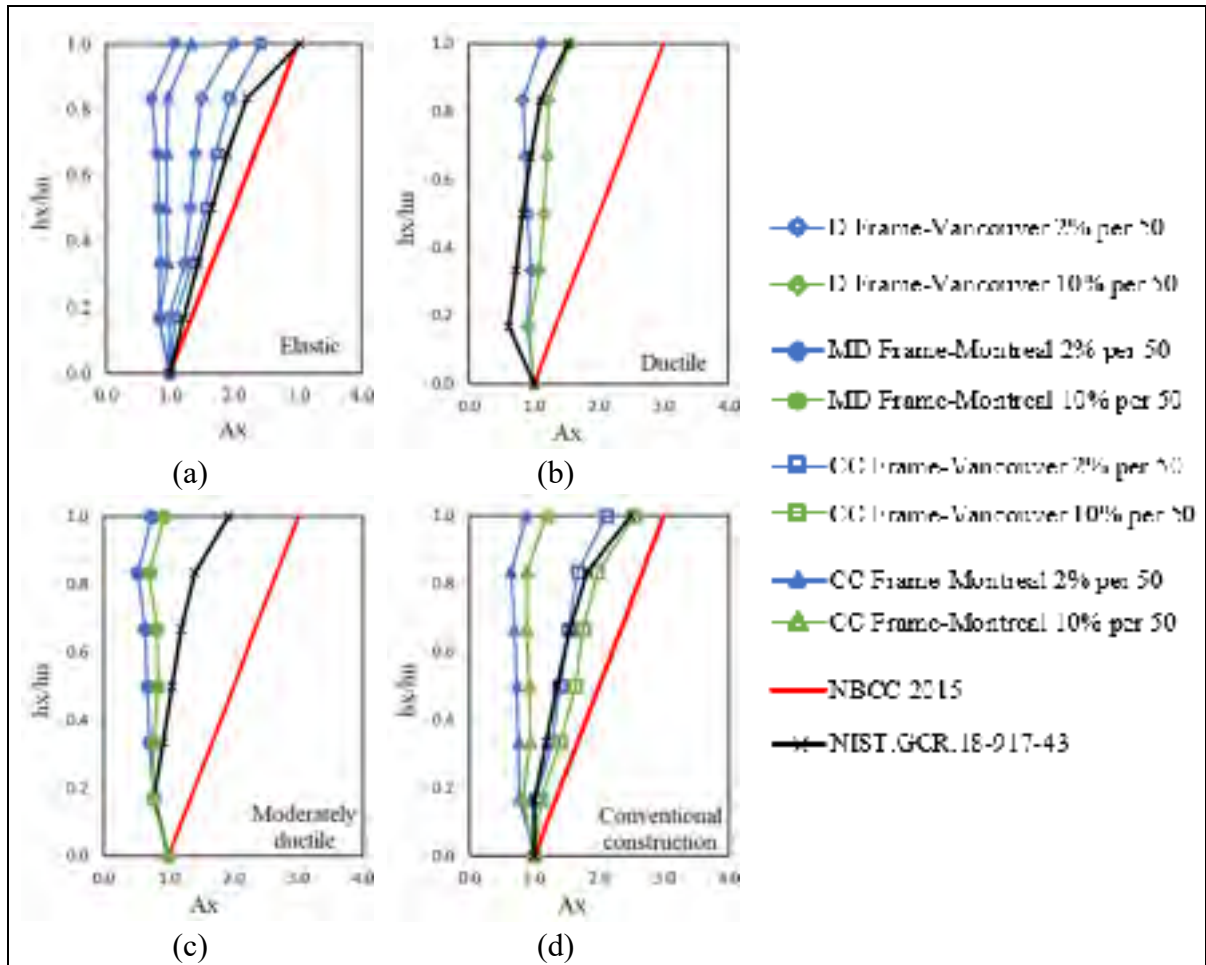


Figure 5.16 Comparison of computed mean elastic and inelastic  $A_x$  profiles with the NIST.GCR.18-917-43 (2018) provisions

It is observed that the profile proposed by NIST GCR 18-917-43 (2018) fits very well the demands of elastic models in Vancouver, but overestimates the demands of the elastic models in Montreal (Figure 5.16a).

In the ductile frame (Figure 5.16b), the profile suggested by NIST GCR 18-917-43 (2018) fits the demands of the upper three floors, but underestimates the demands of the other floors when the ground motion with 2% per 50 years probability of exceedance is used. As for the conventional frame in Vancouver (Figure 5.16d), the profile suggested by NIST fits very well the  $A_x$  profile when the ground motion with 2% per 50 years probability of exceedance is used, but underestimates the  $A_x$  demands when the ground motion with 10% per 50 years probability of exceedance is used.

On the other hand, the  $A_x$  profile when the ground motion with 2% and 10% per 50 years probability of exceedance are used for Montreal frames, the profile suggested by NIST underestimates the demands except for the moderately ductile frame (Figure 5.16c). While the profile proposed by NIST GCR 18-917-43 (2018) overestimates the  $A_x$  demands of the conventional frame in Montreal at the both probabilities of exceedance (Figure 5.16d).

#### 5.4.2 Component amplification factor $A_r$

Figures 5.17 and 5.18 present the mean values of  $A_r$  factors for the elastic and inelastic case of study models in Montreal and Vancouver at the 6<sup>th</sup> and 2<sup>nd</sup> floor levels, respectively compared to the value proposed by NIST GCR 18-917-43 (2018). Values for others floors are presented in Appendix IV.

It can be observed that the  $A_r$  value proposed by NIST GCR 18-917-43 (2018) fits very well the elastic models in Montreal and Vancouver except at the roof level of the conventional construction frame and the second floor of the ductile frame in Vancouver. In the inelastic models, the suggested value by NIST GCR 18-917-43 (2018) fits very well all the frame models in Vancouver and Montreal.

Finally, it is worth to mention that computed  $A_r$  values vary from floor level to another and not constant along the building height as it is supposed in NIST GCR 18-917-43 (2018) and NBC (2015).



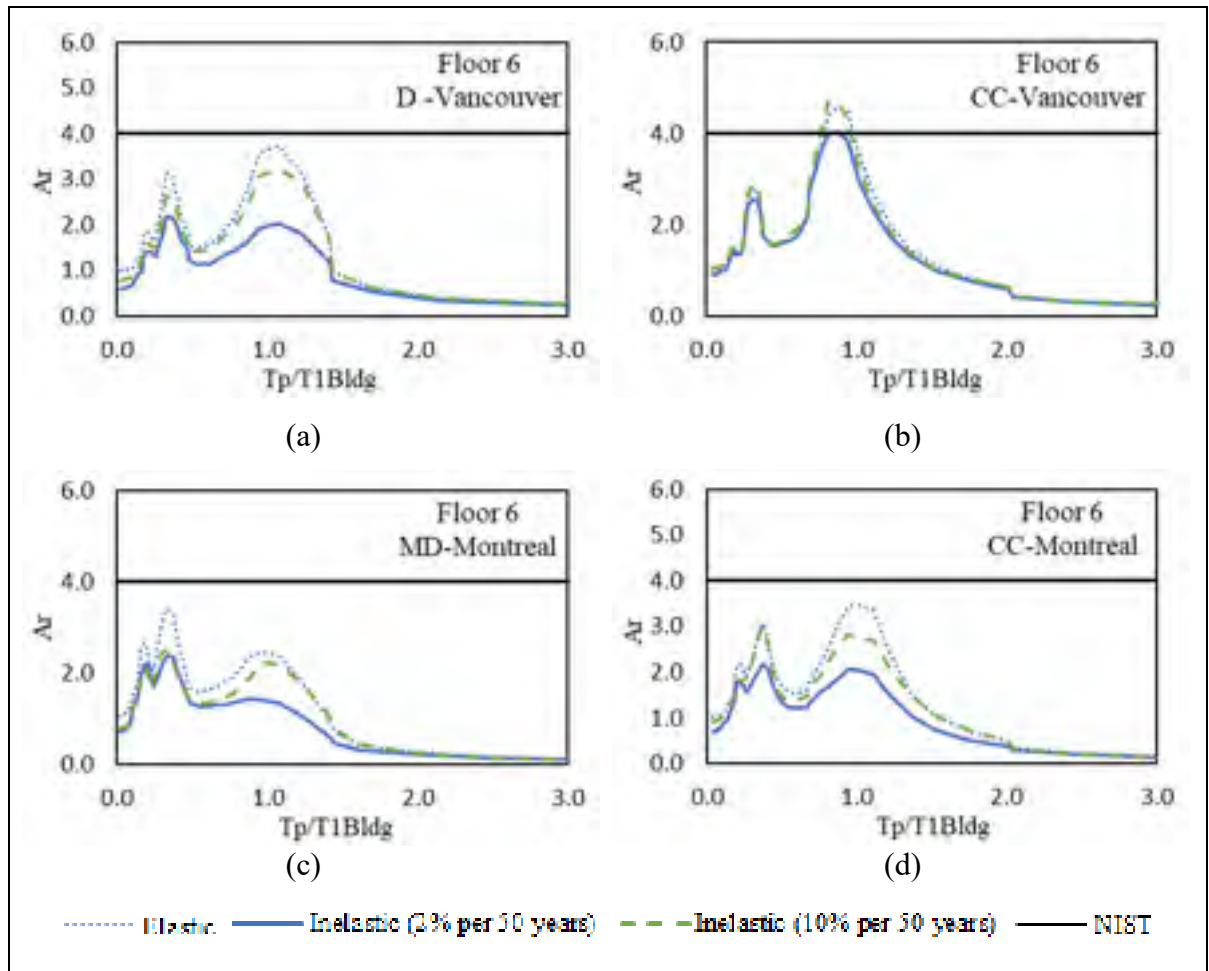


Figure 5.17 Comparison of computed  $A_r$  values in the 6<sup>th</sup> floor compared to the value proposed in NIST.GCR.18-917-43 (2018)

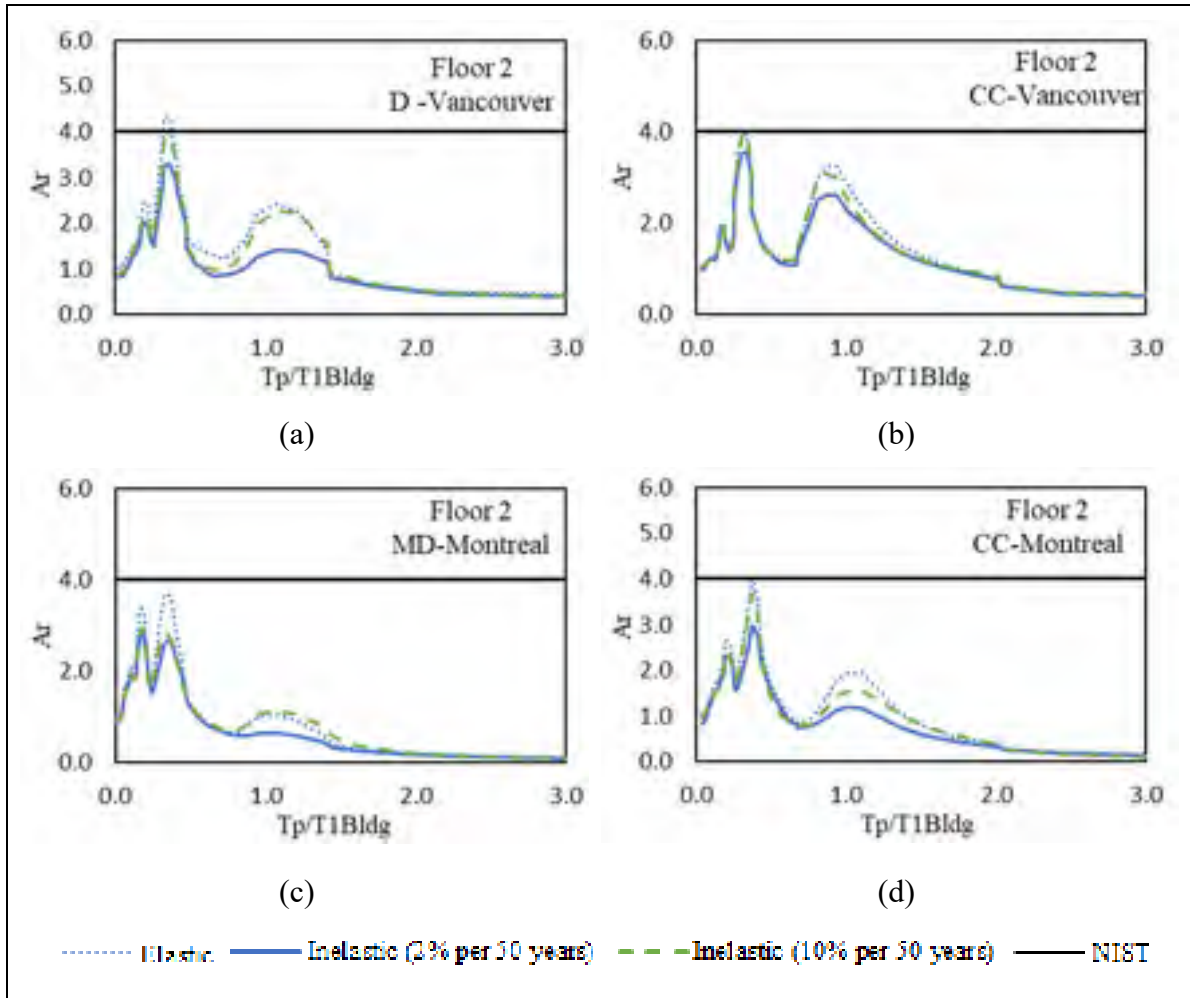


Figure 5.18 Comparison of computed  $A_r$  values in the 2<sup>nd</sup> floor compared to the value proposed in NIST.GCR.18-917-43 (2018)

## 5.5 Evaluation of the product ( $A_x \cdot A_r$ )

As shown in the previous sections, the NBC (2015) and NIST.GCR.18-917-43 (2018) provisions overestimate in general the  $A_x$  factor and underestimate the  $A_r$  factor. For an overall comparison, the product ( $A_x \cdot A_r$ ) is evaluated versus the ( $T_p/T_{1Bldg}$ ) ratio in the 6<sup>th</sup> level (Figure 5.19) and maximum values along the building height are plotted in Figure 5.20.

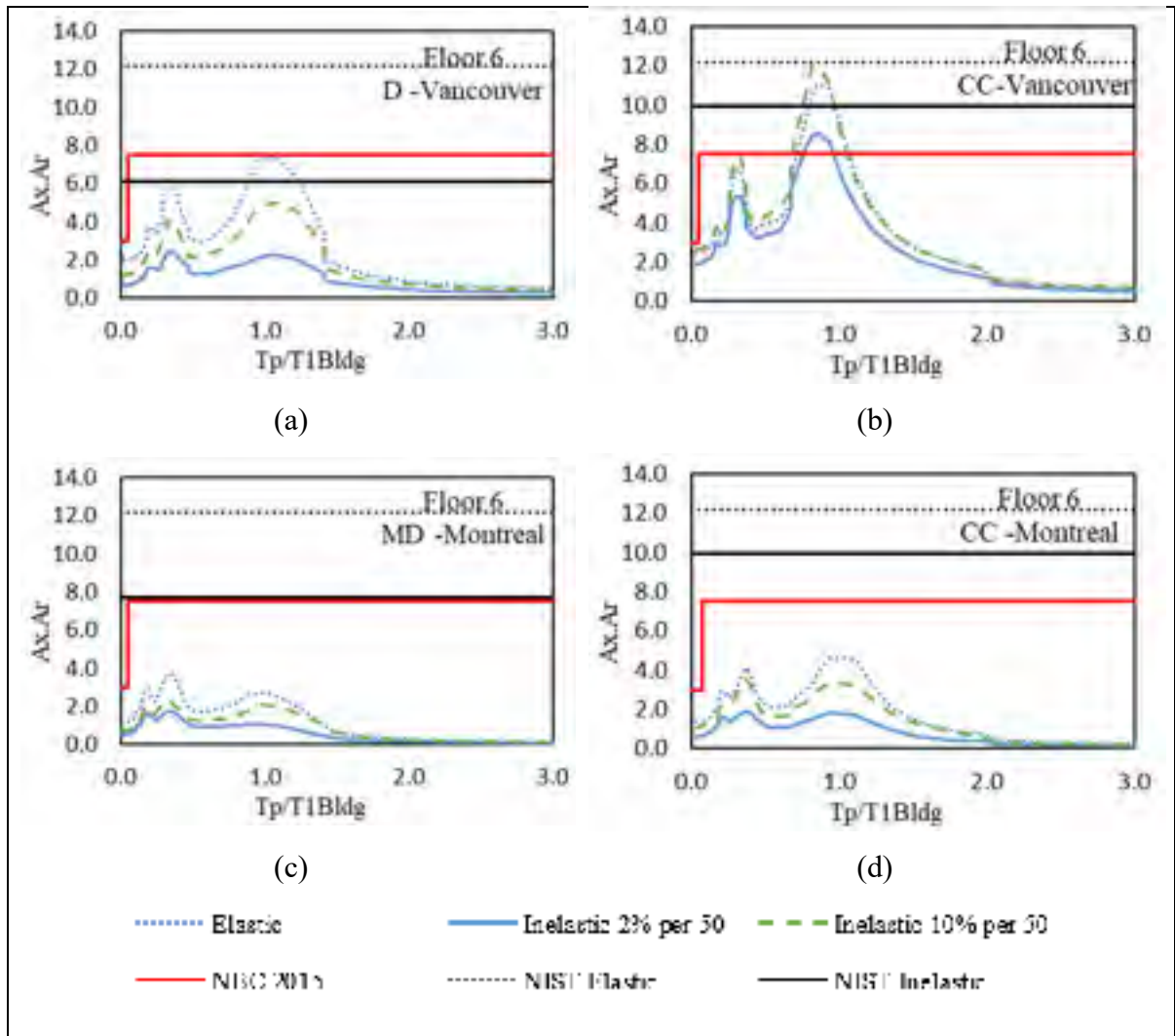


Figure 5.19 Comparison of computed mean ( $A_x \cdot A_r$ ) in the 6<sup>th</sup> level of the studied buildings compared to NBC 2015 and NIST.GCR.18-917-43 (2018) provisions

It can be observed that the product ( $A_x \cdot A_r$ ) is overestimated by the aforementioned provisions for the elastic and inelastic studied models in Montreal (Figure 5.20a, 5.20c, and 5.20d). As for the elastic models in Vancouver, the product ( $A_x \cdot A_r$ ) stated by NBC (2015) underestimate the required ( $A_x \cdot A_r$ ) product while the one proposed by NIST fits well the elastic models (Figure 5.20a). In Figure 5.20b, the product ( $A_x \cdot A_r$ ) stated by NBC (2015) overestimates the required ( $A_x \cdot A_r$ ) product for the ductile frame when the ground motion with 2% per 50 years

probability of exceedance is used, but fits well the  $A_x$  demands when the ground motion with 10% per 50 years probability of exceedance is used.

In Figure 5.20d, the product ( $A_x \cdot A_r$ ) stated by NBC (2015) underestimates the required ( $A_x \cdot A_r$ ) product for the conventional frame in Vancouver at the both ground motion probability of exceedance. As for the ( $A_x \cdot A_r$ ) stated by NIST, it fits well the  $A_x$  demands when the ground motion with 2% per 50 years probability of exceedance is used, but underestimates the required values when the ground motion with 10% per 50 years probability of exceedance is used.

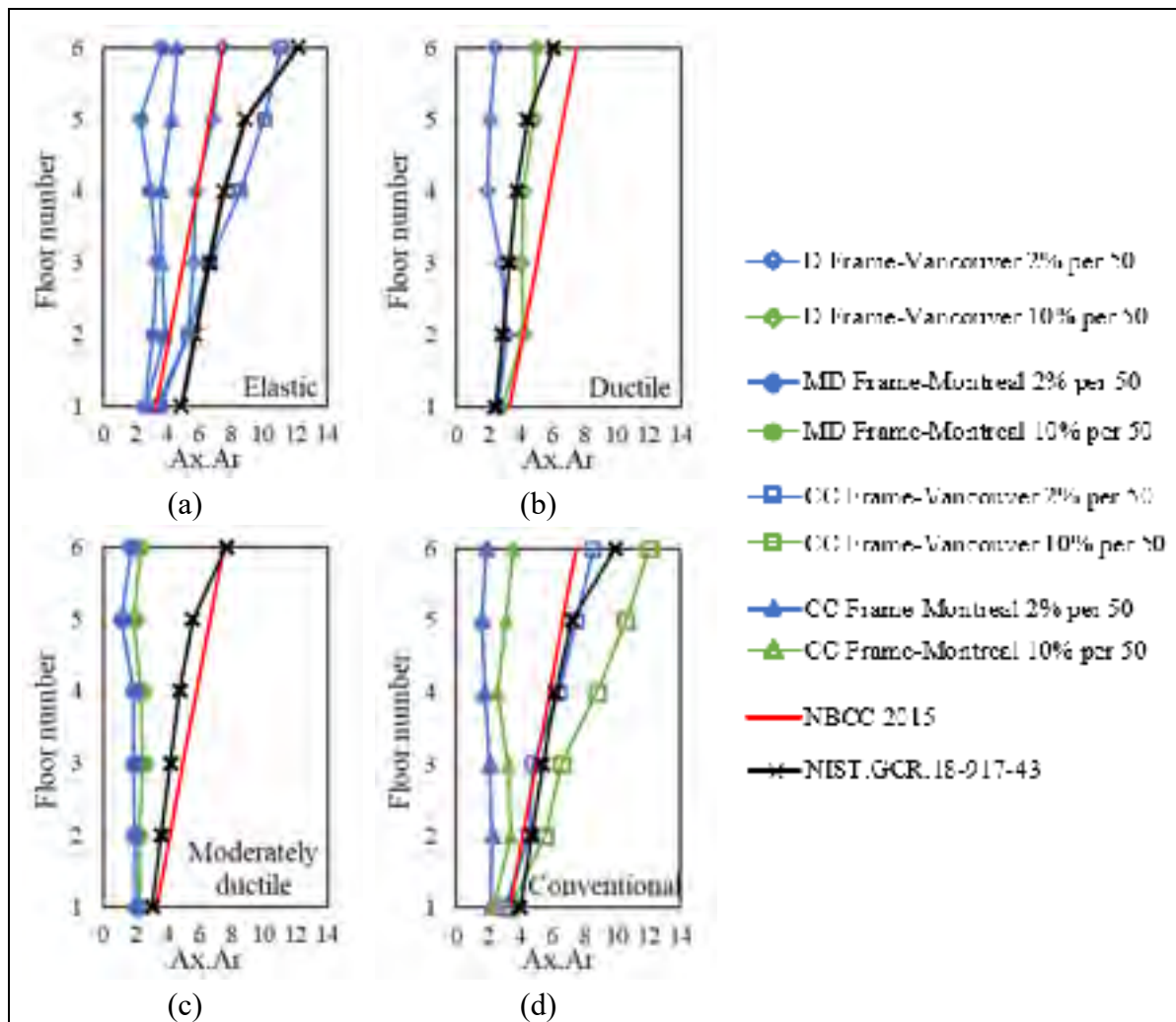


Figure 5.20 Comparison of computed max  $A_x \cdot A_r$  factor of the studied buildings along the building height to NBC 2015 and NIST.GCR.18-917-43 (2018) provisions

## 5.6 Summary

This chapter presented the NSCs demands in terms of  $A_x$ ,  $A_r$ , and FRS resulting from the elastic and inelastic analyses for the studied frames considering the ground motions with 2% and 10% per 50 years probabilities of exceedance. In addition, the results of applying the simplified method of Kothari et al. (2017) to the studied frames were displayed and discussed. The aforementioned output were compared to the NBC (2015) and NIST.GCR.18-917-43 (2018) provisions in aim of evaluation.

In general, the mentioned provisions overestimate the  $A_x$  factor and underestimate the  $A_r$  factor. Therefore, the product ( $A_x \cdot A_r$ ) is evaluated in this chapter too. It is concluded that the product ( $A_x \cdot A_r$ ) suggested by the aforementioned provisions is adequate for the ductile and moderately ductile inelastic frames when the strong ground motions (2% per 50 years probability of exceedance) are used. On the other hand, it is underestimated for conventional construction frames in Vancouver and overestimated for conventional construction on Montreal when moderate ground motions (10% per 50 years probability of exceedance) are used.



## CONCLUSIONS

The main objective of this thesis is to study the effect of building's ductility on the NSCs acceleration demands as well as evaluate the acceleration demands of NSCs suggested by NBC 2015, NIST GCR 18-917-43 and the simplified method of Kothari et al. (2017).

From a practical viewpoint, it can be concluded that considering different building ductility factors ( $R_d$ ) while determining the NSCs acceleration demand reflects the different options of seismic design available in the practice. The conclusions of this study are summarized as follows:

### I. Effect of ductility on the NSCs acceleration demands

- The building's ductility tends to reduce the NSC's acceleration demands.
- The benefit of frame ductility in reducing NSCs demands is less in conventional construction frames as compared to the ductile and moderately ductile frames.

### II. Height factor, $A_x$

- The average decrease in the  $A_x$  factor is equal to 44% and 16% in the ductile and conventional frames in Vancouver, respectively. While it is equal to 34% in the moderately ductile and conventional frames in Montreal. These ratios are obtained when ground motion with 2% per 50 years probability of exceedance is applied.
- The average decrease in the  $A_x$  factor is equal to 22% and 8% in the ductile and conventional frames in Vancouver, respectively. While it is equal to 14% and 11% in the moderately ductile and conventional frames in Montreal, respectively. Therefore, the benefit of frame ductility in reducing NSCs demands is less when the ground motion with 10% per 50 years probability of exceedance is applied.
- The distribution of  $A_x$  factor recommended by NBC 2015 overestimates those obtained from the nonlinear dynamic analysis.

- The  $A_x$  factor predicted by the simplified method at IO performance level is higher than those at LS in the conventional construction frame models while the demands are identical in the ductile and moderately ductile frames.
- The PFA/PGA distribution suggested by NIST GCR 18-917-43 (2018) fits the one obtained from the nonlinear dynamic analysis better than NBC 2015.

### III. Floor response spectra (FRS)

- When ground motions with 2% per 50 years probability of exceedance are applied, the building's ductility reduced the rooftop FRS peaks around the fundamental period of the ductile and conventional frames in Vancouver by 50% and 20%, respectively. These peaks are reduced by 56% and 50% for the moderately ductile and conventional frames in Montreal, respectively.
- When ground motions with 2% per 50 years probability of exceedance are applied, the building's ductility reduced the rooftop FRS peaks around the second period of the ductile and conventional frames in Vancouver by 28% and 13%, respectively. These peaks are reduced by 44% and 33% for the moderately ductile and conventional frames in Montreal, respectively.
- When ground motions with 10% per 50 years probability of exceedance are applied, the building's ductility reduced the rooftop FRS peaks around the fundamental period of the ductile and conventional frames in Vancouver by 57% and 50%, respectively. These peaks are reduced by 68% and 70% for the moderately ductile and conventional frames in Montreal, respectively.
- When the ground motions with 10% per 50 years probability of exceedance are applied, the building's ductility reduced the rooftop FRS around the second period of the ductile and conventional frames in Vancouver by 61% and 44%, respectively. These peaks are reduced by 76% and 68% for the moderately ductile and conventional frames in Montreal, respectively.



- The simplified method proposed by Kothari et al. (2017) predicts well the shape of FRS as compared to the one obtained from the nonlinear dynamic analysis, but underestimates the values of FRS ordinates.
- The FRS predicted by the simplified method at IO performance level is higher than those at LS in the conventional construction frame models while the demands are identical in the ductile and moderately ductile frames.

#### IV. Component amplification factor, $A_r$

- When ground motions with 2% per 50 years probability of exceedance are applied, the building's ductility reduced  $A_r$  in the roof by 46% and 16% around the fundamental period of the ductile and conventional frames in Vancouver, respectively. While the  $A_r$  is reduced by 44% for the moderately ductile and conventional frames in Montreal.
- When ground motions with 10% per 50 years probability of exceedance are applied, the building's ductility reduced  $A_r$  in the roof by 19% and 1% around the fundamental period of the ductile and conventional frames in Vancouver, respectively. While the  $A_r$  is reduced by 12% and 21% for the moderately ductile and conventional frames in Montreal, respectively.
- The value of  $A_r$  factor stated by NBC 2015 underestimates the required demands of NSCs obtained from the nonlinear dynamic analysis.
- The value of 4.0 for  $A_r$  factor suggested by NIST GCR 18-917-43 (2018) for the RC moment resisting frame fits very well the computed values for inelastic frame models in Vancouver, while it overestimates the computed values in Montreal. A value of 3.0 is recommended for frames in Montreal. These values are suggested when ground motions with 2% per 50 years probability of exceedance is applied.
- When ground motions with 10% per 50 years probability of exceedance are applied, a value of 5.0 for  $A_r$  factor is recommended for the RC moment resisting frame for inelastic frame models in Vancouver, and a value of 4.0 for frames in Montreal.

V. The product ( $A_x.A_r$ )

- When ground motions with 2% per 50 years probability of exceedance are applied, the product ( $A_x.A_r$ ) stated by NBC (2015) is overestimated for the inelastic models in Montreal while appropriate the inelastic models in Vancouver.
- When ground motions with 10% per 50 years probability of exceedance are applied, the product ( $A_x.A_r$ ) stated by NBC (2015) is overestimated for the inelastic frame models in Montreal, appropriate for the ductile frame model in Vancouver, but underestimated the conventional frame model in Vancouver.
- When ground motions with 2% per 50 years probability of exceedance are applied, the product ( $A_x.A_r$ ) stated by NIST GCR 18-917-43 (2018) is overestimated for the inelastic models in Montreal and appropriate for the inelastic models in Vancouver.
- When ground motions with 10% per 50 years probability of exceedance are applied, the product ( $A_x.A_r$ ) stated by NIST GCR 18-917-43 (2018) is overestimated for the inelastic frame models in Montreal, but underestimated for the inelastic frame models in Vancouver.

## RECOMMENDATIONS

While the current project have examined several points about the seismic demands of NSCs in inelastic RC frame points, others investigations are recommended for future works as follows:

- Investigate the effect of the hysteretic model used to model the plastic hinges behaviour on the NSCs seismic demands.
- Use historical ground motions database to perform the dynamic analysis.
- Examine the effect of using component damping ratios lower than 5% on the proposed values of  $A_r$  factor.
- Include different building heights to investigate the effect of building period on the NSCs acceleration demands.
- Investigate the effect of gravity loads on the NSCs acceleration demands.
- Investigate the effect of building's ductility on the NSCs seismic displacement demands
- Investigate the seismic acceleration demands in the RC shear wall buildings to examine the effect of the lateral force resisting system.
- Examine the effect of ground motions scaling method by using Method B proposed in the structural commentaries of the NBC 2015.

## APPENDIX I

### SELECTION AND SCALING OF GROUND MOTIONS

Rahaf Sheikh Alard, MScA candidate in ETS; Rola Assi, Prof. in ETS  
 1-4 values are required as input  
 2- Data & procedure are available on <http://www.seismotoolbox.ca/HBCG2005.htm>  
 3- Target spectra is for Vancouver 2% per 50 years

T1 1.17 Enter the fundamental period of the structure!  
 T90% 0.390 Enter the mode period where the contribute d mass are >= 90%!  
 Tmin 0.233  
 Tmax 2.334

Scenario 1						
TRSI min	0.92					
TRSI max	0.3	Enter the upper limit o	selected	F1	F2	F_Final
West6c1	M 6.5	R (km) 12.0	W6c1_2	0.7748		0.7748
			W6c1_21	0.9374		0.9374
			W6c1_17	1.2262		1.2262
West6c2	M 6.5	R (km) 30.0	W6c2_20	1.5331	1.0000	1.5331
			W6c2_10	1.2274		1.2274
			W6c2_22	1.4007		1.4007

Scenario 2						
TRSI min	0.3	Enter the lower limit of the scenario 2!				
TRSI max	1.5	Enter the upper limit o	selected	F1	F2	F_Final
West7c1	M 7.5	R (km) 25.0	W7c1_9	0.6254		0.6663
			W7c1_28	0.8686		0.9255
			W7c1_31	0.7276		0.7753
West7c2	M 7.5	R (km) 100.0	W7c2_16	1.6060	1.0655	1.7112
			W7c2_15	1.6241		1.7305
			W7c2_6	1.7950		1.9126

Scenario 3						
TRSI min	1.0	Enter the lower limit of the scenario 3!				
TRSI max	2.33		selected	F1	F2	F_Final
West9c	M 9.0	R (km) 360.8	W9c_5	1.5991		1.5991
			W9c_9	1.5529		1.5529
			W9c_7	1.6933	1.0000	1.6933
			W9c_15	1.7341		1.7341
			W9c_8	1.7545		1.7545

Figure-A I-1 Excel sheet created to select and scale the ground motions with probability of exceedance 2% per 50 years in Vancouver

**Rahaf Sheikh Alard, MScA candidate in ETS; Rola Assi, Prof. in ETS**

1- 4 values are required as input

2- Data & procedure are available on <http://www.seismotoolbox.ca/NBOC2005.html>

3- Target spectra is for Montreal 2% per 50 years

T1	0.82	Enter the fundamental period of the structure!
T90%	0.28	Enter the mode period where the contributed mass are $\geq 90\%$ !
Tmin	0.16	
Tmax	1.64	

Scenario 1							
TRS1 min	0.16						
TRS1 max	1.0 <span style="color: red;">Enter the upper limit or selected</span>						
East 6c1	M 6.0	R (km) 15.0	E6c1_31	0.7588	1.100	F_Final	
			E6c1_7	0.6096		0.8347	
			E6c1_16	0.6044		0.6706	
East 6c2	M 6.0	R (km) 30.0	E6c2_8	0.9590	1.100	0.6649	
			E6c2_5	1.3994		1.0549	
			E6c2_26	1.5161		1.5394	
						1.6678	

Scenario 2							
TRS1 min	0.5 <span style="color: red;">Enter the lower limit of the scenario 2!</span>						
TRS1 max	1.6 <span style="color: red;">selected</span>						
East7c1	M 7.0	R (km) 25.0	E7c1_25	0.5186	1.000	F_Final	
			E7c1_30	0.5305		0.5186	
			E7c1_28	0.6712		0.5305	
East7c2	M 7.0	R (km) 100.0	E7c2_3	1.1791	1.000	0.6712	
			E7c2_11	1.6754		1.1791	
			E7c2_7	1.0106		1.6754	
						1.0106	

Figure-A I-2 Excel sheet created to select and scale the ground motions with probability of exceedance 2% per 50 years in Montreal

Rahaf Sheikh Alard, Master student in ETS; Rola Assi, Professor in ETS

1- 4 values are required as input

2- Data & procedure are available on: <http://www.seismotoolbox.ca/NBCC2005.html>

3- Target spectra is for Vancouver 10% per 50 years

T1	1.17	Enter the fundamental period of the structure!
T90%	0.390	Enter the mode period where the contributed mass are >= 90%!
Tmin	0.233	
Tmax	2.334	

Scenario 1						
TRSI min	0.23					
TRSI max	0.8	Enter the upper limit of the scenario 1!	selected	F1	F2	F_Final
West 6c1	M 6.5	R (km) 12.0	W6c1_27	0.5587	1.0000	0.5587
			W6c1_17	0.6227		0.6227
			W6c1_25	0.7163		0.7163
West 6c2	M 6.5	R (km) 30.0	W6c2_10	0.5946	1.0000	0.5946
			W6c2_44	0.7615		0.7615
			W6c2_20	0.7576		0.7576

Scenario 2						
TRSI min	0.3	Enter the lower limit of the scenario 2!				
TRSI max	1.5	Enter the upper limit of the scenario 2!				
			selected	F1	F2	F_Final
West7c1	M 7.5	R (km) 25.0	W7c1_22	0.5824	1.0000	0.5824
			W7c1_26	0.5119		0.5119
			W7c1_18	0.6537		0.6537
West7c2	M 7.5	R (km) 100.0	W7c2_16	0.7941	1.0000	0.7941
			W7c2_15	0.8034		0.8034
			W7c2_5	0.8868		0.8868

Scenario 3						
TRSI min	1.0	Enter the lower limit of the scenario 3!				
TRSI max	2.33					
			selected	F1	F2	F_Final
West9c	M 9.0	R (km) 360.8	W9c_15	0.8060	1.0000	0.8060
			W9c_9	0.7222		0.7222
			W9c_5	0.7445		0.7445
			W9c_8	0.8152		0.8152
			W9c_7	0.7878		0.7878

Figure-A I-3 Excel sheet created to select and scale the ground motions with probability of exceedance 10% per 50 years in Vancouver



Rahaf Sheikh Alard, Master student in ETS; Rola Assi, Professor in ETS

1- 4 values are required as input

2- Data & procedure are available on: <http://www.seemotoolbox.ca/NBCC2005.html>

3- Target spectra is for Montreal 10% per 50 years

T1	1.03	Enter the fundamental period of the structure!
T90%	0.34	Enter the mode period where the contributed mass are >= 90%!
Tmin	0.21	
Tmax	2.07	

Scenario 1							
TRS1 min	0.21						
TRS1 max	1.0		Enter the upper limit of t1	selected	F1	F2	F_Final
East 6c1	M 6.0	R (km) 15.0	E6c1_31	0.2582	1.000	0.2582	
			E6c1_1	0.1739		0.1739	
			E6c1_7	0.2007		0.2007	
East 6c2	M 6.0	R (km) 30.0	E6c2_26	0.5357	1.000	0.5357	
			E6c2_31	0.5235		0.5235	
			E6c2_12	0.6516		0.6516	

Scenario 2						
TRS1 min	0.5		Enter the lower limit of the scenario 2!			
TRS1 max	2.1					
			selected	F1	F2	F_Final
East7c1	M 7.0	R (km) 25.0	E7c1_7	0.0990	1.034	0.1024
			E7c1_43	0.0721		0.0746
			E7c1_24	0.0815		0.0843
East7c2	M 7.0	R (km) 100.0	E7c2_11	0.6137	1.034	0.6349
			E7c2_44	0.6742		0.6975
			E7c2_27	0.8396		0.8686

Figure-A I-4 Excel sheet created to select and scale the ground motions with probability of exceedance 10% per 50 years in Montreal

## APPENDIX II

### SECTION ANALYSIS OF PHB1 SECTION BY RESPONSE 2000

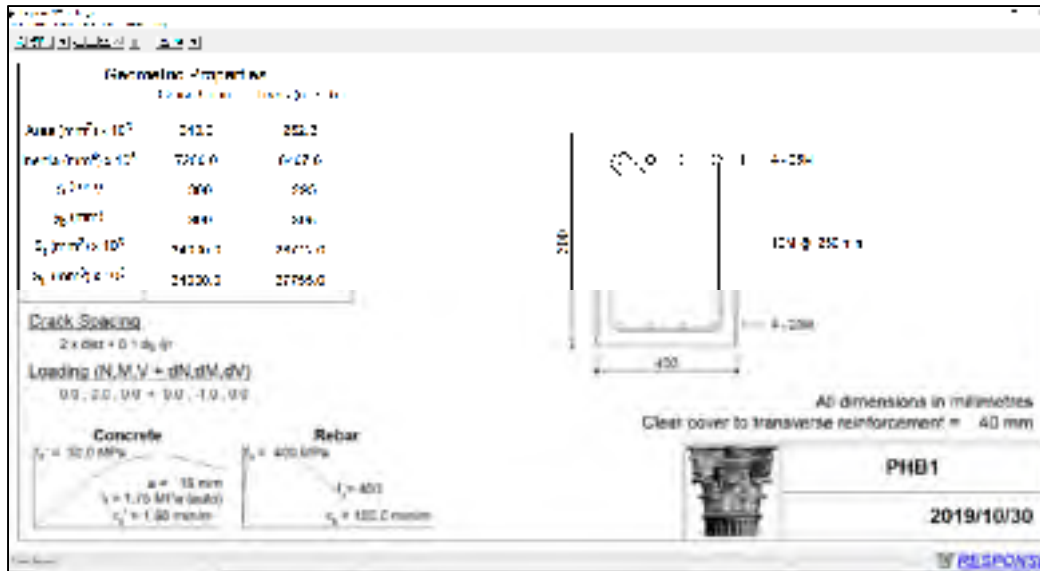


Figure-A II-1 Geometric and material properties used as input in Response 2000 for the section analysis of PHB1 beam in the moderately ductile frame in Montreal

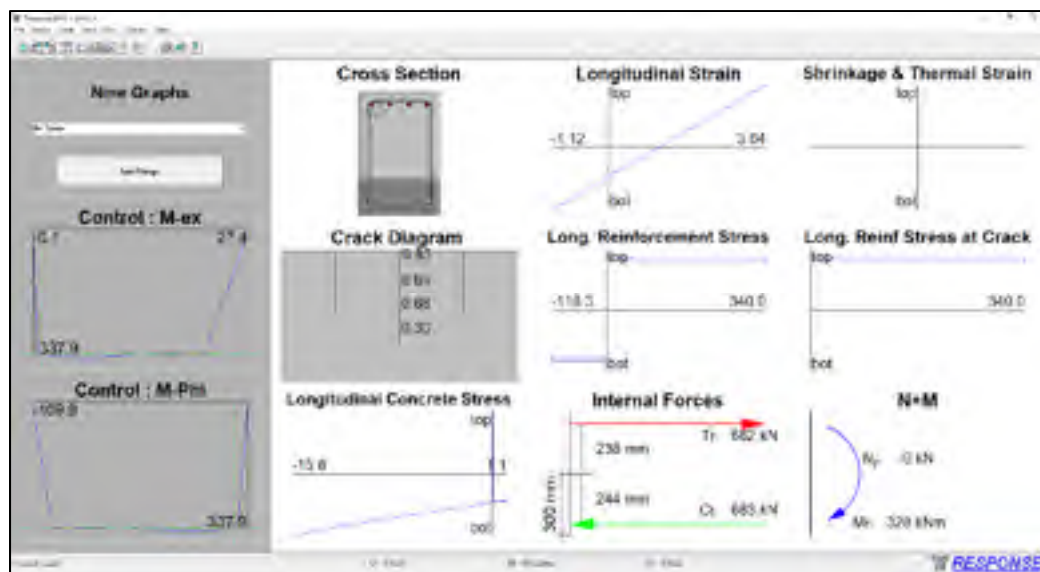


Figure-A II-2 Response 2000 output of the Moment-rotation relationship for PHB1 beam section in the moderately ductile frame in Montreal



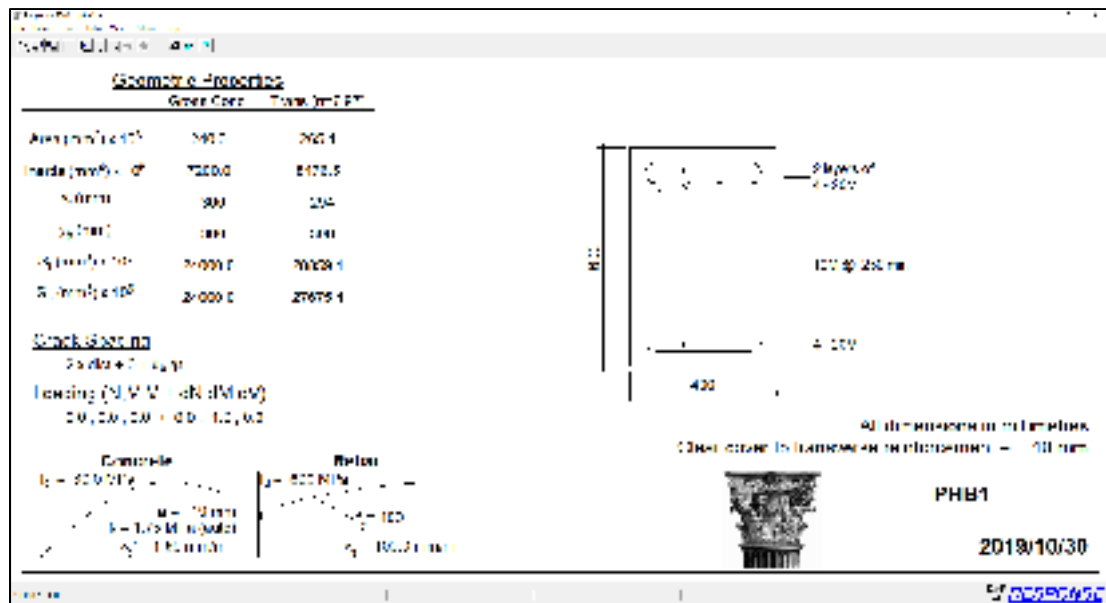


Figure-A II-3 Geometric and material properties used as input in Response 2000 for the section analysis of PHB1<sup>+</sup> beam in the ductile frame in Vancouver

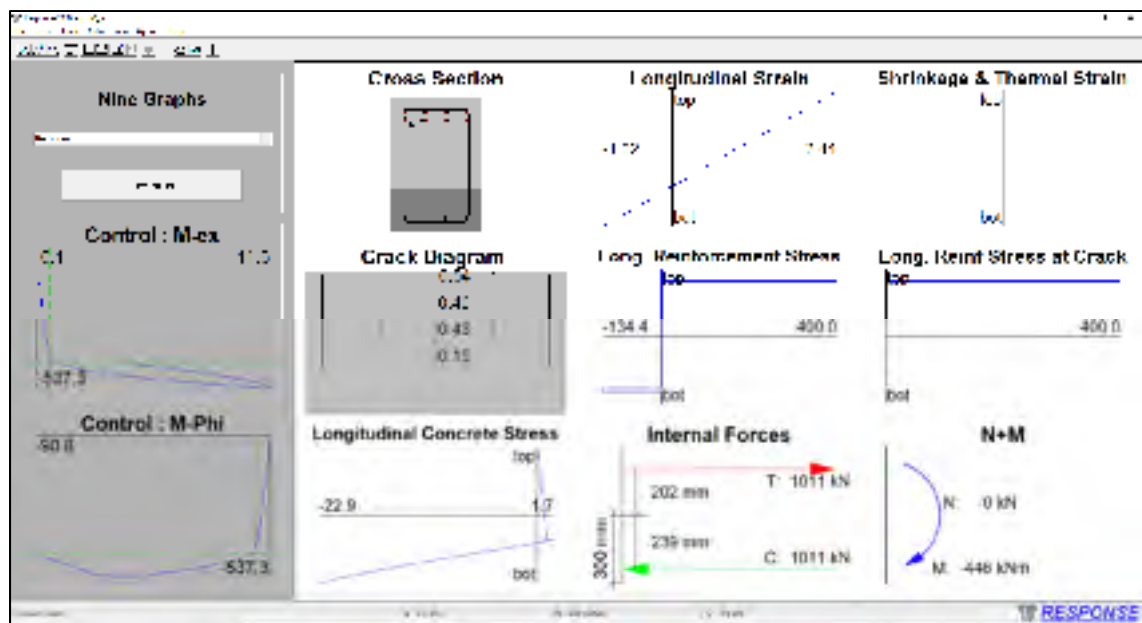


Figure-A II-4 Response 2000 output of the Moment-rotation relationship for PHB1<sup>+</sup> beam section in the ductile frame in Vancouver

### APPENDIX III

#### PLASTIC HINGES PROPERTIES AND ACCEPTTANCE CRITERIA

Table-A III-1 Acceptance criteria of plastic hinges in columns of ductile frame in Vancouver

Hinge	Section	a	b	c	IO	LS	CP
PHCE01	1-1	0.0304	0.0304	0.16	0.0046	0.0152	0.0213
PHCE02		0.0316	0.0316	0.17	0.0047	0.0158	0.0221
PHCE03		0.0314	0.0314	0.17	0.0047	0.0157	0.0220
PHCE04		0.0329	0.0340	0.19	0.0049	0.0170	0.0238
PHCE05		0.0329	0.0340	0.19	0.0049	0.0170	0.0238
PHCE06		0.0342	0.0403	0.20	0.0050	0.0202	0.0282
PHCE07		0.0342	0.0403	0.20	0.0050	0.0202	0.0282
PHCE08		0.0343	0.0412	0.20	0.0050	0.0206	0.0288
PHCE09		0.0343	0.0412	0.20	0.0050	0.0206	0.0288
PHCE10		0.0343	0.0412	0.20	0.0050	0.0206	0.0288
PHCE11		0.0343	0.0412	0.20	0.0050	0.0206	0.0288
PHCE12		0.0342	0.0412	0.20	0.0050	0.0206	0.0288
PHCI01	2-2	0.0253	0.0253	0.12	0.0038	0.0126	0.0177
PHCI02		0.0276	0.0276	0.14	0.0041	0.0138	0.0193
PHCI03		0.0269	0.0269	0.14	0.0040	0.0135	0.0188
PHCI04		0.0290	0.0290	0.16	0.0043	0.0145	0.0203
PHCI05		0.0295	0.0295	0.16	0.0044	0.0148	0.0207
PHCI06		0.0315	0.0315	0.18	0.0047	0.0157	0.0220
PHCI07		0.0316	0.0316	0.18	0.0047	0.0158	0.0221
PHCI08		0.0336	0.0336	0.20	0.0050	0.0168	0.0235
PHCI09		0.0336	0.0336	0.20	0.0050	0.0168	0.0235
PHCI10		0.0341	0.0355	0.20	0.0050	0.0178	0.0249
PHCI11		0.0341	0.0355	0.20	0.0050	0.0178	0.0249
PHCI12		0.0341	0.0355	0.20	0.0050	0.0178	0.0249

Table-A III-2 Properties of plastic hinges in columns of ductile frame in Vancouver

Hinge	$M_y$	$\theta_y$	$M_C/M_y$	$\theta_C / \theta_y$	$M_D/M_y$	$\theta_D / \theta_y$	$M_E/M_y$	$\theta_E / \theta_y$
PHCE01	345.0	0.0041	1.1	5.0	0.16	5.0	0.16	5.0
PHCE02	335.0	0.0042	1.1	5.2	0.17	5.2	0.17	5.2
PHCE03	335.0	0.0042	1.1	5.2	0.17	5.2	0.17	5.2
PHCE04	323.1	0.0044	1.1	5.4	0.19	5.4	0.19	5.5
PHCE05	323.1	0.0044	1.1	5.4	0.19	5.4	0.19	5.5
PHCE06	309.5	0.0045	1.1	5.6	0.20	5.6	0.20	6.4
PHCE07	309.5	0.0045	1.1	5.2	0.20	5.2	0.20	5.9
PHCE08	279.1	0.0045	1.1	5.2	0.20	5.2	0.20	6.0
PHCE09	279.1	0.0045	1.1	5.2	0.20	5.2	0.20	6.0
PHCE10	264.0	0.0045	1.1	5.2	0.20	5.2	0.20	6.0
PHCE11	264.0	0.0045	1.1	5.2	0.20	5.2	0.20	6.0
PHCE12	247.0	0.0045	1.1	5.2	0.20	5.2	0.20	6.0
PHCI01	629.7	0.0034	1.1	3.0	0.12	3.0	0.12	3.0
PHCI02	583.1	0.0037	1.1	3.2	0.14	3.2	0.14	3.2
PHCI03	583.1	0.0036	1.1	3.2	0.14	3.2	0.14	3.2
PHCI04	559.7	0.0039	1.1	3.3	0.16	3.3	0.16	3.3
PHCI05	559.7	0.0040	1.1	3.4	0.16	3.4	0.16	3.4
PHCI06	507.8	0.0042	1.1	3.5	0.18	3.5	0.18	3.5
PHCI07	507.8	0.0042	1.1	3.3	0.18	3.3	0.18	3.3
PHCI08	483.0	0.0045	1.1	3.5	0.20	3.5	0.20	3.5
PHCI09	483.0	0.0045	1.1	3.5	0.20	3.5	0.20	3.5
PHCI10	426.3	0.0045	1.1	3.5	0.20	3.5	0.20	3.6
PHCI11	426.3	0.0045	1.1	3.5	0.20	3.5	0.20	3.6
PHCI12	395.3	0.0045	1.1	3.5	0.20	3.5	0.20	3.6

Units are in kN, m

Table-A III-3 Acceptance criteria of plastic hinges in beams of ductile frame in Vancouver

Hinge	Section	a	b	c	IO	LS	CP
PHB01 <sup>+</sup>	3-3	0.020	0.030	0.200	0.005	0.020	0.030
PHB01 <sup>-</sup>		0.025	0.050	0.200	0.010	0.025	0.050
PHB02 <sup>+</sup>		0.020	0.030	0.200	0.005	0.020	0.030
PHB02 <sup>-</sup>		0.025	0.050	0.200	0.010	0.025	0.050
PHB03 <sup>+</sup>	4-4	0.020	0.031	0.200	0.005	0.020	0.031
PHB03 <sup>-</sup>		0.024	0.048	0.200	0.009	0.024	0.048
PHB04 <sup>+</sup>		0.020	0.031	0.200	0.005	0.020	0.031
PHB04 <sup>-</sup>		0.024	0.048	0.200	0.009	0.024	0.048

Table-A III-4 Properties of plastic hinges in beams of ductile frame in Vancouver

Hinge	$M_y$	$\theta_y$	$M_C/M_y$	$\theta_C/\theta_y$	$M_D/M_y$	$\theta_D/\theta_y$	$M_E/M_y$	$\theta_E/\theta_y$
PHB01 <sup>+</sup>	445.6	0.0042	1.1	5.7	0.2	5.7	0.2	8.1
PHB01 <sup>-</sup>	200.0	0.0042	1.1	6.9	0.2	6.9	0.2	12.8
PHB02 <sup>+</sup>	445.6	0.0042	1.1	3.8	0.2	3.8	0.2	5.2
PHB02 <sup>-</sup>	200.0	0.0042	1.1	4.5	0.2	4.5	0.2	8.1
PHB03 <sup>+</sup>	259.4	0.0046	1.1	5.3	0.2	5.3	0.2	7.8
PHB03 <sup>-</sup>	175.6	0.0046	1.1	6.2	0.2	6.2	0.2	11.4
PHB04 <sup>+</sup>	259.4	0.0046	1.1	3.6	0.2	3.6	0.2	5.1
PHB04 <sup>-</sup>	175.6	0.0046	1.1	4.1	0.2	4.1	0.2	7.2

Units are in kN, m

Table-A III-5 Acceptance criteria of columns hinges of conventional frame in Vancouver

Hinge	Section	a	b	c	IO	LS	CP
PHCE01	5-5	0.0042	0.0115	0.17	0.0006	0.0057	0.0080
PHCE02		0.0042	0.0115	0.17	0.0006	0.0057	0.0080
PHCE03		0.0042	0.0115	0.17	0.0006	0.0057	0.0080
PHCE04		0.0042	0.0115	0.17	0.0006	0.0057	0.0080
PHCE05		0.0042	0.0115	0.17	0.0006	0.0057	0.0080
PHCE06		0.0042	0.0115	0.17	0.0006	0.0057	0.0080
PHCE07	6-6	0.0069	0.0161	0.19	0.0010	0.0080	0.0112
PHCE08		0.0069	0.0161	0.19	0.0010	0.0080	0.0112
PHCE09		0.0069	0.0161	0.19	0.0010	0.0080	0.0112
PHCE10		0.0069	0.0161	0.19	0.0010	0.0080	0.0112
PHCE11		0.0069	0.0161	0.19	0.0010	0.0080	0.0112
PHCE12		0.0069	0.0161	0.19	0.0010	0.0080	0.0112
PHCI01	7-7	0.0078	0.0199	0.20	0.0012	0.0100	0.0140
PHCI02		0.0078	0.0199	0.20	0.0012	0.0100	0.0140
PHCI03		0.0078	0.0199	0.20	0.0012	0.0100	0.0140
PHCI04		0.0078	0.0199	0.20	0.0012	0.0100	0.0140
PHCI05		0.0078	0.0199	0.20	0.0012	0.0100	0.0140
PHCI06		0.0078	0.0199	0.20	0.0012	0.0100	0.0140
PHCI07	8-8	0.0118	0.0220	0.21	0.0018	0.0110	0.0154
PHCI08		0.0118	0.0220	0.21	0.0018	0.0110	0.0154
PHCI09		0.0118	0.0220	0.21	0.0018	0.0110	0.0154
PHCI10		0.0118	0.0220	0.21	0.0018	0.0110	0.0154
PHCI11		0.0118	0.0220	0.21	0.0018	0.0110	0.0154
PHCI12		0.0118	0.0220	0.21	0.0018	0.0110	0.0154

Table-A III-6 Properties of columns plastic hinges of conventional frame in Vancouver

Hinge	$M_y$	$\theta_y$	$M_C/M_y$	$\theta_C/\theta_y$	$M_D/M_y$	$\theta_D/\theta_y$	$M_E/M_y$	$\theta_E/\theta_y$
PHCE01	1042.0	0.0056	1.1	1.7	0.17	1.7	0.17	3.0
PHCE02	1039.0	0.0056	1.1	1.7	0.17	1.7	0.17	3.0
PHCE03	1039.0	0.0056	1.1	1.7	0.17	1.7	0.17	3.0
PHCE04	967.0	0.0056	1.1	1.7	0.17	1.7	0.17	3.0
PHCE05	967.0	0.0056	1.1	1.7	0.17	1.7	0.17	3.0
PHCE06	1043.0	0.0056	1.1	1.7	0.17	1.7	0.17	3.0
PHCE07	503.0	0.0060	1.1	2.2	0.19	2.2	0.19	3.7
PHCE08	510.0	0.0060	1.1	2.2	0.19	2.2	0.19	3.7
PHCE09	510.0	0.0060	1.1	2.2	0.19	2.2	0.19	3.7
PHCE10	483.0	0.0060	1.1	2.2	0.19	2.2	0.19	3.7
PHCE11	483.0	0.0060	1.1	2.2	0.19	2.2	0.19	3.7
PHCE12	460.9	0.0060	1.1	2.2	0.19	2.2	0.19	3.7
PHCI01	1585.0	0.0094	1.1	1.8	0.20	1.8	0.20	3.1
PHCI02	1469.0	0.0094	1.1	1.8	0.20	1.8	0.20	3.1
PHCI03	1469.0	0.0094	1.1	1.8	0.20	1.8	0.20	3.1
PHCI04	1454.0	0.0094	1.1	1.8	0.20	1.8	0.20	3.1
PHCI05	1454.0	0.0094	1.1	1.8	0.20	1.8	0.20	3.1
PHCI06	1445.0	0.0094	1.1	1.8	0.20	1.8	0.20	3.1
PHCI07	822.0	0.0100	1.1	2.2	0.21	2.2	0.21	3.2
PHCI08	781.0	0.0100	1.1	2.2	0.21	2.2	0.21	3.2
PHCI09	781.0	0.0100	1.1	2.2	0.21	2.2	0.21	3.2
PHCI10	696.0	0.0100	1.1	2.2	0.21	2.2	0.21	3.2
PHCI11	696.0	0.0100	1.1	2.2	0.21	2.2	0.21	3.2
PHCI12	468.0	0.0100	1.1	2.2	0.21	2.2	0.21	3.2

Units are in kN, m

Table-A III-7 Acceptance criteria of beams hinges in conventional frame in Vancouver

Hinge	Section	a	b	c	IO	LS	CP
PHB01 <sup>+</sup>	9-9	0.010	0.015	0.200	0.005	0.010	0.015
PHB01 <sup>-</sup>		0.020	0.030	0.200	0.005	0.020	0.030
PHB02 <sup>+</sup>		0.010	0.015	0.200	0.004	0.010	0.015
PHB02 <sup>-</sup>		0.018	0.026	0.200	0.004	0.018	0.026
PHB03 <sup>+</sup>	10-10	0.010	0.015	0.200	0.005	0.010	0.015
PHB03 <sup>-</sup>		0.018	0.027	0.200	0.004	0.018	0.027
PHB04 <sup>+</sup>		0.010	0.015	0.200	0.005	0.010	0.015
PHB04 <sup>-</sup>		0.018	0.027	0.200	0.004	0.018	0.027
PHB05 <sup>+</sup>	11-11	0.020	0.030	0.200	0.005	0.020	0.030
PHB05 <sup>-</sup>		0.018	0.027	0.200	0.004	0.018	0.027
PHB06 <sup>+</sup>		0.020	0.030	0.200	0.005	0.020	0.030
PHB06 <sup>-</sup>		0.018	0.027	0.200	0.004	0.018	0.027

Table-A III-8 Properties of beams plastic hinges in conventional frame in Vancouver

Hinge	M <sub>y</sub>	$\theta_y$	M <sub>C</sub> /M <sub>y</sub>	$\theta_C / \theta_y$	M <sub>D</sub> /M <sub>y</sub>	$\theta_D / \theta_y$	M <sub>E</sub> /M <sub>y</sub>	$\theta_E / \theta_y$
PHB01 <sup>+</sup>	1293.0	0.0032	1.1	4.1	0.2	4.1	0.2	5.7
PHB01 <sup>-</sup>	583.0	0.0032	1.1	7.3	0.2	7.3	0.2	10.4
PHB02 <sup>+</sup>	1293.0	0.0053	1.1	2.9	0.2	2.9	0.2	3.8
PHB02 <sup>-</sup>	583.0	0.0053	1.1	4.3	0.2	4.3	0.2	6.0
PHB03 <sup>+</sup>	880.0	0.0034	1.1	3.9	0.2	3.9	0.2	5.4
PHB03 <sup>-</sup>	436.0	0.0034	1.1	6.3	0.2	6.3	0.2	9.0
PHB04 <sup>+</sup>	880.0	0.0057	1.1	2.8	0.2	2.8	0.2	3.7
PHB04 <sup>-</sup>	436.0	0.0057	1.1	4.2	0.2	4.2	0.2	5.8
PHB05 <sup>+</sup>	426.0	0.0034	1.1	6.9	0.2	6.9	0.2	9.8
PHB05 <sup>-</sup>	426.0	0.0034	1.1	6.3	0.2	6.3	0.2	9.0
PHB06 <sup>+</sup>	426.0	0.0057	1.1	4.5	0.2	4.5	0.2	6.3
PHB06 <sup>-</sup>	426.0	0.0057	1.1	4.2	0.2	4.2	0.2	5.8

Units are in kN, m

Table-A III-9 Acceptance criteria of columns hinges in moderately ductile frame in Montreal

<b>Hinge</b>	<b>Section</b>	<b>a</b>	<b>b</b>	<b>c</b>	<b>IO</b>	<b>LS</b>	<b>CP</b>
PHCE01	12-12	0.0312	0.0312	0.17	0.0047	0.0156	0.0219
PHCE02		0.0314	0.0314	0.18	0.0047	0.0157	0.0220
PHCE03		0.0325	0.0325	0.18	0.0049	0.0162	0.0227
PHCE04		0.0326	0.0326	0.19	0.0049	0.0163	0.0228
PHCE05		0.0337	0.0337	0.20	0.0050	0.0168	0.0236
PHCE06		0.0338	0.0341	0.20	0.0050	0.0170	0.0238
PHCE07		0.0341	0.0354	0.20	0.0050	0.0177	0.0248
PHCE08		0.0341	0.0354	0.20	0.0050	0.0177	0.0248
PHCE09		0.0341	0.0354	0.20	0.0050	0.0177	0.0248
PHCE10		0.0341	0.0354	0.20	0.0050	0.0177	0.0248
PHCE11		0.0341	0.0354	0.20	0.0050	0.0177	0.0248
PHCE12		0.0341	0.0354	0.20	0.0050	0.0177	0.0248
PHCI01	13-13	0.0294	0.0294	0.16	0.0044	0.0147	0.0206
PHCI02		0.0295	0.0295	0.16	0.0044	0.0148	0.0207
PHCI03		0.0309	0.0309	0.17	0.0046	0.0154	0.0216
PHCI04		0.0310	0.0310	0.17	0.0046	0.0155	0.0217
PHCI05		0.0323	0.0323	0.19	0.0048	0.0162	0.0226
PHCI06		0.0338	0.0338	0.20	0.0050	0.0169	0.0236
PHCI07		0.0338	0.0338	0.20	0.0050	0.0169	0.0236
PHCI08		0.0338	0.0338	0.20	0.0050	0.0169	0.0236
PHCI09		0.0338	0.0338	0.20	0.0050	0.0169	0.0236
PHCI10		0.0338	0.0338	0.20	0.0050	0.0169	0.0236
PHCI11		0.0338	0.0338	0.20	0.0050	0.0169	0.0236
PHCI12		0.0338	0.0338	0.20	0.0050	0.0169	0.0236

Table-A III-10 Properties of plastic hinges in columns of moderately ductile frame in  
Montreal

Hinge	$M_y$	$\theta_y$	$M_C/M_y$	$\theta_C / \theta_y$	$M_D/M_y$	$\theta_D / \theta_y$	$M_E/M_y$	$\theta_E / \theta_y$
PHCE01	363.0	0.0075	1.1	5.2	0.17	5.2	0.17	5.2
PHCE02	325.0	0.0075	1.1	5.2	0.18	5.2	0.18	5.2
PHCE03	325.0	0.0075	1.1	5.3	0.18	5.3	0.18	5.3
PHCE04	314.0	0.0075	1.1	5.4	0.19	5.4	0.19	5.4
PHCE05	314.0	0.0075	1.1	5.5	0.20	5.5	0.20	5.5
PHCE06	301.0	0.0075	1.1	5.5	0.20	5.5	0.20	5.5
PHCE07	301.0	0.0082	1.1	5.2	0.20	5.2	0.20	5.3
PHCE08	271.0	0.0082	1.1	5.2	0.20	5.2	0.20	5.3
PHCE09	271.0	0.0082	1.1	5.2	0.20	5.2	0.20	5.3
PHCE10	256.0	0.0082	1.1	5.2	0.20	5.2	0.20	5.3
PHCE11	256.0	0.0082	1.1	5.2	0.20	5.2	0.20	5.3
PHCE12	238.0	0.0082	1.1	5.2	0.20	5.2	0.20	5.3
PHCI01	580.0	0.0125	1.1	3.3	0.16	3.3	0.16	3.3
PHCI02	527.0	0.0125	1.1	3.4	0.16	3.4	0.16	3.4
PHCI03	527.0	0.0125	1.1	3.5	0.17	3.5	0.17	3.5
PHCI04	500.0	0.0125	1.1	3.5	0.17	3.5	0.17	3.5
PHCI05	500.0	0.0125	1.1	3.6	0.19	3.6	0.19	3.6
PHCI06	444.0	0.0125	1.1	3.7	0.20	3.7	0.20	3.7
PHCI07	444.0	0.0136	1.1	3.5	0.20	3.5	0.20	3.5
PHCI08	410.0	0.0136	1.1	3.5	0.20	3.5	0.20	3.5
PHCI09	410.0	0.0136	1.1	3.5	0.20	3.5	0.20	3.5
PHCI10	349.0	0.0136	1.1	3.5	0.20	3.5	0.20	3.5
PHCI11	349.0	0.0136	1.1	3.5	0.20	3.5	0.20	3.5
PHCI12	283.0	0.0136	1.1	3.5	0.20	3.5	0.20	3.5

Units are in kN, m



Table-A III-11 Acceptance criteria of beams hinges in moderately ductile frame in Montreal

Hinge	Section	a	b	c	IO	LS	CP
PHB01 <sup>+</sup>	14-14	0.020	0.030	0.200	0.005	0.020	0.030
PHB01 <sup>-</sup>		0.025	0.050	0.200	0.010	0.025	0.050
PHB02 <sup>+</sup>		0.020	0.030	0.200	0.005	0.020	0.030
PHB02 <sup>-</sup>		0.025	0.050	0.200	0.010	0.025	0.050
PHB03 <sup>+</sup>	15-15	0.020	0.030	0.200	0.005	0.020	0.030
PHB03 <sup>-</sup>		0.024	0.048	0.200	0.009	0.024	0.048
PHB04 <sup>+</sup>		0.020	0.030	0.200	0.005	0.020	0.030
PHB04 <sup>-</sup>		0.024	0.048	0.200	0.009	0.024	0.048
PHB05 <sup>+</sup>	16-16	0.020	0.030	0.200	0.005	0.020	0.030
PHB05 <sup>-</sup>		0.024	0.048	0.200	0.009	0.024	0.048
PHB06 <sup>+</sup>		0.020	0.030	0.200	0.005	0.020	0.030
PHB06 <sup>-</sup>		0.024	0.048	0.200	0.009	0.024	0.048

Table-A III-12 Properties of plastic hinges in beams of moderately ductile frame in Montreal

Hinge	$M_y$	$\theta_y$	$M_C/M_y$	$\theta_C / \theta_y$	$M_D/M_y$	$\theta_D / \theta_y$	$M_E/M_y$	$\theta_E / \theta_y$
PHB01 <sup>+</sup>	329.0	0.0042	1.1	5.7	0.2	5.7	0.2	8.1
PHB01 <sup>-</sup>	200.0	0.0042	1.1	6.9	0.2	6.9	0.2	12.8
PHB02 <sup>+</sup>	329.0	0.0071	1.1	3.8	0.2	3.8	0.2	5.2
PHB02 <sup>-</sup>	200.0	0.0071	1.1	4.5	0.2	4.5	0.2	8.1
PHB03 <sup>+</sup>	295.0	0.0046	1.1	5.3	0.2	5.3	0.2	7.5
PHB03 <sup>-</sup>	180.0	0.0046	1.1	6.2	0.2	6.2	0.2	11.4
PHB04 <sup>+</sup>	295.0	0.0077	1.1	3.6	0.2	3.6	0.2	4.9
PHB04 <sup>-</sup>	180.0	0.0077	1.1	4.1	0.2	4.1	0.2	7.2
PHB05 <sup>+</sup>	222.0	0.0046	1.1	5.3	0.2	5.3	0.2	7.5
PHB05 <sup>-</sup>	180.0	0.0046	1.1	6.2	0.2	6.2	0.2	11.4
PHB06 <sup>+</sup>	222.0	0.0077	1.1	3.6	0.2	3.6	0.2	4.9
PHB06 <sup>-</sup>	180.0	0.0077	1.1	4.1	0.2	4.1	0.2	7.2

Units are in kN, m

Table-A III-13 Acceptance criteria of columns hinges in conventional frame in Montreal

<b>Hinge</b>	<b>Section</b>	<b>a</b>	<b>b</b>	<b>c</b>	<b>IO</b>	<b>LS</b>	<b>CP</b>
PHCE01	17-17	0.0115	0.0218	0.22	0.0017	0.0109	0.0153
PHCE02		0.0115	0.0221	0.22	0.0017	0.0110	0.0154
PHCE03		0.0115	0.0238	0.22	0.0017	0.0119	0.0166
PHCE04		0.0115	0.0240	0.22	0.0017	0.0120	0.0168
PHCE05		0.0115	0.0256	0.22	0.0017	0.0128	0.0179
PHCE06		0.0115	0.0256	0.22	0.0017	0.0128	0.0179
PHCE07	18-18	0.0129	0.0270	0.22	0.0019	0.0135	0.0189
PHCE08		0.0129	0.0270	0.22	0.0019	0.0135	0.0189
PHCE09		0.0129	0.0270	0.22	0.0019	0.0135	0.0189
PHCE10		0.0129	0.0270	0.22	0.0019	0.0135	0.0189
PHCE11		0.0129	0.0270	0.22	0.0019	0.0135	0.0189
PHCE12		0.0129	0.0270	0.22	0.0019	0.0135	0.0189
PHCI01	19-19	0.0123	0.0200	0.23	0.0018	0.0100	0.0140
PHCI02		0.0123	0.0203	0.23	0.0018	0.0101	0.0142
PHCI03		0.0123	0.0229	0.23	0.0018	0.0115	0.0161
PHCI04		0.0123	0.0232	0.23	0.0018	0.0116	0.0162
PHCI05		0.0123	0.0258	0.23	0.0018	0.0129	0.0181
PHCI06		0.0123	0.0260	0.23	0.0018	0.0130	0.0182
PHCI07	20-20	0.0192	0.0330	0.24	0.0029	0.0165	0.0231
PHCI08		0.0192	0.0332	0.24	0.0029	0.0166	0.0233
PHCI09		0.0192	0.0335	0.24	0.0029	0.0168	0.0235
PHCI10		0.0192	0.0335	0.24	0.0029	0.0168	0.0235
PHCI11		0.0192	0.0335	0.24	0.0029	0.0168	0.0235
PHCI12		0.0192	0.0335	0.24	0.0029	0.0168	0.0235

Table-A III-14 Properties of plastic hinges in columns of conventional frame in Montreal

<b>Hinge</b>	<b>M<sub>y</sub></b>	<b><math>\theta_y</math></b>	<b>M<sub>C</sub>/M<sub>y</sub></b>	<b><math>\theta_C / \theta_y</math></b>	<b>M<sub>D</sub>/M<sub>y</sub></b>	<b><math>\theta_D / \theta_y</math></b>	<b>M<sub>E</sub>/M<sub>y</sub></b>	<b><math>\theta_E / \theta_y</math></b>
PHCE01	429.0	0.0056	1.1	3.1	0.22	3.1	0.22	4.9
PHCE02	421.0	0.0056	1.1	3.1	0.22	3.1	0.22	4.9
PHCE03	421.0	0.0056	1.1	3.1	0.22	3.1	0.22	5.2
PHCE04	411.0	0.0056	1.1	3.1	0.22	3.1	0.22	5.3
PHCE05	411.0	0.0056	1.1	3.1	0.22	3.1	0.22	5.5
PHCE06	374.0	0.0056	1.1	3.1	0.22	3.1	0.22	5.5
PHCE07	264.0	0.0060	1.1	3.2	0.22	3.2	0.22	5.5
PHCE08	238.0	0.0060	1.1	3.2	0.22	3.2	0.22	5.5
PHCE09	238.0	0.0060	1.1	3.2	0.22	3.2	0.22	5.5
PHCE10	226.0	0.0060	1.1	3.2	0.22	3.2	0.22	5.5
PHCE11	226.0	0.0060	1.1	3.2	0.22	3.2	0.22	5.5
PHCE12	181.0	0.0060	1.1	3.2	0.22	3.2	0.22	5.5
PHCI01	839.0	0.0094	1.1	2.3	0.23	2.3	0.23	3.1
PHCI02	762.0	0.0094	1.1	2.3	0.23	2.3	0.23	3.2
PHCI03	762.0	0.0094	1.1	2.3	0.23	2.3	0.23	3.4
PHCI04	742.0	0.0094	1.1	2.3	0.23	2.3	0.23	3.5
PHCI05	742.0	0.0094	1.1	2.3	0.23	2.3	0.23	3.8
PHCI06	671.0	0.0094	1.1	2.3	0.23	2.3	0.23	3.8
PHCI07	579.0	0.0100	1.1	2.9	0.24	2.9	0.24	4.3
PHCI08	514.0	0.0100	1.1	2.9	0.24	2.9	0.24	4.3
PHCI09	514.0	0.0100	1.1	2.9	0.24	2.9	0.24	4.4
PHCI10	445.0	0.0100	1.1	2.9	0.24	2.9	0.24	4.4
PHCI11	445.0	0.0100	1.1	2.9	0.24	2.9	0.24	4.4
PHCI12	403.0	0.0100	1.1	2.9	0.24	2.9	0.24	4.4

Units are in kN, m

Table-A III-15 Acceptance criteria of beam hinges of conventional frame in Montreal

Hinge	Section	a	b	c	IO	LS	CP
PHB01 <sup>+</sup>	21-21	0.010	0.015	0.200	0.005	0.010	0.015
PHB01 <sup>-</sup>		0.020	0.030	0.200	0.005	0.020	0.030
PHB02 <sup>+</sup>		0.010	0.015	0.200	0.005	0.010	0.015
PHB02 <sup>-</sup>		0.020	0.030	0.200	0.005	0.020	0.030
PHB03 <sup>+</sup>	22-22	0.010	0.015	0.200	0.005	0.010	0.015
PHB03 <sup>-</sup>		0.018	0.027	0.200	0.004	0.018	0.027
PHB04 <sup>+</sup>		0.010	0.015	0.200	0.005	0.010	0.015
PHB04 <sup>-</sup>		0.018	0.027	0.200	0.004	0.018	0.027
PHB05 <sup>+</sup>	23-23	0.020	0.030	0.200	0.005	0.020	0.030
PHB05 <sup>-</sup>		0.018	0.027	0.200	0.004	0.018	0.027
PHB06 <sup>+</sup>		0.020	0.030	0.200	0.005	0.020	0.030
PHB06 <sup>-</sup>		0.018	0.027	0.200	0.004	0.018	0.027

Table-A III-16 Properties of plastic hinges in beams of conventional frame in Montreal

Hinge	$M_y$	$\theta_y$	$M_C/M_y$	$\theta_C/\theta_y$	$M_D/M_y$	$\theta_D/\theta_y$	$M_E/M_y$	$\theta_E/\theta_y$
PHB01 <sup>+</sup>	453.0	0.0032	1.1	4.1	0.2	4.1	0.2	5.7
PHB01 <sup>-</sup>	279.0	0.0032	1.1	7.3	0.2	7.3	0.2	10.4
PHB02 <sup>+</sup>	453.0	0.0053	1.1	2.9	0.2	2.9	0.2	3.8
PHB02 <sup>-</sup>	279.0	0.0053	1.1	4.8	0.2	4.8	0.2	6.7
PHB03 <sup>+</sup>	379.0	0.0034	1.1	3.9	0.2	3.9	0.2	5.4
PHB03 <sup>-</sup>	254.0	0.0034	1.1	6.3	0.2	6.3	0.2	9.0
PHB04 <sup>+</sup>	379.0	0.0057	1.1	2.8	0.2	2.8	0.2	3.7
PHB04 <sup>-</sup>	254.0	0.0057	1.1	4.2	0.2	4.2	0.2	5.8
PHB05 <sup>+</sup>	261.0	0.0034	1.1	6.9	0.2	6.9	0.2	9.8
PHB05 <sup>-</sup>	261.0	0.0034	1.1	6.3	0.2	6.3	0.2	9.0
PHB06 <sup>+</sup>	261.0	0.0057	1.1	4.5	0.2	4.5	0.2	6.3
PHB06 <sup>-</sup>	261.0	0.0057	1.1	4.2	0.2	4.2	0.2	5.8

Units are in kN, m

## APPENDIX IV

FRS,  $R_{cb}$ , and  $A_r$  in Floors 1, 3, 4, and 5

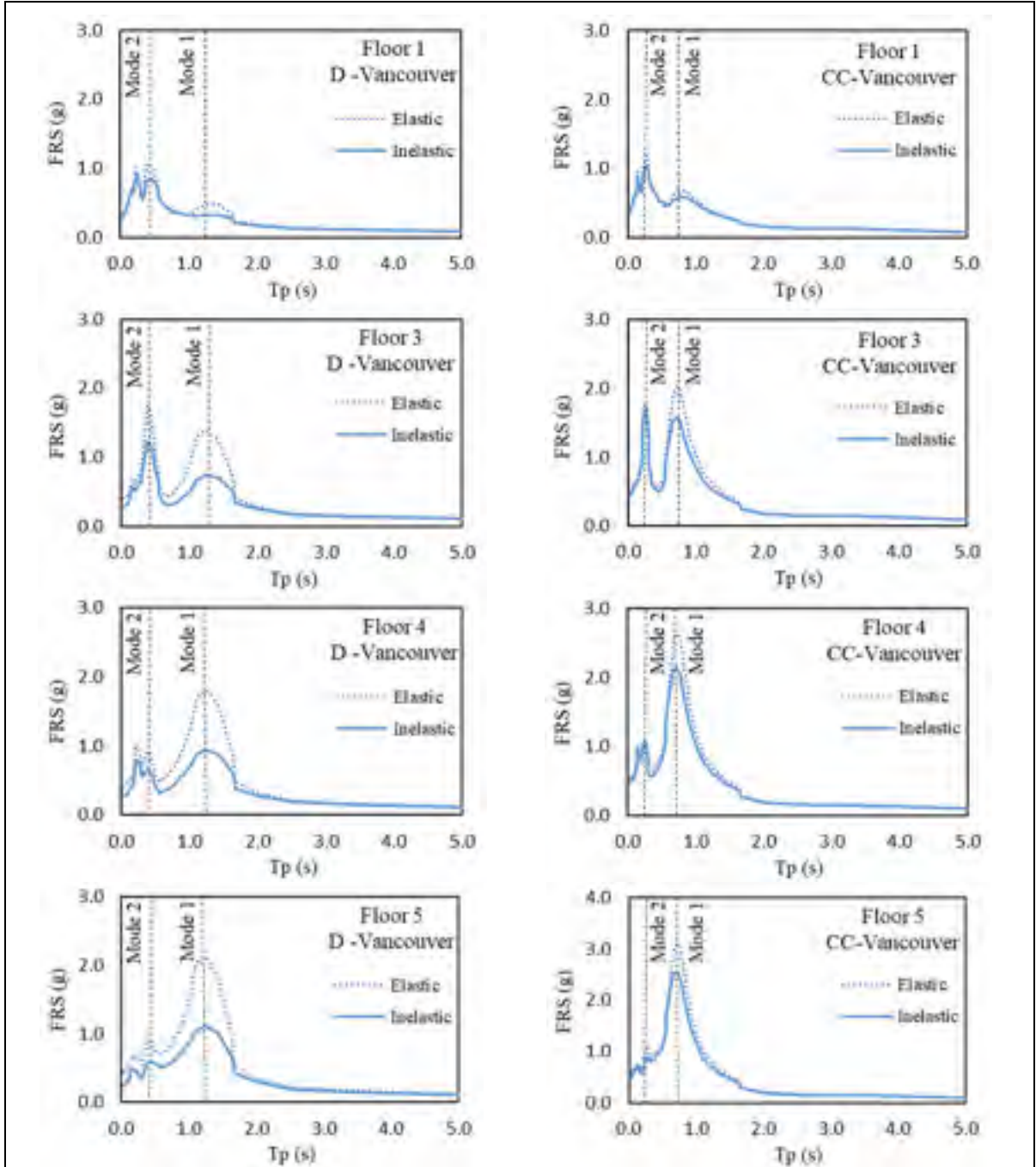


Figure-A IV-1 Computed mean FRS in ductile and conventional construction frames located in Vancouver for component damping ratio 5%

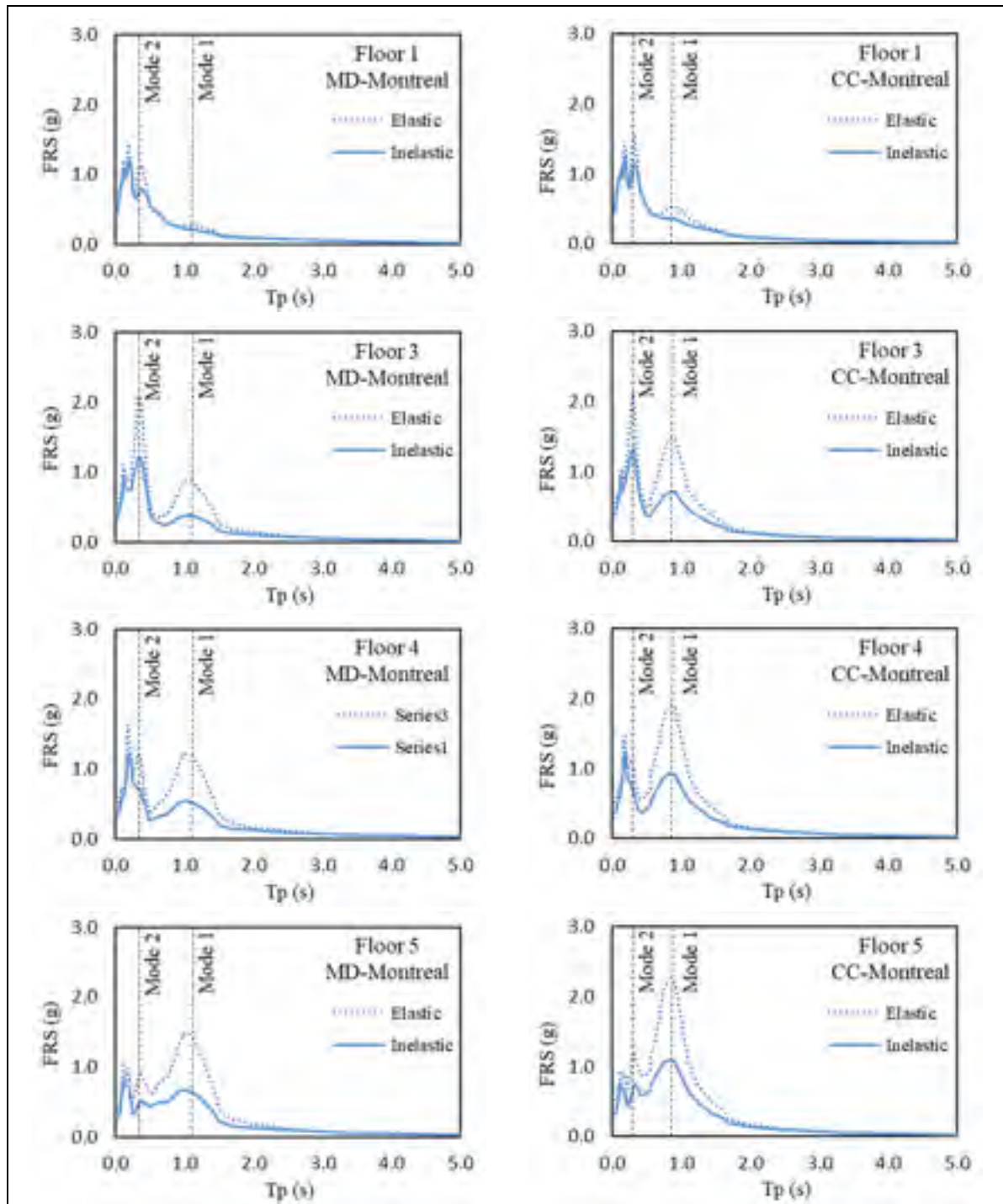


Figure-A IV-2 Computed mean FRS in moderately ductile and conventional frames located in Montreal for component damping ratio 5%

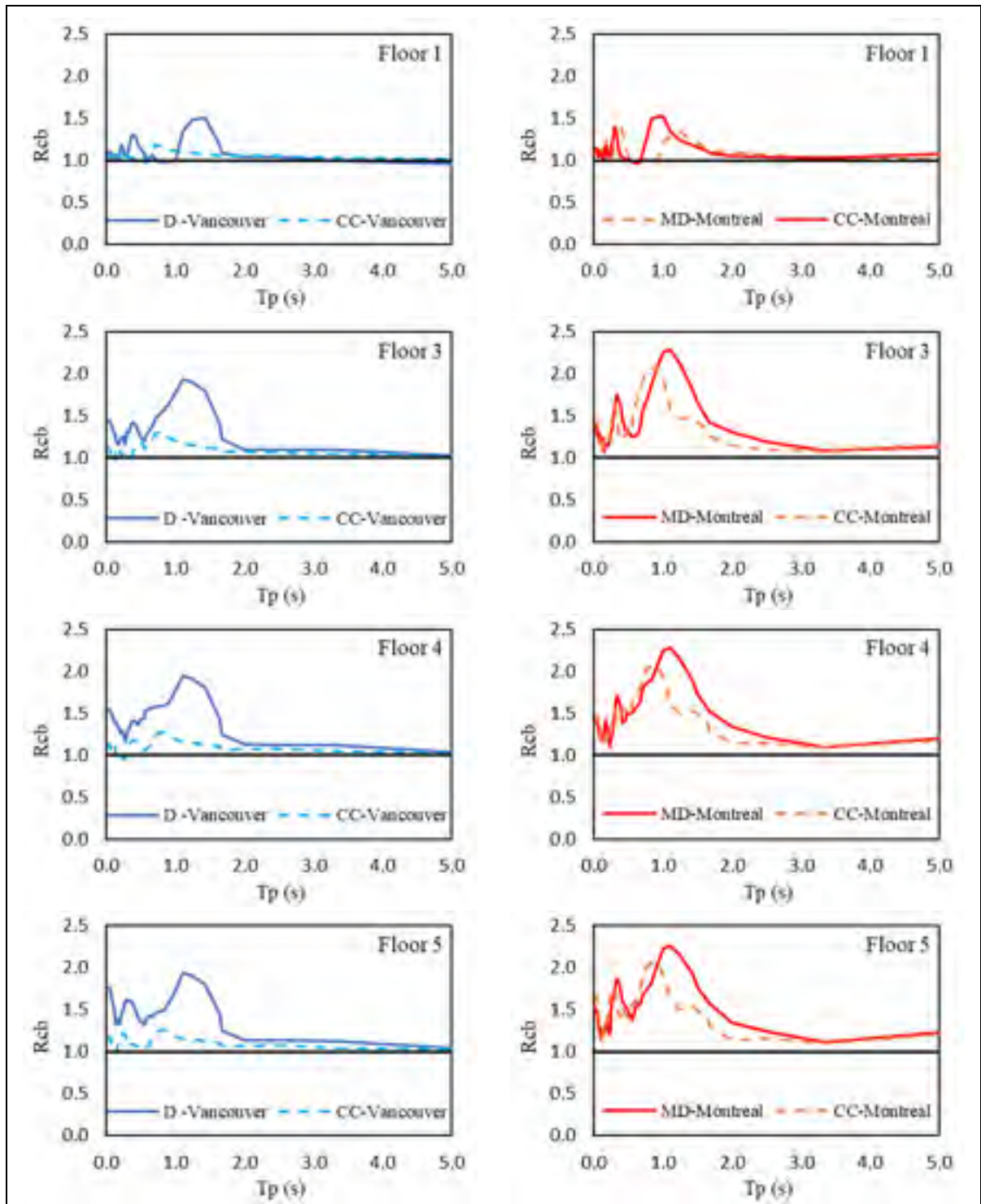


Figure-A IV-3 Mean FRS at different building ductility levels using component damping ratio 5%



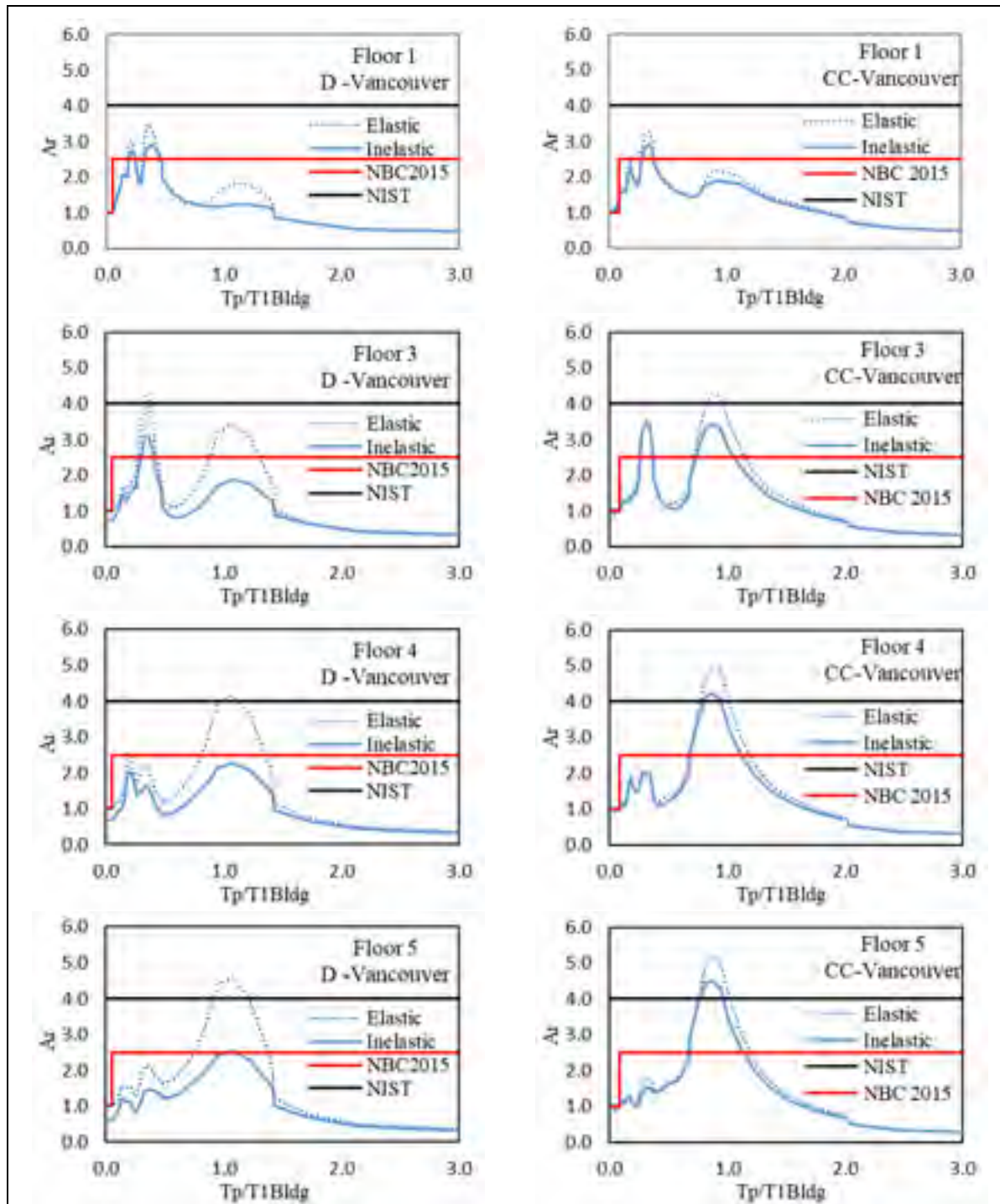


Figure-A IV-4 Computed mean  $A_r$  factors at different floors of frames located in Vancouver compared to the values proposed in NBC (2015) and NIST.GCR.18-917-43 (2018)



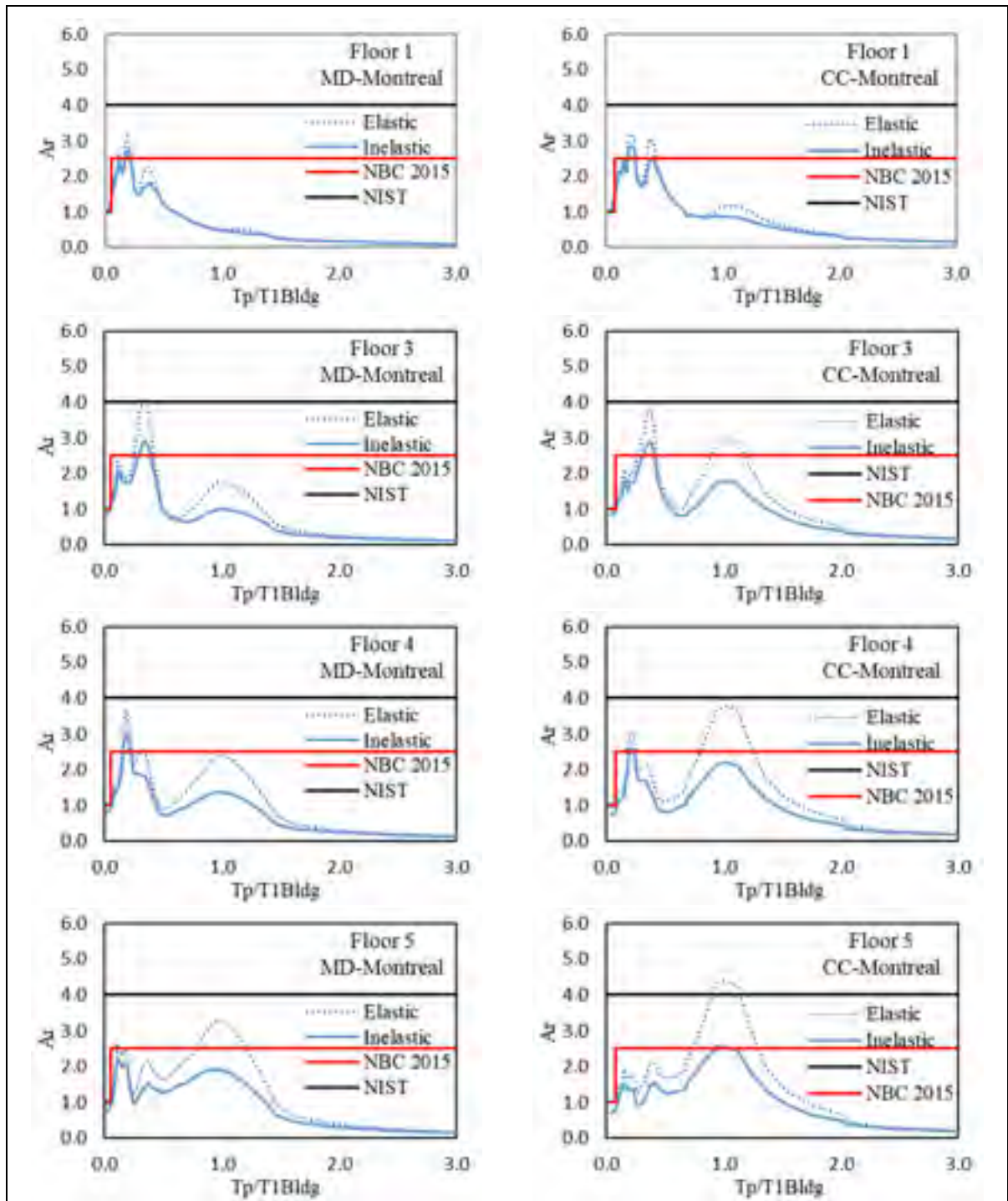


Figure-A IV-5 Computed mean  $A_r$  factors at different floors of frames located in Montreal compared to the values proposed in NBC (2015) and NIST.GCR.18-917-43 (2018)

## LIST OF BIBLIOGRAPHICAL REFERENCES

- American Society of Civil Engineers (ASCE). (2000). *Seismic Analysis of Safety-Related Nuclear Structures and Commentary*. Reston, Virginia, USA: American Society of Civil Engineers.
- American Society of Civil Engineers (ASCE). (2016). *Minimum Design Loads for Buildings and Other Structures*. Reston, Virginia, USA: American Society of Civil Engineers.
- American Society of Civil Engineers (ASCE). (2017). *Seismic Evaluation and Retrofit of Existing Buildings*. Reston, Virginia, USA: American Society of Civil Engineers.
- Assi, R., & McClure, G. (2015). Evolution of the NBCC seismic provisions for operational and functional components in buildings. *Canadian Journal of Civil Engineering*, 42(12), 993-999.
- Atkinson, G. M. (2009). Earthquake time histories compatible with the 2005 National building code of Canada uniform hazard spectrum. *Canadian Journal of Civil Engineering*, 36(6), 991-1000.
- Bachman, R., Drake, R., & Richter, P. (1994). Update to 1991 NEHRP provisions for architectural, mechanical and electrical components and systems. *Letter report to the National Center for Earthquake Engineering Research, Building Seismic Safety Council, Washington, DC*.
- Baird, A., & Yeow, T. (2016). *Estimating the Risk to Life Safety during Earthquakes from Non-Structural Elements in Commercial Buildings in New Zealand*. Retrieved from <https://www.mbie.govt.nz/assets/d1266a58c2/estimating-risk-to-life-safety-during-earthquakes.pdf>
- Bentz, E. (1999). Response-2000. Toronto, Ontario Canada: University of Toronto.
- Calvi, G. M., Priestley, M., & Kowalsky, M. (2008). *Displacement-based seismic design of structures*. Pavia, Italy: IUSS PRESS,.
- Canadian Commission on Building and Fire Codes. (2017). *Structural commentaries (User's guide - NBC 2015: Part 4 of Division B)* (Fourth ed. Vol. 1). Ottawa: National Research Council of Canada.
- Canadian Commission on Building Fire Codes, & National Research Council of Canada. (2015). *National Building Code of Canada, 2015*. Ottawa: National Research Council of Canada.

- Canadian Standards Association (CSA). (2014a). *Design of concrete structures (A23.3-14)*. Mississauga, Ontario, Canada Canadian Standards Association.
- Canadian Standards Association (CSA). (2014b). *Guideline for seismic risk reduction of operational and functional components (OFCs) of buildings (S832-14)*. Mississauga, Ontario, Canada Canadian Standards Association.
- Cement Association of Canada. (2006). *Concrete design handbook* (3rd. ed.). Ottawa: Cement Association of Canada.
- Chaudhuri, S. R., & Villaverde, R. (2008). Effect of building nonlinearity on seismic response of nonstructural components: a parametric study. *Journal of structural engineering*, 134(4), 661-670.
- Chen, Y., & Soong, T. T. (1988). Seismic response of secondary systems. *Engineering Structures*, 10(4), 218-228. doi:[http://dx.doi.org/10.1016/0141-0296\(88\)90043-0](http://dx.doi.org/10.1016/0141-0296(88)90043-0)
- Chopra, A. K. (2012). *Dynamics of structures: theory and applications to earthquake engineering*. (4 ed.). Upper Saddle River, N.J.: Pearson Education, 2012.
- CSI. (2011). CSI Analysis Reference Manual For SAP2000®, ETABS®, SAFE® and CSiBridge™. Berkeley, California, USA: Computers and Structures, Inc.
- CSI. (2017). Hysteresis Types. Retrieved from [https://docs.csiamerica.com/help-files/sap/Menu/Assign/Hysteresis\\_Types.htm](https://docs.csiamerica.com/help-files/sap/Menu/Assign/Hysteresis_Types.htm)
- CSI. (2019). SAP2000 Integrated Software for Structural Analysis and Design (Version 21.0.0). Berkeley, California: Computers & Structures, Inc.
- Deierlein, G. G., Reinhorn, A. M., & Willford, M. R. (2010). Nonlinear structural analysis for seismic design. *NEHRP seismic design technical brief*, 4, 1-36.
- Der Kiureghian, A. (1980). *A response spectrum method for random vibrations*: University of California, Earthquake Engineering Research Center.
- EN1998-1. (2004). Eurocode 8: General rules, seismic actions and rules for buildings.
- Fathali, S., & Lizundia, B. (2011). Evaluation of current seismic design equations for nonstructural components in tall buildings using strong motion records. *The Structural Design of Tall and Special Buildings*, 20(S1), 30-46.
- Federal Emergency Management Agency (FEMA). (2000). *Prestandard And Commentary For The Seismic Rehabilitation Of Buildings*. Reston, Virginia, USA: American Society of Civil Engineers.

- Federal Emergency Management Agency (FEMA). (2005). *Earthquake Hazard Mitigation for Nonstructural Elements*. Reston, Virginia, USA: American Society of Civil Engineers.
- Filiatrault, A., & Sullivan, T. (2014). Performance-based seismic design of nonstructural building components: The next frontier of earthquake engineering. *Earthquake Engineering and Engineering Vibration*, 13(1), 17-46.
- Filiatrault, A., Uang, C.-M., Folz, B., Christopoulos, C., & Gatto, K. (2001). Reconnaissance report of the February 28, 2001 Nisqually (Seattle-Olympia) earthquake. *SSRP*, 02.
- Flores, F. X., Lopez-Garcia, D., & Charney, F. A. (2015). *Floor accelerations in buildings having different structural systems*. Paper presented at the Structures Congress 2015, April 23, 2015 - April 25, 2015, Portland, OR, United States.
- Foo, S., & Cheung, M. (2004). *Seismic risk reduction of operational and functional components of buildings: Standard development*. Paper presented at the 13th World Conference on Earthquake Engineering, Vancouver, B.C., Canada.
- Hakim, R., Alama, M., & Ashour, S. (2014). Seismic assessment of RC building according to ATC 40, FEMA 356 and FEMA 440. *Arabian Journal for Science and Engineering*, 39(11), 7691-7699.
- Jha, S., Roshan, A., & Bishnoi, L. (2015). *FLOOR RESPONSE SPECTRA FOR BEYOND DESIGN BASIS SEISMIC DEMAND*. Paper presented at the 23rd Conference on Structural Mechanics in Reactor Technology, Manchester, United Kingdom.
- Jha, S., Roshan, A., & Bishnoi, L. (2017). Floor response spectra for beyond design basis seismic demand. *Nuclear Engineering and Design*, 323, 259-268.
- Jiang, W. (2016). *Direct Method of Generating Floor Response Spectra*. (Doctor of Philosophy), University of Waterloo, Waterloo, ON. Retrieved from <https://uwspace.uwaterloo.ca/handle/10012/10460>
- Kothari, P., Parulekar, Y., Reddy, G., & Gopalakrishnan, N. (2017). In-structure response spectra considering nonlinearity of RCC structures: Experiments and analysis. *Nuclear Engineering and Design*, 322, 379-396.
- Magliulo, G., Ercolino, M., Petrone, C., Coppola, O., & Manfredi, G. (2014). The Emilia earthquake: seismic performance of precast reinforced concrete buildings. *Earthquake Spectra*, 30(2), 891-912.
- Medina, R. A., Sankaranarayanan, R., & Kingston, K. M. (2006). Floor response spectra for light components mounted on regular moment-resisting frame structures. *Engineering Structures*, 28(14), 1927-1940.

- Miranda, E., & Taghavi, S. (2009). *A comprehensive study of floor acceleration demands in multi-story buildings*. Paper presented at the 2009 ATC and SEI Conference on Improving the Seismic Performance of Existing Buildings and Other Structures, December 9, 2009 - December 11, 2009, San Francisco, CA, United states.
- Mitchell, D., Tinawi, R., & Law, T. (1990). Damage caused by the November 25, 1988, Saguenay earthquake. *Canadian Journal of Civil Engineering*, 17(3), 338-365.
- Mitchell, D., Tremblay, R., Karacabeyli, E., Paultre, P., Saatcioglu, M., & Anderson, D. L. (2003). Seismic force modification factors for the proposed 2005 edition of the National Building Code of Canada. *Canadian Journal of Civil Engineering*, 30(2), 308-327. doi:10.1139/102-111
- National Institute of Standards and Technology (NIST). (2017). *Guidelines for Nonlinear Structural Analysis for Design of Buildings: Part IIb – Reinforced Concrete Moment Frames*. Redwood City, CA, USA: Applied Technology Council.
- National Institute of Standards and Technology (NIST). (2018). *Recommendations for Improved Seismic Performance of Nonstructural Components*. Redwood City, CA, USA: Applied Technology Council.
- Natural Resources Canada. (2018). National Building Code of Canada seismic hazard values. Retrieved from <http://earthquakescanada.nrcan.gc.ca/hazard-alea/interpolat/calc-en.php>
- NEHRP. (2009). NEHRP recommended seismic provisions for new buildings and other structures (FEMA P-750). *Federal Emergency Management Agency, Washington, DC* (Council, Building Seismic Safety).
- Oropeza, M., Favez, P., & Lestuzzi, P. (2010). Seismic response of nonstructural components in case of nonlinear structures based on floor response spectra method. *Bulletin of Earthquake Engineering*, 8(2), 387-400. doi:10.1007/s10518-009-9139-0
- Paultre, P., Castele, D., Rattray, S., & Mitchell, D. (1989). Seismic response of reinforced concrete frame subassemblages. A Canadian code perspective. *Canadian Journal of Civil Engineering*, 16(5), 627-649.
- Petrone, C., Magliulo, G., & Manfredi, G. (2015). Seismic demand on light acceleration-sensitive nonstructural components in European reinforced concrete buildings. *Earthquake engineering & structural dynamics*, 44(8), 1203-1217.
- Pinkawa, M., Hoffmeister, B., & Feldmann, M. (2014). *A critical review of current approaches on the determination of seismic force demands on nonstructural components*. Paper presented at the 9th International Conference on Structural Dynamics, EUROLYN 2014, June 30, 2014 - July 2, 2014, Porto, Portugal.

- Priestley, M. N. (2003). *Myths and fallacies in earthquake engineering, revisited*: IUSS press.
- Rodriguez, M., Restrepo, J., & Carr, A. (2002). Earthquake-induced floor horizontal accelerations in buildings. *Earthquake engineering & structural dynamics*, 31(3), 693-718.
- Saatcioglu, M. (Producer). (2004). Seismic Design and Detailing of Reinforced Concrete Structures Based on CSA A23.3 - 2004. [Powerpoints slides] Retrieved from <https://www.slideserve.com/jeneva/seismic-design-and-detailing-of-reinforced-concrete-structures-based-on-csa-a23-3-2004>
- Saatcioglu, M., Shooshtari, M., Foo, S., & Naumoski, N. (2010). *Assessment of the National Building Code of Canada seismic design requirements for operational and functional components using floor response spectra*. Paper presented at the 9th US National and 10th Canadian Conference on Earthquake Engineering 2010, Including Papers from the 4th International Tsunami Symposium, July 25, 2010 - July 29, 2010, Toronto, ON, Canada.
- Shooshtari, M., Saatcioglu, M., Naumoski, N., & Foo, S. (2010). Floor response spectra for seismic design of operational and functional components of concrete buildings in Canada. *Canadian Journal of Civil Engineering*, 37(12), 1590-1599. doi:10.1139/L10-094
- Singh, M., & Suarez, L. (1986). A perturbation analysis of the eigenproperties of equipment-structure systems. *Nuclear Engineering and Design*, 97(2), 167-185.
- Sucuoğlu, H., & Erberik, A. (2004). Energy-based hysteresis and damage models for deteriorating systems. *Earthquake engineering & structural dynamics*, 33(1), 69-88.
- Sullivan, T. J., Calvi, P. M., & Nascimbene, R. (2013). Towards improved floor spectra estimates for seismic design. *Earthquakes and Structures*, 4(1), 109-132.
- Surana, M., Singh, Y., & Lang, D. H. (2016). Floor Spectra of Inelastic RC Frame Buildings Considering Ground Motion Characteristics. 1-32. doi:10.1080/13632469.2016.1244134
- Surana, M., Singh, Y., & Lang, D. H. (2017). Effect of Response Reduction Factor on Peak Floor Acceleration Demand in Mid-Rise RC Buildings. *Journal of The Institution of Engineers (India): Series A*, 98(1-2), 53-65.
- Taghavi, S., & Miranda, E. (2005). Approximate floor acceleration demands in multistory buildings. II: Applications. *Journal of structural engineering*, 131(2), 212-220.



- Villaverde, R. (1996). *Earthquake resistant design of secondary structures: A report on the state of the art*. Paper presented at the 11th world conference on earthquake engineering, Acapulco, Mexico.
- Villaverde, R. (1997). Method to improve seismic provisions for nonstructural components in buildings. *Journal of structural engineering New York, N.Y.*, 123(4), 432-439. doi:10.1061/(ASCE)0733-9445(1997)123:4(432)
- Vukobratović, V., & Fajfar, P. (2017). Code-oriented floor acceleration spectra for building structures. *Bulletin of Earthquake Engineering*, 15(7), 3013-3026. doi:10.1007/s10518-016-0076-4
- Wieser, J., Pekcan, G., Zaghi, A. E., Itani, A., & Maragakis, M. (2013). Floor accelerations in yielding special moment resisting frame structures. *Earthquake Spectra*, 29(3), 987-1002. doi:10.1193/1.4000167
- Wieser, J., Pekcan, G., Zaghi, A. E., Itani, A. M., & Maragakis, E. (2011). *Assessment of floor accelerations in yielding buildings*. University of Nevada, Reno,